WOLLEGA UNIVERSITY

SCHOOL OF GRADUATE STUDIES

BOUNDARY LAYER FLOW ANALYSIS OF NON-NEWTONIAN NANOFLUID PAST STRETCHING/ SHRINKING SURFACE

PhD Dissertation

Mekonnen Negera

January, 2021

Nekemte, Ethiopia

WOLLEGA UNIVERSITY
SCHOOL OF GRADUATE STUDIES

BOUNDARY LAYER FLOW ANALYSIS OF NON-NEWTONIAN NANOFLUID PAST STRETCHING/ SHRINKING SURFACE

Dissertation Submitted for the award of a Degree of Doctor of Philosophy in Applied Mathematics (Fluid Dynamics)

Mekonnen Negera Woyessa

Supervisor: Wubshet Ibrahim (PhD, Associate Prof.)

January 2021

Nekemte, Ethiopia

Table of Content

Contents

Statement of the Author

I, Mekonnen Negera hereby state that my Ph.D. thesis titled: **Boundary Layer flow Analysis of non-Newtonian Nanofluid Past Stretching/ Shrinking Surface** is my own work and has not been submitted previously by me or by any one for taking any degree from this university (Wollega University) or anywhere else in the country.

At any time if my statement is found to be incorrect even after my doctorate, the university has the right to withdraw my PhD degree.

Signature______________________ Date______________________

Biography

The author of the dissertation, Mr. Mekonnen Negera Woyessa, was born on 21th of January, 1973 in Jemo Kebele Nunu Kumba District East Wollega Zone, Oromia National Regional State, Ethiopia. He attended elementary school (1-6) education at Gombo elementary school from 1979 to 1984. And also he attended junior elementary school (7-8) and Secondary school (9-12) at Arjo Secondary school from 1985 to 1990. After he completed his secondary school education, he joined Nekemte Teacher Training Institute and graduated in 1991by certificate. After his graduation he employed for teaching at East Wollega Zone Nunu Kumba District in 1991. For 9 years he taught in different elementary school. After 9 years' service he joined diploma program at Jima Training Center in 2000 and he graduated in 2005. In 2005 he joined Arjo secondary school and he taught until 2012 at this school. He joined Addis Ababa University and graduated in August, 2010 by Bachelor of degree in Mathematics. In 2011, again he joined Addis Ababa University to attend his second degree program in applied mathematics. He graduated by Masters of Science in Differential Equation in 2012. After his graduation he employed at Wollega University in 2012 for lecturer. In 2016 he started to pursue his PhD studies in applied mathematics (Fluid Dynamics).

Nomenclature

A_1	First Rivlin-Ericson tensor
Bi	Biot Number
B_0	Strength of Magnetic field
c	Volumetric volume expansion coefficient
c_f	The heat capacity of the fluid
c_s	The heat capacity of the solid
C_f	Skin friction coefficient
C_w	Uniform concentration over the surface of the sheet
C_∞	Ambient concentration
d	Permeability parameter
D_B	Brownian diffusion coefficient
D_τ	Thermophoresis diffusion coefficient
E	Velocity Ratio
e	Fitted rate parameter
E_d	Activation energy
Ec	Eckert number
G_t	Temperature buoyancy parameter
G_c	Concentration buoyancy parameter
f	Dimensionless velocity stream function
h	Thermal Biot number
H	Solutal Biot number
h_f	Heat transfer coefficient
k	Thermal conductivity
K	Chemical reaction parameter
k_m	Mass transfer coefficient
k^*	Absorption constant
l	Characteristic length
Le	Lewis number
M	Magnetic parameter
Nb	Brownian motion parameter
Nt	Thermophoresis parameter
Nu_x	Local Nusselt number
p	Pressure
Pr	Prandtl number
m	Dimensionless melting parameter
q_m	Mass flux of the nanofluid
q_w	Heat flux of the nanofluid
r	Radius of cylinder
R	Heat source/sink parameter and radius of cylinder
Rd	Thermal radiation parameter
Re	Reynolds number
Re_x	Local Reynolds number
S	Cauchy stress tensor
Sc	Schmidt number
Sh_x	Local Sherwood number
T	Temperature of the fluid
T_f	Wall temperature
T_w	Uniform temperature over the surface of the sheet
T_m	The temperature of the melting surface
T_∞	Ambient temperature
(u, v)	Velocity component along x- and y direction
u_e	Free steam velocity
u_0	Reference velocity

u_w	The velocity of stretching/ shirnking wedge

Greeks symbols:

α_m	Thermal diffusivity
β	Deborah number
β^*	Wedge angle parameter
Γ	Material constant
χ	Suction-injection parameter
γ	Curvature parameter
γ^*	Stretching parameter
φ	The latent heat of the fluid
λ	Williamson parameter
λ_1	Unsteadiness parameter
υ	Velocity slip parameter
ζ	The ratio of viscosities
ζ^*	Temperature difference
δ^*	Thermal slip parameter
γ_1	Solutal slip parameter
η	Dimensionless similarity variable
θ	Dimensionless temperature function
μ	Dynamic viscosity of the fluid
α	Temperature exponent parameter
ε	Thermal conductivity parameter
β_1	Thermal expansion coefficient
π	Second invariant strain tensor
β_2	Concentration expansion coefficient
ν	Kinematic viscosity of the fluid
σ_1	Reaction rate parameter
σ	Electrical conductivity of the fluid
σ^*	Steffan-Boltzman constant
ς^*	Concentration exponent
ρ_f	Density of the fluid
$(\rho c)_f$	Heat capacity of the fluid
$(\rho c)_p$	Effective heat capacity of a nanoparticle
τ	Extra stress tensor
ρ_p	Density of nanoparticles
ξ	Relaxation time parameter of the fluid
ϕ	Dimensionless concentration function
ψ	Stream function
ϕ_w	Concentration function at the surface
ϕ_∞	Concentration function at large values of y
ω	Parameter defined by $(\rho c)_p/(\rho c)_f$

Subscripts:

∞	Condition at the free stream
w	Condition at the surface

Acknowledgement

First of all I would like to thank the almighty God who led me through all the rough and difficult times and gave me the strength and encouragement to complete this study.

It is my great pleasure to express my sincere gratitude to my advisor, Dr. Wubshet Ibrahim for his constant and comfortable academic supervision with patience and brotherly approach starting from the initial planning to the finalization of this dissertation. During the countless discussions with him, new ideas come to my mind and I broadened my thinking about several aspects and hence I have learnt the research methods used in applied mathematics particularly in fluid dynamics through his guidance. Moreover, his great effort in making me an independent mathematician is also worth beyond mentioning.

I would also like to express my sincerely appreciation to all my family Kuri Tirfe my wife, Gemmechis Mekonnen, Tolassa Mekonnen, Tolawak Mekonnen, Sara Mekonnen, Ferehiwot Mengesha and Kiya Ferew for their support and their encouragement during the period of my study. I would like to thanks my brothers Degefe Negera and Lami Negera for their constructive idea. Also I would like to thanks my colleagues Dr. Alemu Gelata and Dr. Brehanu Bekele for their help when I was writing on computer and sometime correcting grammars.

Lastly, but not the least, I also appreciate the support from Fekadu Yemataw (Former Mathematics head), Andualem Benti (Mathematics Department Head) and Dr. Boka Kumsa (Former College Dean), Dr. Mosissa Geleta (College Dean) . Also I would like to thanks all Wollega University Mathematics Department staff for their encouragement me during the period my study.

Dedication

Dedicated to

My Family

Kuri Tirfe (My Wife)

Gemmechis Mekonnen (Son)

Tolassa Mekonnen (Son)

Tolawak Mekonnen (Son)

Sara Mekonnen (Daughter)

List of Tables

List of Figures

Abstract

This dissertation presents the boundary layer flow analysis of non-Newtonian nanofluid past stretching/shrinking surfaces. In this dissertation heat transfer and mass transfer of MHD flow of non-Newtonian nanofluids over different shaped bodies with different governing parameters considered. The governing partial differential equations with boundary conditions were transformed into set of high order ordinary differential equations using similarity transformations and were solved numerically using implicit finite difference methods known as Keller box methods and Runge-Kutta method with shooting technique with Matlab software 2013a. In this dissertation viscous dissipation, melting heat transfer, variable thermal radiation, chemical reaction, suction/injection, activation energy and MHD effects included in the analysis. Moreover, the effects of magnetic parameter, Prandtl number, Biot-number, Eckert number, Lewis number, Schmidt number, porosity parameter, temperature buoyancy parameter, concentration buoyancy parameter on velocity, temperature and concentration profile are presented graphically. The effects of suction/injection parameter, Deborah number, velocity slip parameter, unsteadiness parameter, Williamson parameter, curvature parameter, activation energy and porosity parameter on skin friction coefficient, Nusselt number and Sherwood number are tabulated and discussed. From the results it can be seen that when the magnetic field is intensified, it reduces velocity profiles, but it increases concentration and temperature profiles. Moreover, when Deborah number increased the velocity profile reduced whereas the temperature profile increased. The numerical solution also noticed that dimensionless melting parameter affects highly the velocity boundary layer of Williamson nanofluid when compared with upper-convected Maxwell nanofliud. Furthermore, with an increase in Williamson parameter the velocity profiles decreased whereas temperature and concentration profiles increased. Still further, from *the result it can be seen that local Sherwood numbers and skin-friction coefficient increased whereas local Nusselt reduced for the higher values of variable thermal conductivity parameter.*

Key words: Non-Newtonian Fluids, Nanofluid, slip effects, Newtonian heating, stagnation point flow, Melting heat transfer, activation energy, Keller box, Runge-Kutta.

Chapter 1

Introduction

1.1. Fluid mechanics

Fluid mechanics deals with transport processes in the molecule–dependent motion of fluids (fluid dynamics or fluid kinematics) or the fluids at rest (fluid statics). Fluid mechanics is a special branch of continuum mechanics which deals with the relationship between forces, motion and statics conditions in a continuous material. In fact, fluid mechanics exists everywhere in our life both in natural or practical environment and we all as a human being observe that this branch of science has significant importance. Life is not possible on earth without flows of fluids and even natural and technical growth would not be possible. Therefore, flows have vital importance like blood in the vessels which transport the essential nutrients to the cells by mass flows, where chemical reactions take place and produces energy for the body, flows of the food chain in flora and fauna, flows into lakes, rivers and seas, transport of clouds through winds and a multitude of other examples in natural and technological environments.

1.2. Fluids

The study of fluid mechanics goes back at least to the days of ancient Greece when Archimedes investigated fluid statics and buoyancy finally to formulate his famous Archimedes Principle. Ancient civilizations had enough knowledge to solve certain flow problems. The developments of sailing ships with oars, water supply, irrigation systems, propulsion of spears and arrow through air and design of boats etc. were known in prehistoric times. These developments were based on trial and error procedures without any core knowledge. However, it was the accumulation of such empirical knowledge that formed the basis for further development. Archimedes first expressed the principles of hydrostatics and flotation. Up to the Renaissance, there was a steady improvement in the design of such flow systems as ships, canals and water conduits. Leonardo da Vinci (1452-1519) described many different types of fluid phenomena through sketches and writings, exactly as they were. The work of Galileo Galilei (1564-1642) marked the beginning of experimental mechanics. In 1687, Isaac Newton (1642-1727) postulated his laws of motion and the law of viscosity of the fluids.

The theory first yielded to the assumption of a perfect or frictionless fluid. In eighteenth century, mathematicians produced many solutions of frictionless flow problems. Daniel Bernoulli (1700-1782) derived Bernoulli's famous equation. Leonhard Euler (1707-1783) proposed the equation, for conservation of momentum and conservation of mass. He also proposed the velocity potential theory. At the beginning of the twentieth century, both fields of theoretical and experimental hydraulics were highly developed, and attempts were being made to unify them. In 1904, a classic research was presented by (Ludwig Prandtl, 1875-1953), to introduce the concept of “fluid boundary layer” and work was started on refining theories of boundary layers and turbulence in fluid flow. Theodore Von Karman (1881-1963) analyzed surface resistance and turbulence.

1.3. Nanofluids

Nano, a Greek word, means dwarf. Science has, however, given this dwarf a numerical value of “one billionth”. A nanometer is a billionth of a meter, and nanofluid is a colloidal suspension which containing nanometer sized particles, called nanoparticles in a base fluid. These fluids are engineered colloidal suspensions of nanoparticles in a base fluid. Nanofluids are important to study because of their heat and mass transfer properties. They enhance the thermal conductivity and convective properties over the properties of the base fluid. Moreover, the presence of the nanoparticles enhance the electrical conductivity of the nanofluid, hence are more susceptible to the influence of magnetic field than the conventional base fluids. Nanofluids have enhanced physical properties such as thermal diffusivity, viscosity, mass diffusivity, thermal conductivity and convective heat transfer coefficients compared to those of base fluids. Due to these novel properties nanofluids became potentially useful in many advanced industrial and engineering applications as found by (Wong & Leon, 2010).

Nanofluids can be used in a plethora of engineering applications ranging from use in the automotive industry to the medical arena to use in power plant cooling systems as well as computers *viz.* heat transfer applications (in industrial cooling applications as smart fluids, in nuclear reactors, in extraction of geothermal energy sources), automotive applications (as nanofluid coolant, nanofluid in fuel, brake and other vehicular nanofluids), electronic applications (cooling of microchips, Micro scale fluidic applications) and biomedical applications (Nano drug delivery, cancer therapeutics, cryopreservation, Nano cryosurgery) etc. For the first time such fluid is experimentally studied by (Choi & Eastman, 1995).

1.4. Non-Newtonian fluids

During the past many years, Newtonian fluids have come a long way in the fluid dynamics in the field of turbulence and multi-phase flows. Most low molecular weight substances such as organic and inorganic liquids, solutions of low molecular weight inorganic salts, molten metals and salts etc. exhibit shear stress is proportional to the rate of shear at constant temperature and pressure and these constant of proportionality is the viscosity. Such fluids are classically known as the Newtonian fluids. In general, for most liquids the viscosity decreases with temperature and increases with pressure. On the other hand for gases it increases with increases of both temperature and pressure (Reid et al., 1977). But, during the past few years, there has been a growing appreciation of the fact that a lot of substances of industrial significance, especially of multi-phase nature (foams, emulsions, dispersions and suspensions, slurries, for instance), and polymeric melts and solutions (both natural and manmade) do not conform to the Newtonian postulate of the linear relationship between shear stress and rate of shear. Accordingly, these fluids are known as non-Newtonian fluids. A non-Newtonian fluid is a fluid that does not follow Newton's law of viscosity, i.e. constant viscosity independent of stress. In non-Newtonian fluids, viscosity can change when a force is undertaken to either more liquid or more solid. These types of fluids exhibit different kinds of behavior with varying strictness of non-Newtonian flow behavior (Chhabra & Richardson, 2008). So the non-Newtonian fluid behavior is more valuable than the Newtonian fluid behavior in nature and in technology. For these types of fluids the constant of proportionality, viscosity, may change with time. A brief introduction of different kinds of non-Newtonian flow characteristics are provided in figure 1.1.

1.4.1. Classification of Non-Newtonian Fluid

Non-Newtonian fluid has been classified by (Shenoyand & Mashelkar, 1982) into two main categories: (A) Inelastic non-Newtonian fluid and (B) viscoelastic non-Newtonian fluid. The first one can be subdivided into two types (i) time independent and (ii) time dependent.

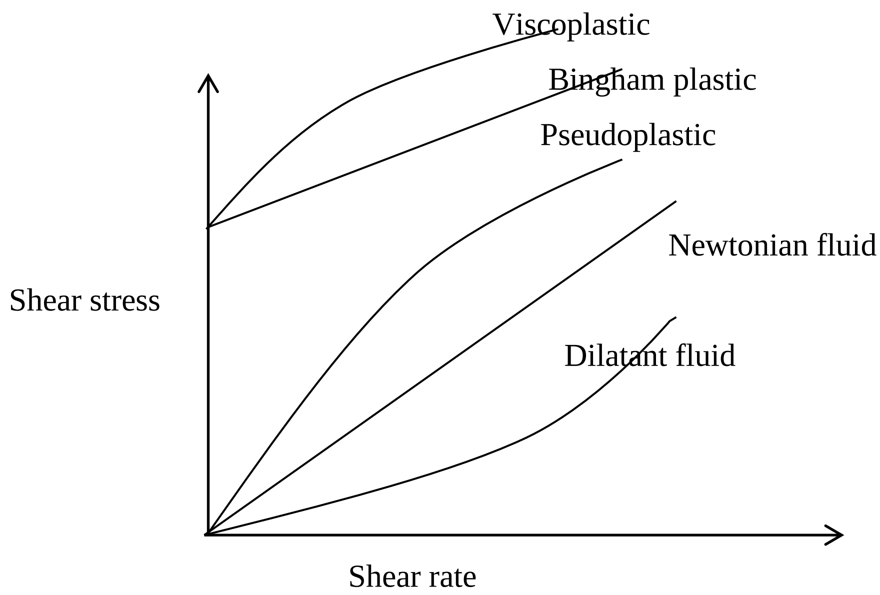

Figure1. 1: Classification of fluids with shear stress as a function of shear rate

(A) Inelastic Non-Newtonian fluid

(i) Time independent Non-Newtonian fluid

In the time-independent fluids properties such as viscosity does not depends on time. The non-linearity relation between the shear stress and strain rate at a given point is solely written by the following way:

$$\tau = f(\dot{Y}) \tag{1.1}$$

where τ and $\dot{Y}$ are the shear stress and strain rate respectively.

The time independent non-Newtonian fluid can be subdivided into three varieties depending on the form of function of above equation:

(i) Pseudoplastic (shear thinning) (ii) Dilatant (shear thickening) (iii) Viscoplastic

i) Pseudoplastic fluids or shear-thinning fluids often exhibit an apparent viscosity which decreases with increasing shear rate. Polymer solutions, polymer melts, printing inks and blood are the pseudoplastic fluids.

ii) Dilatants often referred as shear-thickening fluids, exhibit viscosity increase with increasing shear rate. Gum solution, aqueous suspensions of titanium dioxide, wet sand, starch suspensions are treated as dilatants fluids. Shear-thinning behavior is more common than shear-thickening.

iii) Viscoplastic or "yield stress". This is a fluid that will not flow when only a small shear stress is applied. The shear stress must exceed a critical value known as the yield stress τ_0 for the fluid to flow. For example, when you open a tube of toothpaste, it would be good if the paste does not flow at the application of the slightest amount of shear stress. We need to apply an adequate force before the toothpaste will start flowing. So, viscoplastic fluids behave like solids when the applied shear stress is less than the yield stress. Once it exceeds the yield stress, the viscoplastic fluid will flow just like an ordinary fluid. Examples of viscoplastic fluids are drilling mud, nuclear fuel slurries, mayonnaise, toothpaste, and blood.

(ii) Time-Dependent Fluids

In these types of fluids an apparent viscosity depends on the time of applied shear along with strain rate. Such types of liquids are regarded as complex non-Newtonian fluid. It is recognized that there are two main classes of time-dependent fluids: (a) thixotropic and (b) rheopectic.

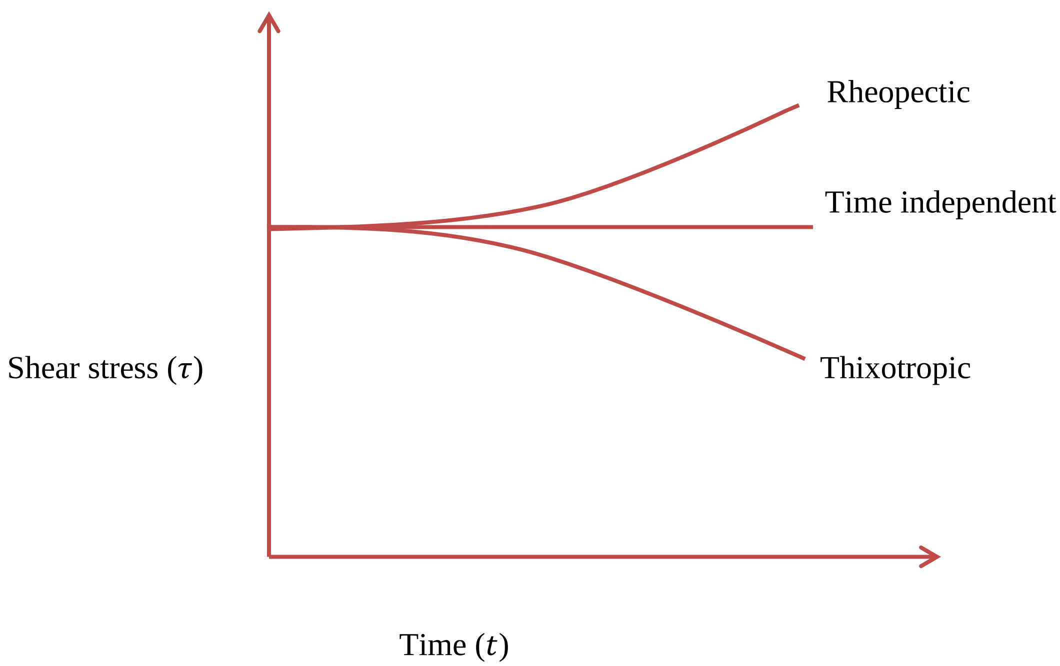

Figure1. 2: Classification of fluids with shear stress as a function of time

Thixotropic fluid: In 1927 the termthixotropy was specified by (Peterfi, 1927) after by (Schalek and Szegvari, 1923) and has been derived from the Greek word 'thixis' which means shaking and 'trepo' means changing. It is most important fluid which exhibits time-dependent shear thinning property. Some more viscous fluids such as gels under static conditions cannot flow but flow when external force applied on or stressed. Such types of fluid acquire the property of flow due to low viscosity. They take a certain time to return to its previous state.

Rheopectic fluid: It is a rare property of a time-dependent of some non-Newtonian fluids in which viscosity increase with time. Examples of some rheopectic fluids are lubricants. The viscosity of these types of fluids increase i.e. thickens or solidifies when shaken for a long time.

The longer the fluid undergoes shearing force, the higher its viscosity. Sometimes the rheopectic behavior of fluid may be considered as time-dependent dilatant behavior (Sato Tatsuo, 1995).
The theories of the time-dependent fluids are less developed. In spite of many proposed models for the time-dependent fluids in the several literatures here two common models have been presented.

(B) Viscoelastic fluids

Viscoelastic fluids are those fluids that illustrate partial elastic recovery upon the removal of a deforming stress. Such materials possess properties of both fluids and elastic solids and obey Hooke's law of elasticity. For viscous fluids constitutive equation (Kairi, 2010) can be written as:

$$`\dot{Y} = \frac{\tau}{\pi} + \frac{\dot{r}}{\varrho} \tag{1.2}$$

Where $\dot{Y}$ and ϱ are the shear rate and rigidity modulus respectively.
An example of a common viscoelastic liquid is egg-white.

1.5. Fluid Flow

Fluid flow occurs due to unbalanced forces or stresses between fluid layers. The motion continues as long as unbalanced forces exist and are applied externally. Fluid flow can be categorized according to direction/dimension and velocity of flow.

- **Laminar and turbulent flow**: A fluid motion is said to be laminar if the tracks of fluid particles form parts of regular curves. If the paths are widely irregular then the motion is called turbulent motion.

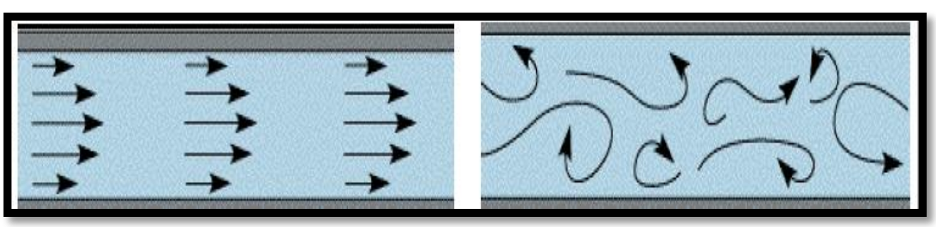

Laminar flow **Turbulent flow**

Figure1. 3: Laminar and Turbulent flow

- **Compressible and incompressible flow**: A fluid flow is said to be compressible when the pressure variation in the flow field is large enough to cause substantial changes in the density of fluid otherwise it is called incompressible.

- **Viscous flow and non-viscous flow**: In a viscous flow the fluid friction has significant effects on the solution where the viscous forces are more significant than inertial forces. Non-viscous flow is the flow of an inviscid fluid, in which the viscosity of the fluid is equal to zero.
- **Uniform and non-uniform flow**: If the flow velocity is the same magnitude and direction at every point in the fluid it is said to be **uniform**. If at a given instant, the velocity is not the same at every point the flow is **non-uniform.** (In practice, by this definition, every fluid that flows near a solid boundary will be non-uniform as the fluid at the boundary must take the speed of the boundary, usually zero. However if the size and shape of the cross-section of the stream of fluid is constant the flow is considered uniform.)
- **Steady and unsteady flow**: A steady flow is one in which the conditions (velocity, pressure and cross section) may differ from point to point but do not change with time. If at any point in the fluid, the conditions change with time, the flow is described as unsteady. (In practice there are always slight variations in velocity and pressure, but if the average values are constant, the flow is considered steady).

Combining the above we can classify any flow in to one of four types:

1. **Steady uniform flow**: Conditions do not change with position in the stream or with time. An example is the flow of water in a pipe of constant diameter at constant velocity.
2. **Steady non-uniform flow**: Conditions change from point to point in the stream but do not change with time. An example is flow in a tapering pipe with constant velocity at the inlet velocity will change as you move along the length of the pipe toward the exit.
3. **Unsteady uniform flow**: At a given instant in time the conditions at every point are the same, but will change with time. An example is a pipe of constant diameter connected to a pump pumping at a constant rate which is then switched off.
4. **Unsteady non-uniform flow**: Every condition of the flow may change from point to point and with time at every point. For example waves in a channel.

1.6. Boundary Layer Concept

Hydrodynamics appeared to be a good theory for flows in the region not close to solid boundaries; however it could not explain concepts like friction and drag. Hydraulics did not provide a solid base to design their experiments since there was too little theory. Ludwig Prandtl provided a theory to connect these fields. He presented the boundary layer theory in 1904 at the third Congress of Mathematicians in Heidelberg, Germany. A boundary layer is the thin region of flow adjacent to a surface, i.e. the layer in which the flow is influenced by the friction between the solid surface and the fluid (Anderson, J.D., 2007). The theory was based on some important observations. The viscosity of the fluid in motion cannot be neglected in all regions. This leads to a significant condition, the no-slip condition. Flow at the surface of the body is at rest relative to that body. At a certain distance from the body, the viscosity of the flow can again be neglected. This very thin layer close to the body in which the effects of viscosity are important is called the boundary layer. This can also be seen as the layer of fluid in which the tangential component of the velocity of the fluid relative to the body increases from zero at the surface to the free stream value at some distance from the surface.

Velocity Boundary Layer:

Transition of zero velocity at the surface to the free stream velocity u_e takes place through a very thin layer δ with the increase in y from the surface, the x velocity component u, must increase until it approaches u_e .The quantity δ is termed as boundary layer thickness (Figure 1.3) and it is formally defined as the value of y for which $u = 0.99\ u_e$. The flow field has two regions.

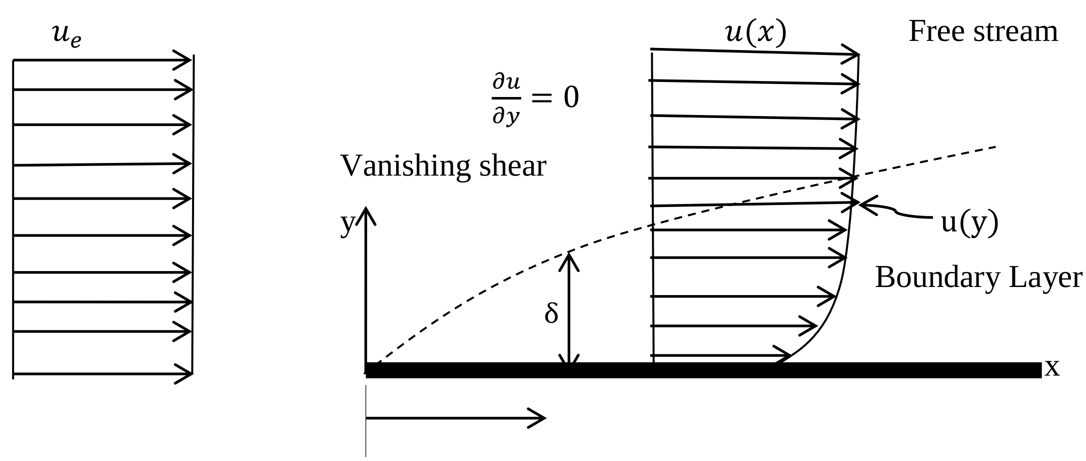

Figure1. 4: Velocity Boundary Layer on a flat Plate

(a) The region where $\frac{\partial u}{\partial y}$ and consequent shear stress is significant.

(b) The region where $\frac{\partial u}{\partial y}$ and shear stress is negligible.

Here $\frac{\partial \boldsymbol{u}}{\partial \boldsymbol{y}}$ determines the local friction coefficient, and $\delta_x = \frac{5.0x}{\sqrt{Re_x}}$

$$C_f = \frac{\tau_w}{\rho u_e^2} \tag{1.3}$$

$$\tau_w = \mu\left(\frac{\partial u}{\partial y}\right)_{y=0} \tag{1.4}$$

Thermal Boundary Layer:

Just as the velocity boundary layer, a thermal boundary layer should develop if the temperatures at the fluid free stream and the solid-surface differ. Fluid particles that come into contact with the plate achieve thermal equilibrium of the plate's surface temperature and the temperature gradient develops in the fluid. The region of the fluid in which these temperature gradients exist, is thermal boundary layer (Figure1.4). We can write

$\delta_T \equiv$ value of y for which $\frac{T_w - T}{T_w - T_\infty} = 0.99$

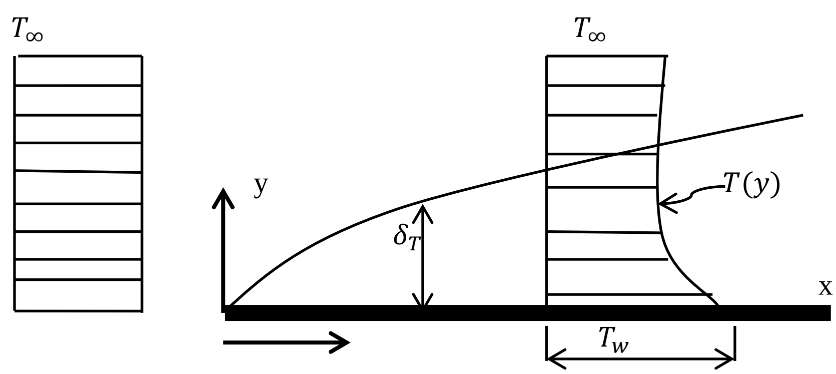

Figure1. 5: Thermal Boundary Layer on a Heated Plate

Concentration Boundary Layer

The water vapor concentration C_w at the body interface is determined by thermodynamic equilibrium condition at the surface. In the free stream the concentration of the working fluid is C_∞. Then the region in which the concentration changes from C_∞ to C_w is called concentration boundary layer. Or concentration boundary layer is defined as that point at which the difference in concentration between the fluid and the surface is 99% of the difference in concentration between the free stream fluid and the surface. The concentration boundary layer has many of the same features as the temperature boundary layer, and in practice the mass transfer coefficient may be determined from heat transfer by analogy. In practice, this means that the same correlations/models may be used to describe both heat and mass transfer.

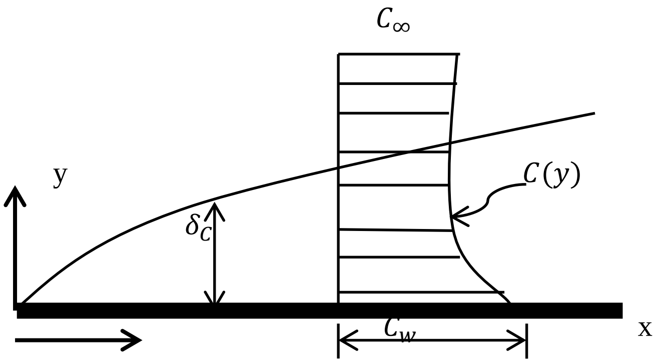

Figure1. 6: Concentration Boundary Layer on a flat Plate

1.7. Heat Transfer

The definition of ‘heat’ is provided by classical thermodynamics. It is defined as an energy that transit due to a difference in temperature. It flows in a direction from higher to lower temperature. This energy can neither be observed nor be measured directly. However, the effects produced by the transfer of this energy are agreeable to observations and measurements. The science of thermodynamics provides the relationship of this energy transfer with the change in the internal energy of a system through which the energy transfer takes place. Therefore, thermodynamic studies how much heat has to be supplied to or rejected from a system between specified equilibrium end states, but fail to predict the rate of energy transfer. This is because of the fact that thermodynamics deals with changes between equilibrium states and does not include time as a variable. The rate of energy transfer, on the other hand, is a time dependent non-equilibrium phenomenon and deals with systems that lack thermal equilibrium.

The science that deals with the mechanism and the rate of energy transfer due to a difference in temperature is known as heat transfer. The driving force for heat transfer is a temperature gradient. If the surface temperature differs from the ambient fluid temperature, this leads to a temperature gradient in the thermal boundary layer. This temperature gradient leads to a body force in the form of buoyancy of the fluid. Aiding flow occurs when the surface temperature is higher than the surrounding temperature. The induced pressure gradient is due to buoyancy force whilst an opposing flow happens when the surface temperature is less than the ambient temperature (Mahmood, 2009).

1.7.1. Modes of Heat Transfer

The process of heat transfer takes place by three distinct modes: conduction, convection and radiation (Cengel & Ghajar, 2014).

(i) Conduction

Heat conduction is a mechanism in which heat or energy passes through high temperature region to low temperature region by direct interaction between molecules of a substance containing temperature differences; that means there exists of a temperature gradient in a fixed medium (Arpaci, 1966 & Ahsan 2011). In this process there is heat transfer through a medium or material without any movement of the medium or material. When heat is applied to one part of a body, the temperature rises in that area. The molecules are made to vibrate more rapidly and though they remain in their places, they bring about increased vibration in their neighbors. The transfer of energy could be primarily by elastic impact as in fluids or by free electron diffusion as predominant in metals or phonon vibration as predominant in insulators.

(ii) Convection

The mode by which heat is transferred between a solid surface and the adjacent fluid in motion when there is a temperature difference between the two is known as convection heat transfer. There are three types of convective heat transfer. Natural convection occurs when the fluid motion is caused by buoyancy forces that result from the density variations due to variations of temperature in the fluid. Forced convection rises when the fluid is forced to flow over the surface by external sources creating an artificially induced convection current (Welty et al. 2008). Many types of mixing also utilize forced convection to distribute one substance within another. Forced convection may produce results more quickly than free convection. Natural and forced convections both occur together in mixed convection.

(iii) Radiation

The radiation mode of heat transport refers to the thermal energy transit in the form of electromagnetic waves (Modest, 2003). In the case of no medium, there exists a net heat transport by radiation between two surfaces at different temperatures. Thermal radiation travels at the speed of light (Bear & Bachmat, 1990).

1.8. Mass Transfer

When a system contains two or more components of varying concentrations then the mass is to be transferred, minimizing the concentration differences within a system. The transport of one constituent from a region of higher concentration to that of a lower concentration is called mass transfer. The driving forces for mass transfer are concentration, temperature or pressure gradient. The pressure difference is the main driving force for fluid flow, whilst for mass transport it is the concentration difference (Hines and Maddox, 1984). The most common mass transfer processes are through diffusion and convection. For mass conduction, it is better to introduce Fick's law of diffusion which states that the rate of diffusion of a chemical species at a point in a mixture is proportional to the concentration gradient of that species at that position (Cengel, 2006). The macroscopic relative movement of a single substance in a region is known as diffusion. In quiescent fluids or solid bodies which are made up of different components, one substance can only be transferred if the average molecular velocities of some components in the mixture are different from each other. This is known as molecular diffusion. Mass convection refers to the mechanism of mass transfer between a surface and a moving fluid that includes both mass conduction and bulk fluid motion (Cengel & Ghajar, 2015). Some examples refer to involve mass transfer as a lump of sugar added to a cup of coffee eventually dissolves and then eventually diffuses to make the concentration uniform; Water evaporates from ponds to increase the humidity of passing-air-stream and; Perfumes present a pleasant fragrance which is imparted throughout the surrounding atmosphere. The mass transfer within a fluid mixture or across a phase boundary is a process that plays a major role in many industrial processes, such as, dispersion of gases from stacks, removal of pollutants from plant discharge streams by absorption, stripping of gases from waste water and Neutron diffusion within nuclear reactors.

1.9. Magnetohydrodynamics

Magnetohydrodynamics is the theory of electrically conducting, neutral fluids in the low-frequency regime. The basic equations of magnetohydrodynamics (MHD) have been proposed by (Hannes Alfvén, 1942) and (Hannes Alfvén, 1953), who realized the importance of the electric currents carried by a plasma and the magnetic field they generate. Alfvén combined the equations of fluid dynamics with Faraday's and Ampere's laws of electrodynamics, thus obtaining a novel mathematical theory, which helped understanding space plasmas in earth and planetary magnetospheres, as well as the physics of the sun, solar wind, and stellar atmospheres.

The interaction of moving conducting fluids with electric and magnetic fields provides for a rich variety of phenomena associated with electro-fluid-mechanical energy conversion. Effects from such interactions can be observed in liquids, gases, two-phase mixtures, or plasmas. Numerous scientific and technical applications exist, such as heating and flow control in metals processing, power generation from two-phase mixtures or seeded high temperature gases, magnetic confinement of high-temperature plasmas even dynamos that create magnetic fields in planetary bodies. Several terms have been applied to the broad field of electromagnetic effects in conducting fluids, such as magneto-fluid mechanics, magneto-gas-dynamics, and the more common one used here magnetohydrodynamics.

Practical magnetohydrodynamics devices have been in use since the early part of the 20th century. For example, a magnetohydrodynamics pump prototype was built as early as 1907 (Northrup 1907). More recently, magnetohydrodynamics devices have been used for stirring, levitating, and otherwise controlling flows of liquid metals for metallurgical processing and other applications (Kolesnichenko, 1990). Gas-phase magnetohydrodynamics is probably best known in magnetohydrodynamics power generation. Since 1959 (Sporn and Kantrowitz, 1959) and (Steg & Sutton,1960) major efforts have been carried out around the world to develop this technology in order to improve electric conversion efficiency, increase reliability by eliminating moving parts, and reduce emissions from coal and gas plants. Closed-cycle liquid metal magnetohydrodynamics systems using both single phase and two-phase flows also have been explored. Still more novel applications are in development or on the horizon. For example, some research has shown the possibility of seawater propulsion using magnetohydrodynamics (Graneau, 1989) and control of turbulent boundary layers to reduce drag (Tsinober, 1990). Extensive worldwide research on magnetic confinement of plasmas has led to attainment of conditions approaching those needed to sustain fusion reactions (Baker et al., 1998).

Magnetohydrodynamics establishes a coupling between the Navier-Stoke's equations of fluid dynamics and Maxwell's-equations of electromagnetism. The simplest form of magnetohydrodynamics, Ideal MHD, assumes that the fluid has so little resistivity that it can be treated as a perfect conductor. This is the limit of infinite magnetic Reynolds number. In ideal magnetohydrodynamics, Lenz's law dictates that the fluid is in a sense tied to the magnetic field lines. The connection between magnetic field lines and fluid in ideal magnetohydrodynamics fixes the topology of the magnetic field in the fluid.

1.10. Physical parameters involved in the study

The physical parameters incorporated in this dissertation are mentioned below.

1.10.1. Viscosity

When two solid bodies in contact, move relative to each other, a friction force develops at the contact surface in the direction opposite to motion. The situation is similar when a fluid moves relative to a solid or when two fluids move relative to each other. The property that represents the internal resistance of a fluid to motion (i.e. fluidity) is called viscosity.

1.10.2. Kinematic viscosity

Kinematic Viscosity is the ratio between dynamic viscosity and densities of the fluid. It is usually denoted by Greek letter ν

1.10.3. Thermal conductivity

It relates the rate of heat flow per unit area $\dot{q}$ to the temperature gradient $\frac{dT}{dx}$ and is governed by Fourier law of heat conduction. Thermal conductivity varies with temperature for liquids as well as gases in the same manner as that of viscosity.

1.10.4. Specific heats

It is the amount of energy required for a unit mass of a fluid for unit rise in temperature. Since the pressure, temperature and density of a gas are interrelated, the amount of heat required to raise the temperature from T_1 to T_2 depend on whether the gas is allowed to expand during the process so that the energy supplied is used in doing the work instead of raising the temperature. For a given gas, two specific heats are defined corresponding to the two extreme conditions of constant volume and constant pressure.

(a) Specific heat at constant volume

(b) Specific heat at constant pressure

1.10.5. Porosity and Permeability

Porosity and permeability are two primary factors that control the movement and storage of fluids. A porous medium is characterized by its porosity, permeability as well as the properties of its constituents. They are intrinsic characteristics of these materials. Porosity is the ratio of the volume of openings or voids to the total volume of material. Porosity represents the storage capacity of the material. Permeability is a measure of the rate of flow of a liquid through porous medium. Just as with porosity, the packing, shape, and sorting of granular materials control their permeability. Although a rock may be highly porous, if the voids are not interconnected, then fluids within the closed, isolated pores cannot move. The degree to which pores within the material are interconnected is known as effective porosity. Rocks such as pumice and shale can have high porosity, yet can be nearly impermeable due to the poorly interconnected voids.

1.10.6. Suction and Injection

Suction is the flow of a fluid into a partial vacuum, or region of low pressure. The pressure gradient between this region and the ambient pressure will force matter toward the low pressure area. Suction is popularly thought of as an attractive effect, which is incorrect since vacuums do not innately attract matter. Suction or blowing is the method of controlling the boundary layer. The effect of suction consists in the removal of decelerated fluid particles from the boundary layer before they are given a chance to cause separation. In more recent times suction was also applied to reduce the drag. Dust being "sucked" into a vacuum cleaner is actually being pushed in by the higher pressure air on the outside of the cleaner. The higher pressure of the surrounding fluid can push matter into a vacuum but a vacuum cannot attract matter. Injection is also an alternative method of preventing separation consists in supplying additional energy to the particles of fluid which are being retarded in the boundary layer.

1.10.7. Chemical reaction

A chemical reaction is a process that leads to the transformation of one set of chemical substances to another. Chemical reactions can be either spontaneous, requiring no input of energy, or non-spontaneous, typically following the input of some type of energy, such as heat, light or electricity. Classically, chemical reactions encompass changes that strictly involve the motion of electrons in the forming and breaking of chemical bonds, although the general concept of a chemical reaction is applicable to transformations of elementary particles as well as nuclear reactions. The substances initially involved in a chemical reaction are called reactants or reagents. Chemical reactions are usually characterized by a chemical change, and they yield one or more products, which usually have properties different from the reactants. Reactions often consist of a sequence of individual sub-steps, the so-called elementary reactions, and the information on the precise course of action is part of the reaction mechanism. Chemical reactions are described with chemical equations, which graphically represent the starting materials, end products, sometimes intermediate products and reaction conditions.

1.10.8. Activation energy

The minimum energy quantity needed to initiate a reaction is termed as activation energy. Such energy makes a vital contribution regarding the evaluation of a reaction (Zhou and Ma. H., 2006). The reaction rate and activation energy are closely associated with each other. Specific examples which comprise chemical reactions and activation energy are geothermal reservoirs, thermal oil recovery, geothermal reservoirs, nuclear reactor cooling and chemical engineering. (Bestman, 1960) initially studied the impact of activation energy on convective mass transportation considering flow analysis in the region of boundary layers. Activation energy and chemical reaction impacts in unsteady convective flow bounded by a heated surface were studied by Makinde et al. (Makinde et al.2011).

1.10.9. Viscous dissipation

Dissipation is the process of converting mechanical energy of downward-flowing water into thermal and acoustical energy. Viscous dissipation is of interest for many applications: significant temperature rises are observed in polymer processing flows such as injection modeling or extrusion at high rates. Aerodynamic heating in the thin boundary layer around high speed aircraft raises the temperature of the skin. In a completely different application, the dissipation function is used to define the viscosity of dilute suspensions (Einstein, 1906). Viscous dissipation for a fluid with suspended particles is equated to the viscous dissipation in a pure Newtonian fluid, both being in the same flow (same macroscopic velocity gradient). (Vajravelu and Hadjinicolaou, 1993) analyzed the heat transfer characteristics over a stretching surface with viscous dissipation in the presence of internal heat generation or absorption. The effect of viscous dissipation is numerically studied on a boundary layer flow of nanofluids over a moving flat plate is studied by (Motsumi and Makinde, 2012). Gebhart (1962) and Gebhart and

Mollendorf (1969) studied the effect of viscous dissipation in natural convection processes. In modeling fluid flow, the dimensionless parameters that describe viscous dissipation are Eckert number (Eldabe et al. 2012).

1.10.10. Slip conditions

Slip condition has significant applications in various industries and is very efficient in manufacturing process. It is a common belief that heat transfer can be increased by adding velocity slip at the boundary. Beavers and Joseph (1967) were the first who used partial slip to the fluid past permeable wall. The addition of velocity slip at wall also plays a vital role for flow in micro devices (Gad-el-hak, 1999). For this reason, researchers have paid considerable attention to include the slip condition at wall rather than no slip condition.

1.10.11. Radiative effects

The radiative effects have important applications in physics and engineering. The radiation heat transfer effects on different flows are very important in space technology and high temperature processes. But very little is known about the effects of radiation on the boundary layer. Thermal radiation effects may play an important role in controlling heat transfer in polymer processing industry where the quality of the final product depends on the heat controlling factors to some extent.

1.10.12. Melting heat transfer

Melting and solidification play a vital role in the advanced technology process. Researchers are interested in exploring melting heat transfer due to a wide range of applications of the melting phenomenon of solid-liquid phase change in the welding process, crystal growth, thermal protection, heat transportation, melting of permafrost, preparation of semiconductors material and the casting of a manufacturing process. Initially, Robert (1958) described the melting phenomenon of ice slab placed in a hot air stream. A boundary layer stagnation point flow of a Maxwell fluid towards a stretching sheet with the melting phenomenon is analyzed by (Hayat et al. 2014). Das (2014) discussed the melting phenomenon in the magneto hydrodynamic flow over a moving surface with thermal radiation. Melting heat transfer in a steady laminar flow over a stationary flat plate was studied by (Epstein and Cho, 1976).

1.11. Dimensionless numbers

A quantity without units, which describes a physical phenomenon but which does not vary in the particular phenomenon, is known as dimensionless number or parameter. Non-dimensional parameters depend on characteristic quantities of the physical system but independent on system of units. Dimensionless Numbers that are used in this study are described below:

1.11.1. Prandtl number

The Prandtl number (Pr) is the ratio of momentum diffusivity and thermal diffusivity. The parameter is named after the Ludwig Prandtl. It is defined as:

$$\mathrm{Pr} = \frac{\text{Momentum diffusivity}}{\text{Thermal diffusivity}} = \frac{\mu_{nf}(C_p)_{nf}}{k_{nf}} \tag{1.5}$$

1.11.2. Reynolds number

The Reynolds number (Re), named in honor of Osborne Reynolds. The ratio of inertial force and viscous force is the Reynolds number, usually denoted as Re.

$$\mathrm{Re} = \frac{\text{Inertial force}}{\text{Viscous force}} = \frac{\rho_{nf}UL}{\mu_{nf}} \tag{1.6}$$

1.11.3. Schmidt number

Schmidt number (Sc) is defined as the ratio of momentum diffusivity and mass diffusivity, and is used to characterize fluid flow in which there are simultaneous momentum and mass diffusion convection processes. It physically relates the relative thickness of the hydrodynamic layer to the mass transfer boundary layer. It is defined as:

$$\mathrm{Sc} = \frac{\text{Momentum diffusivity}}{\text{Mass diffusivity}} = \frac{\mu_{nf}/\rho_{nf}}{D_{nf}} \tag{1.7}$$

1.11.4. Eckert number

The Eckert number (Ec), named for Ernst R. G. Eckert, expresses the relationship between kinetic energy and enthalpy of the flow and is used to characterize dissipation. It is defined as:

$$\mathrm{Ec} = \frac{\text{Kinetic Energy}}{\text{Enthalpy}} = \frac{V^2}{(C_p)_{nf}\Delta T} \tag{1.8}$$

where V is a characteristic velocity of the fluid and ΔT is a characteristic temperature difference of the flow.

1.11.5. Thermal Grashof number

The tendency of a particular system towards natural convection depends on Grashof number (Gr), which is a ratio of buoyancy force and viscous force. It is given as:

$$\mathrm{Gr} = \frac{\text{Temperature buoyancy force}}{\text{Viccous force}} = \frac{g\beta_{nf}\Delta T L^3}{\upsilon_{nf}^2} \tag{1.9}$$

Here ΔT is characteristic temperature difference.

1.11.6. Solutal Grashof number

The Solutal Grashof number is given as:

$$\mathrm{Gc} = \frac{\text{Concentration buoyancy force}}{\text{Viccous force}} = \frac{g\beta_{nf}\Delta C L^3}{\upsilon_{nf}^2} \tag{1.10}$$

Here ΔC is characteristic concentration difference.

1.11.7. Deborah number

The Deborah number is the ratio of fundamentally different characteristic times. Formally, the Deborah number is defined as the ratio of the time it takes for a material to adjust to applied stresses or deformations, and the characteristic time scale of an experiment (or a computer simulation) probing the response of the material:

$$De = \frac{\lambda^*}{\mathrm{T}} \tag{1.11}$$

where λ stands for the relaxation time and T for the "time of observation", typically taken to be the time scale of the process (Poole 2012). The numerator, relaxation time, is the time needed for a reference amount of deformation to occur under a suddenly applied reference load (a more fluid-like material will therefore require less time to flow, giving a lower Deborah number relative to a solid subjected to the same loading rate). The denominator, material time (Franck) is the amount of time required to reach a given reference strain (a faster loading rate will therefore reach the reference strain sooner, giving a higher Deborah number). Equivalently, the relaxation time is the time required for the stress induced, by a suddenly applied reference strain, to reduce by a certain reference amount. The relaxation time is actually based on the rate of relaxation that exists at the moment of the suddenly applied load.

1.11.8. Weissenberg number

The Weissenberg number is a dimensionless number used in the study of viscoelastic flows. It is named after Karl Weissenberg. The dimensionless number compares the elastic forces to the viscous forces. It can be variously defined, but it is usually given by the relation of stress relaxation time of the fluid and a specific process time. For instance, in simple steady shear, the Weissenberg number is defined as the shear rate times the relaxation time. Using the Maxwell Model and the Oldroyd Model, the elastic forces can be written as the first Normal force.

$$\mathrm{We} = \frac{\text{elactic forces}}{\text{viscous forces}} = \frac{\tau_{xx}-\tau_{yy}}{\tau_{xy}} = \frac{\lambda\mu\dot{\gamma}^2}{\mu\dot{\gamma}} = \lambda\dot{\gamma} \tag{1.12}$$

Since this number is obtained from scaling the evolution of the stress, it contains choices for the shear or elongation rate, and the length-scale. Therefore the exact definition of all non-dimensional numbers should be given as well as the number itself.

1.12. Engineering quantity of interest

1.12.1. Skin friction coefficient

Skin friction arises from the friction of the fluid against the "skin" of the object that is moving through it and is directly related to the wetted surface, the area of the surface of the body that is in contact with the fluid. As with other components of parasitic drag, skin friction follows the drag equation and rises with the square of the velocity. The skin friction coefficient (C_f) is given by:

$$\mathrm{C_f} = \frac{2\tau_\mathrm{w}}{\rho_\mathrm{nf}\mathrm{u}_e{}^2} \tag{1.13}$$

1.12.2. Nusselt number

The primary output of a convection experiment is the heat transfer coefficient. The traditional dimensionless form of heat transfer coefficient is the Nusselt number (Nu). In heat transfer at a boundary (surface) within a fluid, the Nusselt number is the ratio of convective to conductive heat transfer across (normal) to the boundary.

$$\mathrm{Nu} = \frac{\text{Convective heat transfer coefficient}}{\text{Conductive heat transfer coefficient}} = \frac{\mathrm{h_w}l}{\mathrm{k_{nf}}} \tag{1.14}$$

where w is width of layer of fluid.

1.12.3. Sherwood number

The Sherwood number (Sh) is used in mass-transfer operation. It represents the ratio of convective to conductive mass transport. Mathematically it is defined as:

$$\mathrm{Sh} = \frac{\text{Convective mass transport}}{\text{Conductive mass transport}} = \frac{\mathrm{h_m L}}{\mathrm{D_{nf}}} \tag{1.15}$$

1.13. Governing equations

Like any mathematical model of the real world, fluid mechanics makes some basic assumptions about the materials being studied. These assumptions are turned into governing equations i.e. Navier–Stokes equations. These equations describe the motion of fluid substances and arise from applying Newton's second law to fluid motion, together with the assumption that the fluid stress is the sum of a diffusing viscous term (proportional to the gradient of velocity), plus a pressure term. The Navier–Stokes equations assume that the fluid being studied is a continuum and every fluid obeys the following assumptions of conservation of mass that forms equation of continuity; conservation of momentum that makes equation of momentum; and conservation of energy that gives equation of energy.

The Navier- Stokes equation, as suggested by **(**Kirby 2010), (Ahmad and Pop 2010), (Devi and Andrews 2011), (Aziz et al. 2012), (Bhattacharyya and Layek 2014) for incompressible nanofluid flow are:

$$\rho_{nf}\frac{D\vec{V}}{Dt} = \vec{F} - \mathrm{grad}p + \mu_{nf}\nabla^2\overrightarrow{V}, \tag{1.16}$$

where $\vec{V} = u\hat{\imath} + v\hat{\jmath} + w\hat{k}$ is the velocity, $\vec{F} = F_x\hat{\imath} + F_y\hat{\jmath} + F_z\hat{k}$ is force, p is pressure and $\nabla^2 = \frac{\partial^2}{\partial x^2} + \frac{\partial^2}{\partial y^2} + \frac{\partial^2}{\partial z^2}$ is Laplace operator.

The equations for the three-dimensional flow of an incompressible, isotropic and homogeneous Newtonian fluid in Cartesian co-ordinate system (x, y, z) according as (Roseanhead 1963) are:

Equation of Continuity:

$$\frac{\partial u}{\partial x} + \frac{\partial v}{\partial y} + \frac{\partial w}{\partial z} = 0 \tag{1.17}$$

Equations of Motion:

$$\rho_{nf}\left(\frac{\partial u}{\partial t} + u\frac{\partial u}{\partial x} + v\frac{\partial u}{\partial y} + w\frac{\partial u}{\partial z}\right) = F_x - \frac{\partial p}{\partial x} + \mu_{nf}\left(\frac{\partial^2 u}{\partial x^2} + \frac{\partial^2 u}{\partial y^2} + \frac{\partial^2 u}{\partial z^2}\right), \tag{1.18}$$

$$\rho_{nf}\left(\frac{\partial v}{\partial t} + u\frac{\partial v}{\partial x} + v\frac{\partial v}{\partial y} + w\frac{\partial v}{\partial z}\right) = F_y - \frac{\partial p}{\partial y} + \mu_{nf}\left(\frac{\partial^2 v}{\partial x^2} + \frac{\partial^2 v}{\partial y^2} + \frac{\partial^2 v}{\partial z^2}\right), \tag{1.19}$$

$$\rho_{nf}\left(\frac{\partial w}{\partial t} + u\frac{\partial w}{\partial x} + v\frac{\partial w}{\partial y} + w\frac{\partial w}{\partial z}\right) = F_z - \frac{\partial P}{\partial z} + \mu_{nf}\left(\frac{\partial^2 w}{\partial x^2} + \frac{\partial^2 w}{\partial y^2} + \frac{\partial^2 w}{\partial z^2}\right), \tag{1.20}$$

Equation of Heat Transfer:

$$\rho_{nf}\left(C_p\right)_{nf}\left(\frac{\partial T}{\partial t} + u\frac{\partial T}{\partial x} + v\frac{\partial T}{\partial y} + w\frac{\partial T}{\partial z}\right) = k_{nf}\left(\frac{\partial^2 T}{\partial x^2} + \frac{\partial^2 T}{\partial y^2} + \frac{\partial^2 T}{\partial z^2}\right) + \mu_{nf}\zeta \tag{1.21}$$

where ζ is dissipation function, which is given by

$$\zeta = 2\left[\left(\frac{\partial u}{\partial x}\right)^2 + \left(\frac{\partial v}{\partial y}\right)^2 + \left(\frac{\partial w}{\partial y}\right)^2\right] + \left[\left(\frac{\partial v}{\partial x} + \frac{\partial u}{\partial y}\right)^2 + \left(\frac{\partial v}{\partial z} + \frac{\partial w}{\partial y}\right)^2 + \left(\frac{\partial w}{\partial x} + \frac{\partial u}{\partial z}\right)^2\right]$$

$$-\frac{2}{3}\left(\frac{\partial u}{\partial x} + \frac{\partial v}{\partial y} + \frac{\partial w}{\partial y}\right)^2 \tag{1.22}$$

Since all terms are quadratic, hence viscous dissipation is always positive. Thus, a viscous flow always tends to lose its energy due to dissipation, in accordance with the second law of thermodynamics.

Equation of Mass Transfer:

$$\left(\frac{\partial C}{\partial t} + u\frac{\partial C}{\partial x} + v\frac{\partial C}{\partial y} + w\frac{\partial C}{\partial z}\right) = D_{nf}\left(\frac{\partial^2 C}{\partial x^2} + \frac{\partial^2 C}{\partial y^2} + \frac{\partial^2 C}{\partial z^2}\right) + D_c \tag{1.23}$$

where D_c is mass diffusion at constant concentration.

The Navier- Stokes equations for the three dimensional flow of an incompressible, isotropic and homogeneous Newtonian fluid are expressed in usual cylindrical co-ordinates system (r, θ, z). The velocity components along r, θ, z directions are denoted by u, v and w respectively.

Equation of Continuity:

$$\frac{\partial u}{\partial r} + \frac{u}{r} + \frac{1}{r}\frac{\partial v}{\partial \theta} + \frac{\partial w}{\partial z} = 0 \tag{1.24}$$

Equations of Motion:

$$\rho_{nf}\left(\frac{\partial u}{\partial t} + u\frac{\partial u}{\partial r} + \frac{v}{r}\frac{\partial u}{\partial \theta} - \frac{v^2}{r} + w\frac{\partial u}{\partial z}\right)$$

$$= F_r - \frac{\partial P}{\partial r} + \mu_{nf}\left(\frac{\partial^2 u}{\partial r^2} + \frac{1}{r}\frac{\partial u}{\partial r} - \frac{u}{r^2} + \frac{1}{r^2}\frac{\partial^2 u}{\partial \theta^2} - \frac{2}{r^2}\frac{\partial v}{\partial \theta} + \frac{\partial^2 u}{\partial z^2}\right) \tag{1.25}$$

$$\rho_{nf}\left(\frac{\partial v}{\partial t} + u\frac{\partial v}{\partial r} + \frac{v}{r}\frac{\partial v}{\partial \theta} - \frac{uv}{r} + w\frac{\partial v}{\partial z}\right)$$

$$= F_\theta - \frac{1}{r}\frac{\partial P}{\partial \theta} + \mu_{nf}\left(\frac{\partial^2 v}{\partial r^2} + \frac{1}{r}\frac{\partial v}{\partial r} - \frac{v}{r^2} + \frac{1}{r^2}\frac{\partial^2 v}{\partial \theta^2} + \frac{2}{r^2}\frac{\partial u}{\partial \theta} + \frac{\partial^2 v}{\partial z^2}\right) \tag{1.26}$$

$$\rho_{nf}\left(\frac{\partial w}{\partial t} + u\frac{\partial w}{\partial r} + \frac{v}{r}\frac{\partial w}{\partial \theta} + w\frac{\partial u}{\partial z}\right) = F_z - \frac{\partial P}{\partial z} + \mu_{nf}\left(\frac{\partial^2 w}{\partial r^2} + \frac{1}{r}\frac{\partial w}{\partial r} + \frac{1}{r^2}\frac{\partial^2 w}{\partial \theta^2} + \frac{\partial^2 u}{\partial z^2}\right) \tag{1.27}$$

Equation of Energy:

$$\rho_{nf}\left(C_p\right)_{nf}\left(\frac{\partial T}{\partial t}+u\frac{\partial T}{\partial r}+\frac{v}{r}\frac{\partial T}{\partial \theta}-\frac{v^2}{r}+w\frac{\partial T}{\partial z}\right)=$$
$$k_{nf}\left(\frac{\partial^2 T}{\partial r^2}+\frac{1}{r}\frac{\partial T}{\partial r}-\frac{u}{r^2}+\frac{1}{r^2}\frac{\partial^2 T}{\partial \theta^2}-\frac{2}{r^2}\frac{\partial v}{\partial \theta}+\frac{\partial^2 T}{\partial z^2}\right)+\mu_{nf}\zeta \tag{1.28}$$

Equation of Mass Transfer:

$$\left(\frac{\partial C}{\partial t}+u\frac{\partial C}{\partial r}+\frac{v}{r}\frac{\partial C}{\partial \theta}-\frac{v^2}{r}+w\frac{\partial C}{\partial z}= k_{nf}\left(\frac{\partial^2 C}{\partial r^2}+\frac{1}{r}\frac{\partial C}{\partial r}-\frac{C}{r^2}+\frac{1}{r^2}\frac{\partial^2 C}{\partial \theta^2}-\frac{2}{r^2}\frac{\partial v}{\partial \theta}+\frac{\partial^2 C}{\partial z^2}\right)+D_c\right) \tag{1.29}$$

1.13.1. Constitutive equation of Newtonian fluids

Fluids in which shear stress is proportional to strain rate (or velocity gradient) are commonly categorized as Newtonian fluids. Mathematically for unidirectional flow it can be written as

$$S \propto \frac{\partial u}{\partial y} \tag{1.30}$$

$$S = \mu\frac{\partial u}{\partial y} \tag{1.31}$$

where μ is the constant of proportionality know as dynamic viscosity. For Newtonian fluid, stress tensor is given by

$$S = -pI + \tau, \tag{1.32}$$

in which p represents the pressure, I is the unite tensor and the extra stress tensor τ has the following form

$$\tau = \mu A_1, \tag{1.33}$$

where A_1 represents the first Rivlin-Ericksen tensor and is defined as

$$A_1 = \nabla V + (\nabla V)^T \tag{1.34}$$

1.13.2. Constitutive equation of Non-Newtonian fluid

The rheological properties of non-Newtonian fluids cannot be illuminated by the classical Naiver-Stokes equations. Also, non- Newtonian fluids characteristics cannot be modeled by single model. To overcome this difficulty ample models have been come into being. The rheological models that were projected were Williamson, Maxwell, Cross, Ellis, power law, Carreau fluid model, Casson fluid model, Walters-B fluid model, etc.

In this study, Williamson, Maxwell and Buongiorno nanofluid model has been investigated.

1.13.2.1. Maxwell fluid model

The Cauchy stress tensor for a Maxwell fluid is;

$$S = -pI + \tau \tag{1.35}$$

where the extra stress tensor τ satisfies the following implicit relation;

$$\tau + \xi \frac{D\tau}{Dt} = \mu A_1 \tag{1.36}$$

where, ξ represent the time relaxation of the material, which is duration of the time over which significant stress persists after termination of deformation. The derivative D/Dt for the vector and tensor can be defined in the following forms:

For a contra variant vector:

$$\frac{D\tau}{Dt} = \frac{\partial \tau}{\partial t} - (\mathrm{V}.\nabla)\tau \tag{1.37}$$

For a contra variant tensor of rank 2:

$$\frac{D\tau}{Dt} = \frac{\partial \tau}{\partial t} + (\mathrm{V}.\nabla)\tau - \tau(\nabla\mathrm{V}) - \tau(\nabla\mathrm{V})^{\mathrm{T}} \tag{1.38}$$

1.13.2.2. Williamson fluid model

A typical example of a non-Newtonian fluid model with shear retreating property is Williamson fluid model and was first expected by (Williamson, 1929). The Williamson fluid model essential equations are specified as follows:

$$S = -pI + \tau \tag{1.39}$$

$$\tau = \left[\mu_\infty + \frac{\mu_0 - \mu_\infty}{1 - \Gamma\dot{\gamma}}\right] A_1 \tag{1.40}$$

where p is pressure, I is identity vector, S is the Cauchy stress tensor, τ is extra stress tensor, μ_0 and μ_∞ are the limiting viscosities at zero and at infinite shear rate. $\Gamma > 0$ is the time constant, A_1 is the first Rivlin-Ericson tensor and $\dot{\gamma}$ is defined as follows

$$\dot{\gamma} = \sqrt{\frac{\pi}{2}}, \pi = trace(A_1^2) \tag{1.41}$$

where π is the second invariant strain tensor. Here if we have considered the case for which $\mu_\infty = 0$ and $\Gamma\dot{\gamma} < 1$. Then we obtain

$\tau = \left[\frac{\mu_0}{1-\Gamma\dot{\gamma}}\right] A_1$ or by using binomial expansion, we get: $\tau = \mu_0(1 + \Gamma\dot{\gamma})A_1$ or (1. 42)

When we consider $\mu_\infty \neq 0$ then we have

$$\tau = \mu_0 \left[\zeta + \frac{1-\zeta}{1-\Gamma\dot{\gamma}}\right] A_1 . \tag{1.43}$$

Here $\zeta = \frac{\mu_\infty}{\mu_0}$ is the ratio of viscosities.

The components of stress tensor for $\mu_\infty = 0$ are

$$\tau_{xx} = 2\mu_0(1 + \Gamma\dot{\gamma})\frac{\partial u}{\partial x}, \tag{1.44}$$

$$\tau_{xy} = \tau_{yx} = \mu_0(1 + \Gamma\dot{\gamma})\left(\frac{\partial u}{\partial y} + \frac{\partial v}{\partial x}\right), \tag{1.45}$$

$$\tau_{yy} = 2\mu_0(1 + \Gamma\dot{\gamma})\frac{\partial v}{\partial y}. \tag{1.46}$$

1.13.2.3. Buongiorno nanofluid model

(Buongiorno, 2006) devices model takes into consideration the effects of Brownian motion and thermophoresis in fluid flow. The energy and transport equations of nanoparticles which represent the Buongiorno nanofluid model are as follows:

$$\frac{DT}{Dt} = \alpha\nabla^2 T + \omega\left(D_B \nabla C.\nabla T + D_\tau \frac{\nabla T.\nabla T}{T_\infty}\right) \tag{1.47}$$

$$\frac{DC}{Dt} = D_B \nabla^2 C + \frac{D_\tau}{T_\infty}\nabla^2 T \tag{1.48}$$

Here $\omega = (\rho c)_p/(\rho c)_f$ is the ratio of effective heat capacity of nanoparticle material and the base fluid, D_B and D_τ are the Brownian and thermophoretic diffusion coefficients and T_∞ is the ambient temperature of the fluid.

1.13.2.3.1. Brownian diffusion

Brownian diffusion is the characteristic random wiggling motion of small airborne particles in still air, resulting from constant bombardment by surrounding gas molecules. Such irregular motions of pollen grains in water were first observed by the botanist Robert Brown, (1827), and later similar phenomena were found for small smoke particles in air. The relationships characterizing Brownian diffusion based on kinetic theory of gases were first derived by Einstein, (1905).

1.13.2.3.2. Thermophoresis

Thermophoresis is defined as the migration of a colloidal particle or large molecule in a solution in response to a macroscopic temperature gradient. The inverse effect, i.e., the formation of a temperature gradient as the result of the mixing of different molecular species, is referred to as the Dufour effect. The Soret coefficient is defined as the ratio of the thermal diffusion coefficient and the normal diffusion coefficient; it is a measure for the degree of separation of the species. These concepts are the same as for a molecular mixture.

1.14. Statement of the problem

Nanofluid is important to study because of their heat and mass transfer properties. They enhance the thermal conductivity and convective properties over the properties of the base fluid. Moreover, the presence of the nanoparticles enhance the electrical conductivity of the nanofluid, hence are more susceptible to the influence of magnetic field than the conventional base fluids. Nanofluid also enhanced physical properties such as thermal diffusivity, viscosity, mass diffusivity, thermal conductivity and convective heat transfer coefficients compared to those of base fluids. Due to these novel properties, nanofluid became potentially useful in many advanced industrial and engineering applications. Some researchers have successfully shown that presence of nanoparticles in water cooled nuclear system can improve the safety margins and produce substantial economic gains (Buongiorno et al., 2008). Although extensive research works have been devoted to heat transfer in viscous (Newtonian) fluids, recently, research in non-Newtonian fluids has gained considerable attention among researchers as well. Nevertheless, theoretical study on these fluids is more challenging and interesting due to the complexity of their constitutive equations. The heat and mass transfer of non-Newtonian nanofluid flow models are appeared to be such complicated systems, on account of their strong nonlinearity. Due to this feature, is being challenged in handling such systems analytically. As a result of this the researchers of the last two decades of this century are engaged in finding the numerical solution of the problems governing the boundary layer flow of the non-Newtonian fluids.

Based on the abovementioned matters, this research has been conducted to study the boundary layer analysis of non-Newtonian nanofluids such as Maxwell and Williamson nanofluid past stretching/shrinking surfaces. In this regards, in order to solve this problem, two essential numerical techniques have been employed namely, (i) Implicit finite difference methods and (ii) Runge-Kutta fifth -order method with shooting technique.

In this study the researcher attempted to answer the following questions.

i. What is the effect of slip condition on MHD stagnation flow on Maxwell non-Newtonian nanofluid?
ii. How melting and viscous dissipation did affect the MHD flow of Maxwell and Williamson nanofluid past stretching sheet?
iii. What is the effect of thermal radiation and chemical reaction Williamson non-Newtonian nanofluid past stretching/shrinking wedge?

iv. What is the effect of activation energy and viscous dissipation on mixed convective heat transfer of MHD flow of Williamson nanofluid above a stretching cylinder in the presence of variable thermal conductivity?

1.15. Research Objectives

1.15.1. General objectives

The general objective of the study is to understand mathematical model and numerical algorism to solve heat and mass transfer equations and also to know the rheological behavior of heat and mass transfer of MHD boundary layer flow of non-Newtonian nanofluids through different shaped bodies due to their wide applications.

1.15.2. Specific objectives

The specific objectives are:

1. To discuss the effect of slip condition on MHD stagnation flow on Maxwell non-Newtonian nanofluid.
2. To describe how melting and viscous dissipation did affect fluid flow, heat transfer and Mass transfer.
3. To study the characteristic of thermal radiation and chemical reaction on non-Newtonian nanofluid above stretching/shrinking sheet.
4. To deliberate the impact of activation energy on the MHD flow of Williamson nanofluid.
5. To scrutinize the influence of viscous dissipation on mixed convective heat transfer of MHD flow of Williamson nanofluid above a stretching cylinder in the presence of variable thermal conductivity.

1.16. Scope of the study

This dissertation focused on the boundary layer analysis of heat and mass transfer of MHD flow of Maxwell non-Newtonian fluid, Williamson non-Newtonian fluid model and Buongiorno nanofluid model over stretching sheet, stretching/shrinking wedge and stretching cylinder. It presents the numerical solutions using Runge-Kutta method with shooting technique and implicit finite difference method (Keller box method).

1.17. Significance of the study

The boundary layer flow of non-Newtonian fluids over a stretching surfaces with mass and heat transfer is of great interest to researchers, scientists, and engineers due to their extensive applications such as thinning of copper wire, extrusion of polymer sheets, annealing, emulsion-coated sheets, and pipe industry. An example of such fluids include soap solutions, cosmetics, toothpaste, magma, lava, gums, honey, blood, saliva, semen, mucus, synovial fluid, cement slurry, paper pulp and many others. Non-Newtonian fluid characteristics cannot be modeled by a single model. Due to these wide areas of application the researchers at present are engaged in exploring the flows of non-Newtonian at various aspects. So the results or output of this research shall enhance the understanding on the fluids flow phenomenon and the effect of nanoparticles with chemical reaction, melting heat transfer, activation energy, variable thermal radiation and slip effects in upper-convected Maxwell and Williamson fluids. Moreover, the present study will have some theoretical contributions for the researchers. In addition that, the generation of efficient algorithm of the non-Newtonian problem shall help in solving the problem of computational fluid dynamics in the future.

1.18. Research Methodology

In many fluid flow problems governing equations are in the form of non-linear partial differential equations. A non-linear differential equation is simply a differential equation where some non-linearity is applied to either the inputs or the outputs of the equation. Due to non-linearity terms in the equations, analytical methods can yield very few solutions. In general, analytical solutions are possible only if these equations can be made linear, either non-linear term naturally drops out or non-linear terms are small in comparison to other terms, so that these terms can be neglected. Therefore, before attempting an analytical solution, it is important to identify whether the equations to be solved are linear or not. If the equations are non-linear then it is generally impossible to solve directly with the help of existing analytical methods so some additional approximations are required. Therefore, the encounter non-linear ordinary differential equations that are incorporated in these papers are solved by implicit finite difference method (Keller box method) and fifth-order Runge-Kutta methods. In non-linear ordinary differential equations missing boundary conditions can be obtained by using shooting technique.

1.18.1. Keller box method

This implicit finite difference scheme that is known as Keller-box in combination with the Newton's linearization techniques as described by (Cebeci and Bradshaw, 1984) is very famous due to its very desirable features that make it appropriate for the solution of all parabolic partial differential equations. The main features of this method are:

i) Unconditionally stable and has a second order accuracy with arbitrary spacing and attractive extrapolation features.

ii) The most reliable and powerful numerical methods for nonlinear boundary layer flows that are generally parabolic in nature.

iii) Tolerates very speedy x variations.

The solution of an equation by this method can be obtained by the following four steps:

1. Reduce the equation or equations to a first-order system.
2. Write difference equations using central differences.
3. Linearize the resulting algebraic equations (if they are nonlinear), and write them in matrix-vector form.
4. Solve the linear system by the block-tridiagonal-elimination method.

We consider the net rectangle in the $x-\eta$ plane shown in figure 1.7 and the net points defined as below

$$x^0 = 0 \qquad x^i = x^{i-1} + k_i \qquad i = 1,2,3,\dots,I$$

$$\eta_0 = 0 \qquad \eta_j = \eta_{j-1} + h_j \qquad j = 1,2,3,\dots,J \qquad \eta_j = \eta_\infty$$

where k_i is the Δx-spacing and h_j is the $\Delta\eta$-spacing. Here i and j are the sequence of numbers that indicate the coordinate location, not tensor indices or exponents.

Since only first derivatives appear in the governing equations, centered differences and two-point averages can be constructed involving only the four corner nodal values of the 'box'. For example, if g represents any of the dependent variables then

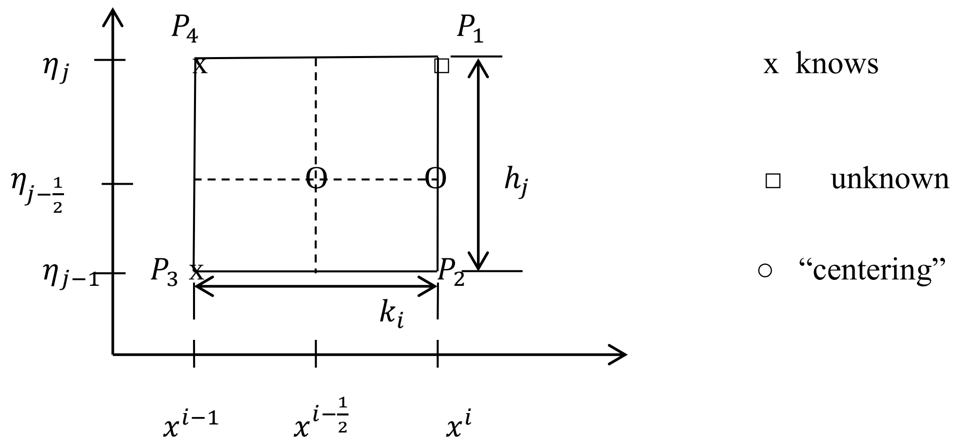

Figure1. 7: Net rectangle for difference approximations

$$
\begin{aligned}
&[g]^i_{j-\frac{1}{2}} = 0.5\left(g^i_{j-1} + g^i_j\right)\\
&[g]^{i-\frac{1}{2}}_{j-\frac{1}{2}} = 0.5\left([g]^{i-1}_{j-\frac{1}{2}} + [g]^i_{j-\frac{1}{2}}\right)\\
&\left[\frac{\partial g}{\partial \eta}\right]^{i-\frac{1}{2}}_{j-\frac{1}{2}} = 0.5\left(\left[\frac{\partial g}{\partial \eta}\right]^{i-1}_{j-\frac{1}{2}} + \left[\frac{\partial g}{\partial \eta}\right]^{i}_{j-\frac{1}{2}}\right)\\
&\left[\frac{\partial g}{\partial \eta}\right]^{i}_{j-\frac{1}{2}} = 0.5\frac{\left([g]^i_{j-\frac{1}{2}} - [g]^i_{1-\frac{1}{2}}\right)}{(\eta_j - \eta_{j-1})}\\
&\left[\frac{\partial g}{\partial x}\right]^{i-\frac{1}{2}}_{j-\frac{1}{2}} = 0.5\frac{\left([g]^i_{j-\frac{1}{2}} - [g]^{i-1}_{1-\frac{1}{2}}\right)}{(x_i - x_{i-1})}
\end{aligned}
\tag{1.49}
$$

1.18.2. Runge-Kutta Method of Fifth Order

Determination of a suitable step size h can be a major challenge in numerical integration. If h is too large, the truncation error may be unacceptable; if h is too small, we are squandering computational resources. Moreover, a constant step size may not be appropriate for the entire range of integration. For example, if the solution curve starts off with rapid changes before becoming smooth (as in a stiff problem), we should use a small h at the beginning and increase it as we reach the smooth region. This is where adaptive methods come in. They estimate the truncation error at each integration step and automatically adjust the step size to keep the error within prescribed limits. The adaptive Runge–Kutta methods use so called embedded integration formulae. These formulae come in pairs: one formula has the integration order m, the other one is of order $(m + 1)$. The idea is to use both formulas to advance the solution from x to $(x + h)$.

Representing the results by $y_m(x + h)$ and $y_{m+1}(x + h)$, we may estimate the truncation error in the formula of order m as

$E(h) = y_{m+1}(x + h) - y_m(x + h)$

Here are the Runge–Kutta embedded formulae of orders 5 and 4 that were originally derived by Fehlberg; hence they are known as Runge–Kutta Fehlberg formulae:

$k_1 = f(x_n, y_n)$

$k_i = f\left(x_n + A_i h,\ y_n + h\sum_{j=1}^{i-1} B_{ij} k_i\right)$, $i = 2, 3, 4, 5, i - 1$

$y_{n+1} = y_n + \sum_{i=0}^{5} C_i k_i$ (5^{th} order formula) (1.50)

$y_{n+1} = y_n + \sum_{i=0}^{4} D_i k_i$ (4^{th} order formula)

1.18.3. Shooting Method

The shooting method reduces the solution of a boundary value problem to the iterative solution of an initial value problem. The usual approaches involve a trial and error procedure. That boundary point having the most known conditions is selected as the initial point. Any other missing initial conditions are assumed and the initial value problem is solved using Runge-Kutta methods. Unless the computed solution agrees with the known boundary conditions, the initial conditions are adjusted and the problem is solved again. The process is repeated until the assumed initial conditions yield, within specified tolerance, a solution that agrees with the known boundary conditions. This method consists of transforming the boundary value problem into an initial value problem. The method requires good initial guesses for the missing initial conditions. The correctness of the guesses is decided based upon how closely the solution satisfies the final boundary conditions. The initial value problem is solved by using Runge-Kutta method and the initial conditions are adjusted. The process is repeated within specified tolerance until the assumed initial conditions yield to a solution with the known boundary conditions.

References

Ahsan A. (2011). Convection and conduction heat transfer, *Intech*.

Arpaci V. S. (1966). Conduction Heat Transfer, *Addison-wesley Company*.

Ahmad, S. and Pop, I. 2010. Mixed convection boundary layer flow from a vertical flat plate embedded in a porous medium filled with nanofluids. *Int. Comm. in Heat and Mass Transfer*. 37: 987-991.

Alfvén H. (1942). Existence of electromagnetic-hydrodynamic waves. *Nature*, 150:405-406.

Alfvén H. (1953). Cosmical Electrodynamics: Fundamental Principles. *The International series of monographs on physics*. Oxford University Press.

Aziz, A., Khan, W.A. and Pop, I. 2012. Free convection boundary layer flow past a horizontal flat plate embedded in porous medium filled by nanofluid containing gyrotactic microorganisms. *Int. J. of Thermal Sc.* 56: 48-57.

Baker C. C. Conn R. W. Najmabadi F. & Tillack M. S. (1998). Status and Prospects for Fusion Energy from Magnetically Confined Plasmas. *Energy* 23 (7/8) pp. 649-694.

Bear J. & Bachmat Y.(1990). Introduction to Modeling of Transport Phenomena in Porous Media. *Kluwer Academic Publisher*, Dordrecht.

Bestman A. R. (1990). Natural convection boundary layer with suction and mass transfer in a porous medium. *Int. J. Energy Res*. (14) 389–396.

Bhattacharyya, K. and Layek, G. C. (2014). Magnetohydrodynamic boundary layer flow of nanofluid over an exponentially stretching permeable sheet. Phy. Research Int. 2014(592536): 1-12.

Buongiorno, J., Hu, L.-W., Kim, S. J., Hannink, R., Truong, B. and Forrest, E. (2008). Nanofluids for enhanced economics and safety of nuclear reactors: an evaluation of the potential features, issues, and research gaps. *Nuclear Technology*. 162(1): pp. 80–91.

Cebeci, T., & Bradshaw, P. (1984). Physical and computational aspects of convective heat transfer. *Springer, New York*.

Cengel Y. A. (2006). Heat and mass transfer: A practical approach. McGraw-Hill, New York.

Cengel Y. & Ghajar A. (2014). Heat and Mass Transfer: Fundamentals and Applications. McGraw-Hill.

Cengel Y. & Ghajar A. (2015). Heat and Mass Transfer: Fundamentals and Applications. McGraw-Hill Education.

Chhabra, R.P. & Richardson, J.F. (2008). Non-Newtonian flow and applied rheology. 2*nd* edn.

Butterworth-Heinemann, Oxford.

Choi SUS & Eastman JA. (1995). Enhancing thermal conductivity of fluids with nanoparticles, presented at ASME. *International Mechanical Engineering Congress and Exposition*, 1217.

Das K. (2014). Radiation and melting effects on MHD boundary layer flow over a moving surface. *Ain Shams Eng. J.,* vol.5, pp.1207-1214.

Devi, S.P. Anjali and Andrews, J. (2011). Laminar boundary layer flow of nanofluid over a flat plate. Int. J. of Appl. Math. And Mech. 7(6): 52 – 71.

Einstein, (1906) *Ann. phys*., 19, (286).

Eldabe, N.T.M, Sallam, S.N., & Abou-zied, M.Y. (2012). Numerical study of viscous dissipation effects on the free convection heat and mass transfer of MHD non-Newtonian fluid flow through a porous medium. Journal of the Egyptian Mathematical Society, 20(2), 139-151. https://doi.org/10.1016/j.joems.2012.08.013.

Epstein E.M. and Cho D.H. (1976). Melting heat transfer in steady laminar flow over a flat plate. J. *Heat Transfer*, 98, pp.531-533.

Franck, A. Viscoelasticity and dynamic mechanical testing. *TA Instruments*. *TA Instruments Germany.*

Gebhart B. (1962). Effect of viscous dissipation in natural convection, *J. Fluid Mech.* (14) 225–232.

Gebhart B. & Mollendorf J. (1969). Viscous dissipation in external natural convection flows, *J. Fluid Mech.*, (38) 97–107.

Gordon S. Beavers & Daniel D. Joseph (1967). Boundary conditions at a naturally permeable wall. *J. Fluid Mech.* (1967), 30(1), pp. 197-207.

Graneau P. (1989). Electro dynamic Seawater Jet: An Alternative to the Propeller. *IEEE* Transactions of Magnetics 25(5) pp. 3275-3277.

Hayat T., Farooq M. and Alsaedi A. (2014). Melting heat transfer in the stagnation point flow of Maxwell fluid with double diffusive convection. Int. J. Numer. Methods Heat Fluid Flow, 24, pp.760-774.

Hines A. L. & Maddox R. N. (1984).Mass Transfer-Fundamentals and Applications. Prentice Hall.

Howard A. Barnes (1997). Thixotropy a review. *J. Non-Newtonian Fluid Mech.*, 70(1997), 1-33 https://doi.org/10.1016/S0377-0257(97)00004-9.

Kairi, R.R. (2010). Convective transport in a power-law fluid Saturated non-Darcy porous medium.

Kirby, B. J. 2010. Micro and Nanoscale Fluid Mechanics. New York. Cambridge University Press.

Kolesnichenko A. F. (1990). Electromagnetic Processes in Liquid Material in the USSR and Eastern European Countries. *Iron and Steel Institute of Japan (ISIJ),* 30 (1) pp. 8–26.

Makinde O. D., Olanrewaju P. O. & Charles W. M. (2011). Unsteady convection with chemical reaction and radiative heat transfer past a flat porous plate moving through a binary mixture, *Afr. Math*. (22) 65–78.

Mahmood M. (2009). Heat and mass transfer analysis of unsteady flow over a horizontal surface inside a squeezing channel. COMSATS *Institute of Information Technology*.

Modest M. (2003). Radiative Heat Transfer. *Academic Press*.

Mohamed Gad-el-Hak (1999). The Fluid Mechanics of Micro devices—The Freeman Scholar Lecture

Motsumi T. G. & Makinde O. D. (2012). Effects of thermal radiation and viscous dissipation on boundary layer flow of nanofluids over a permeable moving flat plate. *Phys. Scr.* 86 045003 (8pp).

Northrup E. F. (1907). Some Newly Observed Manifestations of Forces in the Interior of an Electrical Conductor. *Phys. Rev*., 24 (6), pp.474.

Peterfi, T., Arch. Entwicklungsmech. Organ. 112 (1927) 680, Verhanitlungen 3rd. *Intern. Zellforschung-Kongr.,* Arch. Exp. Zellf, 15(1934): 373.

Poole R. J. (2012). The Deborah and Weissenberg numbers. *The British Society of Rheology, Rheology Bulletin*. 53(2) pp 32-39.

Purna Chandra Barman, Rishi Raj Kairi, Ashoke Das & Md. Rabiul Islam (2016). An Overview of Non-Newtonian Fluid. International Journal of Applied Science and Engineering, 4(2) 97-101. DOI: 10.5958/2322-0465.2016.00011.3

Reid, R.C., Prausnitz, J.M. and Sherwood, T.K. (1977). The properties of gases and liquids. 3rd edn. McGraw-Hill, New York.

Roberts L. (1958). On the melting of a semi-infinite body of ice placed in a hot stream of air. *J. Fluid Mech.*, 4, pp.505-528.

Roseanhead L. (Ed.) (1963). Laminar Boundary Layers, Oxford University Press, Oxford, pp. 427.

Sakiadis B. C. (1961). Boundary-Layer Behavior on Continuous Solid Surfaces *A.1.Ch.E. Journal*

Sato, Tatsuo (1995). Rheology of suspensions. *The Journal of Coatings Technology*: 69.

Schalek, E. and Szegvari, A. and Kolloid Z. (1923) 32 318; 33 (1923) 326.

Shenoyand, A.V. and Mashelkar, R. A. (1982). Thermal convection in non-Newtonian fluids, *Advances in Heat Transfer*, 15: 143-225.

Sporn P. & Kantrowitz A. (1959). Magnetohydrodynamics: Future Power Process. *Power* 103 (11), pp. 62–65.

Tsinober A. (1990). MHD Flow Drag Reduction in Viscous Drag Reduction in Boundary Layers. *American Institute of Astronoutics and Aeronautics*.

Steg L. & Sutton G. W. (1960).Prospects of MHD Power Generation. *Astronautics 5*, pp. 22–25.

Vajravelu K. & Hadjinicolaou A. (1993). Heat transfer in a viscous fluid over a stretching sheet with viscous dissipation and internal heat generation. *Int. Comm. in Heat and Mass Transfer*, 20(3) 417–430.

Welty J. R., Wicks C. E., Wilson R. E., & Rorrer G. L.(2008). Fundamentals of Momentum, Heat and Mass Transfer. *John Wiley and Sons Corporation*.

Williamson R. V. (1929). The flow of pseudo plastic materials. *Industrial and Engineering Chemistry Research*, 21(11): 1108.

Wong, K. V. & De Leon, O. (2010). Applications of nanofluids: current and future. *Advances in Mechanical Engineering*. 2: 1–11.

Zhou C. S. & Ma. H. (2006). Ultrasonic degradation of polysaccharide from red algae (Porphyra yezoensis), *J. Agric. Food Chem*. (54) 2223–2228.

Chapter 2

Literature Review

Recent advancement in nanotechnology has led to the development of a new innovative class of heat transfer in fluids known as nanofluid. Nanofluid can be described as solid-liquid composite materials consisting of solid nanoparticles with size typically of 1-100 nm, which is suspended in conventional fluids such as oil, water and ethylene glycol mixture. This concept introduces advanced heat transfer with substantially higher conductivity to enhance thermal characteristics. Pioneer studies carried out by Choi (1995) and Choi et al. (2001) successfully showed that the addition of a small amount of nanoparticles to convectional heat transfer liquids can increase thermal conductivity of the fluid up to approximately two times. Based on the experimental studies, it can be concluded that, the reason for the increase in thermal conductivity of the fluid is not only attributed to the higher thermal conductivity of the added nanoparticles, but also other mechanisms contributing to the increase in performance. After this discovery, nanofluid has been considered by many researchers to be one of the significant forces that could drive the next major industrial revolution in this century especially in biological sciences, physical sciences, electronic cooling and transportation. Broad range of current and future applications involving nanofluid has been reviewed by Wong and De Leon (2010). Recently, suspensions of metal nanoparticles are also being developed for other purposes, such as medical applications including cancer therapy (Huang and El-Sayed (2010); Ellis et al. (2017); Kang et al. (2017); Mekheimer et al. (2018)).

Numerous models and methods have been proposed by different authors to study convective flows of nanofluid, including the most popular models proposed by Buongiorno (2006) and Tiwari and Das (2007). Buongiorno considered seven slip mechanisms: inertia, Brownian diffusion, thermophoresis, diffusiophoresis, Magnus effect, fluid drainage and gravity that can produce a relative velocity between the nanoparticles and the base fluid. Conclusively, among all the mechanisms, only Brownian diffusion and thermophoresis are found to be important factors in the convective transport process in nanofluid. Based on that, Buongiorno proposed a mathematical model by treating nanofluid as a two-component mixture which are Brownian diffusion and thermophoresis, and introduced these terms in the conservation equations for mass and energy. On the other hand, Tiwari and Das (2007) had proposed a theoretical model to analyze the behaviour of nanofluid by taking into account the solid volume fraction. It is worth mentioning that both proposed nanofluid models were recently used by Habibi Matin et al. (2012), Mahdy (2012), Subhashini and Sumathi (2014), Imtiaz et al. (2014), Uddin et al. (2015), Hayat et al. (2016b), Othman et al. (2017), and Besthapu et al. (2017) in their papers. Several other researchers further proposed the studies of nanofluid in different types of fluid, for example, Sandeep et al. (2015), Abbasi et al. (2016), Madhu and Kishnan (2016), Nabwey et al. (2017) and Naseem et al. (2017). All previous works used Newtonian fluid as the base fluid. Ellahi et al. (2012) pointed out that, non-Newtonian nanofluids have potential roles in physiological transport as biological solutions, as well as in polymer melts and paints. Therefore, for this research, convective mixed heat transfers behaviour of nanofluid with non-Newtonian nanofluids has been considered, by applying Buongiorno model.

In the study of science, fluids can be classified into two categories, known as Newtonian and non-Newtonian fluids. Basically, a Newtonian fluid is a fluid in which the viscous stresses arising from its flow, at every point, are linearly proportional to the local strain rate or the rate of change of its deformation over time (Kirby, 2010). The relation defines the Newtonian fluid behaviour is known as Newton's Law of viscosity, given by

$$S = \mu \frac{\partial u}{\partial y} \tag{2.1}$$

where S denotes the shear stress exerted by the fluid, μ is the dynamic viscosity of the fluid and $\frac{\partial u}{\partial y}$ is the rate of the strain or velocity gradient. On the other hand, fluids which do not obey or opposite of the Newton's law of viscosity are defined as non-Newtonian fluid. This type of fluid is typically not independent on the shear rate and classified on the basis of their properties. In fact, the mathematical systems for non-Newtonian fluid are much more complicated due to the higher order of equation, compared to the Newtonian fluid.

Due to the diversity of non-Newtonian fluids in nature, there is no single constitutive relationship available in the literature that can describe the rheology of all the non-Newtonian fluids. Therefore, various constitutive equations which exhibit different rheological effects have been suggested to predict the behaviour of non- Newtonian fluids by describing the nonlinear relationship between stress and the rate of strain. Many types of non-Newtonian fluid models have become very popular in the literature, such as Maxwell fluid and Williamson fluid which are considered in this dissertation.

Maxwell fluid model is one of the non-Newtonian fluid models which predict the elastic behavior of the fluid. This fluid model can be explained for large elastic effects. However, it does not predict the creep accurately. In last decade, the study on Maxwell fluid model has been considered by many researchers. Wenchang and Mingyu (2002) have considered the constitutive equations of Maxwell fluid model to study the viscoelastic behavior of the fluid. They assumed no slip condition and the fluid near the surface is moving with the surface velocity. Vieru at al. (2008) studied the time dependent flow of fractional Maxwell fluid. The flow is considered between two side walls which are perpendicular to the moving plat. Hayat et al. (2008) have considered magnetic effect on the Maxwell fluid flow through a porous medium in a rotating frame. Hayat and Qasim (2010) considered the hydromagnetic flow and heat transfer of Maxwell fluid influenced by radiation and joule heating. The time dependent two-dimensional heat transfer analysis of Maxwell fluid flow over a stretching surface was studied by Mukhopadhyay (2012). The several other studies of Maxwell fluid are reported in the literature and few of them are Hayat et al. (2012), Prasad et al. (2012), Javed et al. (2016).

Williamson fluid is a non-Newtonian fluid model with shear thinning property. This model is a viscoelastic fluid and it was first proposed by (Williamson, 1929). It is a type of non-Newtonian fluid that belongs to the class of pseudoplastic fluids. This type of fluid has apparent viscosity with an increase in shear rate. The study of this phenomena have attracted the attention of numerous researchers because of its applications in industries such as sheet extrusion of polymer, plastic films, the flow of plasma and blood, etc. Srinivas et al. (2017) studied magnetohydrodynamics (MHD) flow and heat transfer of Williamson nanofluid over a stretching sheet. Hayat et al. (2016) investigated the hydromagnetic boundary layer flow of Williamson fluid by considering thermal radiation and Ohmic dissipation to be significant. Nadeem and Hussain (2014) considered flow and heat transfer analysis of Williamson nanofluid. Liaqat et al. (2017) presented Brownian and thermophoretic analysis of non-Newtonian Williamson fluid flow of thin film. Krishnamurthy et al. (2016) studied MHD boundary layer flow and melting heat transfer of Williamson nanofluid in the presence of chemical reaction. Khan et al. (2018) recently examined heat and mass transfer of Williamson nanofluid flow. Nadeem et al. (2013)

studied the flow of a Williamson fluid over a stretching sheet. Nadeem and Hussain (2014) examined flow and heat transfer analysis of Williamson nanofluid and observed that the flow parameters have a strong influence on heat transfer close to the wall and very slightly far away from the wall.

The study of boundary layer flow and heat transfer over stretching surfaces received remarkable attentions due to its numerous applications in modern industrial and engineering practices. The attributes of the end product are greatly reliant on stretching and the rate of heat transfer at the final stage of processing. Due to this real-world importance, interest developed among scientists and engineers to comprehend this phenomenon. Common examples are the extrusion of metals in cooling liquids, food, plastic products, the reprocessing of material in the molten state under high temperature. During the phase of the manufacturing process, the material undergoes elongation (stretching) with cooling process. Such types of processes are very handy in the production of plastic and metallic made apparatus, such as cutting hardware tools, electronic components in computers, rolling and annealing of copper wires, etc. In many engineering and industrial applications, the cooling of a solid surface is a primary tool for minimizing the boundary layer. Due to these useful and realistic impacts, the problem of cooling of solid moving surfaces has turned out to be an area of concern for scientists and engineers. The dynamics of the boundary layer flow over a stretching surface started from the pioneering work of (Crane, 1970). He solved a primary problem of two-dimensional boundary layer flow of stretching sheet which is extensively used in polymer extrusion industry and assumed that sheet is linearly stretching with a distance from a fixed point. Some representative studies over stretching sheet were presented by (Gupta, 1977, Chakrabarti and Gupta, 1979, Dutta and Roy, 1985, Chen and Char, 1988, Anderson et al., 1992). They provided their analysis by introducing suction and blowing, heat transfer with uniform heat flux, heat transfer with suction and blowing, MHD and heat transfer, analysis of power-law fluids, respectively. Abundant of literature is available over stretching sheet problem with different geometries, physical situations, fluid models and boundary conditions and will be discussed in proceeding paragraphs where necessary.

Some interest has been given to investigate the flow over a shrinking sheet, where the sheet is stretched toward a slot and it would cause a velocity away from the sheet. Wang (1990) first pointed out the flow over a shrinking sheet when he was working on the flow of a liquid film over an unsteady stretching sheet. Later a pioneering paper on this problem has been published by (Miklavčič and Wang, 2006). From the physical grounds vorticity (rotation or non-potential) flow over the shrinking sheet is not confined within a boundary layer, and the flow is unlikely to exist unless adequate suction on the boundary is imposed (Miklavčič and Wang 2006). Fang et al. (2009) extended the problem to unsteady case while Fang and Zhang (2010) obtained an analytical solution for the thermal boundary layers with suction over shrinking sheet. The shrinking sheet problem has also been extended to micropolar fluid (Ishak et al. 2010) as well as magnetohydrodynamic fluid (Fang and Zhang 2009, Noor, & Hashim 2009, Noor et al. 2010, Sajid et al. 2008, Sajid & Hayat 2009). Besides the imposition of suction, an added stagnation flow (which contain the vorticity) towards a shrinking sheet make the solution for such fluids to be existed. This idea is first published by (Wang, 2008) who found that solutions do not exist for large shrinking rates and may be non-unique in the two-dimensional case. Lok et al. (2011) studied the MHD Stagnation Point Flow towards a Shrinking Sheet.

The stagnation point encounters highest pressure, enhancement of heat transfer and rate of mass deposition. Some practical examples are cooling of electronic devices by fans, the aerodynamics of plastic sheets, cooling of nuclear reactors during emergency shutdown, heat exchangers placed in a low velocity environment, solar central receivers exposed to wind current and many others (Burde, 1995). Due to these aspects, the study of stagnation point flow and heat transfer has attracted many researchers and engineers. Hiemenz (1911) initiated the study of two-dimensional stagnation point flow over a stationary flat plate. He transformed the Navier-Stokes equations into ordinary differential equations by using similarity transformations and provided the exact solution of the nonlinear differential equations. Homann (1936) extended this work to three-dimensional problem of axisymmetric stagnation-point flow. Schlichting and Bussmann (1943) provided numerical solution of Hiemenz problem. Eckert (1942) also extended the Heimenz flow by incorporating heat transfer rate in the stagnation point flow. Ariel (1994) obtained the analytical solution by introducing suction in flow field. Stagnation point flow over moving surfaces is also significant in practical purposes including paper production, the spinning of fibers, glass blowing, continuous metal casting, manufacturing of sheeting material through extrusion process especially in the polymer extrusion in a melt spinning process, aerodynamic extrusion of plastic sheets etc. Chiam (1994) investigated the two-dimensional stagnation point flow of a viscous fluid over a linear stretching surface. He considered the situation where stretching velocity is equal to straining (free stream) velocity and concluded that no boundary layer exists in this case. Contrary to the Chiam (1994), Mahapatra and Gupta (2001, 2002) analyzed the effects of Magnetohydrodynamics and heat transfer respectively, in the region of stagnation point flow towards a stretching surface. They show that the boundary layer is formed when $a/b > 1$ (ratio of straining to stretching velocity) and inverted boundary layer is emerging when $a/b < 1$. Unsteady analysis of flow over a stretching sheet is reported by Nazar et al. (2004). Recently, (Mustafa et al. 2011; Sharma and Singh 2009; Javed et al. 2015) reported the investigations on the stagnation point flow over linear and non-linear stretching sheets in different aspects.

Thus, the main aim of the present study is to fill some gaps observed in boundary layer analyses of non-Newtonian fluids past stretching/shrinking surfaces.

References

Abbasi, F., Shehzad, S., Hayat, T. and Alhuthali, M. (2016). Mixed convection flow of Jeffrey nanofluid with thermal radiation and double stratification. *Journal of Hydrodynamics, Ser. B*. 28(5), 840–849.

Anderson, H.I., Bech, K.H., and Dandapat, B.S. (1992). Magnetohydrodynamic flow of a power-law fluid over a stretching sheet. International Journal of Non-Linear Mechanics, 27(6), 929–936.

Ariel, P. D. (1994). Stagnation point flow with suction: an approximate solution. *Journal of Applied Mechanics*, 61(4), 976–978.

Besthapu, P., Haq, R. U., Bandari, S. and Al-Mdallal, Q. M. (2017). Mixed convection flow of thermally stratified MHD nanofluid over an exponentially stretching surface with viscous dissipation effect. *Journal of the Taiwan Institute of Chemical Engineers*. 71, 307–314.

Buongiorno, J. (2006). Convective transport in nanofluids. *Journal of Heat Transfer*. 128(3), 240–250.

Burde, G.I. (1995). Non steady Stagnation-Point Flows over Permeable Surfaces: Explicit Solutions of the Navier-Stokes Equations. *Journal of fluids engineering*, 117(1), 189–191.

Chakrabarti, A., and Gupta, A.S. (1979). Hydromagnetic flow and heat transfer over a stretching sheet. *Quarterly of Applied Mathematics*, 37(1), 73–78.

Chiam, T.C. (1994). Stagnation point flow towards a stretching plate. *Journal of the physical society of Japan*, 63(6), 2443–2444.

Chen C.K., and Char, M.I. (1988). Heat transfer of a continuous, stretching surface with suction or blowing. *Journal of Mathematical Analysis and Applications*, 135(2), 568–580.

Crane, L.J. (1970). Flow past a stretching plate. *Zeitschrift für angewandte Mathematik und Physik*, 21, 645–647.

Choi, S. and JA, E. (1995). Enhancing thermal conductivity of fluids with nanoparticles. *ASME-Publications-Fed.* 231, 99–106.

Choi, S., Zhang, Z., Yu, W., Lockwood, F. and Grulke, E. (2001). Anomalous thermal conductivity enhancement in nanotube suspensions. *Applied Physics Letters*. 79(14): 2252–2254.

Dutta, B.K., Roy, P., and Gupta, A.S. (1985). Temperature field in flow over a stretching sheet with uniform heat flux. *International Communications in Heat and Mass Transfer*, 12, 89–94.

Eckert E.R.G. (1942). Die Berechnung des Warmeüderganges in der laminaren Grenzschicht um stromter Korper, *VDI Forchungsheft*, 416, 1–24.

Ellahi, R., Raza, M. and Vafai, K. (2012). Series solutions of non-Newtonian nanofluids with Reynolds model and Vogels model by means of the homotopy analysis method. *Mathematical and Computer Modelling*. 55(7-8), 1876–1891.

Ellis, E., Zhang, K., Lin, Q., Ye, E., Poma, A., Battaglia, G., Loh, X. J. and Lee, T.-C. (2017). Biocompatible pH-responsive nanoparticles with a core-anchored multilayer shell of triblock copolymers for enhanced cancer therapy. *Journal of Materials Chemistry B.* 5(23), 4421–4425.

Fang, T. and Zhang, J. (2009a), Viscous flow over an unsteady shrinking sheet with mass transfer. *Chin. Phys. Lett*., 26(1):014703, pp. 1-4.

Fang, T. and Zhang, J. (2009b). Closed form exact solutions of MHD viscous flow over a shrinking sheet. *Commun. in Nonlinear Sc. and Numer. Simul*., 14(7), pp. 2853-2857.

Gupta, P.S., and Gupta, A.S. (1977). Heat and mass transfer on a stretching sheet with suction or blowing. *Canadian Journal of Chemical Engineering*, 55,744–746.

Fang, T. and Zhang, J., (2010). Thermal boundary layer over a shrinking sheet : an analytical solution. *Acta Mech*, 209, pp. 325-343.

Habibi Matin, M., Dehsara, M. and Abbassi, A. (2012). Mixed convection MHD flow of nanofluid over a non-linear stretching sheet with effects of viscous dissipation and variable magnetic field. *Mechanics.* 18(4), 415–423.

Hayat, T., Anum, S. and Alsaedi, A. (2016). Hydromagnetic boundary layer flow of Williamson fluid in the presence of thermal radiation and Ohmic dissipation. *Alexandria Engineering Journal*, 55(3), pp. 2229-2240.

Hayat, T., Fetecau, C., and Sajid, M. (2008). On MHD transient flow of a Maxwell fluid in a porous medium and rotating frame. *Physics letters A*, 372(10) 1639–1644.

Hayat, T., Imtiaz, M. and Alsaedi, A. (2016b). Unsteady flow of nanofluid with double stratification and magnetohydrodynamics. *International Journal of Heat and Mass Transfer*. 92, 100–109.

Hayat, T., and Qasim, M. (2010). Influence of thermal radiation and Joule heating on MHD flow of a Maxwell fluid in the presence of thermophoresis. *International Journal of Heat and Mass Transfer*, 53(21), 4780–4788.

Hayat, T., Shehzad, S.A., and Alsaedi, A. (2012). Study on three-dimensional flow of Maxwell fluid over a stretching surface with convective boundary conditions. *International Journal of Physical Sciences*, 7(5), 761–768.

Hiemenz, K. (1911). Die Grenzschicht an einem in den gleichförmigen Flüssigkeitsstrom eingetauchten geraden Kreiszylinder. *Dinglers Polytechn Journal*, 326, 321–324.

Homann, F. (1936). Der Einfluss grosser Zähigkeit bei der Strömung um den Zylinder und um die Kugel. *ZAMM Journal of Applied Mathematics and Mechanics/Zeitschrift für Angewandte Mathematik und Mechanik*, 16(3), 153–164.

Huang, X. and El-Sayed, M. A. (2010). Gold nanoparticles: optical properties and implementations in cancer diagnosis and photothermal therapy. *Journal of Advanced Research.* 1(1), 13–28.

Imtiaz, M., Hayat, T., Hussain, M., Shehzad, S., Chen, G. and Ahmad, B. (2014). Mixed convection flow of nanofluid with Newtonian heating. *The European Physical Journal Plus*. 129(5), 1–11.

Ishak, A. Lok, Y.Y. & Pop, I. (2010). Stagnation-point flow over a shrinking sheet in a micropolar fluid. *Chemical Engineering Communications*. 197, 1417-1427.

Javed, T., and Ghaffari, A. (2016). Numerical Study of Non-Newtonian Maxwell Fluid in the Region of Oblique Stagnation Point Flow over a Stretching Sheet. *Journal of Mechanics*, 32(02), 175–184.

Javed, T., Ghaffari, A., and Ahmad, H. (2015). Numerical study of unsteady MHD oblique stagnation point flow with heat transfer over an oscillating flat plate. *Canadian Journal of Physics*, 93(10), 1138–1143.

Kang, T., Li, F., Baik, S., Shao, W., Ling, D. and Hyeon, T. (2017). Surface design of magnetic nanoparticles for stimuli-responsive cancer imaging and therapy. *Biomaterials.* 136, 98–114.

Kirby, B. J. (2010). Micro-and Nanoscale Fluid Mechanics: *Transport in Microfluidic Devices*. Cambridge University Press.

Krishnamurthy, M.R., Prasannakumara, B.C., Gireesha, B.J. and Gorla, R.S.R. (2016). Effect of chemical reaction on MHD boundary layer flow and melting heat transfer of Williamson nanofluid in porous medium. *Engineering Science and Technology, an International Journal*, 19(1), pp. 53-61.

Liaqat, A., Saeed, I., Gul, T., Khan, I., Dennis, L.C.C., Khan, W. and Aurangzeb, K. (2017). The Brownian and thermophoretic analysis of the non-Newtonian Williamson fluid flow of thin film in a porous space over an unstable stretching surface, *Applied Sciences*.

Lok. Y.Y., Ishak, A. & Pop, I. (2011). MHD stagnation-point flow toward a shrinking sheet. *International Journal of Numerical Methods for Heat and Fluid Flow.* 21, 61-72.

Madhu,M. and Kishan, N. (2016).Magneto-hydrodynamic mixed convection of a non-Newtonian power-law nanofluid past a moving vertical plate with variable density. *Journal of the Nigerian Mathematical Society*. 35(1): 199–207.

Mahapatra, T.R., and Gupta, A.S. (2001). Magnetohydrodynamic stagnation-point flow towards a stretching sheet. *Acta Mechanica*, 152(1–4), 191–196.

Mahapatra, T.R., and Gupta, A.S. (2002). Heat transfer in stagnation-point flow towards a stretching sheet. *Heat and mass transfer,* 38(6), 517521.

Mahdy, A. (2012). Unsteady mixed convection boundary layer flow and heat transfer of nanofluids due to stretching sheet. *Nuclear Engineering and Design*. 249, 248– 255.

Mekheimer, K. S., Hasona, W., Abo-Elkhair, R. & Zaher, A. (2018). Peristaltic blood flow with gold nanoparticles as a third grade nanofluid in catheter: Application of cancer therapy. *Physics Letters A*. 382(2-3), 85–93.

Miklavčič, M. and Wang, C. Y., (2006). Viscous flow due to a shrinking sheet. *Quart. of Appl. Math*., 64(2), pp. 283-290.

Mustafa, I., Javed, T., and Ghaffari, A. (2016). Heat transfer in MHD stagnation point flow of a ferrofluid over a stretchable rotating disk. *Journal of Molecular Liquids*, 219, 526–532.

Mukhopadhyay, S. (2012). Heat transfer analysis of the unsteady flow of a Maxwell fluid over a stretching surface in the presence of a heat source/sink. *Chinese Physics Letters*, 29(5), 054703.

Nabwey, H. A., Boumazgour, M. & Rashad, A. (2017). Group method analysis of mixed convection stagnation-point flow of non-Newtonian nanofluid over a vertical stretching surface. *Indian Journal of Physics*. 91(7): 731–742.

Nadeem, S. and Hussain, S.T. (2014). Flow and heat transfer analysis of Williamson nanofluid. *Applied Nano science*, 4 (8), pp. 1005-1012, doi: 10.1007/s13204-013- 0282-1.

Nadeem, S., Hussain, S.T. & Lee, C. (2013). Flow of a Williamson fluid over a stretching sheet. *Brazilian Journal of Chemical Engineering*, 30(3), pp. 619-625.

Naseem, F., Shafiq, A., Zhao, L. & Naseem, A. (2017). MHD biconvective flow of Powell Eyring nanofluid over stretched surface. *AIP Advances*. 7(6), 065013.

Nazar, R., Amin, N., Filip, D., and Pop, I. (2004). Unsteady boundary layer flow in the region of the stagnation point on a stretching sheet. *International Journal of Engineering Science*, 42(11), 1241–1253.

Noor, N.F.M. & Hashim, I. (2009). MHD flow and heat transfer adjacent to a permeable shrinking sheet embedded in a porous medium. *Sains Malaysiana.* 38(4), 559-565.

Noor, N. F. M., Kechilb, S. A. and Hashimc, I., (2010). Simple non-perturbative solution for MHD viscous flow due to a shrinking sheet. *Commun. in Nonlinear Sc. and Numer. Simul.*, 15(2), pp. 144-148.

Othman, N. A., Yacob, N. A., Bachok, N., Ishak, A. and Pop, I. (2017). Mixed convection boundary-layer stagnation point flow past a vertical stretching/shrinking surface in a nanofluid. *Applied Thermal Engineering*. 115, 1412–1417.

Prasad, K.V., Sujatha, A., Vajravelu, K., and Pop, I. (2012). MHD flow and heat transfer of a UCM fluid over a stretching surface with variable thermo physical properties. *Meccanica*, 47(6), 1425–1439.

Sajid, M. and Hayat, T., (2009). The application of homotopy analysis method for MHD viscous flow due to a shrinking sheet. Chaos, Soliton & Fractals, 39(3), pp. 1317-1323.

Sajid, M., Hayat, T. & Javed, T. (2008). MHD rotating flow of a viscous fluid over a shrinking surface. *Nonlinear Dynamics*. 51, 259-265.

Sandeep, N., Kumar, B. R. and Kumar, M. J. (2015).A comparative study of convective heat and mass transfer in non-Newtonian nanofluid flow past a permeable stretching sheet. *Journal of Molecular Liquids*. 212, 585–591.

Schlichting, H. and Bussmann, K. (1943). Exakte Losungen fur die Laminare Grenzchicht mit Absaugung und Ausblasen, *Schri. Dtsch. Akad. Luftfahrtforschung, Ser. B*, 7(2), pp. 25.

Sharma, P.R., and Singh, G. (2009). Effects of variable thermal conductivity and heat source/sink on MHD flow near a stagnation point on a linearly stretching sheet. *Journal of Applied fluid mechanics*, 2(1), 13–21.

Srinivas, R.C., Naikoti, K. and Rashidi, M.M. (2017). MHD flow and heat transfer characteristics of Williamson nanofluid over a stretching sheet with variable thickness and variable thermal conductivity. *Transactions of A. Razmadze Mathematical Institute.*171(2), pp. 195-211.

Subhashini, S. and Sumathi, R. (2014). Dual solutions of a mixed convection flow of nanofluids over a moving vertical plate. *International Journal of Heat and Mass Transfer*. 71, 117–124.

Tiwari, R. K. and Das, M. K. (2007). Heat transfer augmentation in a two-sided lid-driven differentially heated square cavity utilizing nanofluids. *International Journal of Heat and Mass Transfer*. 50(9), 2002–2018.

Uddin, M. J., Khan, W. A. and Ismail, A. I. M. (2015). G-jitter induced magnetohydrodynamics flow of nanofluid with constant convective thermal and solutal boundary conditions. *PLoS ONE*. 10(5), 1–15.

Vieru, D., Fetecau, C., and Fetecau, C. (2008). Flow of a viscoelastic fluid with the fractional Maxwell model between two side walls perpendicular to a plate. Applied Mathematics and Computation, 200(1), 459-464.

Wang, C. Y., (1990). Liquid film on an unsteady stretching sheet. *Quart. Appl. Math*., 48, pp. 601- 610.

Wang, C.Y. (2008). Stagnation flow towards a shrinking sheet. *International Journal of Non-Linear Mechanics.* 43, 377-382.

Wenchang, T., and Mingyu, X. (2002). Plane surface suddenly set in motion in a viscoelastic fluid with fractional Maxwell model. *Acta Mechanica Sinica*, 18(4), 342–349.

Williamson R. V. (1929). The flow of pseudo plastic materials. *Industrial and Engineering Chemistry Research*, 21(11), 1108.

Wong, K. V. and De Leon, O. (2010). Applications of nanofluids: current and future. *Advances in Mechanical Engineering*, 2, 1–11.

Chapter3

MHD Slip Flow of Upper-Convected Maxwell Nano Fluid over a Stretching Sheet with Chemical Reaction

3.1. Introduction

Nanofluid is a colloidal postponement which containing nano particles in a base fluid. Nanofluids have enhanced physical properties such as mass diffusivity, thermal diffusivity and conductivity, viscosity, and convective heat transfer coefficients compared to those of base fluids. Nanofluids can be used in a plethora of engineering applications extending from use in the automotive industry to the medical field to use in power plant cooling systems as well as computers *viz.* heat transfer applications (in industrial cooling applications as smart fluids, in nuclear reactors, in extraction of geothermal energy sources), automotive applications (as nanofluid coolant, nanofluid in fuel, brake and other vehicular nanofluids), electronic applications (cooling of microchips, Micro scale fluidic applications) and biomedical applications (Nano drug delivery, cancer therapeutics, cryopreservation, Nano cryosurgery) etc. Because of these original properties, nanofluids are important to study. Therefore, more of precise researches are presented in this topic (Macha M. et al., 2017, Macha M. and Naikoti K., 2015, Macha M. and Naikoti K., 2017, Srinivas, C., et al. 2017, & Macha M. et al. 2016).

Because of its comprehensive applications in biomechanics, industry and engineering the research on boundary layer flows of non-Newtonian fluids past a stretching surface is very important. Accordingly, Jayachandra and Sandeep (2016), Reddy et al. (2018), Vijayalakshmi et al. (2017) and Tian et al. (2018) examined with different parameters the non-Newtonian fluid flow past a various stretching surfaces. The effect of thermal radiations on MHD three-dimensional flow over a stretching sheet was studied by (Nasir et al. 2018). In the presence of graphene nanoparticles Khan et al. (2018) investigated Eyring-Powell slip flow of Nano liquid film. The upper-convected Maxwell fluid is a type of a viscoelastic or rate type fluid. This model is very important since it predicts the relaxation time effect and it excludes complicated effects of shear-dependent viscosity. Commonly, many researchers have been studied upper-convected Maxwell fluid flow. Thus, Yu Bai et al. (2017), Imran et al. (2018), Elsayed Mohamed Abdel Rahman Elbashbeshy et al. (2018), Vajravelu et al. (2017). Omowaye and Animasaun (2016), Alireza Rahbari et al. (2018), Gireesha et al. (2018), and Meysam Mohamadali (2016) scrutinized non-Newtonian Maxwell fluid with different physical conditions such as viscous dissipation, Newtonian heating, homogeneous-heterogeneous chemical reactions, thermal stratification etc. past different stretching surfaces. Their result shows that as Prandtl number increases Temperature as well as rate of heat transfer was dwindled.

The stagnation point flow of nanofluid over stretching surface has different applications in industries and technology. As a result, Sajid et al. (2014), Sirinivasulu et al. (2017) and Wubshet (2016) investigated MHD stagnation point flow in different non-Newtonian fluids such as Oldroyd-B fluid casson and upper-convected Maxwell fluid on a stretching sheet with various physical parameters. Similarly, Mageswari and Nirmala (2016) scrutinized stagnation point flow on stretching sheet with Newtonian heating. Moreover, Abuzar et al. (2017) have examined the effect of radiation and convective boundary condition on oblique stagnation point of non-Newtonian nanofluids over the stretching surface. Furthermore, Stagnation point flow of nanofluid due to inclined stretching sheet studied numerically by (Yasin Abdela et al., 2018). The numerical result shows that when velocity ratio parameter, Grashof number, solutal expansion parameter and angle of inclination velocity increased, the boundary layer thickness increases.

The studies of chemical reaction and slip boundary condition with heat transfer have important application in technology and industry. Accordingly, the slip effect on MHD flow with different model of non-Newtonian nanofluids such as Casson fluid and Jeffrey nanofluid past a stretching sheet with various physical conditions are investigated by (Sathies Kumar, 2015), (Raghawendra Mishra, 2017), (Manjula and Jayalakshmi, 2018) and (Mohamed Abd El-Aziz and Ahmed Afify 2018). Their study displays that if velocity ratio, momentum slip, magnetic parameters increase, and then the velocity boundary layer thickness become reduced. Krishnamurthy et al.(2016), Mabood et al. (2016), and Ibrahim et al. (2017) probed the effect of chemical reaction on mass and heat transfer MHD boundary layer flow with viscous dissipation, thermal radiation, mixed convection and etc. past stretching sheet and observed that with an increasing magnetic field the Nusselt number, skin friction coefficient and Sherwood number are increased. Madasi krishnaiah et al. (2016) studied effect of slip conditions, viscous dissipation and chemical reaction on MHD stagnation point flow of nanofluid. They observed that as the values of suction parameter rises the velocity upsurges, whereas the temperature and concentration profiles are reduced. Moreover, the reference covering slip effects and chemical reaction are described in references (Dian-Chen Lu et al.

2018), (Ramzan and Bilal, 2016), Ramzan et al., (2017), (Jae Dong Chung et al., 2017), (Bilal et al., 2017), (Dianchen Lu, 2017), (Shamsa Kanwal et al., 2017), (Umer Farooq et al., 2017), (Hina Gul et al., 2017), (Naeem Ullah et al. 2017) and (Shravani Ittedi et al. 2017).

All the above investigators disregard the effects of nano particles with slip effects in the analysis of the problem of MHD stagnation point flow of upper-convected Maxwell fluid with chemical reaction. So, the objective of present paper is to inspect the effect of nanoparticle and chemical reaction on MHD slip stagnation point flow, the boundary layer flow and heat and mass transfer of upper-convected Maxwell fluid above a stretching sheet via implicit finite difference method. Therefore, the inclusion of the effect of nanoparticles with chemical reaction and slip effect in upper-convected Maxwell fluids makes this study unusual one.

3.2. Mathematical Formulation

Consider time independent and incompressible MHD slip flow of upper-convected Maxwell fluid with chemical reaction along a stretching sheet. It is expected that the free stream velocity $u_e(x)$ and the stretching velocity $u_w(x)$ are of the forms $u_e(x) = ax$ and $u_w(x) = bx$ where a and b are constants. For this study x-axis is along the sheet and normal to the sheet y −axis is chosen. Over the stretching sheet the concentration is represented by C_w and temperature is represented by T_w. Moreover, the ambient temperature and the ambient concentration are represented by T_∞ and C_∞. Under these assumptions the governing equations of time independent and incompressible boundary layer flow a nanofluid over stretching sheet is given by:

$$\frac{\partial u}{\partial x} + \frac{\partial v}{\partial y} = 0 \tag{3.1}$$

$$u\frac{\partial u}{\partial x} + v\frac{\partial u}{\partial y} = \nu\frac{\partial^2 u}{\partial y^2} - \xi\left(u^2\frac{\partial^2 u}{\partial x^2} + v^2\frac{\partial^2 u}{\partial y^2} + 2uv\frac{\partial^2 u}{\partial x\,\partial y}\right) + u_e\frac{\partial u_e}{\partial x} \;\; + \frac{\sigma B_0^2}{\rho_f}(u_e - u) \tag{3.2}$$

$$u\frac{\partial T}{\partial x} + v\frac{\partial T}{\partial y} = \alpha_m\frac{\partial^2 T}{\partial y^2} \;\; + \omega\left\{D_B\frac{\partial C}{\partial y}\frac{\partial T}{\partial y} + \frac{D_\tau}{T_\infty}\left(\frac{\partial T}{\partial y}\right)^2\right\} - \frac{1}{(\rho c_p)_f}\frac{\partial q_r}{\partial y} + \frac{Q_0(T - T_\infty)}{(\rho c_p)_f} \tag{3.3}$$

$$u\frac{\partial C}{\partial x} + v\frac{\partial C}{\partial y} = D_B\frac{\partial^2 C}{\partial y^2} + \frac{D_\tau}{T_\infty}\frac{\partial^2 T}{\partial y^2} - K_r(C - C_\infty) \tag{3.4}$$

The appropriate boundary conditions are:

$$u = u_w + V_r\frac{\partial u}{\partial y},\;\; v = 0,\;\; T = T_w + T_r\frac{\partial T}{\partial y},\;\; C = C_w + C_r\frac{\partial C}{\partial y}, \text{ at } y = 0 \tag{3.5}$$

$$u \to u_e(x) = bx, v \to 0,\;\; T \to T_\infty,\;\; C \to C_\infty \;\text{ as } y \to \infty \tag{3.6}$$

where u and v are the velocity components along the x and y directions, respectively, ρ_f the density of the base fluid, $\alpha_m = \frac{k}{\rho c_f}$ the thermal diffusivity, ξ is the relaxation time parameter of the fluid, B_0 is the strength of the magnetic field, ν is the kinematic viscosity of the fluid, k is the thermal conductivity of the fluid, D_B is the Brownian diffusion coefficient, D_τ is the thermophoretic diffusion coefficient, $\omega = \frac{(\rho c)_p}{(\rho c)_f}$ is the ratio between the effective heat capacity of the nanoparticle material and heat capacity of the fluid, c is the volumetric volume expansion coefficient and ρ is the density of the particles .

We can write for the radiation using Rosseland approximation

$$q_r = -\frac{4\sigma^*}{3k^*}\frac{\partial T^4}{\partial y} \tag{3.7}$$

where σ^* is the Stefan-Boltzman constant, k^* is the absorption coefficient, assuming the temperature difference within the flow is such that T^4 may be expanded in a Taylor series about T_∞ and neglecting higher orders we get $T^4 = 4TT_\infty^3 - 3T_\infty^4$.

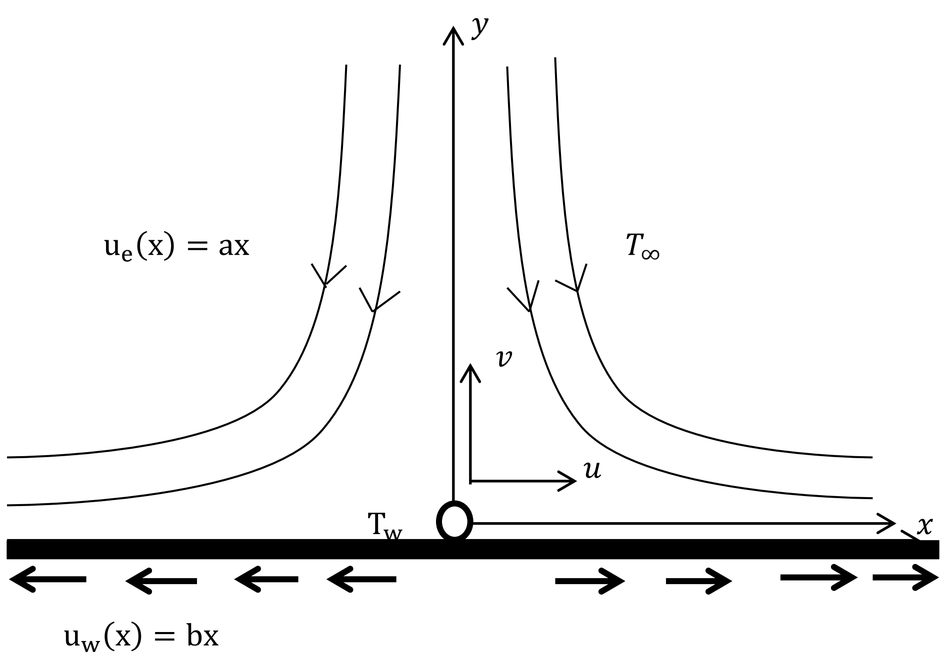

Figure3. 1: Coordinate system and physical model.

Hence

$$\frac{\partial q_r}{\partial y} = -\frac{16\sigma^* T_\infty^3}{3k^*}\frac{\partial^2 T}{\partial y^2} \tag{3.8}$$

Introducing similarity transformations

$$\psi = \sqrt{a\nu} f(\eta), \quad \theta(\eta) = \frac{(T - T_\infty)}{(T_w - T_\infty)}, \quad \phi(\eta) = \frac{(C - C_\infty)}{(C_w - C_\infty)}, \ \eta = \sqrt{\frac{a}{\nu}} y \tag{3.9}$$

We choose the stream function $\psi(x, y)$ such that

$$\frac{\partial \psi}{\partial y} = u, \ \text{and} \ -\frac{\partial \psi}{\partial x} = v \tag{3.10}$$

Using the similarity transformation defined by (3.9), equations 3.1-3.4 is transformed into the non-dimensional ordinary differential equation form as follows:

$$f''' + ff'' - f'^2 + E^2 + M(E - f') + \beta(2ff'f'' - f^2 f''') = 0 \tag{3.11}$$

$$(1 + \frac{4}{3R_d})\theta'' + Prf\theta' + PrNb\phi'\theta' + Nt\theta'^2 + PrR\theta = 0 \tag{3.12}$$

$$\phi'' + Lef\phi' + \frac{Nt}{Nb}\theta'' - KLe\phi = 0 \tag{3.13}$$

The transformed boundary conditions are

$$f(\eta) = \chi, \quad f'(\eta) = 1 + \upsilon f''(\eta), \ \theta(\eta) = 1 + \delta^* \theta'(\eta), \quad \phi(\eta) = 1 + \gamma_1 \phi'(\eta), \text{at } \eta = 0 \tag{3.14}$$

$$f'(\eta) \to E, \theta(\eta) \to 0, \ \phi(\eta) \to 0, \text{as } \eta \to \infty \tag{3.15}$$

where f is dimensionless velocity, θ is dimensionless temperature, ϕ is dimensionless concentration and η is the similarity variable. The prime denotes differentiation with respect to η.

The overall governing parameters are defined as;

$\chi = -v_w(x)\sqrt{\frac{2x}{\nu u_\infty}}$ is the suction-injection parameter, $E = \frac{a}{b}$ is velocity ratio, $\beta = \xi a$ is Deborah number, $M = \frac{\sigma B_0^2 x}{\rho u_\infty}$ is magnetic field parameter,$\upsilon = V_r\sqrt{\frac{b}{\nu}}$ is velocity slip parameter, $\delta^* = T_r\sqrt{\frac{b}{\nu}}$ is thermal slip parameter, $\gamma_1 = C_r\sqrt{\frac{b}{\nu}}$ is solutal slip parameter, $\mathrm{R}_d = \frac{kk^*}{4\sigma^* T_\infty^3}$ is thermal radiation parameter, $Pr = \frac{\nu}{\alpha_m}$ is Prandtl number, $Nb = \frac{(\rho c)_p D_B (C_w - C_\infty)}{(\rho c)_f \nu}$ is Brownian motion parameter, $Nb = \frac{(\rho c)_p D_\tau (T_w - T_\infty)}{(\rho c)_f \nu T_\infty}$ is thermophoresis parameter, $Le = \frac{\nu}{D_B}$ is Lewis number, $K = \frac{K_r}{c}$ is chemical reaction parameter, $\mathrm{R} = \frac{Q_0}{a(\rho c_p)_f}$ is heat source parameter.

The skin friction C_f , local Nusselt number Nu_x and the Sherwood number Sh_x are the important physical quantities of interest in this problem which are defined as

$$C_f = \frac{\tau_w}{\rho u_e^2}, \qquad Nu_x = \frac{x q_w}{k(T_f - T_\infty)}, \qquad Sh_x = \frac{x q_m}{D_B(c_w - c_\infty)}$$

Here $\tau_w = \mu(1+\beta)\frac{\partial u}{\partial y}$ is the surface shear stress, $q_w = -k\left(\frac{\partial T}{\partial y}\right)_{(y=0)} + q_r$ is the surface heat flux and $q_m = -D_B\left(\frac{\partial C}{\partial y}\right)_{(y=0)}$ is the surface mass flux.

Using the similarity transformation in (3.9) we have the following relations;

$C_f\, Re_x^{\frac{1}{2}} = (1+\beta)f''(0)$, $Nu_x\, Re_x^{-\frac{1}{2}} = -(1+\frac{4}{3R_d})\theta'(0)$, $Sh_x\, Re_x^{-\frac{1}{2}} = -\phi'(0)$ where Re_x is local Reynolds number.

3.3. Numerical solution

3.3.1. The Keller-Box Method

The transfigured ordinary differential equations (3.11), (3.12), and (3.13) subject to the boundary conditions (3.14) and (3.15) are solved numerically using an implicit finite difference method (Keller-box) in combination with the Newton's linearization techniques.

3.3.2. The Finite Difference Scheme

We write the governing third order momentum equation (3.11) and second order energy and concentration equations (3.12) and (3.13) in terms of a first order equations. For this purpose we introduce new dependent variable $u, v, t, \theta = s(x,\eta), \phi(\eta) = g(x,\eta)$ such that $f' = u, u' = v, s' = t$, and $g' = z$

Thus equations (3.11), (3.12), and (3.13) can be written as

$$v' + fv - u^2 + E^2 + M(E-u) + \beta(2fuv - f^2v') = 0 \tag{3.16}$$

$$(1+\frac{4}{3R_d})t' + Prft' + PrNbzt + Ntt^2 + PrRs = 0 \tag{3.17}$$

$$z' + Lefz + \frac{Nt}{Nb}t' - KLeg = 0 \tag{3.18}$$

The boundary conditions are

$$f(\eta) = \chi, \quad u(\eta) = 1 + \upsilon v(\eta), \quad s(\eta) = 1 + \delta^* t(\eta), \quad g(\eta) = 1 + \gamma_1 z(\eta), \text{ at } \eta = 0 \tag{3.19}$$

$$u(\eta) \to E, s(\eta) \to 0,\ \ g(\eta) \to 0, \text{as}\ \eta \to \infty \tag{3.20}$$

where prime denotes the differentiation with respect to η.

We know consider the net rectangle in the $x - \eta$ plane shown in figure 2 and the net points defined as below

$x^0 = 0 \qquad x^i = x^{i-1} + k_i \qquad i = 1,2,3, \dots, I$

$\eta_0 = 0 \qquad \eta_j = \eta_{j-1} + h_j \qquad j = 1,2,3, \dots, J \qquad \eta_j = \eta_\infty$

where k_i is the Δx-spacing and h_j is the $\Delta\eta$-spacing. Here i and j are the sequence of numbers that indicate the coordinate location, not tensor indices or exponents

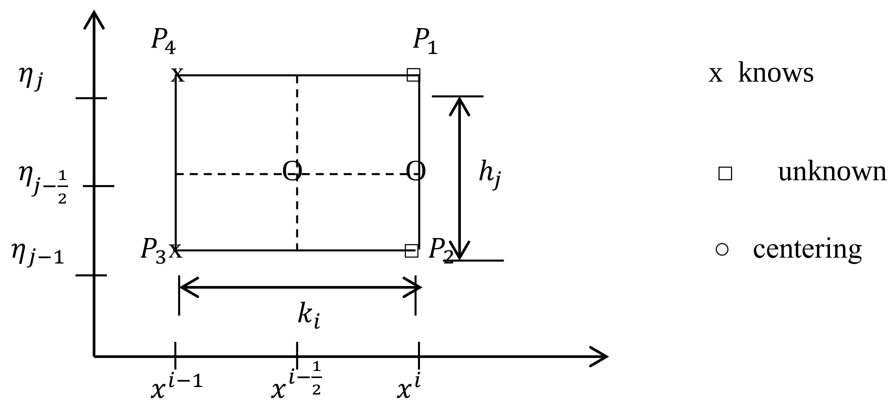

Figure3. 2: Net rectangle for difference approximations

Since only first derivatives appear in the governing equations, centered differences and two-point averages can be constructed involving only the four corner nodal values of the 'box'.

Now write the finite difference approximations of the ordinary differential equation for the mid-point $\left(x^i, \eta_{j-\frac{1}{2}}\right)$ of the segment P_1P_2 using centered difference derivatives. This process is called centering about $\left(x^i, \eta_{j-\frac{1}{2}}\right)$. We get

$$f_j - f_{j-1} - \frac{h_j}{2}\left(u_j + u_{j-1}\right) = 0$$

$$u_j - u_{j-1} - \frac{h_j}{2}\left(\mathrm{v}_j + \mathrm{v}_{j-1}\right) = 0$$

$$s_j - s_{j-1} - \frac{h_j}{2}\left(t_j + t_{j-1}\right) = 0$$

$$g_j - g_{j-1} - \frac{h_j}{2}\left(z_j + z_{j-1}\right) = 0$$

$$(\mathrm{v}_j - \mathrm{v}_{j-1}) + \frac{h_j}{4}(f_j + f_{j-1})(\mathrm{v}_j + \mathrm{v}_{j-1}) - \frac{h_j}{4}(u_j + u_{j-1})^2$$
$$+ \frac{h_j\beta}{4}(f_j + f_{j-1})(u_j + u_{j-1})(\mathrm{v}_j + \mathrm{v}_{j-1}) - \frac{\beta}{4h_j}(f_j + f_{j-1})(f_j + f_{j-1})(\mathrm{v}_j - \mathrm{v}_{j-1})$$
$$+ Mh_j\left(E - \frac{1}{2}(u_j + u_{j-1})\right) + h_jE^2 = P_{j-\frac{1}{2}}$$

$$\left(1 + \frac{4}{3R_d}\right)(t_j - t_{j-1}) + \frac{h_jPr}{4}(f_j + f_{j-1})(t_j + t_{j-1}) + \frac{h_jPrNb}{4}(z_j + z_{j-1})(t_j + t_{j-1})$$
$$+ \frac{h_jPrNt}{4}(t_j + t_{j-1})(t_j + t_{j-1}) + \frac{h_jPrR}{2}(s_j + s_{j-1}) = Q_{j-\frac{1}{2}}$$

$$(z_j - z) + \frac{h_jLe}{4}(f_j + f_{j-1})(\mathrm{z}_j + z_{j-1}) + \frac{Nt}{Nb}(t_j - t_{j-1}) - \frac{Leh_jK}{2}(g_j + g_{j-1}) = S_{j-\frac{1}{2}} \tag{3.21}$$

where $P_{1-\frac{1}{2}} = -(\mathrm{v}_j - \mathrm{v}_{j-1}) - h_j(f\mathrm{v})_{j-\frac{1}{2}} + h_j(u^2)_{j-\frac{1}{2}} - 2h_j(fu\mathrm{v})_{j-\frac{1}{2}} + \frac{\beta}{4h_j}(f^2)_{j-\frac{1}{2}}(\mathrm{v}_j - \mathrm{v}_{j-1}) - Mh_j\left(E - (u)_{j-\frac{1}{2}}\right) - h_jE^2$ and

$$Q_{j-\frac{1}{2}} = -\left(1 + \frac{4}{3R_d}\right)(t_j - t_{j-1}) - h_jPr(f\mathrm{t})_{j-\frac{1}{2}} - h_jPrNb(zt)_{j-\frac{1}{2}} - \beta h_j(t^2)_{j-\frac{1}{2}} - h_jPrR(s)_{j-\frac{1}{2}}$$

$$S_{j-\frac{1}{2}} = -(z_j - z_{j-1}) - h_j(f\mathrm{z})_{j-\frac{1}{2}} - \frac{Nt}{Nb}(t_j - t_{j-1}) + Leh_jK(g)_{j-\frac{1}{2}}$$

We note $P_{1-\frac{1}{2}}$, $Q_{j-\frac{1}{2}}$ and $S_{j-\frac{1}{2}}$ involve only known quantities if we assume that the solution is known on $x = x^{i-1}$.

In terms of the new dependent variables, the boundary conditions become

$$f(x,0) = \chi \;, u(x,0) = 1 + vv(0)\,,\; s(x,0) = 1 + \delta^* t(0), g(0) = 1 + \gamma_1 z(0)$$
$$u(x,\infty) = E, s(x,\infty) = 0\;, s(x,\infty) = 0, \tag{3.22}$$

Equations (4.21) are imposed for $j = 1,2,3,\dots,J$ and the transformed boundary layer thickness, η_J is sufficiently large so that it is beyond the edge of the boundary layer (Cebeci and Bradshaw, 1984). The boundary conditions yields at $x = x^i$ are

$$f_0^i = \chi, u_0^i = 1 + vv_0^i,\; s_0^i = 1 + \delta^* t_0^i,\; g_0^i = 1 + \gamma_1 z_0^i, u_J^i = E, s_J^i = 0\,, g_J^i = 0 \tag{3.23}$$

3.3.3. Newton's Method

Equations (4.21) are nonlinear algebraic equations and therefore have to be linearized before the factorization scheme can be used. Let us write the Newton iterates as follows: For $(k+1)th$ iterates, we write

$$f_j^{(k+1)} = f_j^{(k)} + \delta f_j^{(k)},$$

$$u_j^{(k+1)} = u_j^{(k)} + \delta u_j^{(k)},$$

$$\mathrm{v}_j^{(k+1)} = \mathrm{v}_j^{(k)} + \delta \mathrm{v}_j^{(k)}, \tag{3.24}$$

$$t_j^{(k+1)} = t_j^{(k)} + \delta t_j^{(k)},$$

$$s_j^{(k+1)} = s_j^{(k)} + \delta s_j^{(k)}$$

$$g_j^{(k+1)} = g_j^{(k)} + \delta g_j^{(k)}$$

$$z_j^{(k+1)} = z_j^{(k)} + \delta z_j^{(k)}$$

Equation (4.21) can be written as

$$f_j + \delta f_j - f_{j-1} - \delta f_{j-1} = \frac{h_j}{2}\left(u_j + \delta u_j + u_{j-1} + \delta u_{j-1}\right)$$

$$u_j + \delta u_j - u_{j-1} - \delta u_{j-1} = \frac{h_j}{2}\left(\mathrm{v}_j + \delta \mathrm{v}_{j,} + \mathrm{v}_{j-1} + \delta \mathrm{v}_{j-1}\right)$$

$$g_j + \delta g_j - g_{j-1} - \delta g_{j-1} = \frac{h_j}{2}\left(z_j + \delta z_j + z_{j-1} + \delta z_{j-1}\right)$$

$$s_j + \delta s_j - s_{j-1} - \delta s_{j-1} = \frac{h_j}{2}\left(t_j + \delta t_j + t_{j-1} + \delta t_{j-1}\right) \tag{3.25}$$

$$\mathrm{v}_j + \delta \mathrm{v}_{j,} - \mathrm{v}_{j-1} - \delta \mathrm{v}_{j-1} + \frac{h_j}{4}\left(f_j + \delta f_j + f_{j-1} + \delta f_{j-1}\right)\left(\mathrm{v}_j + \delta \mathrm{v}_{j,} + \mathrm{v}_{j-1} + \delta \mathrm{v}_{j-1}\right) - \frac{h_j}{4}\left(u_j + \delta u_j + u_{j-1} + \delta u_{j-1}\right)^2 + \frac{h_j \beta}{4}\left(f_j + \delta f_j + f_{j-1} + \delta f_{j-1}\right)\left(u_j + \delta u_j + u_{j-1} + \delta u_{j-1}\right)\left(\mathrm{v}_j + \delta v_j + \mathrm{v}_{j-1} + \delta v_{j-1}\right) - \frac{\beta}{4h_j}\left(f_j + \delta f_j + f_{j-1} + \delta f_{j-1}\right)\left(f_j + \delta f_j + f_{j-1} + \delta f_{j-1}\right)\left(\mathrm{v}_j + \delta v_j - \mathrm{v}_{j-1} - \delta v_{j-1}\right) + M h_j \left(E - \frac{1}{2}\left(u_j + \delta u_j + u_{j-1} + \delta u_{j-1}\right)\right) + h_j E^2 = P_{j-\frac{1}{2}}$$

$$\left(1+\frac{4}{3R_d}\right)\left(t_j+\delta t_j-t_{j-1}-\delta t_{j-1}\right)+\frac{h_jPr}{4}\left(f_j+\delta f_j\ +f_{j-1}+\delta f_{j-1}\ \right)\left(t_j+\delta t_j+t_{j-1}+\delta t_{j-1}\right)$$
$$+\frac{h_jPrNb}{4}\left(z_j+\delta z_j\ +z_{j-1}+\delta z_{j-1}\ \right)\left(t_j+\delta t_j\ +t_{j-1}+\delta t_{j-1}\ \right)$$
$$+\frac{h_jPrNt}{4}\left(t_j+\delta t_j\ +t_{j-1}+\delta t_{j-1}\ \right)\left(t_j+\delta t_j\ +t_{j-1}+\delta t_{j-1}\ \right)$$
$$+\frac{h_jPrR}{2}\left(s_j+\delta s_j\ +s_{j-1}+\delta s_{j-1}\ \right)=Q_{j-\frac{1}{2}}$$

$$\left(z_j+\delta z_j\ -z_{j-1}-\delta z_{j-1}\ \right)+\frac{h_jLe}{4}\left(f_j+\delta f_j\ +f_{j-1}+\delta f_{j-1}\ \right)\left(z_j+\delta z_j\ +z_{j-1}+\delta z_{j-1}\ \right)$$
$$+\frac{Nt}{Nb}\left(t_j+\delta t_j-t_{j-1}-\delta t_{j-1}\right)-\frac{Leh_jK}{2}\left(g_j+\delta g_j\ +g_{j-1}+\delta g_{j-1}\ \right)=S_{j-\frac{1}{2}}$$

By dropping the quadratic and higher-order terms in $\delta f_j^{(i)},\delta u_j^{(i)},\delta \mathrm{v}_j^{(i)},\delta s_j^{(i)} and \delta t_j^{(i)}$ a linear tridiagonal system of equations will be obtained, as follows:

$$\delta f_j\ -\delta f_{j-1}-\frac{h_j}{2}\left(\delta u_j\ +\delta u_{j-1}\ \ \right)=(r_1)_{j-\frac{1}{2}}$$

$$\delta u_j\ -\delta u_{j-1}-\frac{h_j}{2}\left(\delta \mathrm{v}_j\ +\delta \mathrm{v}_{j-1}\ \ \right)=(r_2)_{j-\frac{1}{2}}$$

$$\delta s_j\ -\delta s_{j-1}-\frac{h_j}{2}\left(\delta t_j\ +\delta t_{j-1}\ \ \right)=(r_3)_{j-\frac{1}{2}}$$
$$\delta g_j\ -\delta g_{j-1}-\frac{h_j}{2}\left(\delta z_j\ +\delta z_{j-1}\ \ \right)=(r_4)_{j-\frac{1}{2}}$$

$$\delta \mathrm{v}_j-\delta \mathrm{v}_{j-1}\ \ +\frac{h_j}{2}\mathrm{v}_{j-\frac{1}{2}}\left(\delta f_j\ +\delta f_{j-1}\ \right)+\frac{h_j}{2}f_{j-\frac{1}{2}}\left(\delta \mathrm{v}_j+\delta \mathrm{v}_{j-1}\ \ \right)-h_ju_{j-\frac{1}{2}}\left(\delta u_j\ +\delta u_{j-1}\right)+$$
$$h_j\beta(u\mathrm{v})_{j-\frac{1}{2}}\left(\delta f_j\ +\delta f_{j-1}\ \right)+h_j\beta(f\mathrm{v})_{j-\frac{1}{2}}\left(\delta u_j\ +\delta u_{j-1}\ \right)+h_j\beta(fu)_{j-\frac{1}{2}}\left(\delta v_j\ +\delta v_{j-1}\ \right)-$$
$$\beta f_{j-\frac{1}{2}}^2\left(\delta \mathrm{v}_j-\delta \mathrm{v}_{j-1}\ \ \right)-\beta f_{j-\frac{1}{2}}\left(\mathrm{v}_j-\mathrm{v}_{j-1}\right)\left(\delta f_j\ +\delta f_{j-1}\ \right)+M\frac{h_j}{2}\left(\delta u_j\ +\delta u_{j-1}\ \right)=(r_5)_{j-\frac{1}{2}}\quad(3.26)$$

$$\left(1+\frac{4}{3R_d}\right)\left(\delta t_j-\delta t_{j-1}\right)+\frac{h_jPr}{2}f_{j-\frac{1}{2}}\left(\delta t_j\ +\delta t_{j-1}\ \right)+\frac{h_jPr}{2}t_{j-\frac{1}{2}}\left(\delta f_j\ +\delta f_{j-1}\ \right)$$
$$+\frac{h_jPrNb}{2}t_{j-\frac{1}{2}}\left(\delta z_j\ +\delta z_{j-1}\ \right)+\frac{h_jPrNb}{2}z_{j-\frac{1}{2}}\left(\delta t_j\ +\delta t_{j-1}\ \right)$$
$$+h_jPrNtt_{j-\frac{1}{2}}\left(\delta t_j\ +\delta t_{j-1}\ \right)+\frac{h_jPrR}{2}\left(\delta s_j\ +\delta s_{j-1}\ \right)=(r_6)_{j-\frac{1}{2}}$$

$$\left(\delta z_j - \delta z_{j-1}\right) + \frac{h_j Le}{2} z_{j-\frac{1}{2}}\left(\delta f_j + \delta f_{j-1}\right) + \frac{h_j Le}{2} f_{j-\frac{1}{2}}\left(\delta z_j + \delta z_{j-1}\right) + \frac{Nt}{Nb}\left(\delta t_j - \delta t_{j-1}\right) - \frac{Leh_j K}{2}\left(\delta g_j + \delta g_{j-1}\right) = (r_7)_{j-\frac{1}{2}}$$

where $(r_1)_{j-\frac{1}{2}} = f_{j-1} - f_j + \frac{h_j}{2}\left(u_j + u_{j-1}\right)$

$$(r_2)_{j-\frac{1}{2}} = u_{j-1} - u_j + \frac{h_j}{2}\left(\mathrm{v}_j + \mathrm{v}_{j-1}\right)$$

$$(r_3)_{j-\frac{1}{2}} = s_{j-1} - s_j + \frac{h_j}{2}\left(t_j + t_{j-1}\right) \tag{3.27}$$

$$(r_4)_{j-\frac{1}{2}} = g_{j-1} - g_j + \frac{h_j}{2}\left(z_j + z_{j-1}\right)$$

$$(r_5)_{j-\frac{1}{2}} = -(\mathrm{v}_j - \mathrm{v}_{j-1}) - h_j(f\mathrm{v})_{j-\frac{1}{2}} + h_j u^2_{j-\frac{1}{2}} - 2h_j\beta(fu\mathrm{v})_{j-\frac{1}{2}} + \beta f^2_{j-\frac{1}{2}}\left(\mathrm{v}_j - \mathrm{v}_{j-1}\right) - h_j M u_{j-\frac{1}{2}} - E^2 h_j - MEh_j$$

$$(r_6)_{j-\frac{1}{2}} = -\left(1 + \frac{4}{3R_d}\right)\left(t_j - t_{j-1}\right) - Prh_j(f\mathrm{t})_{j-\frac{1}{2}} - Prh_j Nb(z\mathrm{t})_{j-\frac{1}{2}} - h_j Pr Nt t^2_{j-\frac{1}{2}} - Prh_j Q s_{j-\frac{1}{2}}$$

$$(r_7)_{j-\frac{1}{2}} = -\left(z_j - z_{j-1}\right) - Leh_j(f\mathrm{z})_{j-\frac{1}{2}} - \frac{Nt}{Nb}\left(\mathrm{t}_j - t_{j-1}\right) - Leh_j K g_{j-\frac{1}{2}}$$

$$\delta f_j - \delta f_{j-1} - \frac{h_j}{2}\left(\delta u_j + \delta u_{j-1}\right) = (r_1)_{j-\frac{1}{2}}$$

$$\delta u_j - \delta u_{j-1} - \frac{h_j}{2}\left(\delta \mathrm{v}_j + \delta \mathrm{v}_{j-1}\right) = (r_2)_{j-\frac{1}{2}}$$

$$\delta s_j - \delta s_{j-1} - \frac{h_j}{2}\left(\delta t_j + \delta t_{j-1}\right) = (r_3)_{j-\frac{1}{2}}$$

$$\delta g_j - \delta g_{j-1} - \frac{h_j}{2}\left(\delta z_j + \delta z_{j-1}\right) = (r_4)_{j-\frac{1}{2}}$$

$$a_1\delta \mathrm{v}_j + a_2\delta \mathrm{v}_{j-1} + a_3\delta f_j + a_4\delta f_{j-1} + a_5\delta u_j + a_6\delta u_{j-1} = (r_5)_{j-\frac{1}{2}}$$

$$b_1\delta t_j + b_2\delta t_{j-1} + b_3\delta f_j + b_4\delta f_{j-1} + b_5\delta z_j + b_6\delta z_{j-1} + b_7\delta s_j + b_8\delta s_{j-1} = (r_6)_{j-\frac{1}{2}} \tag{3.28}$$

$$c_1\delta z_j + c_2\delta z_{j-1} + c_3\delta f_j + c_4\delta f_{j-1} + c_5\delta t_j + c_6\delta t_{j-1} + c_7\delta g_j + c_8\delta g_{j-1} = (r_7)_{j-\frac{1}{2}}$$

Where $(a_1)_j = 1 + \frac{h_j}{2} f_{j-\frac{1}{2}} + h_j\beta(f\mathrm{u})_{j-\frac{1}{2}} - \beta f^2_{j-\frac{1}{2}}$

$$(a_2)_j = -1 + \frac{h_j}{2} f_{j-\frac{1}{2}} + h_j \beta (f\mathrm{u})_{j-\frac{1}{2}} + \beta f^2_{j-\frac{1}{2}}$$

$$(a_3)_j = (a_4)_j = \frac{h_j}{2} \mathrm{v}_{j-\frac{1}{2}} + h_j \beta (\mathrm{uv})_{j-\frac{1}{2}} - \beta f^2_{j-\frac{1}{2}} (\mathrm{v}_j - \mathrm{v}_{j-1} \ )$$

$$(a_5)_j = (a_6)_j = -\frac{h_j}{2} u_{j-\frac{1}{2}} + h_j \beta (f\mathrm{v})_{j-\frac{1}{2}} + \frac{M h_j}{2}$$

$$(b_1)_j = \left(1 + \frac{4}{3R}\right) + \frac{h_j Pr}{2} f_{j-\frac{1}{2}} + \frac{h_j Pr Nb}{2} z_{j-\frac{1}{2}} + h_j Pr Nt t_{j-\frac{1}{2}}$$

$$(b_2)_j = -\left(1 + \frac{4}{3R_d}\right) + \frac{h_j Pr}{2} f_{j-\frac{1}{2}} + \frac{h_j Pr Nb}{2} z_{j-\frac{1}{2}} + h_j Pr Nt t_{j-\frac{1}{2}} \tag{3.29}$$

$$(b_3)_j = (b_4)_j = \frac{h_j Pr}{2} \mathrm{t}_{j-\frac{1}{2}}$$

$$(b_5)_j = (b_6)_j = \frac{h_j Pr Nb}{2} \mathrm{t}_{j-\frac{1}{2}}, \quad (b_7)_j = (b_8)_j = \frac{h_j Pr R}{2}$$

$$(c_1)_j = 1 + \frac{h_j Le}{2} f_{j-\frac{1}{2}},$$

$$(c_2)_j = -1 + \frac{h_j Le}{2} f_{j-\frac{1}{2}}, (c_3)_j = (c_4)_j = \frac{h_j Le}{2} f_{j-\frac{1}{2}}$$

$$(c_5)_j = \frac{Nt}{Nb}, \ (c_6)_j = -(c_5)_j, \quad (c_7)_j = (c_8)_j = \frac{-h_j Le K}{2}$$

To complete the system (3.28) we recall the boundary conditions (3.23) which can be satisfied exactly with no iteration. Therefore, in order to maintain these correct values in all the iterates, we take

$\delta f_0 = 0, \ \delta u_0 = 0, \ \delta t_0 = 0, \ \delta u_J = 0,$ and $\delta s_J = 0.$

In general case equation (3.28) in vector matrix form;

$$[A][\delta] = [r] \tag{3.30}$$

Where

$$A=\begin{bmatrix} [A_1] & [C_1] & & & & & \\ [B_2] & [A_2] & [C_2] & & & & \\ & [B_3] & [A_3] & [C_3] & & & \\ & & \cdot & \cdot & \cdot & & \\ & & & \cdot & \cdot & \cdot & \\ & & & & \cdot & \cdot & \cdot \\ & & & & [B_{j-1}] & [A_{j-1}] & [C_{j-1}] \\ & & & & & [B_j] & [A_j] \end{bmatrix}, \quad \delta=\begin{bmatrix} [\delta_1] \\ [\delta_2] \\ \cdot \\ \cdot \\ \cdot \\ [\delta_{j-1}] \\ [\delta_j] \end{bmatrix}, r=\begin{bmatrix} [r_1] \\ [r_2] \\ \cdot \\ \cdot \\ \cdot \\ [r_{j-1}] \\ [r_j] \end{bmatrix}$$

In equation (3.28) the elements are defined by

$$[A_1]=\begin{bmatrix} 0 & 0 & 1 & 0 & 0 \\ -\frac{h_1}{2} & 0 & 0 & -\frac{h_1}{2} & 0 \\ 0 & -1 & 0 & 0 & -\frac{h_1}{2} \\ a_2 & 0 & a_3 & a_1 & 0 \\ 0 & 0 & b_3 & 0 & b_1 \end{bmatrix} \quad [A_j]=\begin{bmatrix} -\frac{h_j}{2} & 0 & 1 & 0 & 0 \\ -1 & 0 & 0 & -\frac{h_j}{2} & 0 \\ 0 & -1 & 0 & 0 & -\frac{h_j}{2} \\ a_6 & 0 & a_3 & a_1 & 0 \\ 0 & 0 & b_3 & 0 & b_1 \end{bmatrix} \quad 2 \le j \le J \qquad (3.31)$$

$$[B_j]=\begin{bmatrix} 0 & 0 & -1 & 0 & 0 \\ 0 & 0 & 0 & -\frac{h_j}{2} & 0 \\ 0 & 0 & 0 & 0 & -\frac{h_j}{2} \\ 0 & 0 & a_4 & a_2 & 0 \\ 0 & 0 & b_4 & 0 & b_2 \end{bmatrix} \quad 2 \le j \le J \quad [C_j]=\begin{bmatrix} -\frac{h_j}{2} & 0 & 0 & 0 & 0 \\ 1 & 0 & 0 & 0 & 0 \\ 0 & 1 & 0 & 0 & 0 \\ a_5 & 0 & 0 & 0 & 0 \\ 0 & 0 & 0 & 0 & 0 \end{bmatrix} \quad 1 \le j \le J-1 \quad (3.32)$$

$$[\delta_1]=\begin{bmatrix} \delta v_0 \\ \delta t_0 \\ \delta f_1 \\ \delta v_1 \\ \delta t_1 \end{bmatrix}, \quad [\delta_j]=\begin{bmatrix} \delta u_{j-1} \\ \delta s_{j-1} \\ \delta f_j \\ \delta v_j \\ \delta t_j \end{bmatrix} \quad 2 \le j \le J \qquad [r_j]=\begin{bmatrix} (r_1)_{j-\frac{1}{2}} \\ (r_2)_{j-\frac{1}{2}} \\ (r_3)_{j-\frac{1}{2}} \\ (r_4)_{j-\frac{1}{2}} \\ (r_5)_{j-\frac{1}{2}} \end{bmatrix} \qquad 1 \le j \le J \qquad (3.33)$$

To solve equation (3.30), we assume that A is nonsingular and can be factored in to

$$[A] = [L][U] \tag{3.34}$$

where

$$A = \begin{bmatrix} [\alpha_1] & & & & & \\ [B_2] & [\alpha_1] & & & & \\ & \cdot & \cdot & & & \\ & & \cdot & \cdot & & \\ & & & \cdot & [\alpha_{j-1}] & \\ & & & & [B_J] & [\alpha_J] \end{bmatrix}$$ and

$$U = \begin{bmatrix} [I] & [\Gamma_1] & & & & \\ & [I] & [\Gamma_2] & & & \\ & & \cdot & \cdot & & \\ & & & \cdot & \cdot & \\ & & & & [I] & [\Gamma_{j-1}] \\ & & & & & [I] \end{bmatrix}$$

where $[I]$ is the identity matrix of order 7 and $[\alpha_i]$ and $[\Gamma_i]$ are 7×7 matrices which elements are determined by the following equations:

$$[\alpha_1] = [A_1] \,, \tag{3.35}$$

$$[A_1][\Gamma_1] = [C_1] \,, \tag{3.36}$$

$$[\alpha_j] = [A_j] - [B_j][\Gamma_{j-1}] \,, \qquad j = 2,3, \ldots, J \tag{3.37}$$

$$[\alpha_j][\Gamma_j] = [C_j] \qquad\qquad j = 2,3, \ldots, J-1 \tag{3.38}$$

Equation (3.30) can now be substituted into Equation (3.34), and we get

$$[L][U][\delta] = [r] \tag{3.39}$$

If we define

$$[U][\delta] = [W] \tag{3.40}$$

Equation (3.39) becomes

$$[L][W] = [r] \tag{3.41}$$

where

$$W = \begin{bmatrix} [W_1] \\ [W_2] \\ \cdot \\ \cdot \\ \cdot \\ [W_{j-1}] \\ [W_J] \end{bmatrix},$$

and the [W_j] are 7 $\times$ 1 column matrices. The elements W can be solved from Equation (3.41):

$$[\alpha_1][W_1] = [r_1] \tag{3.42}$$

$$[\alpha_j][W_j] = [r_j] - [B_j][W_{j-1}] \qquad 2 \le j \le J \tag{3.43}$$

The step in which Γ_j, α_j and W_j are calculated is usually referred to as the forward sweep. Once the element of W are found, Equation (3.40) then gives the solution in the so-called backward sweep, in which the elements are obtained by the following relations:

$$[\delta_J] = [W_J] \tag{3.44}$$

$$[\delta_J] = [W_J] - [\Gamma_J][\delta_{j+1}] \qquad 1 \le j \le J-1 \tag{3.45}$$

These calculations are repeated until some convergence criterion is satisfied and calculations are stopped when

$$\left|\delta \mathrm{v}_0^{(i)}\right| \le \varepsilon_1 \tag{3.46}$$

Its exactness and heftiness have been confirmed by different investigators. We have compared our results with the investigators Shravani Ittedi et al. (2017) for a further check on the exactness of our numerical computations and have found to be in an admirable agreement.

3.4. Results and Discussions

This paper analyzed, the effects of slip and chemical reaction on upper-convected Maxwell fluid flow over a stretching sheet. Transfigured governing equations (3.11) - (3.13) with the boundary conditions (3.14) and (3.15) are coupled non-linear differential equations. Thus, it is impossible to solve directly with the analytical method. Therefore, to solve this coupled non-linear differential equations we use implicit finite difference (Keller Box) method by MatLabR2013a software. For various values of effective governing parameters such as suction-injection parameter χ, velocity ratio E, Deborah number β, magnetic field parameter M , velocity slip parameter υ, thermal slip parameter δ^*, solutal slip parameter γ_1, thermal radiation parameter R_d, Prandtl number Pr , Brownian motion parameter Nb, thermophoresis parameter Nt, Lewis number Le, chemical reaction parameter K and heat source parameter R the numerical solutions of velocity, temperature and concentration are obtained with step size $\Delta\eta = 0.1$. Unless otherwise the parameters are specified the values parameters are; $M = 1.0, \beta = 0.1, \upsilon = 0.1, \delta^* = 0.1, \gamma_1 = 0.1, Pr = 2.0, Le = 2.0, Nb = 0.1, \chi = 0.1, Nt = 0.1, R_d = 0.1, K = 0.1, R = 0.0, E = 0.1$. For this study the range of parameters are: $1 \le M \le 4$, $0 \le \beta \le 1$, $0 \le \chi \le 1.5$, $0 \le K \le 1$, $0.1 \le E \le 1.0$, $0.1 \le Nb \le 1.5$, $0.1 \le Nt \le 1.0$, $-1.5 \le R \le 0.0$, $2 \le Le \le 15$, $0 \le R_d \le 1.0$, $0.0 \le \upsilon \le 1.5$, $0 \le \delta^* \le 1.5$, $0 \le \gamma_1 \le 1.0$

Table3. 1: Comparison of skin friction coefficient $-\boldsymbol{f''(0)}$ for different values of magnetic field parameter $\boldsymbol{M}$ when $\boldsymbol{E = 0, \beta = 0, Le = 2.0, Pr = 2.0, K = 0.1}$

M	ShravaniIttedi et al. (2017)	Present Result
0.0	1.2104	1.2105
0.3	1.3578	1.3578
0.5	1.4475	1.4478
1.0	1.6500	1.6504

The comparison of the variation of the skin coefficient $-f''(0)$ for different values of magnetic field parameter M with respect to another study is presented on table 3.1. The values show that our result is an admirable agreement with the results given by researchers (Shravani Ittedi et al., 2017) in limiting conditions. Moreover, a comparison of heat and mass transfer rate for different values of δ^* and γ_1 is made in table 3.2 to check the accuracy of the numerical solution with (Shravani Ittedi et al. 2017) and we have found an admirable agreement with them. Therefore, we are assured that for the analysis of our problem the numerical method is appropriate .

For different values of χ, E, υ and β the variation of $-f''(0)$, $-\theta(0)$ and $-\phi(0)$ is given in table 3.3. From the table, when the suction-injection parameter χ and Deborah number β increase we see that skin friction coefficient increases, but decreases with an increase of velocity ratio E and velocity slip parameter υ . Moreover, the table shows that the local Nusselt number $-\theta'(0)$ and the local Sherwood number $-\phi'(0)$ of the flow field increase as the values of χ and E, whereas decrease with an upsurge of Deborah number β and velocity slip parameter υ.

Table3. 2: Comparison of Nusselt number $-\boldsymbol{\theta}'(\mathbf{0})$ and Sherwood number $-\boldsymbol{\phi}'(\mathbf{0})$ for different values of thermal slip parameter $\boldsymbol{\delta}^{*}$ and concentration slip parameter $\boldsymbol{\gamma}_{\mathbf{1}}$ when $\boldsymbol{E}=\mathbf{0}$, $\boldsymbol{\beta}=\mathbf{0}$, $\boldsymbol{Le}=\mathbf{2.0}, \boldsymbol{Pr}=\mathbf{2.0}$

δ^{*}	γ_1	Shravani Ittedi et al. (2017) (Nu_x)	Present Result	Shravani Ittedi et al. (2017) (Sh_x)	Present Result
0.0	0.1	0.7521	0.5720	0.5958	0.5957
0.3	0.1	0.5874	0.5873	0.6881	0.6880
0.5	0.1	0.5125	0.5120	0.7304	0.7304
1.0	0.1	0.3886	0.3886	0.8009	0.8008
0.1	0.1	0.6810	0.6810	0.7401	0.7401
0.1	0.3	0.6984	0.6984	0.4648	0.4648
0.1	0.5	0.7062	0.7062	0.3424	0.3423
0.1	1.0	0.7191	0.7190	0.1433	0.1432

Table3. 3: Calculation of skin friction coefficient $-\boldsymbol{f}''(\mathbf{0})$ local Nusselt number $-\boldsymbol{\theta}'(\mathbf{0})$ and local Sherwood number $-\boldsymbol{\phi}'(\mathbf{0})$ for different values of $\boldsymbol{\chi}, \boldsymbol{\upsilon}$ and $\boldsymbol{\beta}$ when $\boldsymbol{Nb}=\mathbf{0.1}, \boldsymbol{Nt}=\mathbf{0.1}$, $\boldsymbol{Pr}=\mathbf{2}, \boldsymbol{Le}=\mathbf{2}, \boldsymbol{R}=\mathbf{0.1}, \boldsymbol{\delta}^{*}=\mathbf{0.1}, \boldsymbol{\gamma}_{\mathbf{1}}=\mathbf{0.1}, \boldsymbol{K}=\mathbf{0.1}, \boldsymbol{R}=\mathbf{0.1}$

χ	E	υ	β	$-f''(0)$	$-\theta'(0)$	$-\phi'(0)$
0.0	0.1	0.1	0.1	0.3215	0.6207	0.5638
0.2	-----	-----	-----	1.4387	0.8159	0.6097
0.4	-----	-----	-----	1.5730	1.0272	0.6530
0.7	-----	-----	-----	1.8155	1.3669	0.7178
0.1	0.1	-----	-----	1.4761	0.6842	0.5587
-----	0.2	-----	-----	1.2672	0.7441	0.6138
-----	0.4	-----	-----	1.0091	0.7947	0.6619
-----	0.7	-----	-----	0.5233	0.8663	0.7310
-----	0.1	0.0	-----	1.3969	0. 7191	0.5886
-----	-----	0.2	-----	1.3244	0.7069	0.5835
-----	-----	0.4	-----	1.1418	0.6742	0.5703

-----	-----	0.7	-----	0.8121	0.6068	0.5449
-----	-----	0.1	0.0	1.3494	0.7209	0.5908
-----	-----	-----	0.2	1.4069	0.7111	0.5839
-----	-----	-----	0.4	1.4647	0.7016	0.5776
-----	-----	-----	0.7	1.5517	0.6879	0.5690

The influences of magnetic field parameter on flow velocity, temperature and concentration are displayed through figs.3.3-3.5. From the figures we have perceived that as magnetic field increased the velocity of the fluid decreased; in contrasts the temperature and concentration profiles demonstrated the behavior of increasing. These are because of the magnetic field offerings a retarding body force known as Lorentz force which performs transverse to the direction of the practical magnetic field. The boundary layer flow and the thickness of the momentum boundary layer are abridged by this body force. Similarly, because of Lorentz force is a fractional resistive force which opposes the fluid motion, it produces heat. Due to this fact the strongest the magnetic field the thickest thermal boundary layer and concentration boundary layer. Figs 3.6-3.8 reveal the characteristic of velocity, temperature and concentration profiles with respect to the variation in suction parameter χ. As the values of χ increase the temperature, velocity and concentration profiles diminution. The variations of chemical reaction parameter on concentration profile executed in fig.3.9.This figure gives a clear insight that increasing the value of chemical reaction the concentration in the boundary layer falls. This is due to the fact that chemical reaction in this system results in consumption of the chemical and hence results in decrease of concentration profile. The most important effect is that the first order chemical reaction has a tendency to diminish the overshoot in the profiles of the solute concentration in the solutal boundary layer. The influences of velocity ratio parameter on flow velocity and temperature profiles are revealed through figs.3.10 and 3.11. As the values of velocity ratio upsurges the boundary layer thickness rises and the flow has boundary layer structure. The graph of velocity is possible when the free steam velocity is less than or equal to the velocity of stretching sheet. That is when E is less than or equal to one. But as the value of velocity ratio parameter increases thermal boundary layer thickness decreases.

The influence of Brownian motion parameter on concentration and temperature profiles depicted through figs. 3.12 and 3.13. From the figures it can be seen that as the values of Brownian motion parameter raised the thermal boundary layer thickness increases whereas at the surface the temperature gradient deceases. But we witnessed an opposite result on the concentration profiles and concentration boundary layer thickness as Brownian motion parameter upsurges. Figs. 3.14 and 3.15 are devoted to demonstrate the impact of thermophoresis parameter on temperature and concentration profiles. From figures it is perceived that when thermophoresis parameter rises there is an improvement of the thermal and concentration boundary layer thickness. Fig. 3.16 plotted to examine the effects of heat generation / absorption parameter on temperature profiles. From the figure it can be seen that the temperature profiles increases as heat generation/ absorption parameter upsurges. This is because the thermal state of the fluid rises with an increasing the heat generation. Figs. 3.17 and 3.18 executed that the influence of Deborah number on velocity and temperature profiles. These figures give a clear perception that the velocity boundary thickness falls as the value of Deborah number increases whereas the thermal boundary layer thickness growths, as the values of Deborah number increase. This is because of the fact that as the values of Deborah number upsurges the force due to the parameter opposes the velocity flow and the declines thermal diffusivity in the boundary layer, which encourages the increase of temperature.

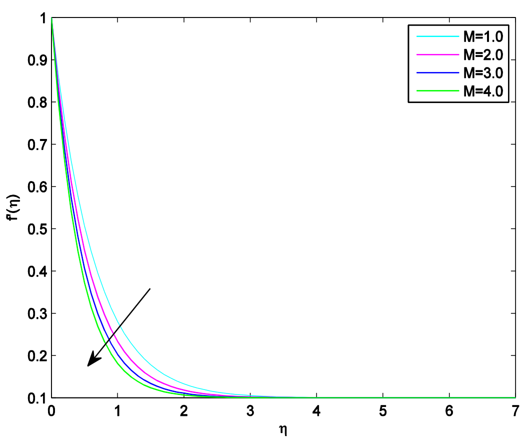

Figure3. 3: Velocity graph for various values of M

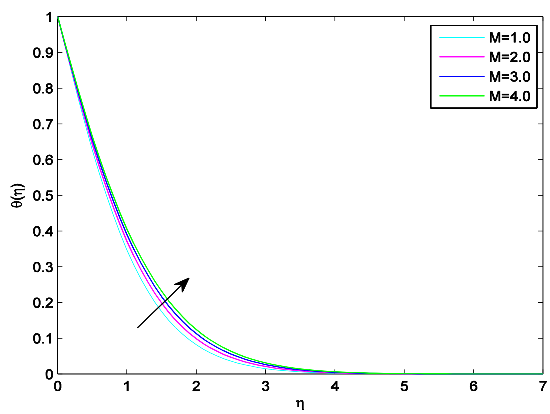

Figure3. 4: Temperature graph for various values oM

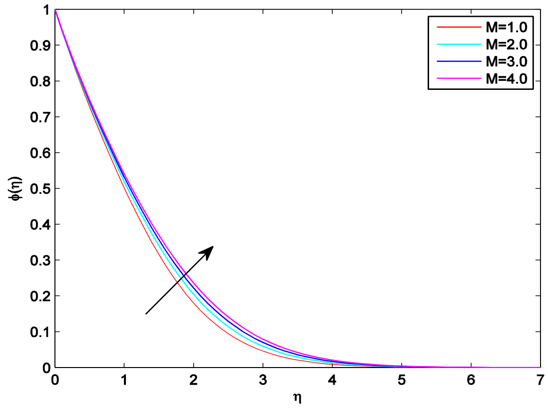

Figure3. 5: Concentration graph for various values of M

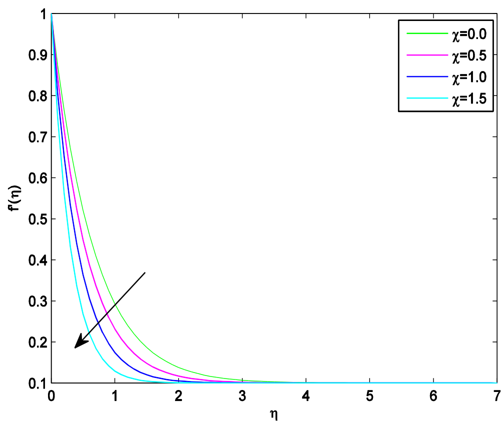

Figure3. 6: Velocity graph for various values of $\boldsymbol{\chi}$

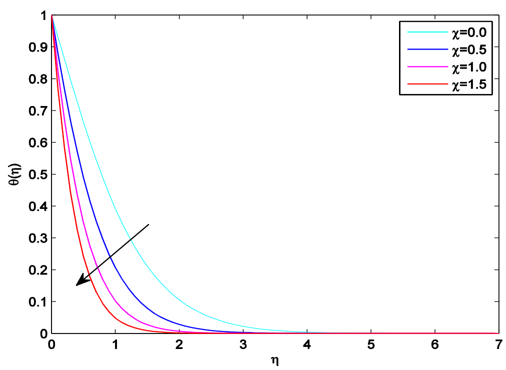

Figure3. 7: Temperature graph for various values of χ

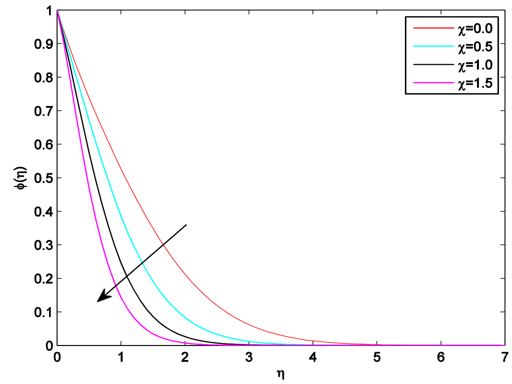

Figure3. 8: Concentration graph for various values of $\boldsymbol{\chi}$

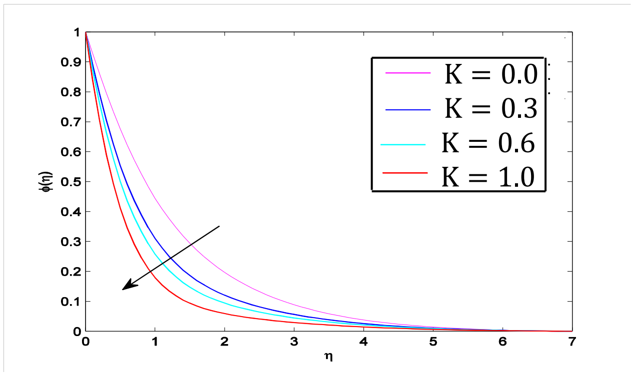

Figure3. 9: Concentration graph for various values of K

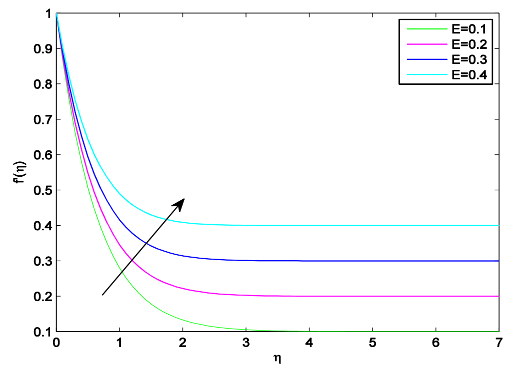

Figure3. 10: Velocity graph for various values of E

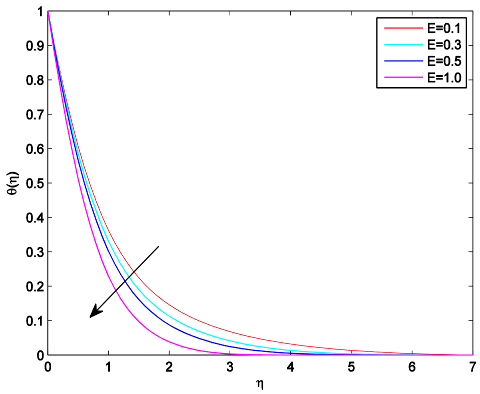

Figure3. 11: Temperature graph for various values of E

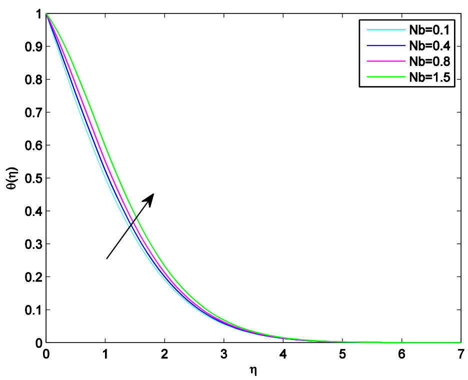

Figure3. 12: Temperature graph for various values of Nb

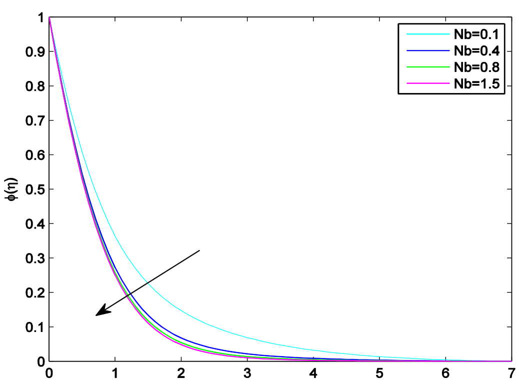

Figure3. 13: Concentraion graph for various values of Nb

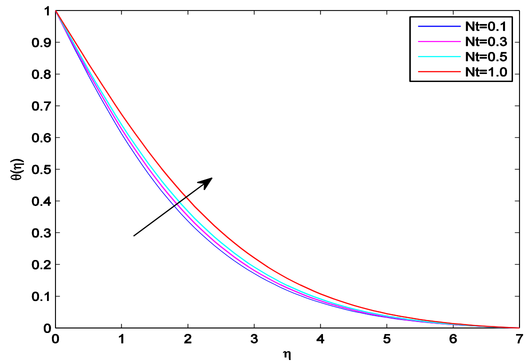

Figure3. 14: Temperature graph for various values of Nt

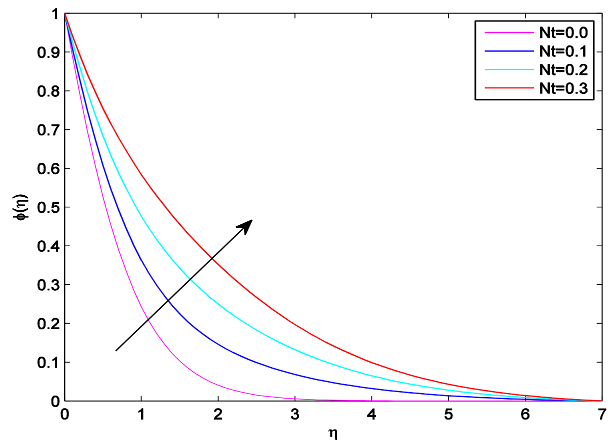

Figure3. 15: Concentration graph for various values of Nt

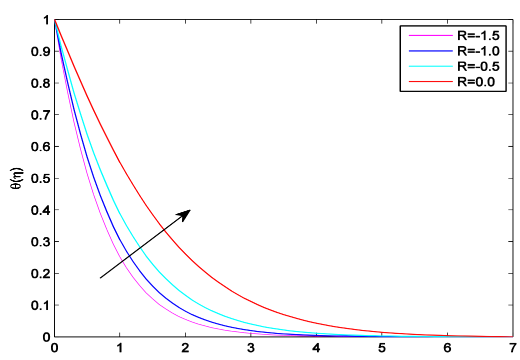

Figure3. 16: Temperature graph for various values of R

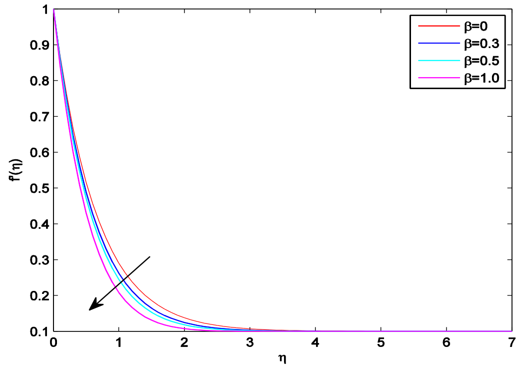

Figure3. 17: Velocity graph for various values of **β**

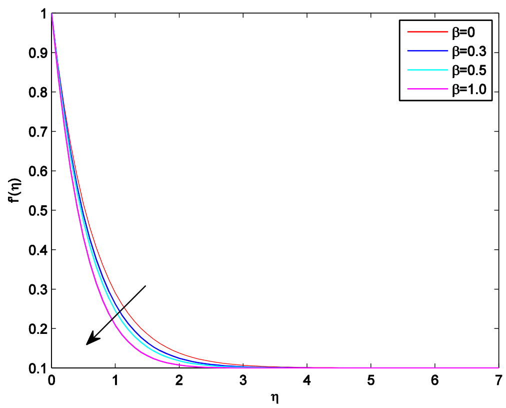

Figure3. 18: Temperature graph for various values of **β**

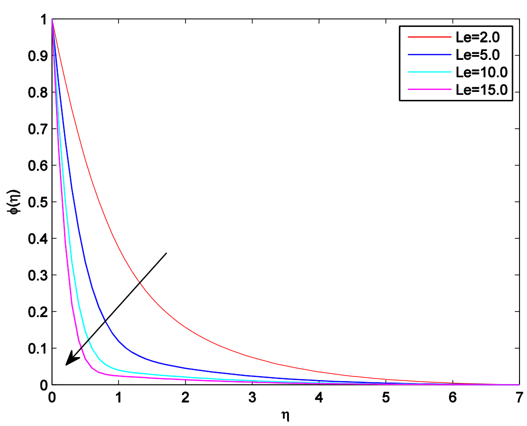

Figure3. 19: Concentration graph for various value of Le

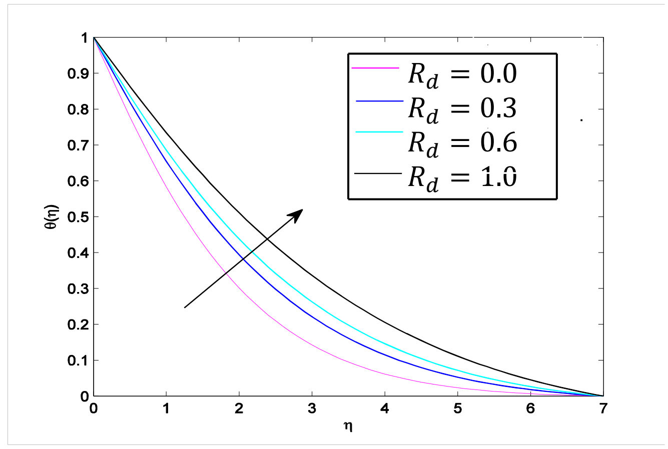

Figure3. 20: Temperature graph for various values of $\mathbf{R_d}$

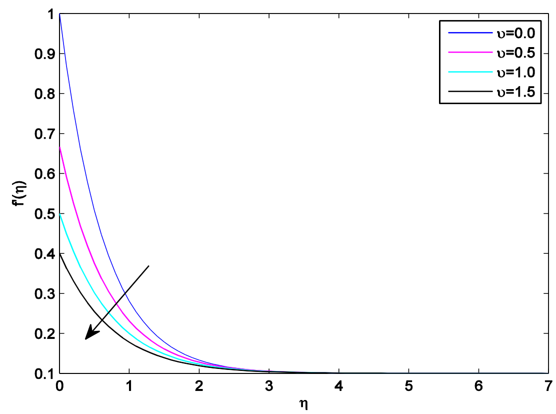

Figure3. 21: Velocity graph for various values of **υ**

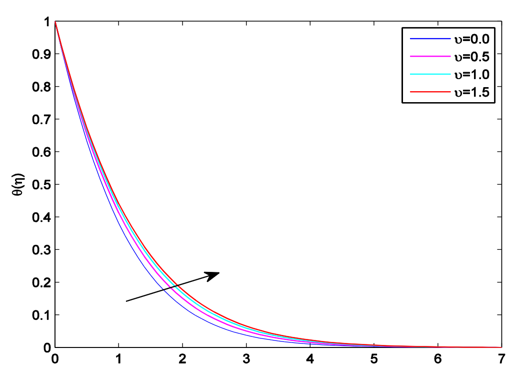

Figure3. 22: Temperature graph for various values of **υ**

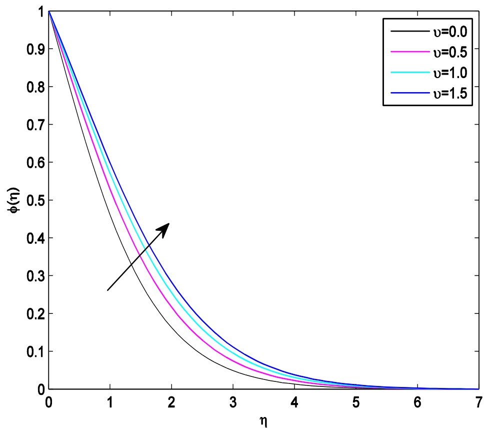

Figure3. 23: Concentration graph for various values of $\boldsymbol{\upsilon}$

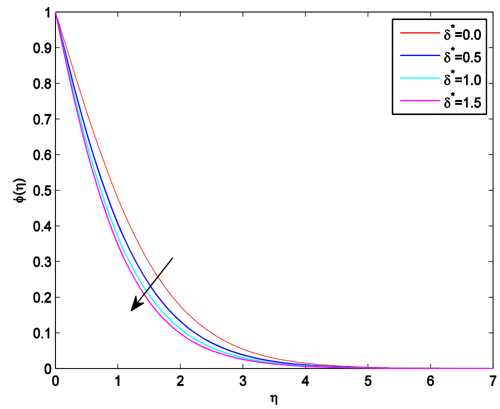

Figure3. 25: Concentration graph for various values of $\boldsymbol{\delta}^*$

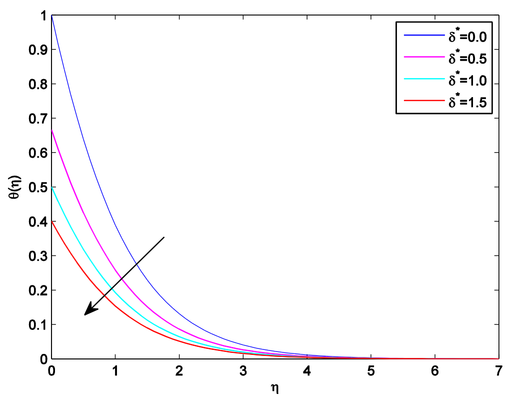

Figure3. 24: Temperature graph for various values of $\boldsymbol{\delta}^*$

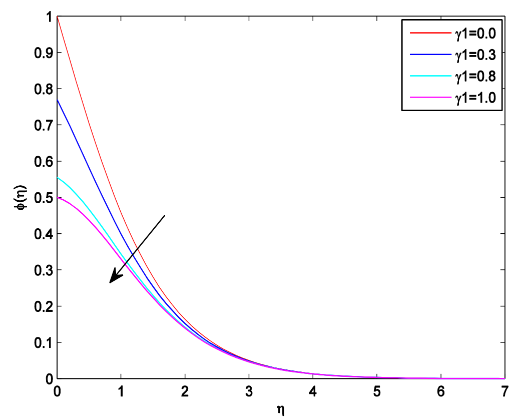

Figure3. 26: Concentration graph for various values of $\boldsymbol{\gamma_1}$

The impact of Lewis number on concentration profiles illustrated through fig. 3.19. From the figure it can be observed that higher values of Lewis number decrease the concentration graph and the concentration boundary layer thickness. The temperature curves for different values of thermal radiation parameter depicted in fig. 3.20. From the graph, it is possible to observe that as the values of thermal radiation parameter upsurge, the temperature graph and the temperature boundary layer thickness are snowballing.

The influences of velocity slip parameter on velocity, temperature and concentration profiles are portrayed in figs. 3.21-3.23. From the graphs it can be seen that as the value of velocity slip parameter upsurges, the velocity profiles decrease, but the temperature and concentration profiles are snowballing. This is due to the fact that as velocity slip rises the velocity of fluid decline because of the pulling of stretching sheet can transmit to the fluid. The Temperature and concentration profiles are presented in figs 3.24 and 3.25 for various values of thermal slip parameter. It is observed that as the values of thermal slip parameter increases both temperature and concentration profiles decline. A decrement of concentration profiles with an increment of concentration slip parameter is executed through fig.3.26. Basically this is due to the fact that slip retards the motion of the fluid which indicates a decline in concentration profiles.

3.5. Conclusions

This study presents MHD slip effect and stagnation point flow of upper-convected Maxwell fluid on a stretching sheet with chemical reaction. Depending on the governing parameters velocity ratio, suction-injection parameter, Lewis numbers, Deborah number, magnetic field, Brownian motion parameter, thermophoresis parameter, chemical reactions parameter, thermal radiation parameter, velocity slip parameter, thermal slip parameter, solutal slip parameter, and heat source parameter a similarity solution is obtained. The clarifications of the present study are précised as:

1. The suction-injection parameter on velocity, concentration and temperature profiles has shown a reduction.
2. When the magnetic field upsurges, then it reduces velocity profiles but it upsurge temperature and concentration profiles.
3. A velocity profile is reduced with rising values of Deborah number, whereas temperature profile is increased with an increasing value of Deborah number.
4. Temperature and concentration profiles are intensified with a snowballing a values of velocity slip parameter but velocity profiles is decreased.
5. By increasing the values of Brownian motion, chemical reaction, Lewis number, thermal slip parameter and solutal slip parameter then there is reduction in concentration profiles.
6. The thickness of thermal boundary layer augmented as thermal radiation parameter R_d upsurges.
7. Both rate of Nusselt number and rate of mass Sherwood number rise with suction-injection parameter χ and velocity ratio E, whereas declines with an increase of velocity slip parameter and Deborah number.

Reference

Abuzar Ghaffari, Tariq Javed & Fotini LABROPULU (2017).Oblique Stagnation Point Flow of a Non-Newtonian Nano-fluid over a stretching surface with radiation. Thermal Science. 21(5), 2139-2153.

Alireza Rahbari, Morteza Abbasi, Iman Rahimipetroudi, Bengt Sundén, Davood Domiri Ganji & Mehdi Gholami, (2018). Heat transfer and MHD flow of non-Newtonian Maxwell fluid through a parallel plate channel. *Mech. Sci.*. 9, 61–70. https://doi.org/10.5194/ms-9-61-2018.

Cebeci, T., & Bradshaw, P. (1984). Physical and computational aspects of convective heat transfer. *Springer−Verlag*, Berlin Heidelberg

Dian-Chen Lu, Ramzan, M., Bilal, M. Jae Dong Chung & Umer Farooq (2018). A Numerical Investigation of 3D MHD Rotating Flow with Binary Chemical Reaction, Activation Energy and Non-Fourier Heat Flux. *Commun. Theor. Phys*. 70, 89–96. DOI: 10.1088/0253-6102/70/1/89.

Dian-Chen Lu, M. Ramzan, M. Bilal, Jae Dong Chung, & Umer Farooq (2018). Upshot of Chemical Species and Nonlinear Thermal Radiation on Oldroyd-B Nanofluid Flow Past a Bi-directional Stretched Surface with Heat Generation/Absorption in a Porous Media. *Commun. Theor. Phys*. 70, 71–80. DOI: 10.1088/0253-6102/70/1/71.

Dianchen Lu, Ramzan M., Shafiq Ahmad, Jae Dong Chung, & Umer Farooq (2017). Upshot of binary chemical reaction and activation energy on carbon nanotubes with Cattaneo-Christov heat flux and buoyancy effects. *Physics of Fluids* 29, 123103. 1-14. https://doi.org/10.1063/1.5010171.

Dianchan Lu, Ramzan, M., Naeem Ullah, Jae Dong Chung & Umer Farooq (2017). Numerical treatment of radiative nanofluid 3D flow containing gyrotactic microorganism with anisotropic slip, binary chemical reaction and activation energy. *SCIENTIFIC REPORT*. 7:17008. 1-22. Doi: 10.1038/s41598-017-16943-9

Elsayed Mohamed Abdel Rahman Elbashbeshy, Khaled Mohamed Abdelgaber & Hamada Galal Asker. (2018). Heat and Mass Transfer of a Maxwell Nanofluid over a Stretching Surface with Variable Thickness Embedded in Porous Medium. *International Journal of Mathematics and Computational Science,* 4 (3), 86-98 http://www.aiscience.org/journal/ijmcs.

Gireesha, B.J., Mahanthesh, B., Rama Subba, & Reddy Gorla, Krupalakshmi K.L. (2018). Mixed convection two-phase flow of Maxwell fluid under the influence of non-linear thermal radiation, non-uniform heat source/sink and fluid-particle suspension. *Ain Shams Engineering Journal*. 9, 735–746. http://dx.doi.org/10.1016/j.asej.2016.04.020.

Ibrahim S.M., Lorenzini G., Vijaya Kumar P., & Raju, C.S.K.: (2017). Influence of chemical reaction and heat source on dissipative MHD mixed convection flow of a Casson nanofluid over a nonlinear permeable stretching sheet. *International Journal of Heat and Mass Transfer*. 111, 346–355.

Imran, M.A., Riaz, M.B., Shah N.A., & Zafar A.A. (2018). Boundary layer flow of MHD generalized Maxwell fluid over an exponentially accelerated infinite vertical surface with slip and Newtonian heating at the boundary. *Results in Physics*, 8, 1061-1067. https://doi.org/10.1016/j.rinp.2018.01.036.

Jayachandra Babu, M. & Sandeep, N. (2016). MHD non-Newtonian fluid flow over a slendering stretching sheet in the presence of cross-diffusion effects. *Alexandria Engineering Journal*, 55, 2193-2201. http://dx.doi.org/10.1016/j.aej.2016.06.009.

Khan, N.S., Zuhra, S., Shah, Z., Bonyah, E., Khan, W., & Islam, S., (2018). Eyring-Powell slip flow of nano liquid film containing graphene nanoparticles. *AIP Adv*., 8, 115302.

Krishnamurthy, M.R., Prasannakumara, B.C., & Gireesha B.J (2016). Effect of chemical reaction on MHD boundary layer flow and melting heat transfer of Williamson nanofluid in porous medium. *Engineering Science and Technology, an International Journal*. 19, 53-6. 1http://dx.doi.org/10.1016/j.jestch.2015.06.010.

Mabood, F., Shateyi,S. , Rashidi, M.M. , Momoniat, E. , & Freidoonimehr N. (2016). The impact of radiation and viscous dissipation on MHD stagnation point flow heat and mass transfer of nanofluids in porous medium with chemical reaction. *Advanced powder Technology*. 27,742-749. http://dx.doi.org/10.1016/j.apt.2016.02.033.

Madhu, Macha, Kishan, Naikoti & Ali J. Chamkha, (2016). MHD flow of a non-Newtonian nanofluid over a non-linearly stretching sheet in the presence of thermal radiation with heat source/sink. *Engineering Computations*, 33(5), 1610-1626. http://dx.doi.org/10.1108/EC-06-2015-0174.

Macha, Madhu, Naikoti Kishan & AliJ.Chamkha (2017). Unsteady flow of a Maxwell nanofluid over a stretching surface in the presence of magnetohydrodynamic and thermal radiation effects. *Propulsion and Power Research*, 6(1), 31–40. http://dx.doi.org/10.1016/j.jppr.2017.01.002.

Macha, Madhua & Naikoti Kishan (2015). Finite Element Analysis of MHD viscoelastic nanofluid flow over a stretching sheet with radiation. *Procedia Engineering*, 127, 432 – 439. doi: 10.1016/j.proeng.2015.11.393.

Macha, Madhu, Naikoti, Kishan, & Chamkha A.: (2016), Boundary layer flow and heat transfer of a non-Newtonian nanofluid over a non-linearly stretching sheet. *International Journal of Numerical Methods for Heat & Fluid Flow*, 26 (7), 2198-2217 (2016). http://dx.doi.org/10.1108/HFF-02-2015-0066.

Macha Madhu & Naikoti Kishan, (2017). MHD flow and heat transfer of Casson nanofluid over a wedge. *Mechanics & Industry*. 18, 210. http://dx.doi.org/10.1051/meca/2016030.

Madasi krishnaiah, Punnam, Rajendar, Vijayalaxmi, T., & Chenna Krishna Reddy, M. (2016). Effect of chemical reaction on MHD Stagnation point flow in Nanofluid over a Nonlinear Stretching sheet with viscous dissipation and slip conditions. *International Journal of Science, Engineering and Technology Research*. 5(12).

Mageswari, M., & Nirmala, M. (2016). Stagnation point flow over a stretching sheet with Newtonian heating using Laplace domain decomposition method. *International Journal of Pure and Applied Mathematics.* 110(1), 95-102. Doi: 10.12732/ijpam.v110i1.11.

Manjula, D. & Jayalakshmi, K. (2018). Slip effects on unsteady MHD and heat transfer flow over a stretching sheet embedded with suction in a porous medium filled with a Jeffrey fluid. *International Journal of Research*.7(8), 609-623. https://doi.org/10.1515/ijnsns-2016-0056.

Meysam Mohamadali & Nariman Ashrafi (2016). Similarity solution for high weissenberg number flow of upper-convected Maxwell fluid on a linearly stretching sheet. *Hindawi Publishing Corporation Journal of Engineering*. http://dx.doi.org/10.1155/2016/9718786.

Mohamed Abd El-Aziz & Ahmed, A. Afify (2018). Influences of Slip Velocity and Induced Magnetic Field on MHD Stagnation-Point Flow and Heat Transfer of Casson Fluid over a Stretching Sheet.

Nasir, S., Islam, S. Gul, T. Shah, Khan Z., M.A. Khan, W. Khan, A.Z. & Khan, S. (2018). Three-dimensional rotating flow of MHD single wall carbon nanotubes over a stretching sheet in presence of thermal radiation. *Appl. Nanosci,* 8, 1361–1378.

Omowaye, A. J. & Animasaun, I. L. (2016). Upper-Convected Maxwell Fluid Flow wit Variable Thermo-Physical Properties over a Melting Surface Situated in Hot Environment Subject to Thermal Stratification. *Journal of Applied Fluid Mechanics*, 9 (4), 1777-1790. DOI: 10.18869/acadpub.jafm.68.235.24939.

Raghawendra Mishra (2017). MHD slip effect of Jeffrey nanofluid flow over a stretching sheet in the presence of nonlinear thermal radiation and chemical reaction. *International journal of engineering sciences and research Technology.* 6(4).

Ramana Reddy, J.V., Anantha Kumar, K., Sugunamma, V., & Sandeep N. (2018). Effect of cross diffusion on MHD non-Newtonian fluids flow past a stretching sheet with non-uniform heat source/sink investigated," *Alexandria Engineering Journal*, 57, 1829-1838. http://dx.doi.org/10.1016/j.aej.2016.06.009.

Ramzan, M. & Bilal M. (2016). Three-dimensional flow of an elastico-viscous nanofluid with chemical reaction and magnetic field effects. *Journal of Molecular Liquids*. 215, 212–220. www.elsevier.com/locate/molliq.

Ramzan, M., Naeem Ullah, Jae Dong Chung, Dianchen Lu & Umer Farooq (2017). Buoyancy effects on the radiative magneto Micropolar nanofluid flow with double stratification, activation energy and binary chemical reaction. *Scientific Reports*. 7: 12901. 1-15. DOI:10.1038/s41598-017-13140-6.

Ramzan, M. Jae Dong Chung, & Naeem Ullah (2017). Radiative magnetohydrodynamic nanofluid flow due to gyrotactic microorganisms with chemical reaction and non-linear thermal radiation. *International Journal of Mechanical Sciences*. (1-29). http://dx.doi.org/10.1016/j.ijmecsci.2017.06.009.

Ramzan, M., M. Bilal, & Jae Dong Chung (2017). Radiative Williamson nanofluid flow over a convectively heated Riga plate with chemical reaction. 1-21. http://dx.doi.org/10.1016/j.cjph.2017.04.014.

Ramzan. M., Bilal, M.& Jae Dong Chung (2017). Soret and Dufour Effects on Three Dimensional Upper-Convected Maxwell Fluid with Chemical Reaction and Non-Linear Radiative Heat Flux. *International Journal of Chemical Reactor Engineering*. 1-17. DOI: 10.1515/ijcre-2016-0136.

Ramzan, M., Bilal, M., Shamsa Kanwal & Jae Dong Chung (2017). Effects of Variable Thermal Conductivity and Non-linear Thermal Radiation past an Eyring Powell Nanofluid Flow with Chemical Reaction. *Commun. Theor. Phys*. 67, 723–731. DOI: 10.1088/0253-6102/67/6/723

Ramzan, M. Muhammad Bilal & Jae Dong Chung (2017). Radiative Flow of Powell-Eyring Magneto-Nanofluid over a Stretching Cylinder with Chemical Reaction and Double Stratification near a Stagnation Point. *PLoS ONE*. 12(1), 1-19. doi:10.1371/journal.

Ramzan, M, Bilal, M, Chung & Jae Dong (2017). Numerical Simulation of Magnetohydrodynamic Radiative Flow of Casson Nanofluid with Chemical Reaction past a Porous Media. *Journal of Computational and Theoretical Nano science*. 14(12), 5788-5796. DOI: https://doi.org/10.1166/jctn.2017.7013.

Ramzan, M., Hina Gul & Jae Dong Chung (2017). Double stratified radiative Jeffery magneto nanofluid flow along an inclined stretched cylinder with chemical reaction and slip condition. *Eur. Phys. J. Plus*. 132: 456. 1-17. DOI 10.1140/epjp/i2017-11748-5.

Sajid, M., Ahmed, B., Abbas, & Z. (2014). Steady mixed convection stagnation point flow of MHD Oldroyd-B fluid over a stretching sheet. *Journal of the Egyptian Mathematical Society*. 23, 440-444. http://dx.doi.org/10.1016/j.joems.2014.05.013.

Sathies Kumar, P. & Gangadhar, K. (2015).Slip flow of MHD Casson fluid over a stretching sheet with heat, chemical reaction and mass transfer is investigated by Sathies Kumar. *Advances in Applied Science Research*. 6(8), 205-223.

Shravani Ittedi, Dodda Ramya, & Sucharitha (2017). Slip effect of MHD heat transfer of Nanofluids above a stretching sheet with chemical reaction. *International Journal of latest Engineering research and Application(IJLERA)*. 02(08), 10-20.

Srinivas, C., Reddy, Kishan, N., & Macha, Madhu, (2017). Finite Element Analysis of Eyring–Powell Nano Fluid Over an Exponential Stretching Sheet. *Int. J. Appl. Comput. Math.* 4(8), 1-13. https://doi.org/10.1007/s40819-017-0438-x

Srinivasulu, T. Shankar Bandari & Chenna Sumalatha (2017). The effect of Viscous Dissipation MHD Stagnation Point flow of casson Nano-Fluid over Stretching sheet. *Global Journar of Pure and applied mathematics*. 13(8), 0973-1768.

Tian, X., Li, B., & Hu, Z. (2018).Convective stagnation point flow of a MHD non-Newtonian nanofluid towards a stretching plate. Int. J. Heat Mass Transf. 127, 768–780.

Vajravelu, K., Ronald Li, Dewasurendra, M., Joseph Benarroch, Nicholas Ossi, Ying Zhang, Michael Sammarco & Prasad K. V. (2017). Analysis of MHD boundary layer flow of an Upper- Convected Maxwell fluid with homogeneous-heterogeneous chemical reactions. *Communications in Numerical Analysis*, 2, 202-216. doi:10.5899/2017/cna-00324.

Vijayalakshmi, R., Sreelakshmi, K., Sandhya, G. & Sarojamma, G. (2017). Flow of upper-convected Maxwell Micropolar fluid over a stretching sheet with slip effect. *International Journal of Innovative Research in Science, Engineering and Technology*, 6(13).

Wubshet, I. (2016). Magnetohydrodynamic stagnation point Flow and heat transfer of upper-convected Maxwell fluid past a stretching sheet in the Presence of nanoparticles with convective Heating. *Frontiers in Heat and Mass Transfer (FHMT).* 7(4). DOI: 10.5098/hmt.7.4.

Yasin A., Bandari Sh., & Srinivasulu, T. (2018). Numerical solution of stagnation point flows of nano fluid due to an inclined stretching sheet. *International Journal of Computational Engineering Research*. 8(2) 2250 – 3005.

Yu Bai, Yuehua Jiang, Fawang Liu & Yan Zhang, (2017). Numerical analysis of fractional MHD Maxwell fluid with the effects of convection heat transfer condition and viscous dissipation. *AIP Advances*, 7, 12530. https://doi.org/10.1063/1.5011789.

Chapter 4

Melting and Viscous Dissipation Effect on Upper-Convected Maxwell and Williamson Nanofluid

4.1. Introduction

An engineered fluid that can be used in modern high technological area with huge heat diffusivity capacity is called nanofluid. For the first time such fluid is experimental studied by (Choi and Eastman, 1995). The experimental result reveals the pumping powers during heat exchange were significantly reduced when nanofluid is involved in the processes. Das (2003), Pak and Choi (1998), Xuan and Li (2003) experimentally discovered that convectional fluid thermal conductivity can be elevated up 10-50 percent with addition of small amount of volumetric fraction of nanoparticles. The study further indicates that in common fluids, to improve the heat transfer by a factor of 2, the pumping power were increased by a factor of 10. The examinations of nanofluids were encompassing wide area of fluid dynamic studies. Accordingly, Ramesh and Gireesha (2017) have computed the impacts of nanofluid past a Riga plate with non-linear radiative heat transfer. Moreover, the influences of energy generation of Nano liquid past a disk were studied by (Mahanthesh et al., 2017). They reckoned out that the Nusselt number is boosted with an addition of nanoparticle. Furthermore, the influences of velocity slip on MHD flow of Eyring-Powel nanofluid past isothermal sphere were deliberated by (Swarnalathamma, 2018).The thermal performance of single-walled carbon nanotube nanofluid under turbulent flow conditions was investigated by (Olatomide Gbenga Fadodun et.al., 2019). Their results indicates that convective heat transfer (average Nusselt number) increases by 7.48% while the pressure drop and pumping power increase by 119% and 199%, respectively. Mathematical modeling of non-Newtonian fluid with chemical aspects via numerical technique was investigated by (Tasawar Hayat et al., 2017). IjazKhan et al. (2018) examined new thermodynamics of entropy generation minimization in the presence of nonlinear thermal radiation and nanomaterial. Adigoppula Raju and Odelu Ojjela (2019) examined the effects of the induced magnetic field motion on mixed convective Jeffrey nanofluid flow through a porous channel due to thermophoresis and Brownian. They found that when the values of viscoplastic Eyring-Powell fluid parameter increase the flow, thermal and concentration boundary layer thickness decelerates. The Brownian motion and thermophoresis aspects in nonlinear flow of micropolar nanoliquid over stretching surface have been investigated by (Hayat et al., 2017).

A substantial amount of experimental and theoretical work has been voted for to determine the role of natural convection in the kinetics of heat transfer escorted with melting or solidification effect. The study of heat transfer escorted by melting has received much attention because of its important applications in areas such as liquid polymer extrusion, frozen ground thawing, permafrost melting, casting and welding processes as well as phase change material, hot extrusion, polymers, ceramics, geothermal energy recovery, silicon wafer process, thermal insulation, etc. The dynamics of melting processes under different circumstances were described by (Roberts, 1958), (Tien and Yen, 1965)], (Epstein and Cho, 1976) and (Kairi and Murthy, 2009). The result reveals that melting enhances heat and mass transfer. Moreover, different researchers such as, Krishnamurthy et al. (2016), Kumar and Gireesha, 2018), Khan et al. (2017), Kairi and RamReddy (2015) and Babu and Narayana (2019) have discussed the influences of melting on non-Newtonian fluids like Williamson and Burgers fluid exposed to different physical conditions like porosity, radiation, etc. Still further, simultaneous effects of melting heat transfer and inclined magnetic field flow of tangent hyperbolic fluid over a nonlinear stretching surface with homogeneous-heterogeneous reactions was studied by (Sajid Qayyum et al., 2017).

As indicated in different literatures viscous dissipation is the unidirectional processes by which the work done by a fluid on adjacent layers due to the action of shear forces are transformed into heat. It has significant impact on heat transfer; especially for high-velocity flows, fluids with a moderate Prandtl number, highly viscous flows at moderate velocities and moderate velocities with small wall-to-fluid temperature difference. Accordingly, Pop (2010) and Yasin et al. (2015) remarked that energy dissipation and Joule heating in fluid dynamic has a great significance for the design of energy-conversion systems and energy-efficient circuits. Further, the impact of Joule heating, viscous dissipation and heat generation of fluid like Oldroyd B and Casson nanofluid has been discussed by (Kumar et al. 2018), (Reddy et al., 2107), (Ajayi et al., 2017) and (Yohannes and Shankar, 2013). A modified homogeneous-heterogeneous reaction for MHD stagnation flow with viscous dissipation and Joule heating was investigated by (Muhammad Imran Khan, 2017). Still further, Tasawar Hayat (2018) examined by Entropy generation in magnetohydrodynamic radiative flow due to rotating disk in presence of viscous dissipation and Joule heating.

In most industries nowadays the importance of non-Newtonian fluids dominates the Newtonian fluids. The rheological possessions of non-Newtonian fluids cannot be elucidated by the classical Naiver-Stokes equations. Also no single model is sufficient to describe non- Newtonian fluids characteristics. To overcome this difficulty several models have come into being. The rheological models that were proposed were Williamson, Cross, Ellis, power law, Carreau fluid model, etc. Typical of a non-Newtonian fluid model with shave retreating property is Williamson fluid model and was first projected by (Williamson, 1919). The examination of Williamson fluid has been carried out by researchers such as, Dapra and Scarpi (2007), Reddy et al. (2017), Sreelakshmi et al. (2017), Talha et al. (2018), Immaculate et al. (2016), Eswaramoorthi et al. (2017) and AL-Qaissy and Abdulhadi (2017) past different physical geometry like stretching surface, vertical porous plate and asymmetric channels. Furthermore, Magnetohydrodynamic bio convective flow of Williamson nanofluid containing gyro tactic microorganisms subjected to thermal radiation and Newtonian conditions was studied by (Salma Zaman and Mahwish Gul, 2019). Still further Tasawar Hayata et al. (2017) studied mathematical modeling of non-Newtonian fluid with chemical aspects. From their simulation it can be seen that increasing values of Sc enhance the concentration field but opposite trend is seen for higher values of K_1 and K_2.

A Maxwell fluids model can predict the stress lessening and become the most popular model. This model excludes the complicated effects of shear-dependent viscosity and thus enables us to focus merely on the effects of fluid's elasticity on the characteristics of its boundary layer. Typically, many researchers have been studied non- Newtonian upper-convected Maxwell fluid flows. Accordingly, the slip effect on non-Newtonian upper-convected Maxwell and Micropolar fluid flow over a stretching sheet were studied by (Vijayalakshmi et al., 2017). Further, the study of the influence of cross diffusion on Casson and Maxwell fluid flows past a stretching surface was examined by (Kumaran et al., 2017). In a porous medium mass and heat transfer of a non-Newtonian Maxwell nanofluid above a stretching surface with variable thickness was investigated by (Elbashbeshy et al., 2017). With variable thermo-physical possessions mass and heat transfer of upper convected Maxwell fluid flow properties over a horizontal melting surface were studied by (Kolawole et al., 2015). The result indicated when thermal conductivity parameter increases the temperature of the fluid increases. Hayat et al. (2016) investigated the effect of Cattaneo-Christov heat flux stagnation point flow with homogeneous-heterogeneous reactions. Muhammad Imran Khana et al. (2017) studied the influence of chemically reaction on the flow of Maxwell liquid with variable ticked surface. The heat, mass and motile microorganisms transfer rates in the convective stretched flow of Maxwell fluid consisting of nanoparticles and gyrotactic microorganisms were studied by (Ijaz Khan et al., 2017). From their result it is observed that thermal, concentration and motile density stratification parameters result in the reduction of temperature, concentration and motile microorganisms' density distributions respectively.

In view of all the above mentioned studies, it is decided that impacts of melting and viscous dissipation on boundary flow of upper-convected Maxwell and Williamson nanofluids in porous medium with chemical reaction is not inspected yet. Thus, to fill this gap, the main object of this paper is to explore the effect of melting heat transfer and viscous dissipation on boundary flow of upper-convected Maxwell and Williamson nanofluids in porous medium with chemical reaction. For the information our work is innovative in terms of the proposed fluids and incorporated parameters in the boundary layer flow. By employing appropriate similarity transformations the nonlinear coupled dimensionless equations from the governing equations are achieved. Finally, the resulting dimensionless equations are solved computationally by instigating the Keller Box method via MATLAB software. We scrutinize the influence of dimensionless melting, magnetic field, Thermal radiation, chemical reaction, Brownian motion, Thermophoresis, permeability parameter, Prandtl number, Eckert number and Lewis number on Williamson and Maxwell nanofliuds that are derived from the governing equations. From the result we observed that the dimensionless melting parameter affects highly the velocity boundary layer of Williamson nanofluid when compared with upper-convected Maxwell nanofliud.

The rest of this problem is structured as follows. The second section describes statement of the problem and mathematical formulation. Solution of methodology and scheme of methodology are provided under section 3. Section 4 tells us that result and discussion of the paper. Conclusion is provided under section 5. Finally, under section 6 references are provided.

4.2. Mathematical formulation

The main theme in this problem is based on a time independent flow of an upper-convected Maxwell and Williamson nanofluid with melting heat transfer, chemical reaction and viscous dissipation effect past a stretching surface embedded in porous medium. The study considered uniform stretching velocity u_w and the uniform free stream velocity u_e in the similar direction as revealed in fig.4.1. Above the stretching sheet the concentration and the ambient concentration respectively represented by C_w and C_∞. The melting surface of wall subjected to fixed temperature T_m and the free stream condition T_∞ with $T_\infty > T_m$ is considered. Also, thermal radiation influence is taken into account. The Williamson fluid model essential equations are specified as follows:

$$S = -pI + \tau, \tag{4.1}$$

$$\tau = \left[\mu_\infty + \frac{\mu_0 - \mu_\infty}{1 - \Gamma\dot{\gamma}}\right] A_{1,} \tag{4.2}$$

where p is pressure, I is identity vector, S is the Cauchy stress tensor, τ is extra stress tensor, μ_0 and μ_∞ are the limiting viscosities at zero and at infinite shear rate, $\Gamma > 0$ is the time constant, A_1 is the first Rivlin-Ericson tensor and $\dot{\gamma}$ is defined as follows

$$\dot{\gamma} = \sqrt{\frac{\pi}{2}}, \pi = trace(A_1^2), . \tag{4.3}$$

where π is the second invariant strain tensor. Here we have only considered the case for which $\mu_\infty = 0$ and $\Gamma\dot{\gamma} < 1$. Then we obtain

$$\tau = \left[\frac{\mu_0}{1 - \Gamma\dot{\gamma}}\right] A_1 \text{ or } \tau = \mu_0(1 - \Gamma\dot{\gamma}) A_{1.} \tag{4.4}$$

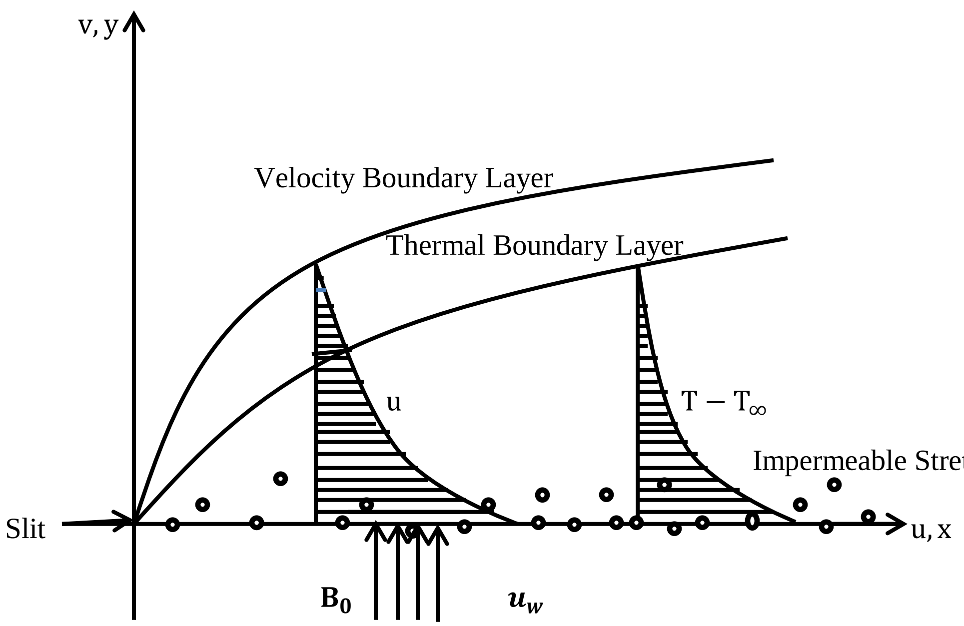

Figure4. 1: Physical Model and Coordinate system

Under these assumptions the governing equations can be described in Cartesian system as listed below.

$$\frac{\partial u}{\partial x}+\frac{\partial v}{\partial y}=0, \tag{4.5}$$

$$u\frac{\partial u}{\partial x}+v\frac{\partial u}{\partial y}=\nu\frac{\partial^2 u}{\partial y^2}+\sqrt{2}\nu\Gamma\frac{\partial u}{\partial y}\frac{\partial^2 u}{\partial y^2}-\xi\left(u^2\frac{\partial^2 u}{\partial x^2}+v^2\frac{\partial^2 u}{\partial y^2}+2uv\frac{\partial^2 u}{\partial x\,\partial y}\right)+u_e\frac{\partial u_e}{\partial x}+\frac{\sigma B_0^2}{\rho_f}\left(\xi v\frac{\partial u}{\partial y}+u\right)-\frac{\nu}{k'}u, \tag{4.6}$$

$$u\frac{\partial T}{\partial x}+v\frac{\partial T}{\partial y}=\alpha_m\frac{\partial^2 T}{\partial y^2}+\omega\left\{D_B\frac{\partial C}{\partial y}\frac{\partial T}{\partial y}+\frac{D_\tau}{T_\infty}\left(\frac{\partial T}{\partial y}\right)^2\right\}-\frac{1}{(\rho c_p)_f}\frac{\partial q_r}{\partial y}+\frac{\nu}{\rho_f}\left(\frac{\partial u}{\partial y}\right)^2, \tag{4.7}$$

$$u\frac{\partial C}{\partial x}+v\frac{\partial C}{\partial y}=D_B\frac{\partial^2 C}{\partial y^2}+\frac{D_\tau}{T_\infty}\frac{\partial^2 T}{\partial y^2}-K_r(C-C_\infty). \tag{5.8}$$

The appropriate boundary conditions are:

$$u=u_w=ax,\qquad T=T_m,\qquad C=C_w\qquad \text{at } y=0, \tag{4.9}$$

$$u\to 0,\ \ T\to T_\infty,\ \ C\to C_\infty\quad \text{as}\ \ y\to\infty,\quad \text{and}\ \ k\left(\frac{\partial u}{\partial y}\right)_{y=0}=\rho[\varphi+c_s(T_m-T_\infty)]v(x,0). \tag{4.10}$$

where u and v are the velocity components along the x and y directions respectively, ρ_f the density of the base fluid, $\alpha_m = \frac{k}{\rho c_f}$ the thermal diffusivity, ξ is the relaxation time parameter of the fluid, B_0 is the strength of the magnetic field, ν is the kinematic viscosity of the fluid, k is the thermal conductivity of the fluid, D_B is the Brownian diffusion coefficient, D_τ is the thermophoretic diffusion coefficient,$\omega = \frac{(\rho c)_p}{(\rho c)_f}$ is the ratio between the effective heat capacity of the nanoparticle material and heat capacity of the fluid, c is the volumetric volume expansion coefficient and ρ is the density of the particles, k' is the permeability of porous medium, φ is the latent heat of the fluid and c_s is the heat capacity of the solid surface, c_f is the heat capacity of the fluid, σ is electrical conductivity. We can write for the radiation using Rosseland approximation

$$q_r=-\frac{4\sigma^*}{3k^*}\frac{\partial T^4}{\partial y}, \tag{4.11}$$

where σ^* is the Stefan-Boltzman constant, k^* is the absorption constant. Assuming the temperature difference within the flow such that T^4 may be expanded in a Taylor series about T_∞ and neglecting higher orders we get $T^4=4TT_\infty^3-3T_\infty^4$,

Hence

$$\frac{\partial q_r}{\partial y}=-\frac{16\sigma^* T_\infty^3}{3k^*}\frac{\partial^2 T}{\partial y^2}. \tag{4.12}$$

Introducing similarity transformations

$$\psi = \sqrt{a\nu} f(\eta), \quad \theta(\eta) = \frac{(T - T_\infty)}{(T_w - T_\infty)}, \quad \phi(\eta) = \frac{(C - C_\infty)}{(C_w - C_\infty)}, \ \eta = \sqrt{\frac{a}{\nu}} y. \tag{4.13}$$

We choose the stream function $\psi(x, y)$ such that

$$\frac{\partial \psi}{\partial y} = u, \text{ and } -\frac{\partial \psi}{\partial x} = v. \tag{4.14}$$

By applying the similarity transformation in equation (4.13) equations (4.6-4.8) are transformed into the non-dimensional ordinary differential equation form as follows:

$$f''' + (\beta M + 1) f f'' - f'^2 + \beta(2 f f' f'' - f^2 f''') + \lambda f'' f''' - (M + d) f' = 0, \tag{4.15}$$

$$(1 + \tfrac{4}{3} R_d)\theta'' + Pr\{f\theta' + Nb\phi'\theta' + Nt\theta'^2 + Ecf''^2\} = 0, \tag{4.16}$$

$$\phi'' + Lef\phi' + \frac{Nt}{Nb}\theta'' - KLe\phi = 0. \tag{4.17}$$

With corresponding boundary conditions

$$f'(\eta) = 1, \quad m\theta'(\eta) + Prf(\eta) = 0, \ \theta(\eta) = 0, \quad \phi(\eta) = 0, \text{ at } \eta = 0, \tag{4.18}$$

$$f'(\eta) \to 0, \theta(\eta) \to 1, \ \phi(\eta) \to 1, \text{ as } \eta \to \infty. \tag{4.19}$$

where f' is dimensionless velocity, θ is dimensionless temperature, ϕ is dimensionless concentration and η is the similarity variable. The prime denotes differentiation with respect to η. The overall governing parameters are defined as;$\lambda = \sqrt{\frac{2a^3}{\nu}} x\Gamma$ is non- Newtonian Williamson parameter, $d = \frac{\nu}{k\prime}$ is permeability parameter, $\beta = \xi a$ is Deborah number, $M = \frac{\sigma B_0^2}{a\rho}$ is magnetic field parameter, $R_d = \frac{4\sigma^* T_\infty^3}{kk^*}$ is thermal radiation parameter, $k = \alpha_m(\rho c)_f$ is thermal conductivity, $Pr = \frac{\nu}{\alpha_m}$ is Prandtl number, $Nb = \frac{\omega D_{B(C_w - C_\infty)}}{\nu}$ is Brownian motion parameter, $Nt = \frac{\omega D_\tau (T_w - T_\infty)}{T_\infty \nu}$ is thermophoresis parameter, $Le = \frac{\nu}{D_B}$ is Lewis number, $K = \frac{K_r}{a}$ is chemical reaction parameter, $Ec = \frac{u_w^2}{c_p(T_\infty - T_m)}$ is Eckert number, $m = \frac{c_{f(T_\infty - T_m)}}{\varphi + c_s(T_m - T_0)}$ is dimensionless melting parameter.

The skin friction C_f, local Nusselt number Nu_x and the Sherwood number Sh_x are the important physical quantities of interest in this problem which are defined as

$$C_f = \frac{\tau_w}{\rho u_w^2}, \quad Nu_x \frac{x q_w}{k(T_\infty - T_m)}, \quad Sh_x = \frac{x q_m}{D_B(C_\infty - C_w)}, \tag{4.20}$$

Here $\tau_w = \mu(1+\beta)\left(1 + \frac{\Gamma}{\sqrt{2}}\frac{\partial u}{\partial y}\right)\frac{\partial u}{\partial y}$ at $y = 0$ is the surface shear stress, $q_w = -k\left(\frac{\partial T}{\partial y}\right)_{(y=0)} + q_r$ is the surface heat flux and $q_m = -D_B\left(\frac{\partial C}{\partial y}\right)_{(y=0)}$ is the surface mass flux.

$$C_f Re_x^{\frac{1}{2}} = (1+\beta)\left(f''(0) + \frac{\lambda}{2} f''^2(0)\right), -\left(1 + \frac{4}{3}R_d\right)\theta'(0) = Nu_x Re_x^{-\frac{1}{2}}, -\phi(0) = Sh_x Re_x^{-\frac{1}{2}}, \tag{4.21}$$

where $Re_x^{\frac{1}{2}} = \frac{x u_w(x)}{\nu}$ is local Reynolds number.

4.3. Solution Methodology

4.3.1. Keller Box Method

The transformed ordinary differential equations (4.15), (4.16) and (4.17) subject to boundary conditions (4.18) and (4.19) are solved numerically using an implicit finite difference method (Keller box) in combination with the Newton linearization techniques.

Accuracy and strength of this method has been confirmed by different investigators. We have compared our results with the investigators (Krishnamurthy et al., 2016) for a further check on the exactness of our numerical computations and we have found an admirable agreement.

4.3.2.The Finite Difference Scheme

We write the governing third order momentum equation (4.15) and second order energy and concentration equations (4.16) and (4.17) in terms of a first order equations. For this purpose we introduce new dependent variable $\mathrm{u, v, t}, \theta = \mathrm{s}(\mathrm{x}, \eta), \phi(\eta) = \mathrm{g}(\mathrm{x}, \eta)$ such that $\mathrm{f}' = \mathrm{u}, \mathrm{u}' = \mathrm{v}, \mathrm{s}' = \mathrm{t}$, and $\mathrm{g}' = \mathrm{z}$.

Thus equations (4.15), (4.16), and (4.17) can be written as

$$\mathrm{v}' + \mathrm{fv} - \mathrm{u}^2 + \lambda \mathrm{vv}' - (\mathrm{M} + \mathrm{d})\mathrm{u} + \beta(2\mathrm{fuv} - \mathrm{f}^2\mathrm{v}') = 0, \tag{4.22}$$

$$(1 + \tfrac{4}{3}\mathrm{R}_d)\mathrm{t}' + \mathrm{Prft} + \mathrm{PrNbzt} + \mathrm{PrNtt}^2 + \mathrm{PrEcv}^2 = 0, \tag{4.23}$$

$$z' + \text{Lefz} + \frac{\text{Nt}}{\text{Nb}} t' - \text{KLeg} = 0. \tag{4.24}$$

The boundary conditions are

$$u(\eta) = 1,\ \ mt(0) + Prf(0) = 0, s(0) = 0, \quad g(\eta) = 0, \text{ at } \ \eta = 0, \tag{4.25}$$

$$u(\eta) \to 0, s(\eta) \to 1,\ \ g(\eta) \to 1, \text{as } \eta \to \infty. \tag{4.26}$$

where prime denotes the differentiation with respect to η.

We know consider the net rectangle in the $x - \eta$ plane shown in figure 4.2 and the net points defined as below

$x^0 = 0, \qquad x^i = x^{i-1} + k_i, \qquad i = 1,2,3, \dots, I,$

$\eta_0 = 0, \qquad \eta_j = \eta_{j-1} + h_j, \qquad j = 1,2,3, \dots, J, \qquad \eta_j = \eta_\infty.$

where k_i is the Δx-spacing and h_j is the $\Delta\eta$-spacing. Here i and j are the sequence of numbers that indicate the coordinate location, not tensor indices or exponents.

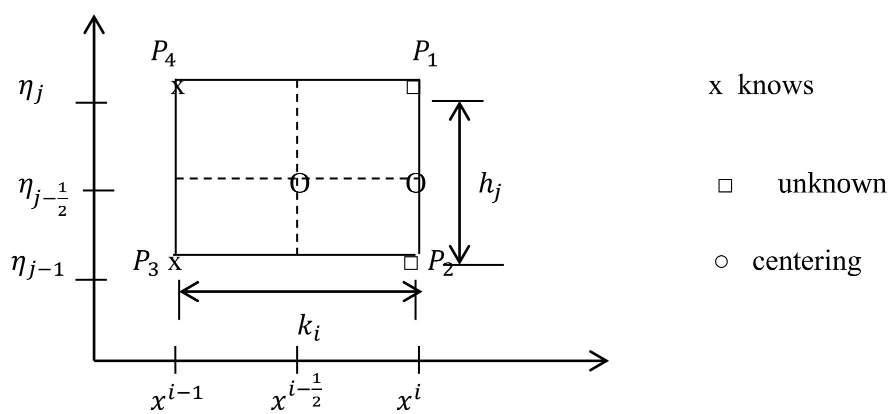

Figure4. 2: Net rectangle for difference approximations

Since only first derivatives appear in the governing equations, centered differences and two-point averages can be constructed involving only the four corner nodal values of the 'box'.

Now write the finite difference approximations for first order ordinary differential equation for the mid-point $\left(x^i, \eta_{j-\frac{1}{2}}\right)$ of the segment P_1P_2 using centered difference derivatives. This process is called centering about $\left(x^i, \eta_{j-\frac{1}{2}}\right)$. We get

$$f_j - f_{j-1} - \frac{h_j}{2}\left(u_j + u_{j-1}\right) = 0,$$

$$u_j - u_{j-1} - \frac{h_j}{2}\left(\mathrm{v}_j + \mathrm{v}_{j-1}\right) = 0,$$

$$s_j - s_{j-1} - \tfrac{h_j}{2}\left(t_j + t_{j-1}\right) = 0,$$

$$g_j - g_{j-1} - \tfrac{h_j}{2}\left(z_j + z_{j-1}\right) = 0, \tag{4.27}$$

$$\left(\mathrm{v}_j - \mathrm{v}_{j-1}\right) + \tfrac{h_j}{4}\left(f_j + f_{j-1}\right)\left(\mathrm{v}_j + \mathrm{v}_{j-1}\right) - \tfrac{h_j}{4}\left(u_j + u_{j-1}\right)^2 + \tfrac{h_j\beta}{4}\left(f_j + f_{j-1}\right)\left(u_j + u_{j-1}\right)\left(\mathrm{v}_j + \mathrm{v}_{j-1}\right) \; - \tfrac{\beta}{4}\left(f_j + f_{j-1}\right)\left(f_j + f_{j-1}\right)\left(\mathrm{v}_j - \mathrm{v}_{j-1}\right) + \tfrac{\lambda}{2}\left(\left(\mathrm{v}_j + \mathrm{v}_{j-1}\right)\left(\mathrm{v}_j - \mathrm{v}_{j-1}\right)\right) - \tfrac{h_j}{2}(M+d)\left(u_j + u_{j-1}\right) = Q_{j-\frac{1}{2}},$$

$$\left(1 + \frac{4}{3}R_d\right)\left(t_j - t_{j-1}\right) + \frac{h_j Pr}{4}\left(f_j + f_{j-1}\right)\left(t_j + t_{j-1}\right) + \frac{h_j PrNb}{4}\left(z_j + z_{j-1}\right)\left(t_j + t_{j-1}\right) + \frac{h_j PrNt}{4}\left(t_j + t_{j-1}\right)\left(t_j + t_{j-1}\right) + \frac{h_j PrEc}{4}\left(v_j + v_{j-1}\right)^2 = T_{j-\frac{1}{2}},$$

$$\left(z_j - z\right) + \frac{h_j Le}{4}\left(f_j + f_{j-1}\right)\left(\mathrm{z}_j + z_{j-1}\right) + \frac{Nt}{Nb}\left(t_j - t_{j-1}\right) - \frac{Leh_j h}{2}\left(g_j + g_{j-1}\right) = S_{j-\frac{1}{2}},$$

where $Q_{1-\frac{1}{2}} = -\left(\mathrm{v}_j - \mathrm{v}_{j-1}\right) - h_j(f\mathrm{v})_{j-\frac{1}{2}} + h_j(u^2)_{j-\frac{1}{2}} - 2\beta h_j(fu\mathrm{v})_{j-\frac{1}{2}} + \frac{\beta}{4}(f^2)_{j-\frac{1}{2}}\left(\mathrm{v}_j - \mathrm{v}_{j-1}\right) - \lambda v_{j-\frac{1}{2}}\left(\mathrm{v}_j - \mathrm{v}_{j-1}\right) + (M{+}d)h_j(u)_{j-\frac{1}{2}}$,

$$T_{j-\frac{1}{2}} = -\left(1 + \tfrac{4}{3}R_d\right)\left(t_j - t_{j-1}\right) - h_j Pr(f\mathrm{t})_{j-\frac{1}{2}} - h_j PrNb(zt)_{j-\frac{1}{2}} - \beta h_j(t^2)_{j-\frac{1}{2}} - h_j PrEc(v^2)_{j-\frac{1}{2}},$$

$$S_{j-\frac{1}{2}} = -\left(z_j - z_{j-1}\right) - h_j(f\mathrm{z})_{j-\frac{1}{2}} - \frac{Nt}{Nb}\left(t_j - t_{j-1}\right) + Leh_j K g_{j-\frac{1}{2}}.$$

We note $Q_{1-\frac{1}{2}}$, $T_{j-\frac{1}{2}}$ and $S_{j-\frac{1}{2}}$ involve only known quantities if we assume that the solution is known on $x = x^{i-1}$. In terms of the new dependent variables, the boundary conditions become

$$u(x,0) = 1, \;\; mt(x,0) + Prf(x,0) = 0, s(x,0) = 0, \quad g(x,0) = 0, \tag{4.28}$$

$$u(x,\infty) \to 0, s(x,\infty) \to 1, \;\; g(x,\infty) \to 1. \tag{4.29}$$

Equations (4.27) are imposed for $j = 1,2,3,\dots,J$ and the transformed boundary layer thickness η_J is sufficiently large so that it is beyond the edge of the boundary layer (Cebeci and Bradshaw, 1984). The boundary conditions yields at $x = x^i$ are

$$,u_0^i = 1,\ 0 = mt_0^i + Prf_0^i, s_0^i = 0, g_0^i = 0, u_J^i = 0, s_J^i = 1\,, g_J^i = 1. \tag{4.30}$$

4.3.3. Newton's Method

Equations (4.27) are nonlinear algebraic equations and therefore have to be linearized before the factorization scheme can be used. Let us write the Newton iterates as follows: For $(k+1)th$ iterates, we write

$$
\begin{aligned}
f_j^{(k+1)} &= f_j^{(k)} + \delta f_j^{(k)}, \\
u_j^{(k+1)} &= u_j^{(k)} + \delta u_j^{(k)}, \\
\mathrm{v}_j^{(k+1)} &= \mathrm{v}_j^{(k)} + \delta \mathrm{v}_j^{(k)}, \\
t_j^{(k+1)} &= t_j^{(k)} + \delta t_j^{(k)}, \\
s_j^{(k+1)} &= s_j^{(k)} + \delta\, s_j^{(k)}, \\
g_j^{(k+1)} &= g_j^{(k)} + \delta\, g_j^{(k)}, \\
z_j^{(k+1)} &= z_j^{(k)} + \delta\, z_j^{(k)}.
\end{aligned} \tag{4.31}
$$

Equation (4.27) can be written as

$$
\begin{aligned}
f_j + \delta f_j - f_{j-1} - \delta f_{j-1} &= \frac{h_j}{2}\left(u_j + \delta u_j + u_{j-1} + \delta u_{j-1}\right), \\
u_j + \delta u_j - u_{j-1} - \delta u_{j-1} &= \frac{h_j}{2}\left(\mathrm{v}_j + \delta \mathrm{v}_{j,} + \mathrm{v}_{j-1} + \delta \mathrm{v}_{j-1}\right), \\
g_j + \delta g_j - g_{j-1} - \delta g_{j-1} &= \frac{h_j}{2}\left(z_j + \delta z_j + z_{j-1} + \delta z_{j-1}\right), \\
s_j + \delta s_j - s_{j-1} - \delta s_{j-1} &= \frac{h_j}{2}\left(t_j + \delta t_j + t_{j-1} + \delta t_{j-1}\right),
\end{aligned} \tag{4.32}
$$

$$\mathrm{v}_j + \delta\mathrm{v}_{j,} - \mathrm{v}_{j-1} - \delta\mathrm{v}_{j-1} + \frac{h_j}{4}\left(f_j + \delta f_j + f_{j-1} + \delta f_{j-1}\right)\left(\mathrm{v}_j + \delta\mathrm{v}_{j,} + \mathrm{v}_{j-1} + \delta\mathrm{v}_{j-1}\right)$$
$$- \frac{h_j}{4}\left(u_j + \delta u_j + u_{j-1} + \delta u_{j-1}\right)^2$$
$$+ \frac{h_j\beta}{4}\left(f_j + \delta f_j + f_{j-1} + \delta f_{j-1}\right)\left(u_j + \delta u_j + u_{j-1} + \delta u_{j-1}\right)\left(\mathrm{v}_j + \delta v_j + \mathrm{v}_{j-1}\right.$$
$$\left. + \delta v_{j-1}\right) - \frac{\beta}{4}\left(f_j + \delta f_j + f_{j-1} + \delta f_{j-1}\right)^2\left(\mathrm{v}_j + \delta v_j - \mathrm{v}_{j-1} - \delta v_{j-1}\right)$$
$$- \frac{h_j}{2}(M + d)\left(u_j + \delta u_j + u_{j-1} + \delta u_{j-1}\right)$$
$$+ \frac{\lambda}{2}\left(\mathrm{v}_j + \delta\mathrm{v}_{j,} + \mathrm{v}_{j-1} + \delta\mathrm{v}_{j-1}\right)\left(\mathrm{v}_j + \delta v_j - \mathrm{v}_{j-1} - \delta v_{j-1}\right) = Q_{j-\frac{1}{2}},$$

$$\left(1 + \frac{4}{3}R_d\right)\left(t_j + \delta t_j - t_{j-1} - \delta t_{j-1}\right)$$
$$+ \frac{h_j Pr}{4}\left(f_j + \delta f_j + f_{j-1} + \delta f_{j-1}\right)\left(t_j + \delta t_j + t_{j-1} + \delta t_{j-1}\right)$$
$$+ \frac{h_j PrNb}{4}\left(z_j + \delta z_j + z_{j-1} + \delta z_{j-1}\right)\left(t_j + \delta t_j + t_{j-1} + \delta t_{j-1}\right)$$
$$+ \frac{h_j PrNt}{4}\left(t_j + \delta t_j + t_{j-1} + \delta t_{j-1}\right)^2 + \frac{h_j PrEc}{4}\left(v_j + \delta v_j + v_{j-1} + \delta v_{j-1}\right)^2$$
$$= T_{j-\frac{1}{2}},$$

$$\left(z_j + \delta z_j - z_{j-1} - \delta z_{j-1}\right) + \frac{h_j Le}{4}\left(f_j + \delta f_j + f_{j-1} + \delta f_{j-1}\right)\left(z_j + \delta z_j + z_{j-1} + \delta z_{j-1}\right)$$
$$+ \frac{Nt}{Nb}\left(t_j + \delta t_j - t_{j-1} - \delta t_{j-1}\right) - \frac{Leh_jK}{2}\left(g_j + \delta g_j + g_{j-1} + \delta g_{j-1}\right) = S_{j-\frac{1}{2}}.$$

By dropping the quadratic and higher-order terms in $\delta f_j^{(i)}, \delta u_j^{(i)}, \delta \mathrm{v}_j^{(i)}, \delta s_j^{(i)}, \delta g_j^{(i)}, \delta t_j^{(i)}\ and \delta z_j^{(i)}$ a linear tridiagonal system of equations will be obtained, as follows:

$$\delta f_j - \delta f_{j-1} - \frac{h_j}{2}\left(\delta u_j + \delta u_{j-1}\right) = (r_1)_{j-\frac{1}{2}},$$

$$\delta u_j - \delta u_{j-1} - \frac{h_j}{2}\left(\delta \mathrm{v}_j + \delta \mathrm{v}_{j-1}\right) = (r_2)_{j-\frac{1}{2}},$$

$$\delta s_j - \delta s_{j-1} - \frac{h_j}{2}\left(\delta t_j + \delta t_{j-1}\right) = (r_3)_{j-\frac{1}{2}},$$

$$\delta g_j - \delta g_{j-1} - \frac{h_j}{2}\left(\delta z_j + \delta z_{j-1}\right) = (r_4)_{j-\frac{1}{2}}, \tag{4.33}$$

$$a_1\delta \mathrm{v}_j + a_2\delta \mathrm{v}_{j-1} + a_3\delta f_j + a_4\delta f_{j-1} + a_5\delta u_j + a_6\delta u_{j-1} = (r_5)_{j-\frac{1}{2}},$$

$$b_1\delta t_j + b_2\delta t_{j-1} + b_3\delta f_j + b_4\delta f_{j-1} + b_5\delta z_j + b_6\delta z_{j-1} + b_7\delta v_j + b_8\delta v_{j-1} = (r_6)_{j-\frac{1}{2}},$$

$$c_1\delta z_j + c_2\delta z_{j-1} + c_3\delta f_j + c_4\delta f_{j-1} + c_5\delta t_j + c_6\delta t_{j-1} + c_7\delta g_j + c_8\delta g_{j-1} = (r_7)_{j-\frac{1}{2}},$$

Where $(r_1)_{j-\frac{1}{2}} = f_{j-1} - f_j + \frac{h_j}{2}\left(u_j + u_{j-1}\right)$,

$$(r_2)_{j-\frac{1}{2}} = u_{j-1} - u_j + \frac{h_j}{2}\left(\mathrm{v}_j + \mathrm{v}_{j-1}\right),$$

$$(r_3)_{j-\frac{1}{2}} = s_{j-1} - s_j + \frac{h_j}{2}\left(t_j + t_{j-1}\right),$$

$$(r_4)_{j-\frac{1}{2}} = g_{j-1} - g_j + \frac{h_j}{2}\left(z_j + z_{j-1}\right),$$

$$(r_5)_{j-\frac{1}{2}} = -(\mathrm{v}_j - \mathrm{v}_{j-1}) - h_j(f\mathrm{v})_{j-\frac{1}{2}} + h_j u^2_{j-\frac{1}{2}} - 2h_j\beta(fu\mathrm{v})_{j-\frac{1}{2}} + \beta f^2_{j-\frac{1}{2}}\left(\mathrm{v}_j - \mathrm{v}_{j-1}\right) - \lambda v_{j-\frac{1}{2}}\left(\mathrm{v}_j - \mathrm{v}_{j-1}\right) + h_j\,(M+d)u_{j-\frac{1}{2}},$$

$$(r_6)_{j-\frac{1}{2}} = -\left(1 + \frac{4}{3}R_d\right)\left(t_j - t_{j-1}\right) - Prh_j(f t)_{j-\frac{1}{2}} - Prh_jNb(z\mathrm{t})_{j-\frac{1}{2}} - h_jPrNtt^2_{j-\frac{1}{2}} - Prh_jEcv^2{}_{j-\frac{1}{2}},$$

$$(r_7)_{j-\frac{1}{2}} = -\left(z_j - z_{j-1}\right) - Leh_j(fz)_{j-\frac{1}{2}} - \frac{Nt}{Nb}\left(\mathrm{t}_j - t_{j-1}\right) - Leh_jKg_{j-\frac{1}{2}},$$

$$(a_1)_j = 1 + \frac{h_j}{2}f_{j-\frac{1}{2}} + h_j\beta(f\mathrm{u})_{j-\frac{1}{2}} - \beta f^2_{j-\frac{1}{2}} + \frac{\gamma}{2}\left(\mathrm{v}_j + \mathrm{v}_{j-1}\right) + \frac{\lambda}{2}\left(\mathrm{v}_j - \mathrm{v}_{j-1}\right),$$

$$(a_2)_j = -1 + \frac{h_j}{2}f_{j-\frac{1}{2}} + h_j\beta(f\mathrm{u})_{j-\frac{1}{2}} + \beta f^2_{j-\frac{1}{2}} - \frac{\gamma}{2}\left(\mathrm{v}_j + \mathrm{v}_{j-1}\right) + \frac{\lambda}{2}\left(\mathrm{v}_j - \mathrm{v}_{j-1}\right),$$

$$(a_3)_j = (a_4)_j = \frac{h_j}{2}\mathrm{v}_{j-\frac{1}{2}} + h_j\beta(\mathrm{uv})_{j-\frac{1}{2}} - \beta f_{j-\frac{1}{2}}\left(\mathrm{v}_j - \mathrm{v}_{j-1}\right),$$

$$(a_5)_j = (a_6)_j = -\frac{h_j}{2} u_{j-\frac{1}{2}} + h_j \beta (f\mathrm{v})_{j-\frac{1}{2}} + \frac{h_j}{2}(M + d),$$

$$(b_1)_j = \left(1 + \frac{4}{3} R\right) + \frac{h_j Pr}{2} f_{j-\frac{1}{2}} + \frac{h_j Pr Nb}{2} z_{j-\frac{1}{2}} + h_j Pr Nt t_{j-\frac{1}{2}},$$

$$(b_2)_j = -\left(1 + \frac{4}{3R_d}\right) + \frac{h_j Pr}{2} f_{j-\frac{1}{2}} + \frac{h_j Pr Nb}{2} z_{j-\frac{1}{2}} + h_j Pr Nt t_{j-\frac{1}{2}},$$

$$(b_3)_j = (b_4)_j = \frac{h_j Pr}{2} \mathrm{t}_{j-\frac{1}{2}},$$

$$(b_5)_j = (b_6)_j = \frac{h_j Pr Nb}{2} \mathrm{t}_{j-\frac{1}{2}}, \quad (b_7)_j = (b_8)_j = \frac{h_j Pr Ec}{2} \mathrm{v}_{j-\frac{1}{2}},$$

$$(c_1)_j = 1 + \frac{h_j Le}{2} f_{j-\frac{1}{2}},$$

$$(c_2)_j = -1 + \frac{h_j Le}{2} f_{j-\frac{1}{2}}, (c_3)_j = (c_4)_j = \frac{h_j Le}{2} f_{j-\frac{1}{2}},$$

$$(c_5)_j = \frac{Nt}{Nb}, \ (c_6)_j = -(c_5)_j, \quad (c_7)_j = (c_8)_j = \frac{-h_j LeK}{2}.$$

To complete the system (4.33) we recall the boundary conditions (4.30) which can be satisfied exactly with no iteration. Therefore, in order to maintain these correct values in all the iterates, we take

$\delta f_0 = 0, \ \ \delta u_0 = 0, \ \ \delta s_0 = 0, \ \delta g_0 = 0 \ \ \delta u_J = 0, \delta s_J = 0, and \ \ \delta g_J = 0.$

In general case equation (4.33) in vector matrix form;

$$[A][\delta] = [r] \tag{4.34}$$

where

$$A=\begin{bmatrix} [A_1] & [C_1] & & & & & & \\ [B_2] & [A_2] & [C_2] & & & & & \\ & [B_3] & [A_3] & [C_3] & & & & \\ & & . & . & . & & & \\ & & & . & . & . & & \\ & & & & . & . & . & \\ & & & & & [B_{J-1}] & [A_{J-1}] & [C_{J-1}] \\ & & & & & & [B_J] & [A_J] \end{bmatrix}, \quad \delta=\begin{bmatrix} [\delta_1] \\ [\delta_2] \\ . \\ . \\ . \\ [\delta_{J-1}] \\ [\delta_J] \end{bmatrix}, r=\begin{bmatrix} [r_1] \\ [r_2] \\ . \\ . \\ . \\ [r_{J-1}] \\ [r_J] \end{bmatrix}$$

In equation (4. 34) the elements are defined by

$$[A_1]=\begin{bmatrix} 0 & 0 & 0 & 1 & 0 & 0 & 0 \\ -\frac{h_1}{2} & 0 & 0 & 0 & -\frac{h_1}{2} & 0 & 0 \\ 0 & -\frac{h_1}{2} & 0 & 0 & 0 & -\frac{h_1}{2} & 0 \\ 0 & 0 & -\frac{h_1}{2} & 0 & 0 & 0 & -\frac{h_1}{2} \\ a_2 & 0 & 0 & a_3 & a_1 & 0 & 0 \\ b_8 & b_2 & b_6 & b_3 & b_7 & b_1 & b_5 \\ 0 & c_6 & c_2 & c_3 & 0 & c_5 & c_1 \end{bmatrix},$$

$$[A_j]=\begin{bmatrix} -\frac{h_j}{2} & 0 & 0 & 1 & 0 & 0 & 0 \\ -1 & 0 & 0 & 0 & -\frac{h_j}{2} & 0 & 0 \\ 0 & -1 & 0 & 0 & 0 & -\frac{h_j}{2} & 0 \\ 0 & 0 & -1 & 0 & 0 & 0 & -\frac{h_j}{2} \\ a_6 & 0 & 0 & a_3 & a_1 & 0 & 0 \\ 0 & 0 & 0 & b_3 & b_7 & b_1 & b_5 \\ 0 & 0 & c_8 & c_3 & 0 & c_5 & c_1 \end{bmatrix}, \quad 2 \le j \le J,$$

$$[B_j] = \begin{bmatrix} 0 & 0 & 0 & -1 & 0 & 0 & 0 \\ 0 & 0 & 0 & 0 & -\frac{h_j}{2} & 0 & 0 \\ 0 & 0 & 0 & 0 & 0 & -\frac{h_j}{2} & 0 \\ 0 & 0 & 0 & 0 & 0 & 0 & -\frac{h_j}{2} \\ 0 & 0 & 0 & a_4 & a_2 & 0 & 0 \\ 0 & 0 & 0 & b_4 & b_8 & b_2 & b_6 \\ 0 & 0 & 0 & c_4 & 0 & c_6 & c_2 \end{bmatrix}, \quad 2 \le j \le J,$$

$$[C_j] = \begin{bmatrix} -\frac{h_j}{2} & 0 & 0 & 0 & 0 & 0 & 0 \\ 1 & 0 & 0 & 0 & 0 & 0 & 0 \\ 0 & 1 & 0 & 0 & 0 & 0 & 0 \\ 0 & 0 & 1 & 0 & 0 & 0 & 0 \\ a_5 & 0 & 0 & 0 & 0 & 0 & 0 \\ 0 & 0 & 0 & 0 & 0 & 0 & 0 \\ 0 & 0 & c_7 & 0 & 0 & 0 & 0 \end{bmatrix}, 1 \le j \le J,$$

$$[\delta_1] = \begin{bmatrix} \delta v_0 \\ \delta t_0 \\ \delta z_0 \\ \delta f_1 \\ \delta v_1 \\ \delta t_1 \\ \delta z_1 \end{bmatrix}, [\delta_j] = \begin{bmatrix} \delta u_{j-1} \\ \delta s_{j-1} \\ \delta g_{j-1} \\ \delta f_j \\ \delta v_j \\ \delta t_j \\ \delta z_j \end{bmatrix}, \quad 2 \le j \le J, \quad [r_j] = \begin{bmatrix} (r_1)_{j-\frac{1}{2}} \\ (r_2)_{j-\frac{1}{2}} \\ (r_3)_{j-\frac{1}{2}} \\ (r_4)_{j-\frac{1}{2}} \\ (r_5)_{j-\frac{1}{2}} \\ (r_6)_{j-\frac{1}{2}} \\ (r_7)_{j-\frac{1}{2}} \end{bmatrix}, \quad 1 \le j \le J, \tag{4.35}$$

To solve equation (4.34), we assume that A is nonsingular and can be factored in to

$$[A] = [L][U] \tag{4.36}$$

where

$$A = \begin{bmatrix} [\alpha_1] & & & & & \\ [B_2] & [\alpha_1] & & & & \\ & \cdot & \cdot & & & \\ & & \cdot & \cdot & & \\ & & & \cdot & [\alpha_{j-1}] & \\ & & & & [B_J] & [\alpha_J] \end{bmatrix} \quad \text{and}$$

$$U = \begin{bmatrix} [I] & [\Gamma_1] & & & & \\ & [I] & [\Gamma_2] & & & \\ & & \cdot & \cdot & & \\ & & & \cdot & \cdot & \\ & & & & [I] & [\Gamma_{j-1}] \\ & & & & & [I] \end{bmatrix}$$

where $[I]$ is the identity matrix of order 7 and $[\alpha_i]$ and $[\Gamma_i]$ are 7×7 matrices which elements are determined by the following equations:

$$[\alpha_1] = [A_1]\ , \tag{4.37}$$

$$[A_1][\Gamma_1] = [C_1]\ , \tag{4.38}$$

$$[\alpha_j] = [A_j] - [B_j][\Gamma_{j-1}]\ , \qquad j = 2,3, \dots, J \tag{4.39}$$

$$[\alpha_j][\Gamma_j] = [C_j]\ , \qquad\qquad j = 2,3, \dots, J-1. \tag{4.40}$$

Equation (4.36) can now be substituted into Equation (4.34), and we get

$$[L][U][\delta] = [r], \tag{4.41}$$

If we define

$$[U][\delta] = [W]. \tag{4.42}$$

Equation (4.41) becomes

$$[L][W] = [r], \tag{4.43}$$

where

$$W = \begin{bmatrix} [W_1] \\ [W_2] \\ \cdot \\ \cdot \\ \cdot \\ [W_{j-1}] \\ [W_J] \end{bmatrix},$$

and the $[\,W_j]$ are $7 \times\ 1$ column matrices. The elements W can be solved from Equation (4.43):

$$[\alpha_1][W_1] = [r_1], \tag{4.44}$$

$$[\alpha_j][W_j] = [r_j] - [B_j][W_{j-1}], \quad 2 \leq j \leq J. \tag{4.45}$$

The step in which Γ_j, α_j and $W_j$are calculated is usually referred to as the forward sweep. Once the element of W are found, equation (4.38) then gives the solution in the so-called backward sweep, in which the elements are obtained by the following relations:

$$[\delta_J] = [W_J], \tag{4.46}$$

$$[\delta_J] = [W_J] - [\Gamma_J][\delta_{j+1}], \qquad 1 \leq j \leq J - 1. \tag{4.47}$$

These calculations are repeated until some convergence criterion is satisfied and calculations are stopped when

$$\left|\delta \mathrm{v}_0^{(i)}\right| \leq \varepsilon_1, \tag{4.48}$$

where $\varepsilon_1$is small arranged value.

4.4. Results and Discussions

Fig. 4.3-fig.4.5 portrays the temperature, velocity, and concentration profiles for different values of dimensionless melting parameter. It is noticed that when dimensionless melting parameter increases the flow and velocity boundary layer rises whereas the thermal and concentration profiles decreases. This is due to the fact that an increase in *m* will upsurge the intensity of melting, which acts as blowing boundary condition at the stretching surface and hence tends to thicken the boundary layer. Melting parameter affects harmfully the velocity boundary layer thickness of Williamson nanofluid when compared to upper-convected Maxwell nanofliud. The influences of thermal radiation parameter on temperature and concentration profiles are re-counted through fig.4. 6 and fig.4.7. From the figures it is noticed that an increment in the

thermal radiation parameter causes the reduction in temperature profiles, but opposite effect on concentration profile is obtained. This is because an increase in the radiation parameter R_d leads to a decrease in the boundary layer thickness and enhances the heat transfer rate on melting surface in the presence of chemical effect. The behavior of the concentration profiles in contradiction of chemical reaction parameter is offered in fig.4. 8. From the graph it can be seen that if the chemical reaction parameter increased the concentration boundary layer thickness and concentration profiles reduced. This is due to the fact that chemical reaction in this system results in consumption of the chemical and hence results in reduction of concentration profile. The most important outcome is that the first order chemical reaction has a tendency to reduce the overshoot in the profiles of the solute concentration in the solutal boundary layer.

Prandtl number is a ratio of momentum diffusivity to thermal diffusivity. When Prandtl number is high fluid has low thermal conductivity, which decreases the thermal boundary layer thickness and conduction. Accordingly, form fig. 4.9 it is seen that with increasing Prandtl number the thermal boundary layer and temperature profiles upsurges. The impact of magnetic field parameter on velocity, temperature and concentration profiles is plotted in fig. 4.10-fig. 4.12. From the figures it is noticed that as the values of magnetic parameter goes up, the velocity of the fluid, the temperature and concentration decline. The physical significance of this behavior is an increase in the values of magnetic field parameter develops the force opposite to the flow, which is known as Lorentz force. This body force abridged the boundary layer flow and congeals the velocity boundary layers.

The impact of thermophoresis and Brownian motion parameter on concentration and temperature profiles are portrayed in figs. 4.13- fig. 4.16. A phenomenon in which small particles are pulled away from the hot surface to cold one is called thermophoresis. So, when the surface is heated large number of nanoparticles is moved away which raises the temperature of fluid. Therefore the temperature of fluid increases whereas the concentration of the fluid declines. Because of more heat is produced an increase in Nb enhances the random motion of fluid particles. This causes an increase of fluid temperature and concentration. fig. 4.17- fig. 4.19 is devised to demonstrate the influence of permeability parameter on the flow of the fluid, temperature and concentration profiles. It is obvious that the presence of porous medium causes higher restriction to the fluid flow, which in turn slows its motion. Therefore, an increment of permeability parameter causes the reduction in boundary layer thickness and the profiles of velocity, temperature and concentration. In particular, the boundary layer of Williamson nanofluid more affected by permeability parameter when compared with the boundary layer of upper-convected Maxwell nanofluid. From fig. 4.20 it is noticed that as the value of Lewis number escalated the concentration boundary layer and concentration profiles rises. This is probably due to the fact that higher values of Lewis number create the smaller Brownian diffusion coefficient. fig. 4.21 reveals that when the values of Eckert number upsurges the thermal boundary layer and the temperature profiles are enhanced. This is because of the point that heat energy is put in the liquid because of the frictional heating.

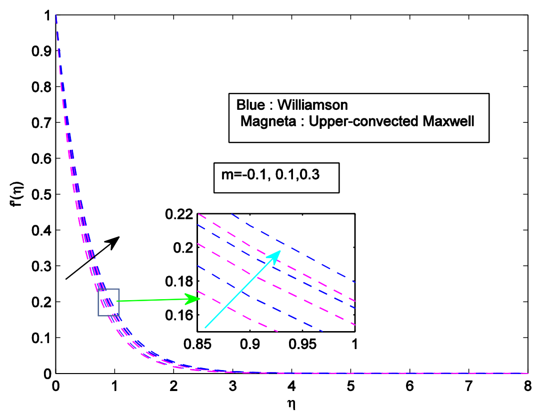

Figure4. 3: Velocity graph for different values of m

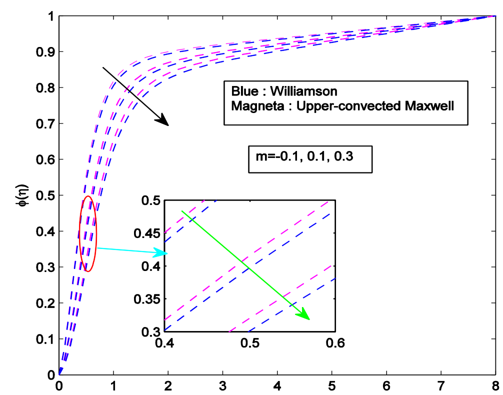

Figure4. 5: Concentration graph for different values of m

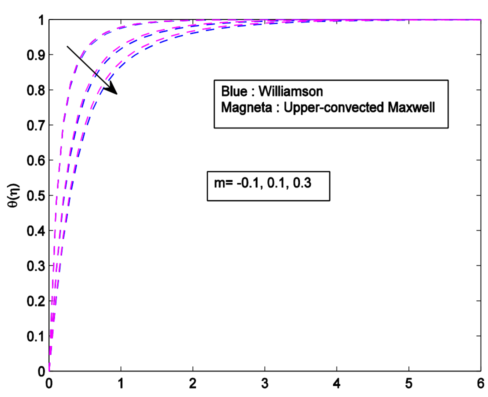

Figure4. 4: Temperature graph for different values of m

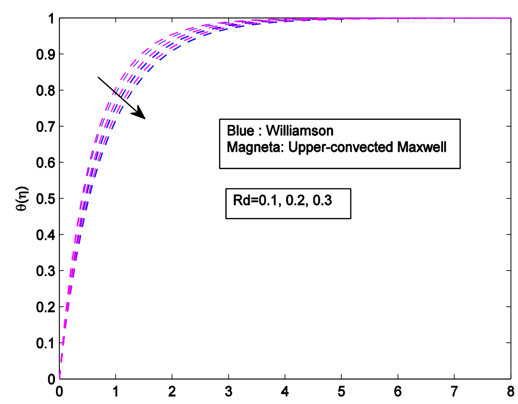

Figure4. 6: Temperature graph for different values of R_d

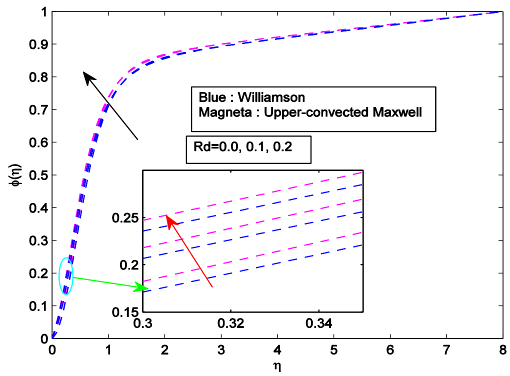

Figure4. 7: Concentration graph for different values of $\mathbf{R_d}$

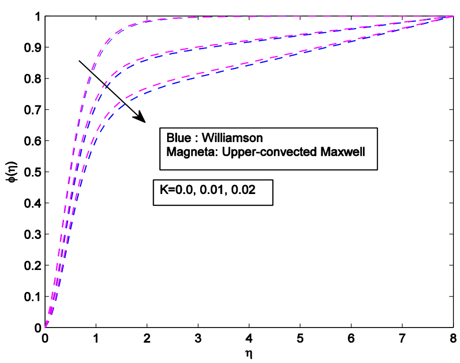

Figure4. 8: Concentration graph for different values of K

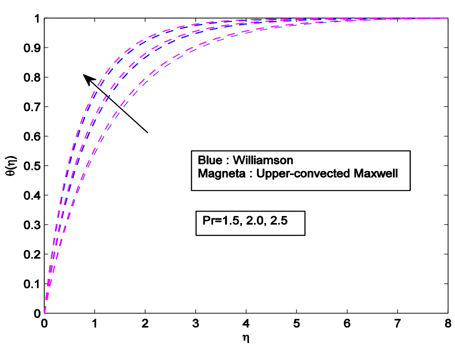

Figure4. 9: Temperature graph for different values of Pr

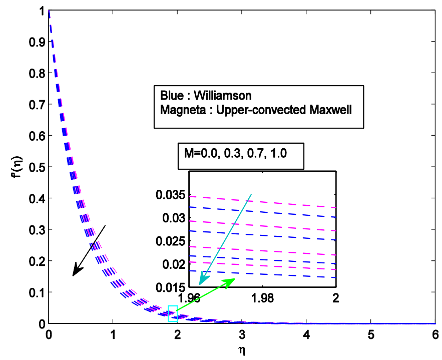

Figure4. 10: Velocity graph for different values of M

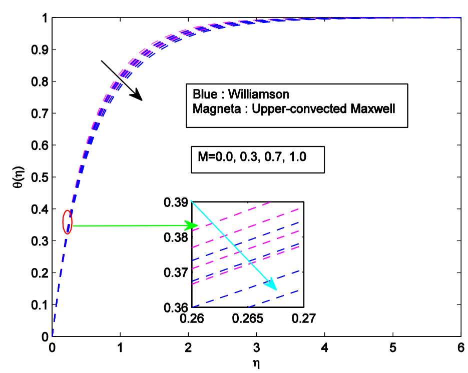

Figure4. 11: Temperature graph for different values of M

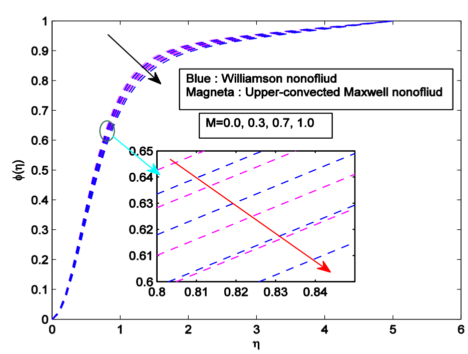

Figure4. 12: Concentration graph for different values of M

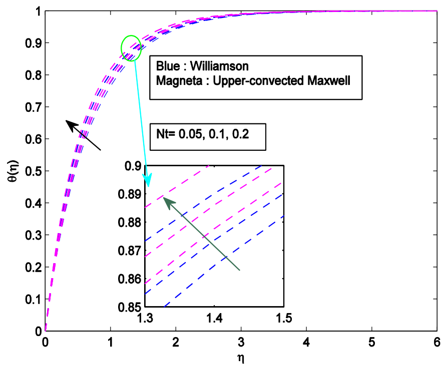

Figure4. 13: Temperature graph for different values of **Nt**

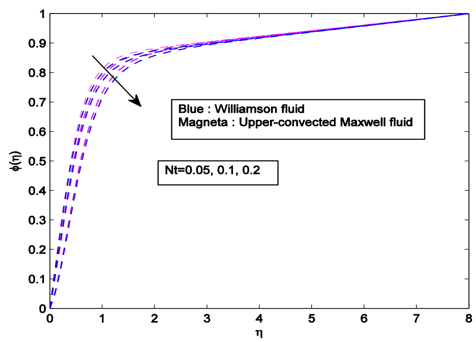

Figure4. 14: Concentration graph for different values of **Nt**

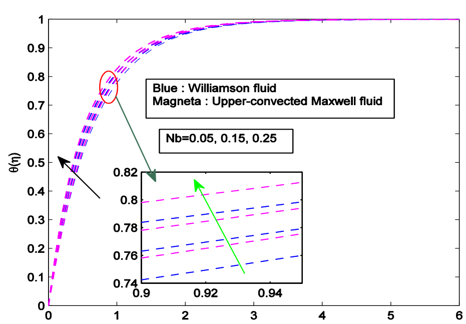

Figure4. 15: Temperature graph for different values of **Nb**

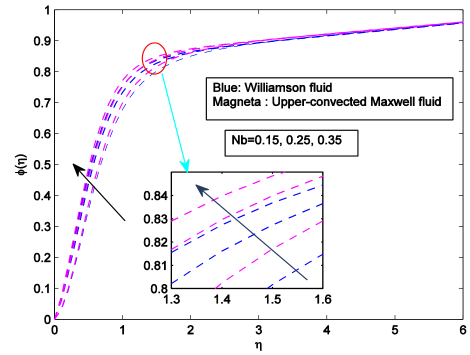

Figure4. 16: Concentration graph for different values of **Nb**

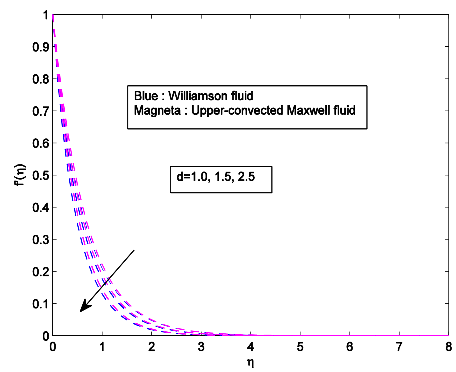

Figure4. 17: Velocity graph for different values of **d**

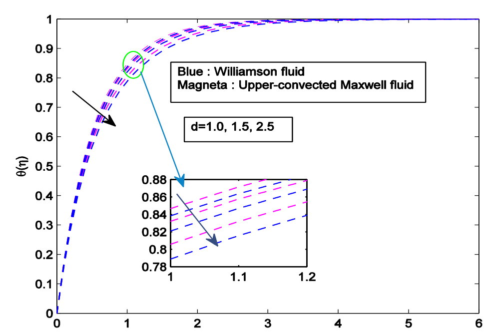

Figure4. 18: Temperature graph for different values of **d**

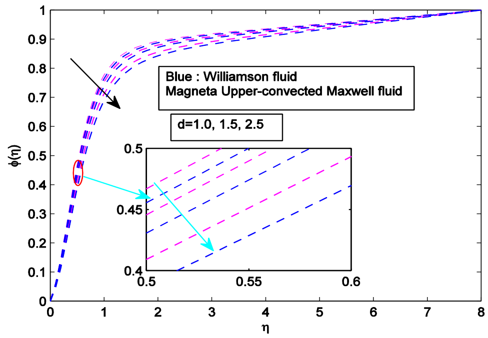

Figure4. 19: Concentration graph for different values of d

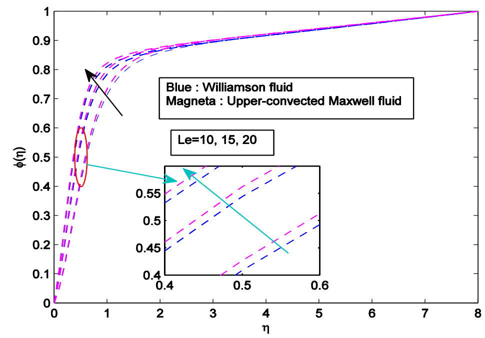

Figure4.20: Concentration graph for different values of **Le**

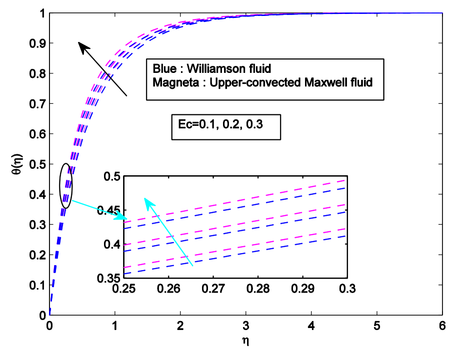

Figure4. 21: Temperature graph for different values of **Ec**

Table4. 1: Comparison of Nusselt number $-\boldsymbol{Nu_x(0)}$ and Sherwood number $-\boldsymbol{Sh_x(0)}$ for different values of permeability parameter $\boldsymbol{d}$ and Williamson parameter $\boldsymbol{\lambda}$ when $\boldsymbol{Ec = 0}$, and $\boldsymbol{\beta = 0, Q = 0{:}5, K = 0.01}$

d	λ	Krishnamurthy et al. (2016) $-\theta(0)$	Present result	Krishnamurthy et al. (2016) $-\phi(0)$	Present result
0.0	0.2	2.1656	2.16565	0.3345	0.33458
1.0	0.2	1.9578	1.95781	0.2975	0.29757
2.0	0.2	1.7914	1.79143	0.2698	0.26982
0.0	0.01	1.8511	1.85112	0.2780	0.27803
0.0	0.1	1.8256	1.82567	0.2744	0.27448
0.0	0.2	1.7914	1.7914	0.2698	0.26987

To check the validity of the numerical solution obtained a comparison of Nusselt and Sherwood number with (Krishnamurthy et al. 2016) for different values of d and

λ is exhibited in Table 4.1 and reasonable agreement with them has been found. The changes in physical quantities at various relevant parameters are displayed in Table 4.2 and Table 4.3. From the tables it is noticed that with an increment in Eckert number Ec and thermophoresis parameter Nt a decrement in friction factor and mass transfer rate attained, whereas, the heat transfer rate is amplified. Moreover, when magnetic field parameter M upsurges skin friction coefficient upsurges but Nusselt number $-Nu_x(0)$ and Sherwood number $-Sh_x(0)$ are decreased. Furthermore, from the tables it can be seen that with an increase in Brownian motion parameter Nb there is a decrement in a friction factor, in contrast, there is an increment in both Sherwood and Nusselt number.

Table4. 2: Calculation of skin friction coefficient $f''(0)$, local Nusselt number $-Nu_x(0)$ and local Sherwood number $-Sh_x(0)$ for different values of λ, Ec, Nb, Nt and M when $d = 2.0$ $Pr = 3.2, Le = 10, K = 0.01, R = 0.01, m = 0.2$ for Williamson nanofluid

λ	Ec	Nb	Nt	M	$f''(0)$	$-Nu_x(0)$	$-Sh_x(0)$
0.1	0.1	0.25	0.25	0.3	-1.872267	1.969929	0.063527
0.2	-----	-----	-----	-----	-2.047295	1.946866	0.043231
0.3	-----	-----	-----	-----	-2.404276	1.916175	0.010166
0.1	0.1	-----	------	------	-1.872267	1.969929	0.063527
-------	0.2	-----	------	------	-1.863774	2.205993	-0.182168
-------	0.3	-----	------	------	-1.855431	2.439110	-0.418728
-------	0.1	0.1	-----	------	-1.884558	1.630553	-0.934150
-------	------	0.2	------	------	-1.876417	1.855036	-0.082370
-------	------	0.3	------	------	1.868094	2.085765	0.148010
-------	------	0.25	0.2	------	-1.875426	1.882452	0.368256
-------	------	------	0.3	------	1.868972	2.061364	-0.269270
-------	------	------	0.4	-------	-1.861986	2.255834	-1.025984
-------	------	------	0.25	0.1	-1.807712	1.986533	0.075362
-------	------	-------	-------	0.2	-1.840199	1.978144	0.069415
-------	------	-------	-------	0.3	-1.872267	1.969929	0.063527

Table4. 3: Calculation of skin friction coefficient $f''(0)$, local Nusselt number $-Nu_x(0)$ and local Sherwood number $-Sh_x(0)$ for different values of β, Ec, Nb, Nt and M when $d = 2.0$ $Pr = 3.2, Le = 10, K = 0.01,, R_d = 0.01, m = 0.2$ for Maxwell nanofluid

β	Ec	Nb	Nt	M	$f''(0)$	$-Nu_x(0)$	$-Sh_x(0)$
0.1	0.1	0.25	0.25	0.3	-1.756946	1.987314	0.077509
0.2	-----	-----	-----	-----	-1.758375	1.985692	0.076464
0.3	-----	-----	-----	-----	-1.759786	1.984084	0.075423
0.1	0.1	-----	------	------	1.756946	1.987314	0.077509
-------	0.2	-----	------	------	-1.749135	2.216304	-0.158271
-------	0.3	-----	------	------	-1.741450	2.442636	-0.385522
-------	0.1	0.1	-----	------	-1.768794	1.642032	-0.910417
-------	------	0.2	------	------	-1.760948	1.870408	-0.066449
-------	------	0.3	------	------	-1.752921	2.105189	0.160509
-------	------	0.25	0.2	------	-1.759997	1.898168	0.383877
-------	------	------	0.3	------	-1.753763	2.080503	-0.257463
-------	------	------	0.4	-------	-1.747012	2.255834	-1.020299
-------	------	------	0.25	0.1	1.700836	2.278734	0.088168
-------	------	-------	-------	0.2	-1.729108	1.995063	0.082807
-------	------	-------	-------	0.3	-1.756946	1.987314	0.077509

4.5. Conclusion

This topic was aimed at exploring the effect of melting heat transfer, viscous dissipation and chemical reaction on the flow of upper-convected Maxwell and Williamson nanofluids above a stretching surface. By employing well-known similarity transformations the nonlinear coupled dimensionless equations from the governing equations are achieved. Then, the resulting dimensionless equations are solved computationally by implementing Keller Box method with MATLAB software. The graphs and tables for velocity profiles, skin-friction coefficient, temperature field, local Nusselt number, concentration field and local Sherwood number for different values of dimensionless melting, magnetic field, Thermal radiation, chemical reaction, Brownian motion, Thermophoresis, permeability parameter, Prandtl number, Eckert number and Lewis number are revealed and pondered. The result shows that when the melting parameter enhance the fluid flow and boundary layer thickness increases but opposite trends happens to the temperature and concentration profiles. In addition upper-convected Maxwell fluids are less affected by melting parameter when compared to Williamson fluids. The interpretations of the conclusion are summarized as follows:

1. Melting and magnetic field parameter affects highly the velocity boundary layer of Williamson nanofluid when compared with upper-convected Maxwell nanofliud.
2. Melting parameter m have similar effect on both temperature and concentration graphs. That is, when melting parameter increases both temperature and concentration profiles are reduces.
3. Radiation parameter R_d has opposite effect on temperature and concentration graph. As the values of radiation parameter upsurges the temperature decreases whereas concentration rises.
4. An increment of Eckert number causes an increment of temperature profiles.
5. With an increment of Eckert number and thermophoresis parameter a decrement in friction factor and mass transfer rate attained whereas heat transfer rate is enhance.
6. An augmentation of permeability parameter causes the reduction of the profiles of velocity, temperature and concentration.
7. When the Williamson parameter upsurges the velocity, temperature and concentration declines.
8. When magnetic field parameter M upsurges skin friction coefficient is upsurges but Nusselt number $-Nu_x(0)$ and Sherwood number $-Sh_x(0)$ are decreased.

References

Adigoppula Raju and Odelu Ojjela (2019). Effects of the induced magnetic field, thermophoresis and Brownian motion on mixed convective Jeffrey nanofluid flow through a porous channel, *John Wiley and Sons Ltd.*. https://doi.org/10.1002/eng2.12053.

Ajayi T. M., Omowaye A. J., and Animasaun I. L. (2017). Viscous dissipation effects on the motion of Casson fluid over an upper horizontal thermally stratified melting surface of a paraboloid of revolution. *Journal of Applied Mathematics*. Article ID 1697135, 13 pages. https://doi.org/10.1155/2017/1697135.

Cebeci T. and Bradshaw P. (1984). Physical and Computational Aspects of Convective Heat Transfer. *springer-Verlag*, Berlin Heidelberg.

Choi SUS, Eastman JA. (1995). Enhancing thermal conductivity of fluids with nanoparticles, presented at ASME. *International Mechanical Engineering Congress and Exposition*. 1217.

Dapra I., Scarpi G. (2007). Perturbation solution for pulsatile flow of a non-Newtonian Williamson fluid in a rock fracture. *International Journal of Rock Mechanics and Mining Sciences*. 44, 271-278.

Das S. 2003. Temperature dependence of thermal conductivity enhancement for nanofluids. *J. Heat Transfer.*; 125, 56774.

Dharmendar Reddy Y., Srinivasa Rao V. and Anand Babu L. (2017). Viscous dissipation and partial slip effects on MHD boundary layer flow of nano fluid and heat transfer over a nonlinear stretching sheet with non-uniform heat source. *International Journal of Mathematical Archive*. 8(8), 1-14. http://www.ijma.info/.

Elsayed Mohamed Abdel Rahman Elbashbeshy, Khaled Mohamed Abdelgaber and Hamada Galal Asker (2018). Heat and mass transfer of a Maxwell nanofluid over a stretching surface with variable thickness embedded in porous medium. *International Journal of Mathematics and Computational Science.* 4(3), 86-98. http://www.aiscience.org/journal/ijmcs.

Epstein M., Chao D.H. (1976). Melting heat transfer in steady laminar flow over a flat plate, *J. Heat Transf.* 98 (3): 531533.

Eswaramoorthi S., Bhuvaneswari M. Sivasankaran S. and Rajan S. (2017). Hydrodynamic slip effect on MHD combined convection of a Williamson nanofluid. *International Journal of Pure and Applied Mathematics*. 117(11), 327-333. url: http://www.ijpam.eu.

Ganesh Kumar K., Ramesh G.K., Gireesha B.J., Gorla R.S.R. (2018). Characteristics of Joule heating and viscous dissipation on three-dimensional flow of Oldroyd B nanofluid with thermal radiation. *Alexandria Engineering Journal.* 57, 21392149. http://dx.doi.org/10.1016/j.aej.2017.06.006.

Harish Babu D., Satya Narayana P.V. (2019). Melting heat transfer and radiation effects on Jeffrey fluid flow over a continuously moving surface with a parallel free stream. *J. Appl. Comput. Mech*. . 5(2), 468-476. DOI: 10.22055/JACM.2019.26479.1335.

Hayat T., Ijaz Khan M., Waqas M., Alsaedi A., Muhammad Imran Khan (2017). Radiative flow of micropolar nanofluid with thermophoresis and Brownian moment on stretching surface. *International journal of hydrogen energy*. 1-13. http://dx.doi.org/10.1016/j.ijhydene.2017.05.006.

Hayat T., Sumaira Qayyum, Muhammad Ijaz Khan and Ahmed Alsaedi (2018). Entropy generation in magnetohydrodynamic radiative flow due to rotating disk in presence of viscous dissipation and Joule heating. *Physics of fluids.* 30, 017101. https://doi.org/10.1063/1.5009611.

Hayat T., Muhammad Ijaz Khana, Muhammad Waqasa and Ahmed Alsaedi (2017) Mathematical modeling of non-Newtonian fluid with chemical aspects: A new formulation and results by numerical technique. *Physicochem. Eng. Aspects.* 518, 263272. doi.org/10.1016/j.colsurfa.2017.01.007.

Hayata T., Muhammad Ijaz Khana, Muhammad Waqasa and Ahmed Alsaedi. (2017). Mathematical modeling of non-Newtonian fluid with chemical aspects. *Physicochem. Eng. Aspects*, 518, 263–272. http://dx.doi.org/10.1016/j.colsurfa.2017.01.007.

Hayat T., Ijaz Khan M., Farooq M., Tabassam Yasmeen and Alsaedi A. (2016). Stagnation point flow with Cattaneo-Christov heat flux and homogeneous-heterogeneous reactions. *Journal of Molecular Liquids.* 220, 4955. http://dx.doi.org/10.1016/j.molliq.2016.04.032.

IjazKhan M., Hayat T., Sumaira Qayyum, Alsaedi A. and ImranKhan M. (2018). New thermodynamics of entropy generation minimization with nonlinear thermal radiation and nanomaterial's, *Physics Letters A.*

Ijaz Khana M., Waqasa M., Hayata T., Imran Khan M. and Alsaedi A. (2017). Behavior of stratification phenomenon in flow of Maxwell nanomaterial with motile gyrotactic microorganisms in the presence of magnetic field. *International Journal of Mechanical Sciences.* http://dx.doi.org/10.1016/j.ijmecsci.2017.07.009.

Kairi R.R. and Murthy P.V.S.N. (2009). Effect of melting and thermo-diffusion on natural convection heat and mass transfer in a non-Newtonian fluid saturated non-darcy porous medium. *The Open Transport Phenomena Journal.*; 1: 7-14.

Kairi R.R. and RamReddy Ch. (2015). The effect of melting on mixed convection heat and mass transfer in non-Newtonian nanofluid saturated in porous medium. *Frontiers in Heat and Mass Transfer (FHMT)*. (6) (6). DOI: 10.5098/hmt.6.6.

Khalid AL-Qaissy and Ahmed Abdulhadi M. (2017). Effect of magnetic field on peristaltic flow of Williamson fluid in a symmetric channel. *IOSR Journal of Mathematics (IOSR-JM).* 13(1), 30-39.

Kolawole S. Adegbie, Adeola J. Omowaye, Akeem B. Disu and Isaac L. Animasaun (2015). Heat and mass transfer of upper convected Maxwell fluid flow with variable thermo physical properties over a horizontal melting surface. *Applied Mathematics*. 6, 1362-1379. http://dx.doi.org/10.4236/am.2015.68129.

Krishnamurthy M.R., Prasannakumara B.C., Gireesha B.J., Rama Subba Reddy Gorla (2016). Effect of chemical reaction on MHD boundary layer flow and melting heat transfer of Williamson nanofluid in porous medium. *Engineering Science and Technology, an International Journal.* 19, 5361. http://dx.doi.org/10.1016/j.jestch.2015.06.010.

Kumar K.G. and Gireesha B.J. (2018). Scrutinization of joule heating and viscous dissipation on MHD flow and melting heat transfer over a stretching sheet. *Int. J. of Applied Mechanics and Engineering*. 23 (2), 429-443, DOI: 10.2478/ijame-2018-0025.

Kumaran G., Sandeep N. and Ali M.E (2017). Computational analysis of magnetohydrodynamic Casson and Maxwell flows over a stretching sheet with cross diffusion. *Results in Physics*. 7, 147155. http://dx.doi.org/10.1016/j.rinp.2016.12.011.

Lourdu Immaculate D., Muthuraj R., Anant Kant Shuklac and Srinivas S. (2016). MHD unsteady flow of a Williamson nanofluid in a vertical porous space with oscillating wall temperature. *Frontiers in Heat and Mass Transfer (FHMT)*. 7(12). DOI: 10.5098/hmt.7.12.

Mahanthesh B., Gireesha B.J., Prasannakumara B.C. and Sampathkumar P.B. (2017). Magneto-Thermo-Marangoni convective flow of Cu-H2O nanoliquid past an infinite disk with particle shape and exponential space based heat source effects. *Results in physics*. 7, 2990-2996.

Muhammad Imran Khana, Ijaz Khan M., Waqas M., Hayat T. and Alsaedic A. (2017). Chemically reactive flow of Maxwell liquid due to variable thicked surface. *International Communications in Heat and Mass Transfer.* 6, 231238. http://dx.doi.org/10.1016.

Olatomide Gbenga Fadodun, Adebimpe Amos Amosun, Ayodeji Olalekan Salau and Johnson Ayodeji Ogundeji (2019). Thermal performance of single-walled carbon nanotube nanofluid under turbulent flow conditions. *Wiley*.. https://doi.org/10.1002/eng2.12024.

Pak BC, Cho Y. (1998). Hydrodynamic and heat transfer study of dispersed fluids with submicron metallic oxide particles. *Exp. Heat Transfer*. 11: 15170.

Pop, E. (2010). Energy dissipation and transport in nanoscale devices. *Nano Research*. 3 (3):147169.

Ramesh, G. K., and Gireesha B. J. (2017).Non-Linear Radiative Flow of Nanofluid past a Moving/ Stationary Riga Plate. *Frontiers in Heat and Mass Transfer (FHMT).* 9.

Muhammad Imran Khan, Tasawar Hayat, Muhammad Ijaz Khan and Ahmed Alsaed (2017). A modified homogeneous-heterogeneous reaction for MHD stagnation flow with viscous dissipation and Joule heating. *International Journal of Heat and Mass Transfer*. 113: 310317, http://dx.doi.org/10.1016/j.ijheatmasstransfer.2017.05.082.

Roberts L. (1958). On the melting of a semi-infinite body of ice placed in a hot stream of air. *J. Fluid Mech.*; 4: 505528.

Sajid Qayyum, Rimsha Khan and Humera Habib (2017). Simultaneous effects of melting heat transfer and inclined magnetic field flow of tangent hyperbolic fluid over a nonlinear stretching surface with homogeneous-heterogeneous reactions. *International Journal of Mechanical Sciences.* 133, 110. http://dx.doi.org/10.1016/j.ijmecsci.2017.07.026.

Salma Zaman and Mahwish Gul (2019). Magnetohydrodynamic bio convective flow of Williamson nanofluid containing gyrotactic microorganisms subjected to thermal radiation and Newtonian conditions. *Journal of Theoretical Biology* 479, 2228. https://doi.org/10.1016/j.jtbi.2019.02.015.

Sreelakshmi K., Prasanthi K. and Sarojamma G. (2017). MHD three dimensional flow of a Williamson fluid over a stretching sheet with velocity slip. *International Journal of Innovative Research in Science, Engineering and Technology*. 6(13).

Srinivas Reddy C. Kishan Naikoti and Mohammad Mehdi Rashidi (2017). MHD flow and heat transfer characteristics of Williamson nanofluid over a stretching sheet with variable thickness and variable thermal conductivity. *Transactions of A. Razmadze Mathematical Institute.* http://dx.doi.org/10.1016/j.trmi.2017.02.004.

Swarnalathamma B.V. (2018). Heat and Mass transfer on MHD flow of Nanofluid with thermal slip effects. *International Journal of Applied Engineering Research ISSN.* 13(18), 13705-13726. http://www.ripublication.com.

Talha M.A., Osman Gani M.and Ferdwos M. (2018). Numerical solution of MHD boundary layer flow due to Gyrotactic Microorganism for Williamson nanofluid over stretching sheet in the presence of exponential internal heat generation. *International Journal of Mathematical and Computational Sciences*. 12(2). Waset.org/publication10008777.

Tien C., Yen Y. C. (1965). The effect of melting on forced convection heat transfer. *J. Appl. Meteorol.* 4, 523-527. https:// doi.org/10.1175//(1965).: 1520-0450:0040523:TEOMOF/2.0.CO;2

Vijayalakshmi R., Sreelakshmi, Sandhya G. and Sarojamma G. (2017). Flow of upper-convected Maxwell Micropolar fluid over a stretching sheet with slip effect. *International Journal of Innovative Research in Science, Engineering and Technology*. 6(13). http://www.ijirset.com/.

Waqar Azeem Khan, Masood Khan, Muhammad Irfan and Alshomrani A.S. (2017). Impact of melting heat transfer and nonlinear radiative heat flux mechanisms for the generalized Burgers fluids. *Results in Physics.* 7, 4025-4032. https://doi.org/10.1016/j.rinp.2017.10.004.

Williamson R. V. (1929). The flow of pseudo plastic materials. *Industrial and Engineering Chemistry Research*. 21(11), 1108.

Xuan Y, Li Q. (2003). Investigation on convective heat transfer and flow features of nanofluids. *J. Heat Transfer*. 125, 1515.

Yasin M. H. M., Ishak A., and Pop (2015). MHD stagnation-point flow and heat transfer with effects of viscous dissipation, Joule heating and partial velocity slip. *Scientific Reports*. 5.

Yohannes K.Y. and B. Shankar (2013). Heat and mass transfer in MHD flow of nanofluids through a porous media due to a stretching sheet with viscous dissipation and chemical reaction effects. *Carib.J.SciTech*. (1), 001-017.

Chapter5

The Effect of Viscous Dissipation on Unsteady Williamson Nanofluid over Stretching/ Shrinking Wedge with Thermal Radiation and Chemical reaction

5.1. Introduction

Due to its applications the flow of fluid in a boundary adjacent to the wedge has great attention to the researchers and Engineers. Some of its applications are geothermal systems, polymer processes, crude oil extraction, cooling or heating of films/sheets, etc .Firstly the steady laminar flow above a wedge was investigated by (Fankner and Skan, 1931). They projected a well-known Falkner-Skan equation to define the flow above a wedge, which has delivered many successful sources of information about the behavior of incompressible boundary layers. Later many reaserchers have investigated the flow above a wedge. Among them Seddeek et al., (2009), Michael and Iain, (2009), Alam et al., (2017), Sattar (2011), Bharathi Devi and Gangadhar, (2015), Mohammadi et al., (2012) and Ali and Alim, (2018) have studied Falkner-Skan flow over a wedge with different boundary conditions and with various parameters. Their study shows that with an increasing pressure gradient parameter the magnitude velocity increases. Moreover, unsteady MHD heat and mass transfer boundary layer flow along a wedge with different dimensionless parameter were inspected by (Radiah Bte Mohamad, 2013), (Kandasamy, 2014), (Rahman, 2011), (Alam et al., 2015), (Muhaimin et al., 2013), (Ali et al., 2017), (Rahman et al., 2013) and (Mohd Rijal Ilias et al., 2017). Their results indicates that unsteadiness significantly control the flow, heat transfer and mass transfer of non-Newtonian nanofliuds. Furthermore, in the presence of variable viscosity dual solutions of a boundary layer problem for MHD nanofluids through a permeable wedge was studied by (Xiaoqin Xu and Shumei Chen, 2018). Futhermore, Rama Subba Reddy Gorla and Mahesh Kumari, (2012) have investigated mixed convective heat transfer of boundary layer flow along a vertical porous wedge with a nanofluid. The heat transfer of MHD nanofluid flow along a wedge with viscous effects of embedded in Porous Media were examined by (Wubshet Ibrahim and Ayele Tulu, 2019).

In most industries nowadays the importance of non-Newtonian fluids dominates the Newtonian fluids. The rheological properties of non-Newtonian fluids cannot be illuminated by the classical Naiver-Stokes equations. Also no single model is sufficient to describe non- Newtonian fluids characteristics. To overcome this difficulty abundant models have come into being. The rheological models that were projected were Williamson, Cross, Ellis, power law, Carreau fluid model, etc. Typical of a non-Newtonian fluid model with shear withdrawing property is Williamson fluid model and was first projected by (Williamson, 1929). Nadeem et al., (2013) studied the two dimensional flow of Williamson flud above stertching sheet. Moreover, Nadeem and Hussain, (2014) have scrutinized the impacts of nanoparticles on Williamson fluid over a stretching sheet. Furthermore, the inspection of Williamson fluid has been carried out by investigators such as, (Abegunrinand and Animasaun, 2017), (Kumaran et al., 2017), (Nagendra et al., 2018), (Wubshet Ibrahim and Dachasa Gamachu, 2019), (Hashim et al., 2019), (Aamir Hamid et al., 2019) and (Talha, 2018) past different physical geometry like radially stretching surface, static/moving wedge and streching sheet.

Choi and Eastman, (1995) introduced nanofluid, which is a mixture of nanoparticles and the base fluid such as water, ethylene glycol, and propylene glycol.The most imprtant properties of nanofliud are to increase effective thermal heat conductivty and heat transfer coefficient. Therefore, many researchers were attracted to this fact. Accordingly, Gireesha et al., (2018), Sulochana et al., (2016) and Mahanthesh et al., (2016) investigated the heat and mass transfer characteristics in nanofluids in three dimensions and they found that in the presence of the nanoparticles the effective thermal conductivity of the fluid upsurges appreciably and consequently improves the heat transfer characteristics. Furthermore, unsteady MHD nanofluid flow over a slendering stretching surface with slip effects was studied by (Ramana Reddy et al., 2018). The result indicates that with an increase of unsteadiness parameter, the heat and mass transfer coeficient are increased.

The influence of radiation on flow and heat transfer is significant in the framework of space technology and processes involving high temperature. Some of the application of thermal radiation are in the design of nuclear power plant, fire propagtion, plume dynamics, materials processing, rocket propulsion, missiles, aircraft, space technology, hypersonic fights,gas turbines and etc. The application and the effect of radiations on fluid flow was firstly investigated by (Plum et al., 1981). Later, Anuradha and Yegammai, (2017), Majeed et al., (2019), Abdul Maleque, (2013) and Sajid et al., (2018) investigated the effect of thermal radiation and activation energy on boundary layer flow of nanofluids on different surfaces.

Moreover, the influence of thermal radiation on hydromagnetic boundary layer flow of Williamson fluid with Ohmic dissipation was examined by (Hayat et al., 2016). From their result it can be seen that when the values of Weissenberg number, magnetic parameter, radiation parameter and the Eckert number Ec, rises the heat transfer rate reduces. Furthermore, Hameed Khan et al., (2018), Abdul Samad Khan et al., (2019) and Sameh et al., (2019)] have studied the impact of thermal radiation on boundary layer flow non-Newtonian Maxwell nanofluids with heat generation/ absorption. Still further, the enhancement of thermal radiation on hydromagnetic Casson fluid flow over a stretched cylinder in the presence of suspension of liquidparticles was inspected by (Ramesh et al., 2017). Rajput and Gaurav kumar, (2017) examined the effect of thermal radiation on heat and mass transfer of MHD flow through an oscillating inclined plate. The effect of chemical reaction and thermal radiation on free convective heat and mass transfer of MHD fluid flow from over stretching surface embedded in a saturated Porous medium was examined by (Rashad et al., 2011).

The main aim of this study is to investigate the effect of viscous dissipation on unsteady Williamson nanofluid over stretching/ shrinking wedge with thermal radiation and chemical reaction. The novelty of this paper are (i) inclusion of viscous dissipation on energy equation, since it has significant impact on heat transfer; especially for high-velocity flows, fluids with a moderate Prandtl number, highly viscous flows at moderate velocities and moderate velocities with small wall-to-fluid temperature difference. (ii) consideration of Falkner-Skan flow of Williamson fluid over stretcing /shrinking wedge. It palys a vital role in geothermal systems, polymer processes, crude oil extraction, cooling or heating of films/sheet. The novel govrning partial differential equation of momentum, energy and concentration are reduced in to non linear ordinary differential equation and then solved by implicit finite difference method known as Keller box. Inaddtion graphically the impact of different physical parametres such as Suction/Injection, Streching/shrinking, Biot number, Williamson parameter, wedge angle parameter, unsteady parameter, Prandtl number, Lewis number, Thermophoresis parameter, Brownian motion paremeter, Eckret number, radiation parameter and chemical reaction parameter on velocity, temperature and concentration profiles scrutinized. Moreover, in tabular the numerical values of volume friction, mass and heat transfer rate were examined.

5.2. Mathematical Formulation

Unsteady two-dimensional incompressible laminar boundary flow of non-Newtonian Williamson nanofliuds over stretching/ shrinking wedge is considered. In this study we consider $u_w(x)$ the velocity of stretching/ shirnking wedge, $u_e(x)$ free steam velocity, T_∞ ambient temperature, T_w stretching/ shirnking wedge tempearture, C_w nanoparticle at stretching/ shirnking wedge and C_∞ ambient nanopaticle. The physical coordinate system is chosen with x along the surface of the wedge and is measured from the origin and y is the coordinate normal to the surface (see fig.5.1.).

For an incompressible Williamson fluid the continuity and momentum equation are given by

$$\nabla . V = 0, \tag{5.1}$$

$$\rho \frac{dV}{dt} = \nabla . S + \rho b. \tag{5.2}$$

where ρ is the density, V is the velocity vector, S is the Cauchy stress tensor, b represents the specific body force vector and $d\,/\,dt$ represents the material time derivative. The essential equations for Williamson fluid model are specified as follows:

$$S = -pI + \tau A_1, \tag{5.3}$$

$$\tau = \left[\mu_\infty + \frac{\mu_0 - \mu_\infty}{1 - \Gamma\dot{\gamma}}\right]. \tag{5.4}$$

where p is pressure, I is identity vector, τ is extra stress tensor, μ_0 and μ_∞ are the limiting viscosities at zero and at infinite shear rate respectively, $\Gamma > 0$ is the time constant, A_1 is the first Rivlin-Ericson tensor and $\dot{\gamma}$ is defined as follows;

$$\dot{\gamma} = \sqrt{\frac{\pi}{2}}, \pi = trace(A_1^2), \tag{5.5}$$

where π is the second invariant strain tensor. Here we consider the case in which $\mu_\infty \neq 0$ and $\Gamma\dot{\gamma} < 1$. Then we obtain

$$\tau = \mu_0 \left[\zeta + \frac{1-\zeta}{1-\Gamma\dot{\gamma}}\right]. \tag{5.6}$$

Here $\zeta = \frac{\mu_\infty}{\mu_0}$ is the ratio of viscosities.

The components of stress tensor are

$$\tau_{xx} = 2\mu_0(1-\Gamma\dot{\gamma})\frac{\partial u}{\partial x}, \tag{5.7}$$

$$\tau_{xy} = \tau_{yx} = \mu_0(1-\Gamma\dot{\gamma})\left(\frac{\partial u}{\partial y}+\frac{\partial v}{\partial x}\right), \tag{5.8}$$

$$\tau_{yy} = 2\mu_0(1-\Gamma\dot{\gamma})\frac{\partial v}{\partial y}. \tag{5.9}$$

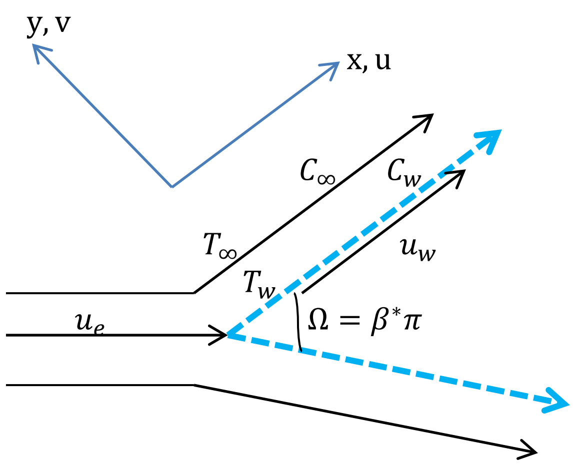

Figure5. 1: Flows configuration and the coordinate system.

In the absence of body force the governing equations can be described in Cartesian system as listed below (See Aamir Hamid et al., 2019).

.

$$\frac{\partial u}{\partial x}+\frac{\partial v}{\partial y} = 0, \tag{5.10}$$

$$\frac{\partial u}{\partial t}+u\frac{\partial u}{\partial x}+v\frac{\partial u}{\partial y} = \frac{\partial u_e}{\partial t}+v\frac{\partial^2 u}{\partial y^2}\left[\zeta+(1-\zeta)\left(1-\Gamma\frac{\partial u}{\partial y}\right)^{-1}\right]+v\Gamma\frac{\partial u}{\partial y}\frac{\partial^2 u}{\partial y^2}\left[(1-\zeta)\left(1-\Gamma\frac{\partial u}{\partial y}\right)^{-2}\right]+ u_e\frac{\partial u_e}{\partial x}, \tag{5.11}$$

$$\frac{\partial T}{\partial t}+u\frac{\partial T}{\partial x}+v\frac{\partial T}{\partial y} = \alpha_m\frac{\partial^2 T}{\partial y^2}\ +\omega\left\{D_B\frac{\partial C}{\partial y}\frac{\partial T}{\partial y}+\frac{D_\tau}{T_\infty}\left(\frac{\partial T}{\partial y}\right)^2\right\}-\frac{1}{(\rho c_p)_f}\frac{\partial q_r}{\partial y}+\frac{\nu}{\rho_f}\left(\frac{\partial u}{\partial y}\right)^2, \tag{5.12}$$

$$\frac{\partial C}{\partial t}+u\frac{\partial C}{\partial x}+v\frac{\partial C}{\partial y} = D_B\frac{\partial^2 C}{\partial y^2}+\frac{D_\tau}{T_\infty}\frac{\partial^2 T}{\partial y^2}-K_r(C-C_\infty). \tag{5.13}$$

The appropriate boundary conditions are (See Aamir Hamid et al. 2019)

$$u = \gamma^* u_e + U_{slip},\ v = v_w, -k\frac{\partial T}{\partial y} = h_f(T_f-T),\quad D_B\frac{\partial C}{\partial y}+\frac{D_T}{T_\infty}\frac{\partial T}{\partial y} = 0,\quad \text{at } y = 0, \tag{5.14}$$

$$u \to u_e(x),\ T \to T_\infty,\ C \to C_\infty,\quad \text{as}\ y \to \infty. \tag{5.15}$$

U_{slip} is a velocity slip for Williamson fluid model and defined as (See Aamir Hamid et al. 2019).

$$U_{slip} = L\frac{\partial u}{\partial y}\left[\zeta + (1-\zeta)\left(1-\Gamma\frac{\partial u}{\partial y}\right)^{-1}\right]$$

where u and v are the velocity components along the x and y directions respectively, ρ_f is the density of the base fluid, $\alpha_m = \frac{k}{\rho c_f}$ is the thermal diffusivity, ν is the kinematic viscosity of the fluid, k is the thermal conductivity of the fluid, D_B is the Brownian diffusion coefficient, D_τ is the thermophoretic diffusion coefficient, $\omega = \frac{(\rho c)_p}{(\rho c)_f}$ is the ratio between the effective heat capacity of the nanoparticle material and heat capacity of the fluid, c is the volumetric volume expansion coefficient and ρ_p is the density of the particles, L is the velocity slip length with dimension of length, h_f is heat transfer slip, T_f is the temperature of the fluid and v_w is suction velocity at the wall. We can write the thermal radiation using Rosseland approximation for heat flux q_r as follows (See Hayat et al., 2016) and Ramesh et al., 2017).

$$q_r = -\frac{4\sigma^*}{3k^*}\frac{\partial T^4}{\partial y}, \tag{5.16}$$

where σ^* is the Stefan-Boltzman constant, k^* is the absorption constant. Assuming the temperature difference within the flow such that T^4 may be expanded in a Taylor series about T_∞ and neglecting higher orders. We get $T^4 = 4TT_\infty^3 - 3T_\infty^4$,

Hence

$$\frac{\partial q_r}{\partial y} = -\frac{16\sigma^* T_\infty^3}{3k^*}\frac{\partial^2 T}{\partial y^2}. \tag{5.17}$$

In order to obtain similarity solution for equation (5.10)-(5.15) assume the free steam velocity for the wedge (See Sattar, 2011) and (Rahman et al., 2013);

$$u_e(x,t) = \frac{\nu x^m}{\delta^{m+1}}. \tag{5.18}$$

Where $\delta = \delta(t)$ is time dependent length scale (See Sattar, 2011), (Rahman et al., 2011) and (Rahman et al., 2013), m is a positive constant related to the wedge angle which is $m = \frac{\beta^*}{2-\beta^*}$

$(0 \leq m \leq 1)$and β^* is Hartree pressure gradient parameter which resembles to $\beta^* = \frac{\Omega}{\pi}$ for a total angle Ω of the wedge. The constant moving parameter γ^* is defined as $\gamma^* = \frac{u_w}{u_e}$, so that $\gamma^* > 0$ corresponds to stretching wedge, $\gamma^* < 0$ corresponds to a shrinking wedge, and $\gamma^* = 0$ corresponds to flat plate.

In order to transform equations (5.11)-(5.13) subjected boundary condition (5.14) and (5.15) in to non-linear ordinary differential equations we introduce similarity transformations as follows (See Sattar, 2011) and (Rahman et al., 2013);

$$\psi = \nu\sqrt{\frac{2x^{m+1}}{(m+1)\delta^{m+1}}}f(\eta), \quad \theta(\eta) = \frac{(T-T_\infty)}{(T_w-T_\infty)}, \quad \phi(\eta) = \frac{(C-C_\infty)}{(C_w-C_\infty)}, \ \eta = y\sqrt{\frac{(m+1)x^{m-1}}{2\delta^{m+1}}}. \tag{5.19}$$

We choose the stream function $\psi(x, y)$ such that

$$\frac{\partial\psi}{\partial y} = u, \text{ and } -\frac{\partial\psi}{\partial x} = v. \tag{5.20}$$

Equations (5.11) – (5.13) are transformed into the non-dimensional ordinary differential equation by applying the similarity transformation equation (5.19) as follows:

$$f'''[\zeta + (1-\zeta)(1-\lambda f'')^{-1} + \lambda f''(1-\zeta)(1-\lambda f'')^{-2}] + ff'' + \beta^*(1-f'^2) + \lambda_1(2-2f' - \eta f'') = 0, \tag{5.21}$$

$$(1 + \frac{4}{3}R_d)\theta'' + Pr\{f\theta' + Nb\phi'\theta' + Nt\theta'^2 + Ecf''^2 + \lambda_1\eta\theta'\} = 0, \tag{5.22}$$

$$\phi'' + Lef\phi' + \frac{Nt}{Nb}\theta'' - KLe\phi + Le\lambda_1\eta\phi' = 0. \tag{5.23}$$

With corresponding boundary conditions

$$f(\eta) = \chi, f'(\eta) = \gamma^* + \iota f''(\eta)[\zeta + (1-\zeta)(1-\lambda_2 f''(\eta))^{-1}], \quad \theta'(\eta) = Bi(\theta(\eta) - 1), \quad Nb\,\phi'(\eta) + Nt\theta'(\eta) = 0, \text{ at } \eta = 0, \tag{5.24}$$

$$f'(\eta) \to 1, \theta(\eta) \to 0, \ \phi(\eta) \to 0, \text{ as } \eta \to \infty. \tag{5.25}$$

where f' is dimensionless velocity, θ is dimensionless temperature, ϕ is dimensionless concentration and η is the similarity variable. The prime denotes differentiation with respect to η. The overall governing parameters are defined as; $\lambda = \sqrt{\frac{(m+1)x^{3m-1}}{\delta^{3m+3}}}\nu\Gamma$ is non- Newtonian

Williamson parameter, $\beta^* = \frac{2m}{m+1}$ is the wedge angle parameter that corresponds to $\Omega = \beta^*\pi$, $\lambda_1 = \frac{\delta^m}{\nu x^{m+1}}\frac{\partial\delta}{\partial t}$ is unsteadiness parameter, $R_d = \frac{4\sigma^* T_\infty^3}{kk^*}$ is thermal radiation parameter, $k = \alpha_m(\rho c)_f$ is thermal conductivity, $Pr = \frac{\nu}{\alpha_m}$ is Prandtl number, $Nb = \frac{\omega D_{B(C_w - C_\infty)}}{\nu}$ is Brownian motion parameter, $Nt = \frac{\omega D_T(T_w - T_\infty)}{T_\infty \nu}$ is thermophoresis parameter, $Le = \frac{\nu}{D_B}$ is Lewis number, $K = \frac{2K_r\delta^{m+1}}{(m+1)x^{m-1}}$ is chemical reaction parameter, $Ec = \frac{u_e^2}{c_p(T_f - T_\infty)}$ is Eckert number, $\iota = L\sqrt{\frac{(m+1)x^{m-1}}{2\delta^{m+1}}}$ the slip parameter, $Bi = \sqrt{\frac{2}{(m+1)R_e}}\frac{h_f x}{k}$ Biot number or surface convention parameter and $\chi = \frac{v_w}{\nu\sqrt{\frac{(m+1)x^{m-1}}{2\delta^{m+1}}}}$ is the suction-injection parameter.

The skin friction C_f, local Nusselt number Nu_x and the Sherwood number Sh_x are the important physical quantities of interest in this problem which are defined as

$$C_f = \frac{2\tau_w}{\rho u_e^2}, \quad Nu_x = \frac{xq_w}{k(T_\infty - T_m)}, \quad Sh_x = \frac{xq_m}{D_B(C_\infty - C_w)} \ , \tag{5.26}$$

Here $\tau_w = \mu_0\left[\zeta + (1-\zeta)\left(1 - \Gamma\frac{\partial \mathrm{u}}{\partial \mathrm{y}}\right)^{-1}\right]\frac{\partial u}{\partial y}$ at $y = 0$ is the surface shear stress, $q_w = -k\left(\frac{\partial T}{\partial y}\right)_{(y=0)} + q_r$ is the surface heat flux and $q_m = -D_B\left(\frac{\partial C}{\partial y}\right)_{(y=0)}$ is the surface mass flux.

$$C_f Re_x^{\frac{1}{2}} = \frac{1}{\sqrt{2-\beta^*}}f''(0)[\zeta + (1-\zeta)(1-\lambda_2 f''(0))^{-1}], -\frac{1}{\sqrt{2-\beta^*}}\left(1+\frac{4}{3}R\right)\theta'(0) = Nu_x Re_x^{-\frac{1}{2}}, \quad -\phi(0) = Sh_x Re_x^{-\frac{1}{2}}, \tag{21}$$

where $Re_x^{\frac{1}{2}} = \frac{xu_w(x)}{\nu}$ is local Reynolds number.

5.3. Solution Methodology

5.3.1. Keller Box Method

The transmuted ordinary differential equations (5.21), (5.22) and (5.23) subject to boundary conditions (5.24) and (5.25) are solved numerically using an implicit finite difference method (Keller box) in combination with the Newton linearization techniques.

We consider the net rectangle in the $x - \eta$ plane shown in figure 2 and the net points defined as below

$x^0 = 0 \qquad x^i = x^{i-1} + k_i \qquad i = 1,2,3,\dots,I$

$\eta_0 = 0 \qquad \eta_j = \eta_{j-1} + h_j \qquad j = 1,2,3,\dots,J \qquad \eta_j = \eta_\infty$

where k_i is the Δx-spacing and h_j is the $\Delta\eta$-spacing. Here i and j are the sequence of numbers that indicate the coordinate location, not tensor indices or exponents.

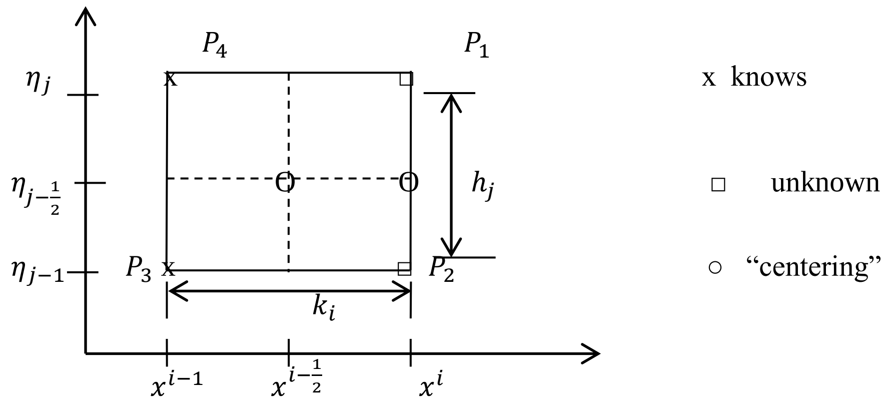

Figure5. 2: Net rectangle for difference approximations

Since only first derivatives appear in the governing equations, centered differences and two-point averages can be constructed involving only the four corner nodal values of the 'box'.

5.4. Rerult and Discussion

By taking $Bi = 2.0, Nb = Nt = 0.1, K = 0.1 = R_d = \iota = Ec = \gamma^* = \lambda_1 = \lambda, \beta^* = 0.5, Pr = 1.0,$ and $Le = 1.0$ numerical calculations are carried out unless otherwise specified. The results are revealed in a graphical and in tabular form for different values of parameters such as wedge angle parameter (β^*), unsteadiness parameter (λ_1) , Williamson parameter(λ), Lewis number (Le) , Brownian motion parameter (Nb), thermophoresis parameter (Nt), stretching parameter (γ), Prandtl number (Pr) , slip parameter ι, Eckert number (Ec), Radiation parameter (R_d), Chemical reaction parameter (K) and Biot number (Bi) on the flow, heat and mass transfer characteristics. The results are compared with those of others authors (Watanaba, 1990) and (Wubshet and Ayele, 2019) and found to be in good agreement as shown in Table 5.1. This ensures the validity and accuracy of the present work. Also, various values of the skin friction, rate of heat transfer and rate of nanoparticle concentration are presented in Table 5.2 for different values of $\beta^*, \lambda_1, \lambda, A,$ and Ec. From table 5.2 it is observed that as value of wedge β^* and suction χ parameter increases the skin friction, local Nusselt number and local Sherwood number are increased. Moreover, from this table we see that $-\theta'(0)$ and $-\phi(0)$ upsurges with an increase of unsteady parameter λ_1 but opposite results happened for $-f''(0)$. Furthermore, when the values of Williamson parameter increase the skin friction coefficient upsurges whereas the local Nusselt number and Sherwood number declines. The table also indicates that skin friction coefficient remains constant with an increase of Eckert number but local Nusselt number rises and local Sherwood number declines.

Table5. 1: Comparison of current result of $-\boldsymbol{f}''(\mathbf{0})$ and $-\boldsymbol{\theta}'(\mathbf{0})$ with Watanaba and Wubshet and Ayele.

m	$-\mathbf{f}''(\mathbf{0})$			$-\boldsymbol{\theta}'(\mathbf{0})$		
	Watanaba, (1990)	Wubshet and Ayele, (2019)	Present Result	Watanaba, (1990)	Wubshet and Ayele, (2019)	Present Result
0.0000	0.46960	0.46960	0.469646	0.42016	0.42016	0.420152
0.0141	0.50461	0.50461	0.504476	0.42578	0.42578	0.425656
0.0435	0.56898	0.56898	0.568979	0.43548	0.43548	0.435469
0.0909	0.65498	0.65498	0.655006	0.44730	0.44730	0.447302
0.1429	0.73200	0.73200	0.732004	0.45693	0.45694	0.456933
0.2000	0.80213	0.80213	0.802130	0.45503	0.45503	0.455026
0.3333	0.92765	0.92765	0.927653	0.47814	0.47814	0.458139

Table5. 2: Calculation of skin friction ($-\boldsymbol{f}''(\mathbf{0})$), local Nusselt number ($-\boldsymbol{\theta}'(\mathbf{0})$) and local Sherwood number ($-\boldsymbol{\phi}'(\mathbf{0})$) for different values of $\boldsymbol{\beta}^*, \boldsymbol{\lambda_1}, \boldsymbol{\lambda}, \boldsymbol{A},$ and $\boldsymbol{Ec}$.

$\boldsymbol{\beta}^*$	$\boldsymbol{\lambda_1}$	$\boldsymbol{\lambda}$	$\boldsymbol{A}$	$\boldsymbol{Ec}$	$-\boldsymbol{f}''(\mathbf{0})$	$-\boldsymbol{\theta}'(\mathbf{0})$	$-\boldsymbol{\phi}'(\mathbf{0})$
0.2					0.078400	0.535463	0.722917
0.4					0.241552	0.556469	0.772358
0.6					0.368587	0.575692	0.835371
0.8					0.469646	0.589358	0.916954
1.0					0.551879	0.591315	1.024316
	0.0				0.392314	0.426145	0.589306
	0.01				0.365288	0.432299	0.597823
	0.02				0.337470	0.438380	0.606393
	0.03				0.308868	0.444387	0.615013

0.04				0.279493	0.450319	0.623681
	0.1			0.308868	0.444387	0.615013
	0.5			0.322775	0.443652	0.614005
	1.0			0.345883	0.442548	0.612500
	1.5			0.382273	0.441085	0.610521
	2.0			0.490683	0.438461	0.606843
		0.01		0.308869	0.497249	0.702157
		0.03		0.311218	0.501663	0.709569
		0.05		0.313564	0.506072	0.717042
		0.07		0.315905	0.510477	0.724578
		0.09		0.318241	0.514877	0.732176
			1.0	0.490683	0.514635	0.531957
			2.0	0.490683	0.536659	0.514055
			3.0	0.490683	0.546684	0.496152
			4.0	0.490683	0.562711	0.478246
			5.0	0.490683	0.578740	0.460339

Fig.5.3 revealed that the impact of the slip parameter on the velocity profiles within the boundary layer. From the figure it can be observed that the velocity profiles increase with a growing in values of slip parameter. The horizontal line which approaches to one (converges to 1) is an asymptote to the graph as η tends to infinity (∞) . The boundary layer thickness of velocity profile is an increasing function for slip parameter (ι). The boundary layer thickness decreases as the fluid velocity increases.

The influence of the stretching parameter $\gamma^* > 0$ on the velocity profile is displayed in fig.5.4. From the figure it can be observed that the velocity profiles within the boundary layer intensified with the rising values of the stretching parameter. Moreover, the velocity boundary layer thickness increases with an increasing stretching parameter. Fig.5.5 displayed that the effect of shrinking parameter on the velocity profile. The figure reveals that the velocity boundary layer width declines when the shrinking parameter γ^* rises from -0.01 to -0.1.

Fig.5.6-fig.5.11 displayed the impact of suction parameter (χ) and injection parameter $(-\chi)$ on velocity profiles, temperature profiles and concentration profiles. Fig.5.6 describes that the fluid

velocity within the boundary layer upsurges whereas the thickness of the boundary layer reduces with the growing values of the suction parameter (χ). This is because the removal of the decelerated fluid particles through the porous wedge surface reduces the growth of the boundary layer thickness. Fig. 5.7 displays that the fluid velocity within the boundary layer diminutions with the growing in the values of injection parameter $(-\chi)$. Fig.5.8 displays when the values of suction parameter (χ) upsurges the thermal boundary layer thickness decreases.

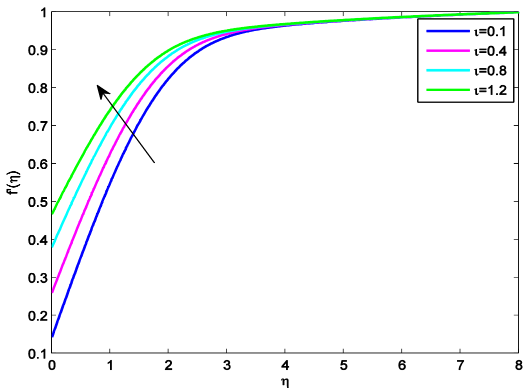

Figure5. 3Velocity graph for different values of Slip parameter

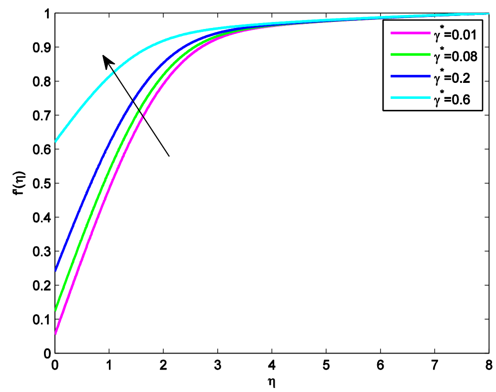

Figure5. 4: Velocity graph for different values of Stretching parameter

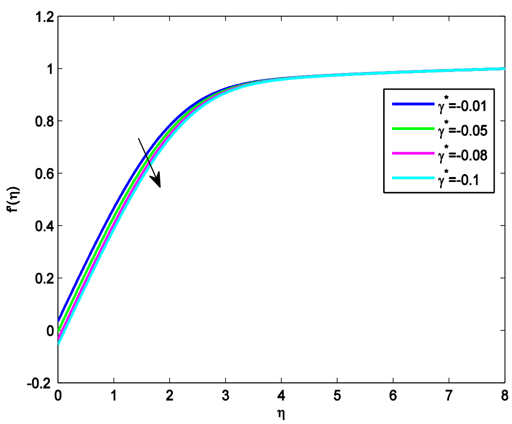

Figure5. 5: Velocity graph for different values of shrinking parameter

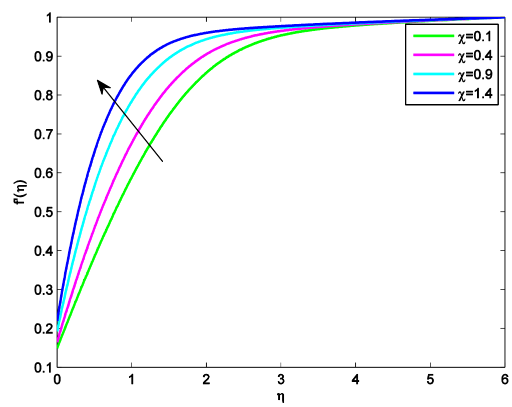

Figure5. 6: Velocity graph for different values of Suction parameter

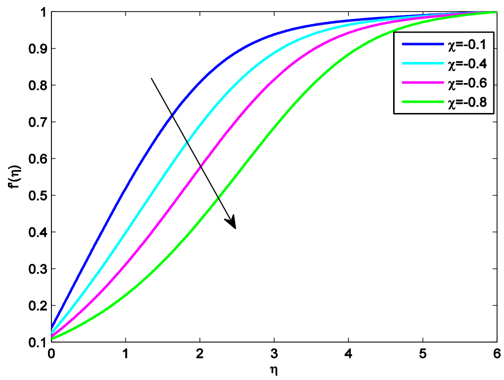

Figure5. 7: Velocity graph for different values of Injection parameter

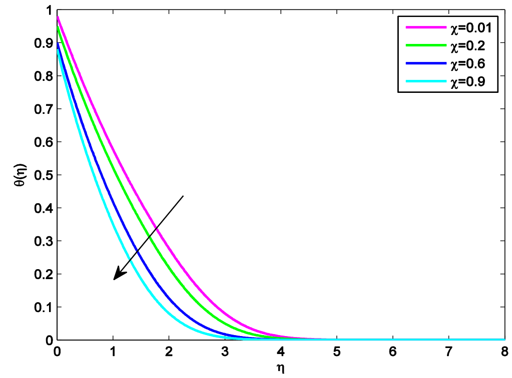

Figure5. 8: Temperature graph for different values of Suction parameter

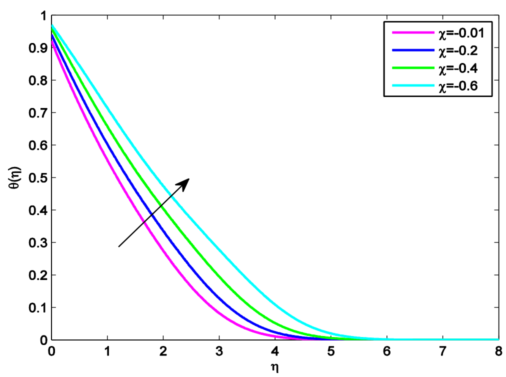

Figure5. 9: Temperature graph for different values of Injection parameter

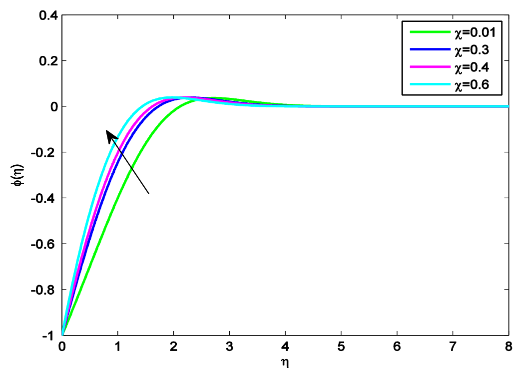

Figure5. 10: Concentration graph for different values of Suction parameter

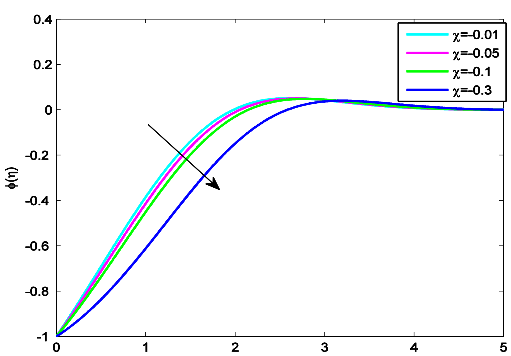

Figure5. 11: Concentration graph for different values of Injection parameter

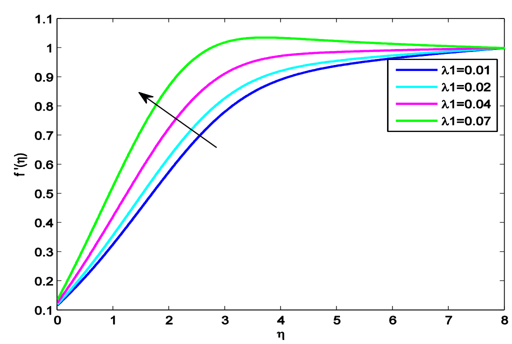

Figure5. 12: Velocity graph for different values of unsteady parameter

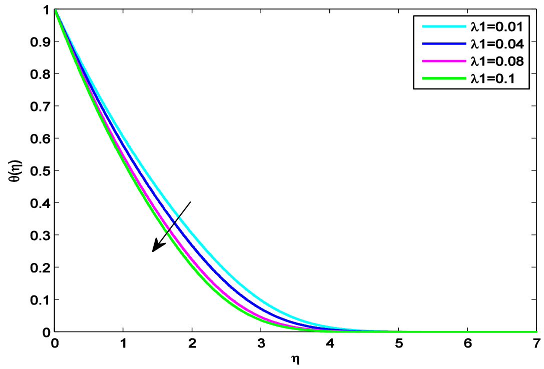

Figure5. 13: Temperature graph for different values of unsteady parameter

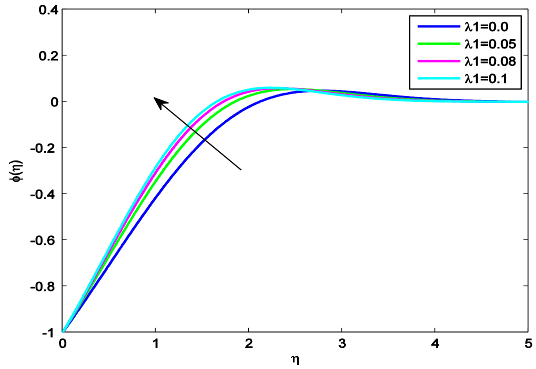

Figure5. 14: Concentration graph for different values of unsteady parameter

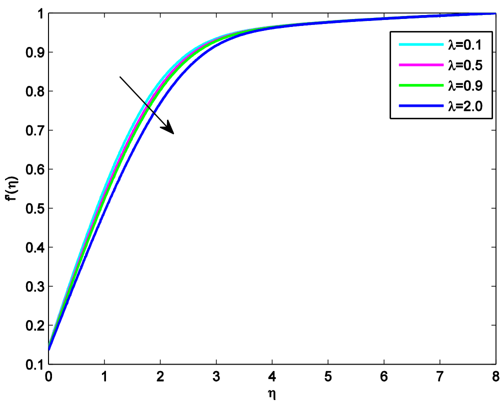

Figure5. 15: Velocity graph for different values of Williamson parameter

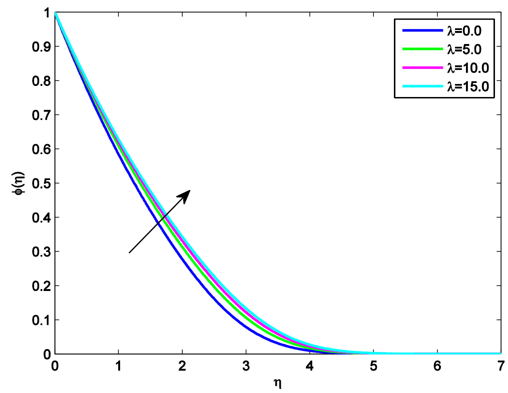

Figure5. 16: Concentration graph for different values of Williamson parameter

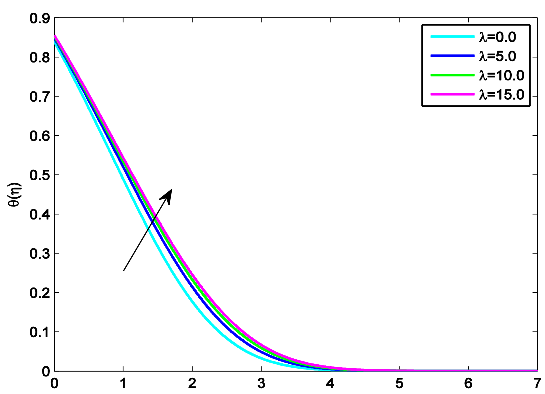

Figure5. 17: Temperature graph for different values of Williamson parameter

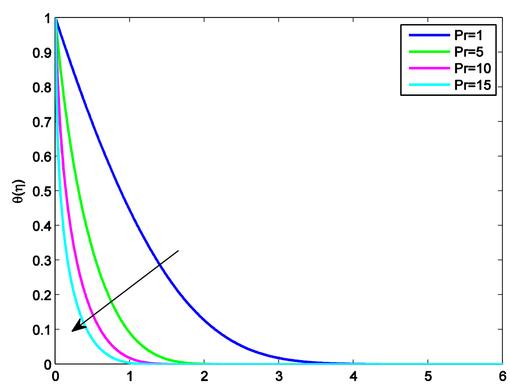

Figure5. 18: Temperature graph for different values of Prandtl Number

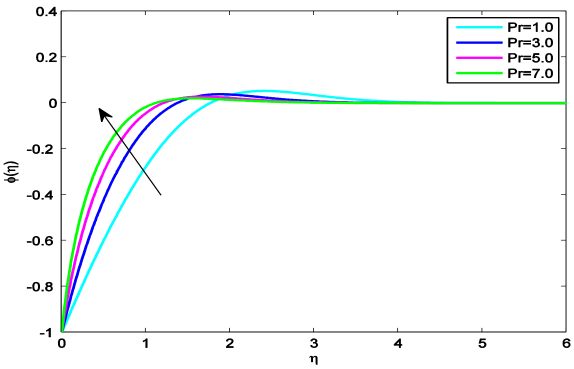

Figure5. 19: Concentration graph for different values of Prandtl Number

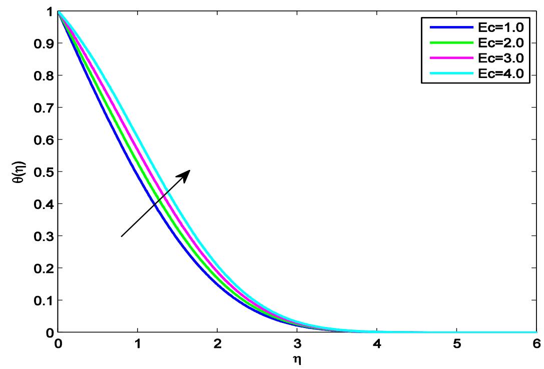

Figure5. 20: Temperature graph for different values of Eckert Number

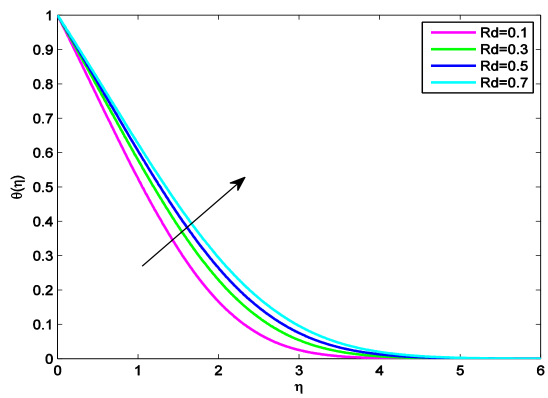

Figure5. 21: Temperature graph for different values of Thermal Radiation parameter

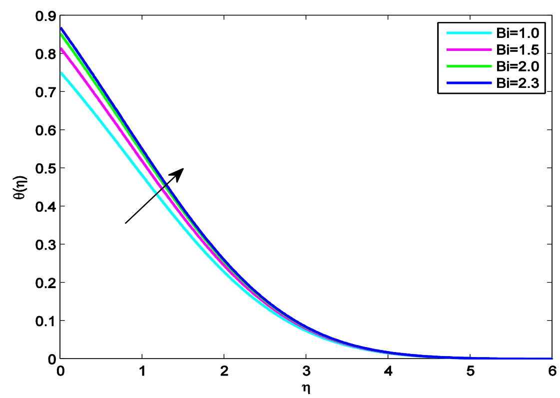

Figure5. 22: Temperature graph for different values of Biot Number

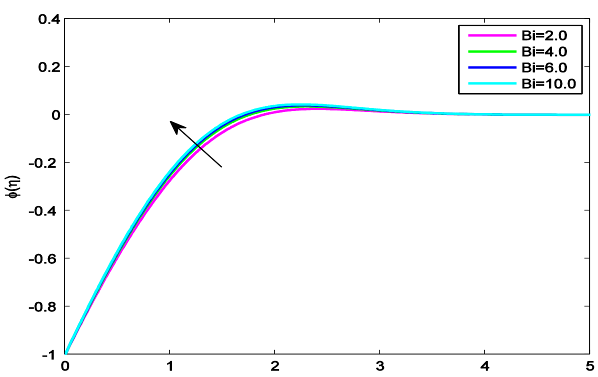

Figure5. 23: Concentration graph for different values of Biot Number

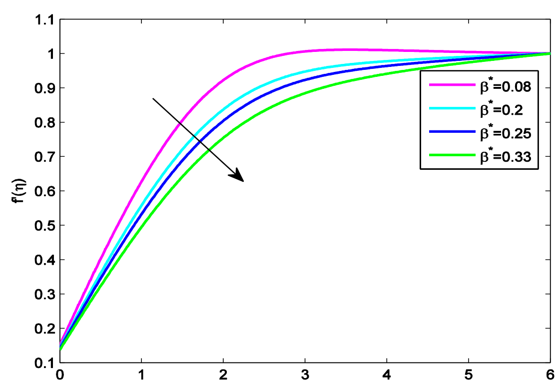

Figure5. 24: Velocity graph for different values of Wedge angle parameter

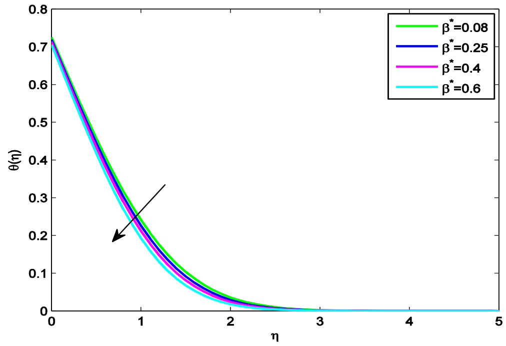

Figure5. 25: Temperature graph for different values of Wedge angle parameter

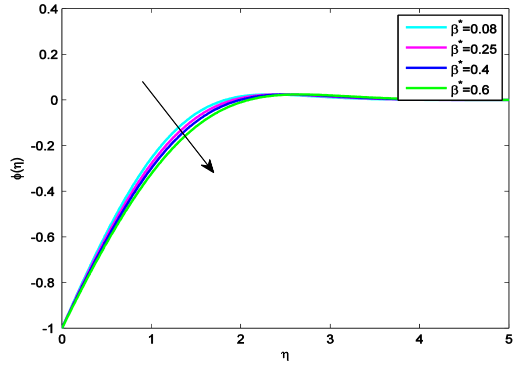

Figure5. 26: Concentration graph for different values of Wedge angle parameter

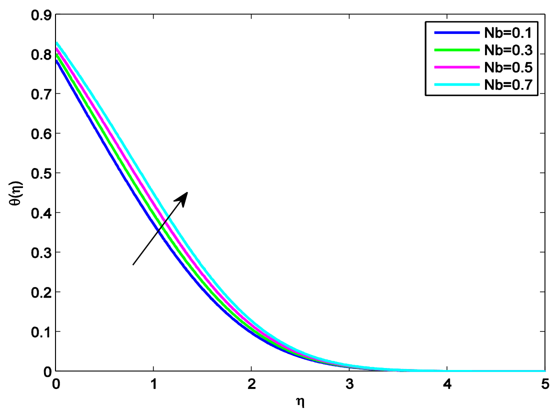

Figure5. 27: Temperature graph for different values of Brownian motion parameter

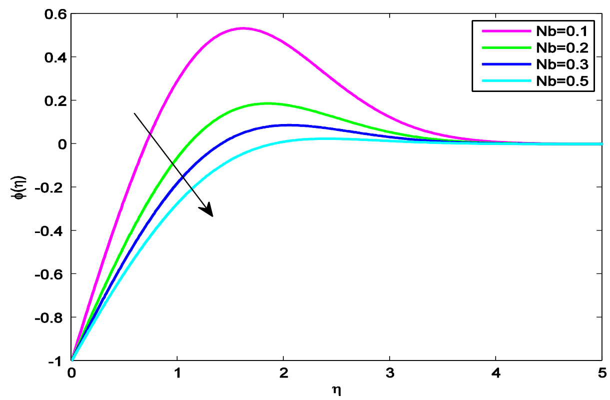

Figure5. 28: Concentration graph for different values of Brownian motion parameter

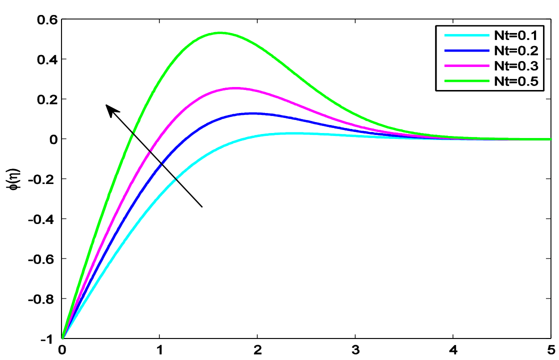

Figure5. 29: Concentration graph for different values of Thermophoresis parameter

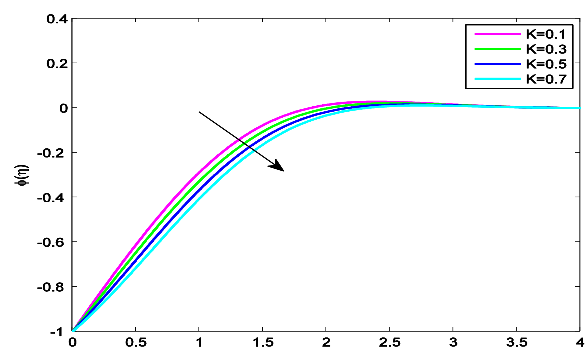

Figure5. 30: Concentration graph for different values of Chemical reaction parameter

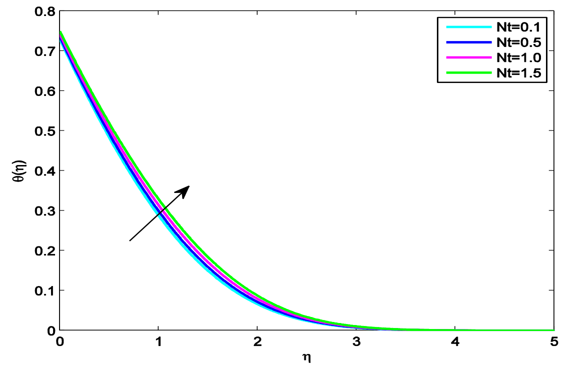

Figure5. 31: Temperature graph for different values of Thermophoresis parameter

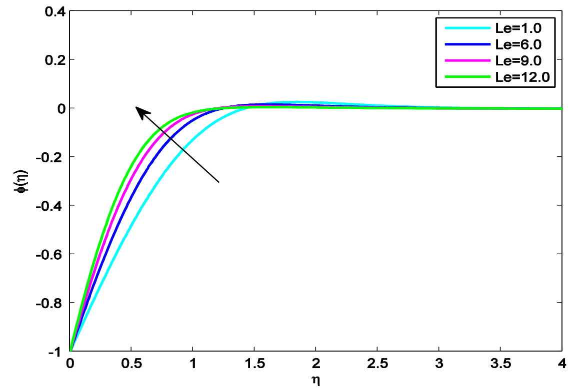

Figure5. 32: Concentration graph for different values of Lewis number parameter

Fig.5.9 demonstrates that as the values of injection parameter $(-\chi)$ increases from -0.01 to -0.6 temperature of the fluid within the boundary layer increases.Fig.5.10 and fig.5.11 reveal that the graph of concentration for different values suctions parameter (χ) and injection parameter $(-\chi)$ respectively. The graphs show that when the values of suctions parameter (χ) raises the concentration profiles within boundary layer increase whereas with an increase of injection parameter $(-\chi)$ the concentration declines. The effects of unsteady parameter (λ_1) on velocity, temperature and concentration profiles are displayed through figs.5.12-5.14. From the graphs we can see that as the values of unsteady parameter (λ_1) upsurges the concentration and the velocity profiles are rise whereas the temperature profiles are decline within boundary layer. Figs.5.15-5.17 illustrates that the influence of Williamson parameter on velocity, concentration and temperature profiles. The graphs demonstrate that when the values of non-Newtonian Williamson parameter (λ) growths the concentration and temperature increases but opposite result is obtained for velocity within the boundary layer.

For different values of Prandtl number (Pr) the graph of temperature and concentration is displayed through figs.5.18-5.19. From fig.5.18 it is found that as the values of Pr rises the temperature at the wedge surface decreases and the thermal boundary layer width shrinks. This shows that a fluid with higher Pr has relatively low thermal conductivity, which results in heat conduction and there by the thermal boundary layer thickness, and temperature drops. The concentration profile within the boundary layer increases with an increasing the value of Prandtl number (Pr) was displayed in fig.5.19. Near the wall of the wedge, the concentration growths with a growth in Pr and at some point away from the wall it starts falling before coming to a point far away from where it becomes to a stable position. The effect Eckert number (Ec) (viscous dissipation parameter) on temperature is plotted in fig. 5. 20. It is found that the temperature profile is increased with an increase of Eckert number (Ec). This is due to the fact that heat energy is stored in the liquid due to the frictional heating. The impact of rising Eckert number is to increase the temperature at any point. Fig. 5.21 is plotted to indicate the effect of radiation parameter (R_d) on temperature profiles. It is observed that the temperature profile decreases for increasing values of R_d. This is due to the fact that an increase in the radiation parameter R_d leads to decrease in the boundary layer thickness and enhances the heat transfer rate.

A ratio of the hot fluid side convection resistance to the cold fluid side convection resistance on a surface is the heat convection parameter (Biot number). From this fact we observed that when the values of heat convection parameter upsurge the hot fluid side convection resistance reduces and as a result the surface temperature rises. Accordingly, fig.5.22 reveals that with an increase of Biot number the temperature profiles within the boundary layer raises. The impact of heat convection parameter on concentration profiles is plotted in fig.5.23. As the values of heat convection parameter raises the concentration profiles upsurges within boundary layer.

In figs.5.24-5.26 the effect of wedge angle parameter on velocity, temperature and concentration were plotted. From fig.5.24 we observed that as the value of wedge angle parameter raises the velocity increased within boundary layer. This displays that velocity boundary layer width reduced with an increase of wedge angle parameter(β^*). Fig.5.25 and fig.5.26 illustrates that with an increment of wedge angle parameter (β^*) the profiles of temperature and concentration decreases. The temperature and concentration graphs with various values of Brownian motion (Nb) are depicted in figs.5.27-5.28. Fig.27 indicates that when Brownian motion (Nb) parameter increases, the movement of nanoparticles from the hot surface to cold surface is happened and ambient fluid occurred. Due to this the temperature and thermal boundary layer thickness rises. From fig.5.28 we see that when Brownian motion (Nb) upsurges volume fraction of nanoparticles within the boundary layer upsurges. It is interesting to note that Brownian motion of the nanoparticles at the molecular and nanoscale levels is a key mechanism in governing their thermal behavior. In nanofluid system, due to the size of the nanoparticles, Brownian motion affects the heat transfer properties. As the particle size scale approaches to the nano-meter scale, Brownian motion on the surrounding liquids play an important role in heat transfer. The influence of Thermophoresis on concentration and temperature was displayed in figs.5.29-5.30. The graphs indicated that when the value of Thermophoresis increases both temperature and concentration profiles and boundary layer thickness are increased. This is because of the fact that temperature difference between surface and ambient growths for larger thermophoresis parameter and hence the fluid temperature accelerates for both cases.

Fig.5.31 displays the effects of Chemical reaction parameter on the nanoparticles volume fraction profile. From this figure we have observed that increasing the value of the chemical reaction reduces the concentration profile in the boundary layer. The physical reason of this phenomenon is chemical reaction declines the concentration boundary layer thickness and upsurges the mass transfer. The concentration curves for different values of Lewis number (Le) have been shown in fig.5.32. From the definition of Lewis number, it is clear that an increase in Lewis number (Le) may be because of a larger thermal diffusivity of the fluid for a constant mass diffusivity. This causes an increase of the flow within the boundary layer. Therefore, the graph reveals that when Lewis number (Le) increases the concentration upsurges at the wedge wall and at some point away from the wall it starts falling before coming to a stable position.

5.5. Conclusions

This study presents a mathematical model of unsteady boundary layer flow of Williamson nanofluid past a stretching/Shrinking permeable wedge with thermal radiation, viscous dissipation and chemical reaction. The study extended the previous work of Wubshet and Ayele, (2019) by taking into consideration the effects of unsteadiness parameter, Williamson fluid, chemical reaction, slip effect\and the passively controlled boundary condition. Fluid suction/injection is imposed on the wedge surface. The governing unsteady higher order non-linear ordinary deferential equations(ODEs) are reduced to a set of a first order non-linear differential equations(DEs) by introducing appropriate similarity transformations and then solved numerically by using Keller Box scheme with MATLAB software(R2013a) for different values of the parameters. The obtained numerical results are in good agreement with the previously published data in limiting condition. The numerical results of velocity, temperature and concentration for the dimensionless parameters are presented graphically. As well as the numerical values of local skin friction, local Nusselt number and local Sherwood number are presented in tabular form. Depending on these the result of the study is summarized as follows:

1. Increasing suction χ and unsteady λ_1 parameters raises both the velocity and concentration profiles near the surface of the wedge but it diminutions the thermal boundary layer thickness.
2. Both temperature and concentration profiles are declining function within the boundary layer but the velocity boundary layer thickness enhanced for raising the values of β^*parameter.
3. For growing the values of Bi and Nt the thermal boundary layer thickness and the concentration profiles growths near the wedge surface.
4. The temperature profile declines within the boundary layer and the concentration profile enhanced near the wedge surface for rising values of Pr.
5. When the values of thermal radiation and Eckert number rises, the temperature profiles are amplified.
6. As the values of chemical reaction upsurges the concentration profiles diminutions but the concentration profiles grows with a rise of Lewis number.
7. For increasing the values of Nb both the temperature and concentration profiles are increased.
8. The skin friction coefficient rises with growing values of λ, β^* and χ. But it declines for enlargement values of λ_1.
9. The heat transfer rate $(-\theta'(0))$ and the mass transfer rate $(-\phi'(0))$ enhances with rising values of β, χ and λ_1.
10. The heat transfer rate is improved for rising values of Ec but it declines for rising values of λ.
11. The mass transfer rate reduces for an increase of λ and Ec.

References

Aamir Hamid, Masood Khan and Alshomrani A.S. (2019). Non-linear radiation and chemical reaction effects on slip flow of Williamson nanofluid due to a static/moving wedge. *Applied Nano science.*

Abdul Maleque Kh. (2013). Effects of Exothermic/Endothermic Chemical Reactions with Arrhenius Activation Energy on MHD Free Convection and Mass Transfer Flow in Presence of Thermal Radiation. *Journal of Thermodynamics,* 692516.

Abdul Samad Khan, Yufeng Nie and Zahir Shah (2019). Impact of Thermal Radiation and Heat Source/Sink on MHD Time-Dependent Thin-Film Flow of Oldroyed-B, Maxwell, and Jeffry Fluids over a Stretching Surface. Processes. 7(191), 1-18.

Abegunrin O.A. and Animasaun I.L. (2017). Motion of Williamson Fluid over an Upper Horizontal Surface of a Paraboloid of Revolution due to Partial Slip and Buoyancy. Defect and Diffusion Forum. 378, 16-27.

Alam M. S., Ali M., Alim M. A., Haque Munshi M. J. and Uddin Chowdhury M. Z. (2017). Solution of Falkner- Skan Unsteady MHD Boundary Layer Flow and Heat Transfer past a Moving Porous Wedge in a Nanofluid. *Procedia Engineering*. 194 414 – 420.

Alam M. S., Tariku Islam and Rahman M. M. (2015). Unsteady Hydromagnetic Forced Convective Heat Transfer Flow of A Micropolar Fluid Along A Porous Wedge With Convective Surface Boundary Condition. *International Journal of Heat and Technology*, 33(2).

Ali M., Alim M. A., Nasrin R., Alam M. S., Haque Munshi M. J. (2017). Similarity Solution of Unsteady MHD Boundary Layer Flow and Heat Transfer past a Moving Wedge in a Nanofluid using the Buongiorno Model. Procedia Engineering. 194, 407 – 413.

Ali M.and Alim M.A. (2018). Boundary Layer Analysis In Nanofluid Flow Past A Permeable Moving Wedge In Presence Of Magnetic Field By Using Falkner – Skan Model. Int. J. of Applied Mechanics and Engineering. 23(4), 1005-1013.

Anuradha S. and Yegammai M. (2017). MHD Radiative Boundary Layer Flow of Nanofluid Past a Vertical Plate with Effects of Binary Chemical Reaction and Activation Energy. Global Journal of Pure and Applied Mathematics. 13(9), 6377-6392.

Bharathi M. Devi and Gangadhar K. (2015). Effect of viscous dissipation on Falkner-skin boundary layer flow past a Wedge through a porous medium with slips boundary condition. *International Journal of Engineering Inventions*. 4(11), 21-35.

Choi SUS, Eastman JA. (1995). Enhancing thermal conductivity of fluids with nanoparticles, presented at ASME. *International Mechanical Engineering Congress and Exposition*.:1217.

Falkner V.M., Skan S.W. (1931). Some Approximate Solutions of Boundary Layer Equations. *Philosophical Magazine and Journal of Science*. 12(80), 865-896.

Gireesha B.J., Ganesh Kumar K., Ramesh G.K. and Prasannakumara B.C. (2018). Nonlinear convective heat and mass transfer of Oldroyd-B nanofluid over a stretching sheet in the presence of uniform heat source/sink*; Results in Physics*. (9), 1555-1563.

Hameed Khan, Muhammad Haneef, Zahir Shah, Saeed Islam, Waris Khan and Sher Muhammad. (2018). The Combined Magneto Hydrodynamic and Electric Field Effect on an Unsteady Maxwell Nanofluid Flow over a Stretching Surface under the Influence of Variable Heat and Thermal Radiation. *Appl. Sci*. 8(160), 1-17.

Hashim, Aamir Hamid and Masood Khan. (2019). Multiple solutions for MHD transient flow of Williamson nanofluids with convective heat transport. Journal of the Taiwan Institute of Chemical Engineers 103, 126–137.

Hayat T., Anum Shafiq and Alsaedi A. (2016).Hydromagnetic boundary layer flow of Williamson fluid in the presence of thermal radiation and Ohmic dissipation. *Alexandria Engineering Journal.*

Kandasamy R., Muhaimin I. and Rosmila A.I. (2014).The performance evaluation of unsteady MHD non-Darcy nanofluid flow over a porous wedge due to renewable (solar) energy. *Renewable Energy*. 64. 1-9.

Kumaran G., Sandeep N. and Vijayaragavan R. (2017). Melting heat transfer in magnetohydrodynamic radiative Williamson fluid flow with non-uniform heat source/sink. Materials Science and Engineering 263 062022.

Mahanthesh B., Gireesha B.J. and Rama Subba Reddy Gorla. (2016). Nonlinear radiative heat transfer in MHD three-dimensional flow of water based nanofluid over a non-linearly stretching sheet with convective boundary condition. *Journal of the Nigerian Mathematical Society*. (35) 178–198.

Majeed A., Zeeshan A. and Noori F. M. (2019). Numerical study of Darcy-Forchheimer model with activation energy subject to chemically reactive species and momentum slip of order two. AIP Advances. 9, 045035.

Michael J. Martin and Iain D. Boyd. (2009). Falkner-Skan flow over a wedge with slip boundary conditions. *American Institute of Aeronautics and Astronautics.*

Mohammadi F., Hosseini M.M, Dehgahn A. and Maalek Ghaini F.M. (2012). Numerical Solutions of Falkner-Skan Equation with Heat Transfer. *Studies in Nonlinear Sciences*. 3 (3), 86-93

Mohd Rijal Ilias, Nur Sa'aidah Ismail and Wan Siti Esah C Hussain. (2018). Unsteady Aligned MHD Boundary Layer Flow of a Magnetic Nanofluid Over A Wedge. *International Journal of Civil Engineering and Technology (IJCIET).* 9(11), 794–810.

Muhaimin I., Kandasamy R., Khamis Azme B. and Rosalan Rozaini (2013). Influence of thermophoresis particle deposition and chemical reaction on unsteady non-Darcy MHD mixed convective flow over a porous wedge in the presence of temperature dependent viscosity. Journal of Mechanical Science and Technology 27(5), 1545-1555.

Nadeem S. and Hussain S. T. (2014).Flow and heat transfer analysis of Williamson nanofluid. *Appli Nanosci*, 4, 1005-1012.

Nadeem S., Hussain S. T. and Lee C. (2013). Flow of a Williamson fluid over a stretching sheet. *Brazilian journal of Chemistry Engineering*, 30 (3), 619-625.

Nagendra N., Amanulla C.H. and Sudhakar Reddy M. (2018). Slip Effects on MHD Flow of a Williamson Fluid from an Isothermal Sphere. AMSE Journals. 86(3), 782-807.

Plum O.A., Huenfeld J.S. and Eschbach E.J. (1981). The effect of cross flow and radiation on natural convection from vertical heated surfaces in saturated porous media. In Proceedings of the AIAA. 23–25.

Radiah Bte Mohamad, Kandasamy R. and Muhaimin I. (2013). Enhance of heat transfer on unsteady Hiemenz flow of nanofluid over a porous wedge with heat source sink due to solar energy radiation with variable stream condition. *Heat Mass Transfer.* 231(1163), 1-9.

Rahman ATM. M., Alam M. S., Alim M. A. and Chowdhury M. K. (2013). Unsteady MHD forced convective heat and mass transfer flow along a wedge with variable electric conductivity and thermophoresis. *Procedia Engineering*. 56, 531 – 537.

Rahman ATM. M., Alam M. S., Chowdhury M. K. and Rahman M.M. (2011). Unsteady Two-Dimensional Convective Heat and Mass Transfer Flow along a Wedge with Thermophoresis. *International Conference on Mechanical Engineering.*

Rajput U S and Gaurav Kumar (2017). Radiation effect on MHD flow past an oscillating inclined plate with heat and mass transfer. *Journal of Mathematics and Informatics*, 09(01).

Rama Subba Reddy Gorla and Mahesh Kumari. (2012). Mixed convective boundary layer flow over a vertical wedge embedded in a porous medium saturated with a nanofluid. *J Nano engineering and Nano systems.* 225(2) 55–66.

Ramana Reddy J.V., V. Sugunamma and Sandeep N. (2018). Thermophoresis and Brownian motion effects on unsteady MHD nanofluid flow over a slendering stretching surface with slip effects *Alexandria Engineering Journal*. (57), 2465–2473.

Ramesh G.K., Ganesh Kumar K., Shehzad S.A. and Gireesha B.J. (2017). Enhancement of radiation on hydromagnetic Casson fluid flow towards a stretched cylinder with suspension of liquid-particles. *Canadian Journal of Physics.* Cjp-2017-0307.R1, 1-24.

Rashad A.M., Modather M. Abdou M., and Ali Chamkha (2011). MHD Free Convective Heat and Mass Transfer of a Chemically-Reacting Fluid from Radiate Stretching Surface Embedded in a Saturated Porous Medium. *International Journal of Chemical Reactor Engineering,* 9, 1-15.

Sajid T., Sagheer M., Hussain S., and Bilal M. (2018). Darcy-Forchheimer flow of Maxwell nanofluid flow with nonlinear thermal radiation and activation energy. *AIP ADVANCES* 8, 035102.

Sameh E. Ahmed, Ramadan A. Mohamed, Abd Elraheem M. Aly, Mahmoud S. Soliman. (2019). Magnetohydrodynamic Maxwell Nanofluids Flow over a Stretching Surface through a Porous Medium with the effects of Non-Linear Thermal Radiation, Convective Boundary Conditions and Heat Generation/Absorption. *International Journal of Mechanical, Industrial and Aerospace Sciences*, 13(6).

Sattar M. A. (2011). A local similarity transformation for the unsteady two-dimensional hydrodynamic boundary layer equations of a flow past a wedge. *Int. J. Appl. Math. and Mech*., 7(1), 15-28.

Seddeek M. A., Afify A. A. and Al- Hanaya A. M. (2009). Similarity Solutions for a Steady MHD Falkner-Skan Flow and Heat Transfer over a Wedge Considering the Effects of Variable Viscosity and Thermal Conductivity. *An International Journal Applications and Applied Mathematics.* 4(2), 301 – 313.

Sulochana C., Ashwinkumar G.P. and Sandeep N. (2016). Similarity solution of 3D Casson nanofluid flow over a stretching sheet with convective boundary conditions. *Journal of the Nigerian Mathematical Society*. (35) 128–141.

Talha M.A. Osman Gani M. and Ferdwos M. (2018). Numerical solution of steady Magnetohydrodynamic boundary layer flow due to Gyrotactic microorganism for Williamson nonofluid over stretched surface in the presence of exponential internal heat generation. *International Journal of Mathematical and Computational Sciences*. 12(2).

Watanabe T. (1990). Thermal boundary layer over a wedge with uniform suction and injection in forced flow. *Acta Mechanica.* 83(3-4), 119–126.

Williamson R. V. (1929). The flow of pseudo plastic materials. *In*

dustrial and Engineering Chemistry Research. 21(11): 1108.

Wubshet Ibrahim and Ayele Tulu. (2019). Magnetohydrodynamic (MHD) Boundary Layer Flow Past a Wedge with Heat Transfer and Viscous Effects of Nanofluid Embedded in Porous Media. *Mathematical Problem in Engineering*.

Wubshet Ibrahim and Dachasa Gamachu. (2019). Nonlinear convection flow of Williamson nanofluid past a radially stretching surface. *AIP Advances* 9, 085026.

Xiaoqin Xu and Shumei Chen. (2017). Dual solutions of a boundary layer problem for MHD nanofluids through a permeable wedge with variable viscosity. *Xu and Chen Boundary Value Problems.* 2017:147.

Chapter6

The investigation of MHD Williamson nanofluid over stretching cylinder with the effect of activation energy

6.1. Introduction

The heat and mass transfer of boundary layer flow of non- Newtonian fluids over a stretching cylinder is of great interest for scientists, engineers and researchers due to its wide applications. Some examples of its applications are extrusion process, extraction of metals, annealing, thinning of copper wire, pipe industry, etc. Nowadays in most industries the significance of non-Newtonian fluids governs the Newtonian fluids. The rheological properties of non-Newtonian fluids cannot be illuminated by the classical Naiver-Stokes equations. Also, non- Newtonian fluids characteristics can not be modeled by single model. To overcome this difficulty ample models have been come into being. The rheological models that were projected were Williamson, Cross, Ellis, power law, Carreau fluid model, etc. Typical of a non-Newtonian fluid model with shear retreating property is Williamson fluid model and was first expected by (Williamson, 1929). Some recent investigations concerning the flow and heat and mass transfer MHD flow of Williamson fluid can be mentioned through investigations [2-6].

Heat and mass transfer in non-Newtonian fluid flow through porous medium in engineering has extensive application, such as ventilation procedure, oil production, solar collector, cooling of nuclear reactors, electronic cooling etc. Accordingly, Srinivas Maripala and Kishan, (2015) investigated the effect of thermal radiation and chemical reaction on time dependent MHD flow and heat transfer of nanofluid over a permeable shrinking sheet. Their result indicates that with an increase of suction parameter the temperature profiles decreases whereas the concentration profiles upsurges. Moreover, Kairi and RamReddy, (2015), Vijaya Lakshmi et al., (2018), Ambreen et al.(2019), Aurangzaib et al., (2013), Bal Reddy et al., (2019), Abdullah Al-Mamun et al., (2019) and Sameh E. Ahmed et al., (2019) studied mixed convective heat and mass transfer of MHD nano fluids embedded in porous medium over stretching surfaces. From their result it can be seen that temperature distribution and thermal boundary layer reduces with an increase of dimensionless thermal free convection parameter, dimensionless mass free convection parameter and Prandtl number.

The miracle of heat generation/absorption in working fluid plays an important role in several engineering and industries. The influence of heat generation may increase the temperature distribution in moving fluids, and consequently, impacts the heat transfer rate. Some of its application in many industries is geothermal system, thermal absorption, and removal of heat from nuclear wreckage, food storage, microelectronics manufacturing and cooling of nuclear reactors. Consequently, heat generation or absorption in MHD flow of casson fluid over a stretching wedge with viscous dissipation and Newtonian heating was investigated by (Imran Ullaha et al., 2018). Moreover, Zeeshan Khan et al., (2018) and Padmavathi and Anitha Kumari, (2017) examined the effect of heat generation or absorption on mixed heat and mass transfer nanofluids embedded over stretching surfaces. Some researchers have studied for the impact of heat source/sink on MHD non-Newtonian nanofluids over stretching surfaces [18–23].

Activation energy is the smallest amount of energy needed by chemical reactants to endure a chemical reaction. The influence of activation energy on convective heat and mass transfer in the region of boundary layers was initially inspected by (Bestman, 1990). Later many researcher have been studied the impact of activation energy on heat and mass transfer of boundary layer flow of the fluids. Among those researchers, Faiz G. Awad et al., 2014), Mlamuli Dhlamini et al., (2018), Anuradha and Sasikala, (2018) and Aamir Hamid et al., (2018) scrutinized the influence of activation energy on heat and mass transfer in unsteady fluid flow under different geometry. Moreover, Chuo-Jeng Huang, (2019) and Mustafa, (2017) studied the effect of activation energy on MHD boundary layer flow of nano fluids past vertical surface and permeable horizontal cylinder. Further investigations on the effect of activation energy on non-Newtonian fluid under different surfaces are stated in [31-34]. From their plots it can be seen that as the values of activation energy parameter upsurges the concentration nanoparticles increases.

In view of all the above revealed studies, it is decided that the effect of activation energy on mixed convective heat and mass transfer of Williamson nano fluid over stretching cylinder embedded in porous medium with heat generation/absorption is not examined yet. Thus, to fill this gap, we aim to explore the effect of activation energy on mixed convective heat and mass transfer of Williamson nano fluid over stretching cylinder embedded in porous medium with heat generation/absorption. For the information our work is innovative in terms of the proposed fluids and incorporated parameters in the boundary layer flow. Numerical solution is obtained by using Runge-Kutta method in conjugation with shooting technique. Numerical results of Nusselt number, skin friction coefficient and Sherwood number for different values of physical parameter are computed in tables. The effects of different physical parameter on dimensionless velocity, temperature and concentration are presented in graphs.

6.2. Mathematical formulation

Two dimensional time independent Williamson nanofluid over stretching cylinder in the presence of boundary layer slip has been considered. Porous cylinder is chosen. Magnetic field of constant strength B_0 is applied normal to the flow along r-axis in radial direction with the assumption of small Reynolds number so that the induced magnetic field is neglected. The fluid is infinite in magnitude of positive $x-$direction. The mixed convective mass and heat transfer phenomenon are included in the existence of heat generation/absorption. T_w and $C_w$are surface temperature and concentration respectively. The ambient fluid temperature and concentration are denoted by T_∞ and C_∞ respectively. Further, u and v are the velocity components in the direction of x and r respectively. All the physical properties of the fluid are considered constant.

Using the assumptions given above the governing equations of continuity, momentum, energy and mass are specified as follows:

$$\frac{\partial}{\partial x}(ru)+\frac{\partial}{\partial y}(rv)=0 \tag{6.1}$$

$$u\frac{\partial u}{\partial x}+v\frac{\partial u}{\partial r}=\nu\left(\frac{1}{r}\frac{\partial u}{\partial r}+\frac{\partial^2 u}{\partial r^2}\right)+\nu\left(\frac{\Gamma}{\sqrt{2}r}\left(\frac{\partial u}{\partial r}\right)^2+\sqrt{2}\Gamma\frac{\partial u}{\partial r}\frac{\partial^2 u}{\partial r^2}\right)-\frac{\nu}{k'}u-\frac{\sigma_1 B_0^2}{\rho}u+g\beta_1(T-T_\infty)+ g\beta_2(C-C_\infty)=0, \tag{6.2}$$

$$u\frac{\partial T}{\partial x}+v\frac{\partial T}{\partial r}=\frac{k}{\rho c_p}\left(\frac{1}{r}\frac{\partial T}{\partial r}+\frac{\partial^2 T}{\partial r^2}\right)+\omega\left\{D_B\frac{\partial C}{\partial r}\frac{\partial T}{\partial r}+\frac{D_T}{T_\infty}\left(\frac{\partial T}{\partial r}\right)^2\right\}+\frac{Q}{\rho c_p}(T-T_\infty), \tag{6.3}$$

$$u\frac{\partial C}{\partial x}+v\frac{\partial C}{\partial r}=D_B\left(\frac{1}{r}\frac{\partial C}{\partial r}+\frac{\partial^2 C}{\partial r^2}\right)+\frac{D_T}{T_\infty}\left(\frac{1}{r}\frac{\partial T}{\partial r}+\frac{\partial^2 T}{\partial r^2}\right)-k_r^2(C-C_\infty)\left(\frac{T}{T_\infty}\right)^e\exp\left(\frac{E_a}{k_1 T}\right). \tag{6.4}$$

The boundary conditions are

$$u = u_0 \frac{x}{L} + b_0 \nu \frac{\partial u}{\partial r}, \qquad v = -v_w, \qquad T = T_w, \qquad C = C_w \ \text{at}\ r = R, \tag{6.5}$$

$$u \to u_\infty, \ \ T \to T_\infty, \ \ C \to C_\infty, \quad \text{as}\ \ r \to \infty. \tag{6.6}$$

where $T_w = T_\infty + T_0 \left(\frac{x}{L}\right)^{\alpha}$, $C_w = C_\infty + C_0 \left(\frac{x}{L}\right)^{\varsigma^*}$ are surface temperature and surface concentration respectively. u_0, T_0 and C_0 are reference velocity, temperature and concentration respectively, α is temperature exponent and ς^* is concentration exponent signifying the change of amount of solute in x −direction.

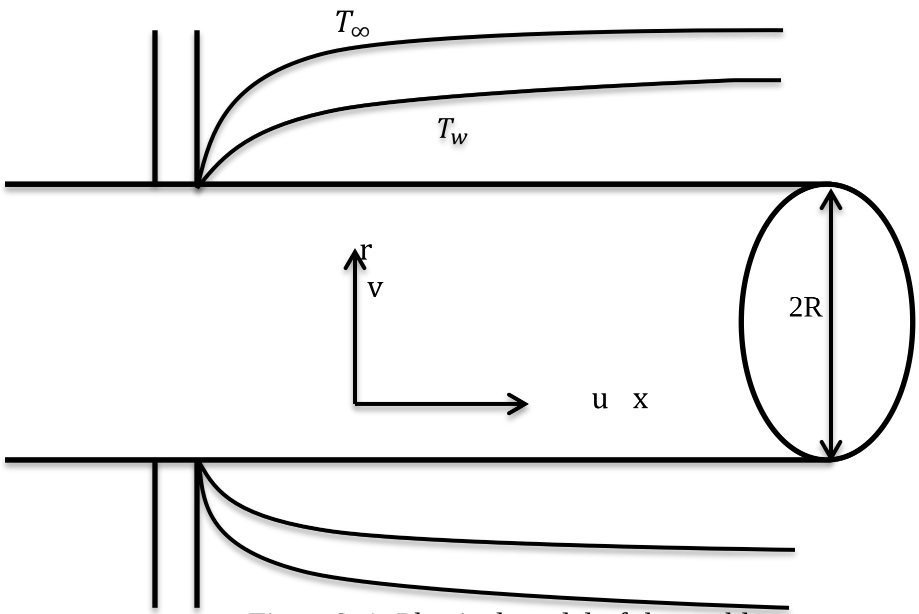

Figure6. 1: Physical model of the problem

The partial differential equations given in equations (6.2)-(6.4) are converted to system of ordinary differential equations by inspiring the following similarity transformations.

$$\eta = \frac{r^2 - R^2}{2R}\left(\frac{u_0}{x\nu}\right)^{\frac{1}{2}}, \qquad \psi = Rf(\eta)(x\nu u_0)^{\frac{1}{2}}, \qquad \theta(\eta) = \frac{T - T_\infty}{T_w - T_\infty}, \qquad \phi(\eta) = \frac{C - C_\infty}{C_w - C_\infty} \tag{6.7}$$

$$u = \frac{1}{r}\frac{\partial \psi}{\partial r} \ \text{and}\ v = -\frac{1}{r}\frac{\partial \psi}{\partial x} \tag{6.8}$$

Thus, the system of ordinary differential equations is:

$$(1+2\eta\gamma)f''' + 2\gamma f'' + {}^{3}\!/_{2}\,(1+2\eta\gamma)^{\frac{1}{2}}\lambda f''^{2} + \lambda(1+2\eta\gamma)^{\frac{3}{2}} f'' f''' - f'^{2} - (d+M)f' + G_t\theta + G_c\phi = 0, \tag{6.9}$$

$$(1+2\eta\gamma)\theta'' + PrNb(1+2\eta\gamma)\theta'\phi' + 2\gamma\theta' + Prf'\theta' + PrNt(1+2\eta\gamma)\theta'^{2} + PrR\theta - Pr\beta f'\theta = 0, \tag{6.10}$$

$$(1+2\eta\gamma)\phi'' + Scf\phi' + 2A\phi' + 2\frac{Nt}{Nb}\gamma\theta' + \frac{Nt}{Nb}(1+2\eta\gamma)\theta'' - Sc\sigma_1(1+\zeta^*\theta)^e exp\left(\frac{-E_d}{1+\zeta\theta}\right) - Sc\varsigma^* f'\phi = 0. \tag{6.11}$$

With the boundary conditions

$$f(0) = \chi,\ \ f'(0) = 1 + \gamma^* f''(0), \quad \theta(0) = 1, \quad \phi(0) = 1, \tag{6.12}$$

$$f'(\infty) = 0, \quad \theta(\infty) = 0, \quad \phi(\infty) = 0. \tag{6.13}$$

Where $M = \left(\frac{\sigma_1 B_0^2 L}{\rho u_0}\right)^{\frac{1}{2}}$ is magnetic parameter, $\gamma = \sqrt{\frac{\nu L}{u_0 R^2}}$ is curvature parameter, $\gamma^* = B_0\sqrt{\frac{\nu u_0}{L}}$ is slip parameter, $\lambda = \Gamma\sqrt{\frac{2u_0^3}{\nu L}}$ is Weissenberg number (Williamson parameter), $G_t = \frac{g\beta_1(T_w - T_\infty)}{Re_x \nu}$ is local temperature buoyancy parameter, $G_c = \frac{g\beta_2(C_w - C_\infty)}{Re_x \nu}$ is concentration buoyancy parameter, $d = \frac{\nu L}{u_0 k}$ is porosity parameter, $Nb = \frac{\omega D_{B(C_w - C_\infty)}}{\nu}$ is Brownian motion parameter, $Nb = \frac{\omega D_{T(T_w - T_\infty)}}{\nu T_\infty}$ is thermophoresis parameter, $R = \frac{QL}{\rho c u_0}$ is the heat source/sink parameter, $Pr = \frac{\mu c_p}{k}$ is Prandtl number, $Sc = \frac{\nu}{D_B}$ is Schmidt number, $\sigma_1 = \frac{k_r^2}{c}$ is the reaction rate parameter, $E_d = \frac{E_a}{k_1 T_\infty}$ is activation energy parameter, $\zeta^* = \frac{T_w - T_\infty}{T_\infty}$ is temperature difference parameter.

Local skin friction coefficient (C_f), Local Nusselt number (Nu_x) and Local Sherwood number (Sh_x) are defined as follows.

$$C_f = \frac{2\tau_w}{\rho u_e^2}, \quad Nu_x = \frac{x p_w}{k(T_w - T_\infty)}, \quad Sh_x = \frac{x q_w}{D_B(C_w - C_\infty)}, \tag{6.14}$$

where $\tau_w = \mu\left(\frac{\partial u}{\partial r} + \frac{\Gamma}{\sqrt{2}}\left(\frac{\partial u}{\partial r}\right)^2\right)_{r=R}, \quad q_w = -k\left(\frac{\partial T}{\partial r}\right)_{r=R}, \qquad q_m = -D_B\left(\frac{\partial C}{\partial r}\right)_{r=R}.$ (6.15)

The non-dimension forms of Local Nusselt number, Local skin friction coefficient, Local Sherwood number are:

$$C_f \frac{\sqrt{Re_x}}{2} = f''(0) + \frac{\lambda}{2} f''^2(0), \qquad Nu_x Re_x^{-1/2} = -\theta(0), \qquad Sh_x Re_x^{-1/2} = -\phi(0). \tag{6.16}$$

where $Re_x = \frac{u_0^2 x}{\nu}$ is local Reynolds number.

6.3. Solution methodology

The coupled non-linear ordinary differential equation (6.9)-(6.11) subjected to the boundary conditions (6.12) and (6.13) are solved numerically using Runge-Kutta method with shooting technique. For the minor change of initial guesses u_1, u_2 and u_3 Newton Raphson method is applied subject to the tolerance $\varepsilon_1 = 10^{-5}$. On the origin of a number of computational experiments, there is no important change in the results after $\eta = 5$. So, it was considered $[0, 5]$ as the domain of the problem in terms of $[0, \infty)$. To solve this problem by using these method equations (6.19)-(6.11) are converted to system of first order ordinary differential equations. System of first order ordinary differential equations is defined below.

$$f = y_1, f' = y_2, f'' = y_3, f''' = y'_3, \theta = y_4, \theta' = y_5, \theta'' = y'_5, \phi = y_6, \phi' = y_7, \phi'' = y'_7 \tag{6.17}$$

Thus, the systems of first order concurrent ODEs are

$$y'_1 = y_2 \tag{6.18}$$

$$y'_2 = y_3 \tag{6.19}$$

$$y'_3 = \frac{-2Ay_3 - \frac{3}{2}(1+2\eta\gamma)^{\frac{1}{2}}\gamma\lambda y_3^2 - y_1 y_3 + y_2^2 + (d+M)y_2 - py_4 - qy_6}{(1+2\eta\gamma) + \lambda(1+2\eta\gamma)^{\frac{3}{2}} y_3} \tag{6.20}$$

$$y'_4 = y_5 \tag{6.21}$$

$$y'_5 = \frac{-PrNb(1+2\eta\gamma)y_5 y_7 - 2\gamma y_5 - Pry_1 y_5 - PrNt(1+2\eta\gamma)y_5^2 + PrRy_4 + Pr\beta y_2 y_4}{(1+2\eta A)} \tag{6.22}$$

$$y'_6 = y_7 \tag{6.23}$$

$$y'_7 = \frac{\begin{array}{c}-Scy_1y_7+PrNt(1+2\eta\gamma)y_5y_7+2\gamma y_7+4\frac{Nt}{Nb}Ay_5-2\frac{Nt}{Nb}Pry_1y_5+2Pr\frac{Nt^2}{Nb}(1+2\eta\gamma)y_5^2 \\ +2\frac{Nt}{Nb}PrSy_4-2\frac{Nt}{Nb}Pr\beta y_2y_4+Sc\sigma_1(1+\zeta^*y_4)^e exp\left(\frac{-E_d}{1+\zeta^*y_4}\right)y_6+Sc\varsigma^*y_2y_6\end{array}}{(1+2\eta\gamma)} \tag{6.24}$$

Here prime represents the derivative with respect to η and the transformed boundary conditions are $y_1(0)=\delta, y_2(0)=1+\gamma^*u_1, y_3(0)=u_1, y_4(0)=1, y_5(0)=u_2, y_6=1,\ y_7=u_3$ (6.25)

6.4. Result and discussion

Figs.6.2 (a)-(c) are plotted to show the distribution of velocity, temperature and concentration for different values of suction (χ) parameter respectively. From these figures it can be seen that when the values of suction parameter increases the velocity, temperature and concentration boundary layer thickness are reduced. This is due to the fact that suction or blowing is the method of controlling the boundary layer. The effect of suction consists in the removal of decelerated fluid particles from the boundary layer before they are given a chance to cause

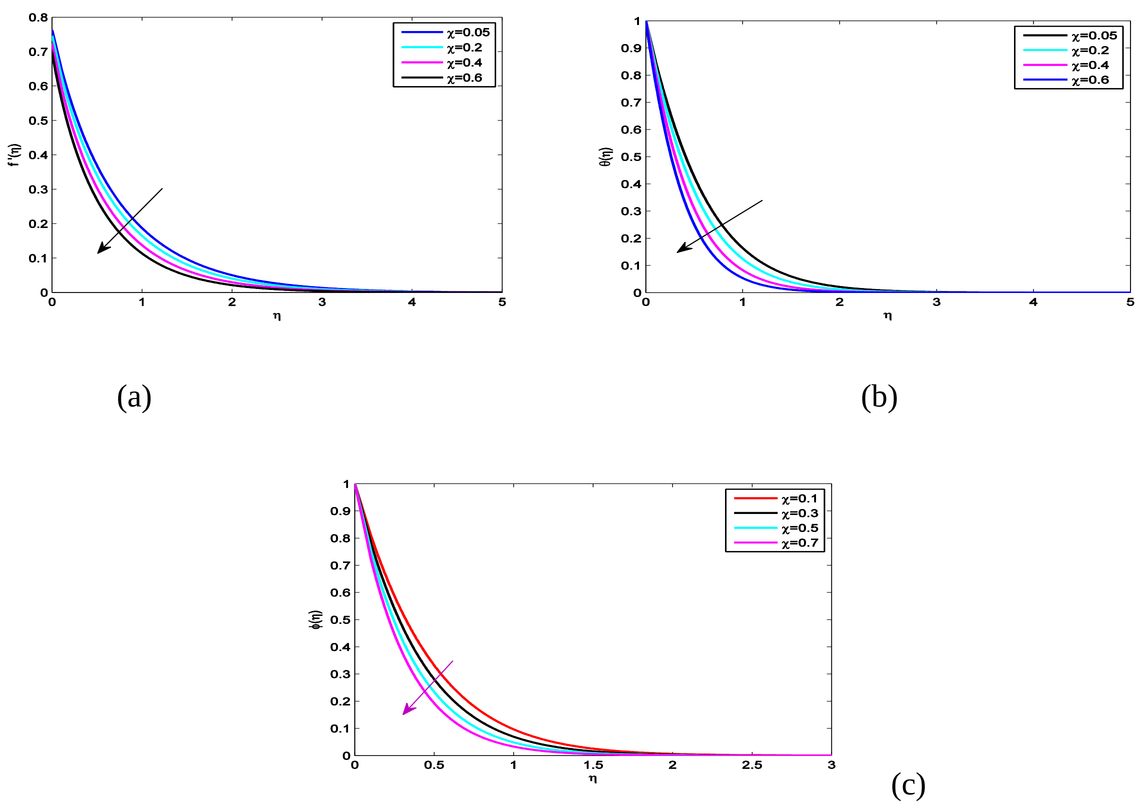

(a) (b)

(c)

Figure6. 2: The graph of Velocity, Temperature and Concentration for different values of Suction (χ)

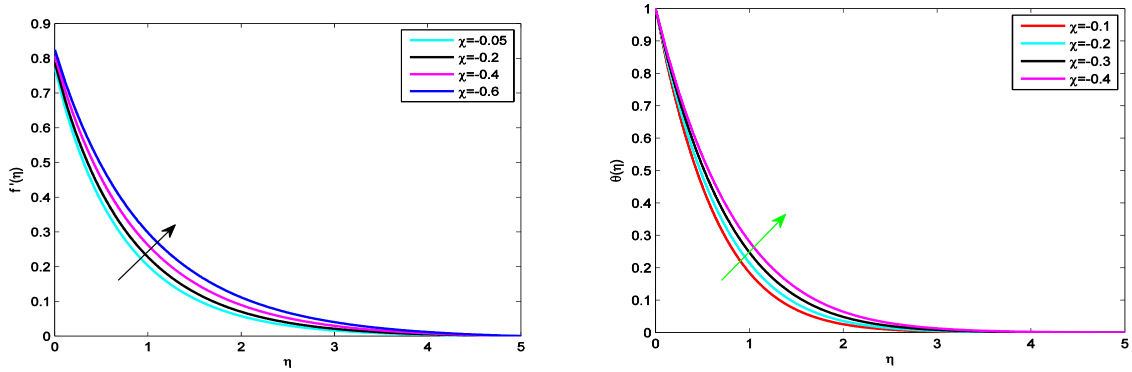

(a) (b)

Figure6. 3: The graph of Velocity and Temperature for different values of Injection $(-\boldsymbol{\chi})$

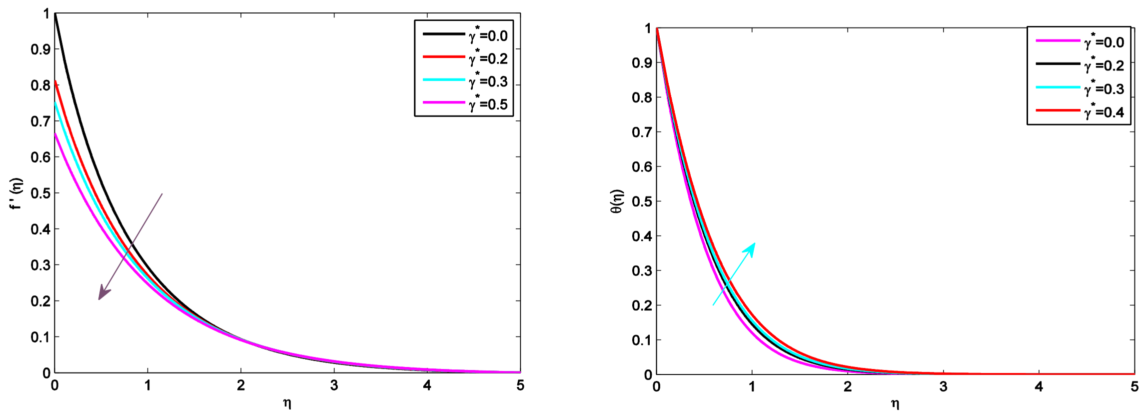

(a) (b)

Figure6. 4: The graph of Velocity and Temperature for different values of Slip parameter $(\boldsymbol{\gamma}^*)$

separation. Figs.6.3 (a)-(b) reveal that the profiles of velocity and temperature for different values of injection $(-\chi)$. The graph shows that with an increase of injection parameter velocity and temperature are upsurges.

For different values of slip parameter (γ^*) the variation of velocity and temperature are plotted in figs. 6.4 (a)-(b). Fig.6.4 (a) shows that when the value of slip parameter raises the velocity profiles reduces. This is because of the fact that when the slip parameter increase, slip velocity increases and consequently fluid velocity declines because under the slip condition, the pulling of the stretching wall can only be partly taken to the fluid. Fig.6.4 (b) displayed that the temperature profiles is raise with an increase of slip parameter.

Figs.6.5 (a)-(c) plotted to show the velocity, temperature and concentration profiles respectively for various values of magnetic field. It is noticed that in fig.6.5 (a) the velocity declines with an increase of magnetic field parameter. From figs.6.5 (b)-(c) it can be seen that the temperature and concentration are upsurges with an increase of magnetic field parameter (M). The physical meaning of this behavior is an upsurge in the values of magnetic field parameter develops the force opposite to the flow, which is known as Lorentz force.

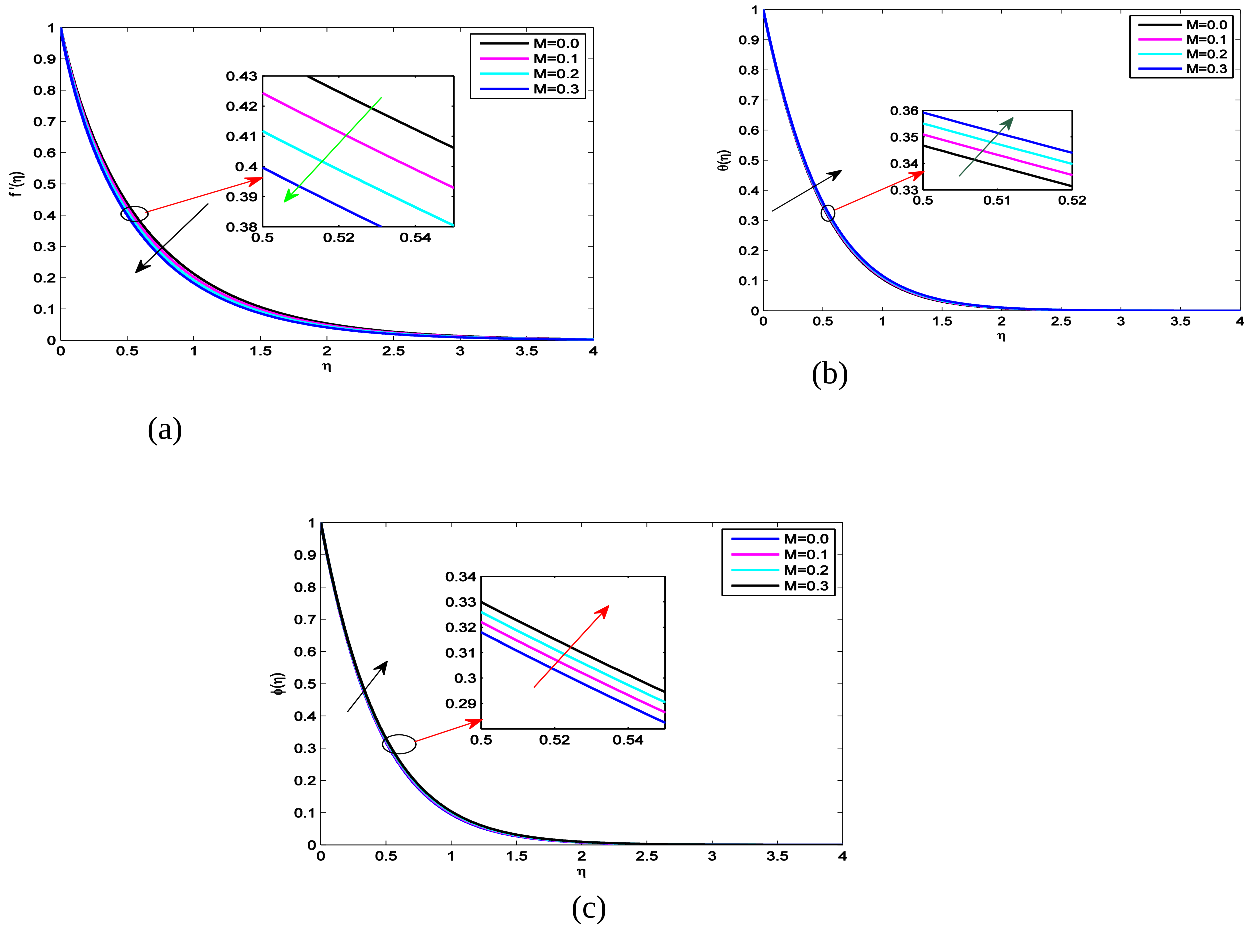

Figure6. 5: The graph of Velocity, Temperature and Concentration for different values of Magnetic field (M)

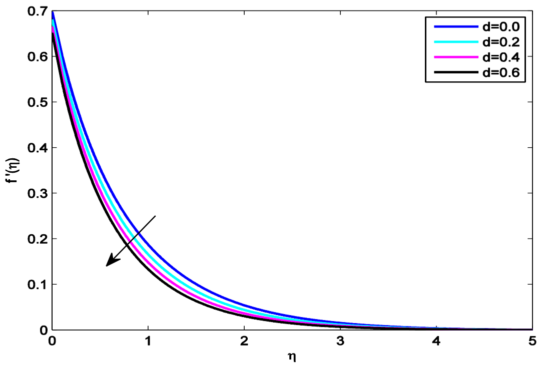

(a)

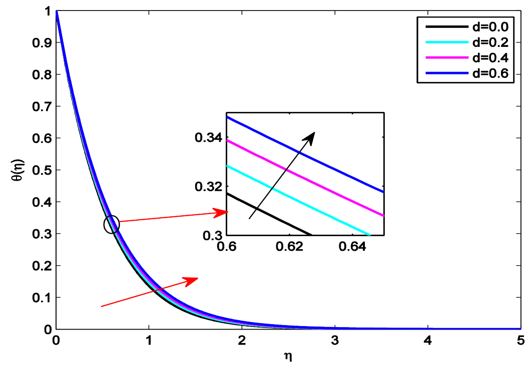

(b)

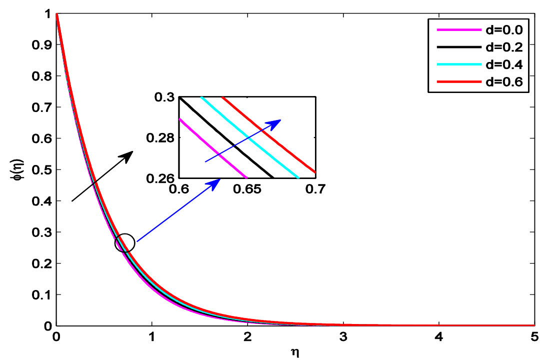

(c)

Figure6. 6: The graph of Velocity, Temperature and Concentration for different values of Porous parameter (d)

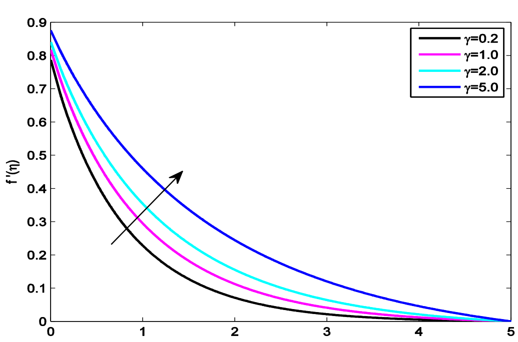

(a)

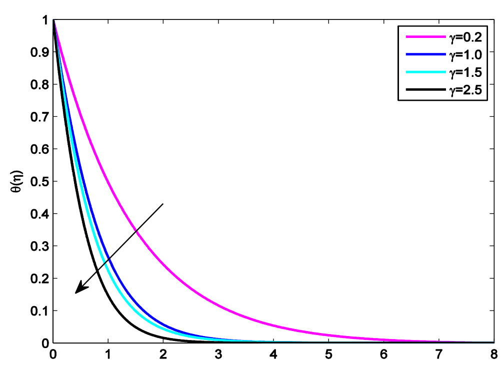

(b)

Figure6. 7: The graph of Velocity and Temperature for different values of Curvature parameter $(\boldsymbol{\gamma})$

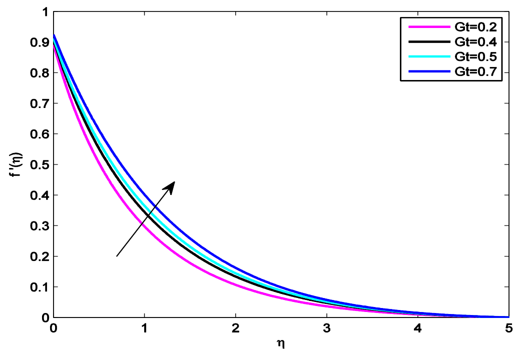

(a)

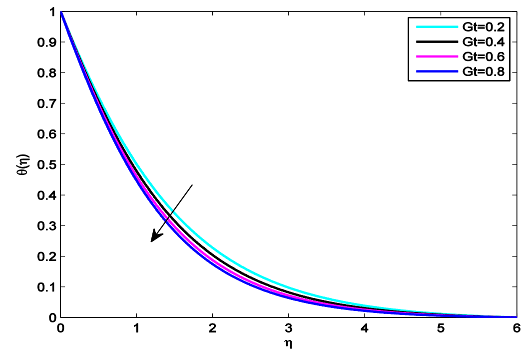

(b)

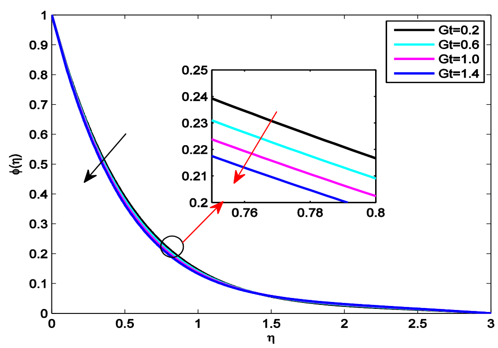

(c)

Figure6. 8: The graph of Velocity, Temperature and Concentration for different values of Temperature Buoyancy parameter ($\mathbf{G_t}$)

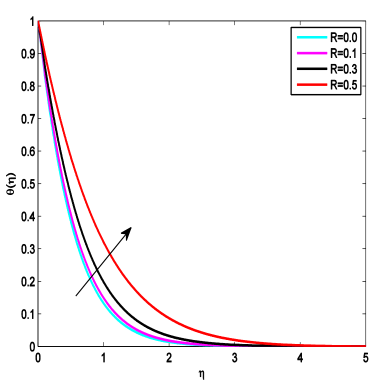

(a)

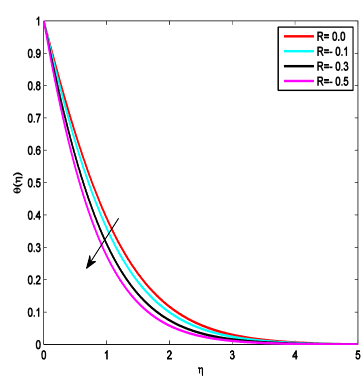

(b)

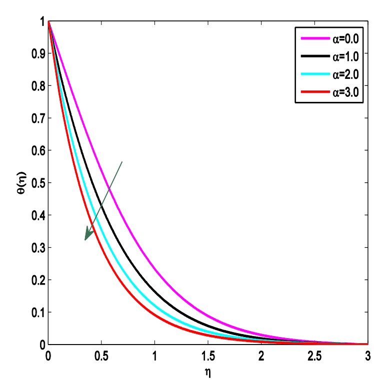

(c)

Figure6. 9: The graph of Temperature for different values of heat source/sink parameter (R) and temperature exponent ($\boldsymbol{\alpha}$)

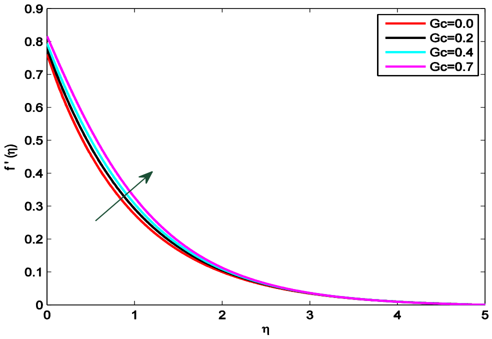

(a)

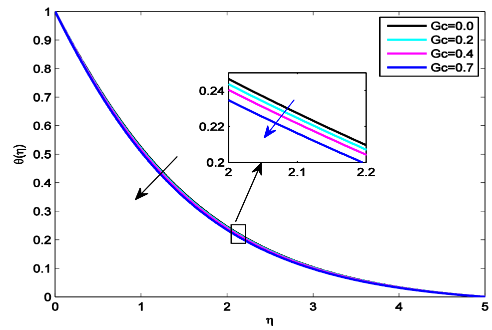

(b)

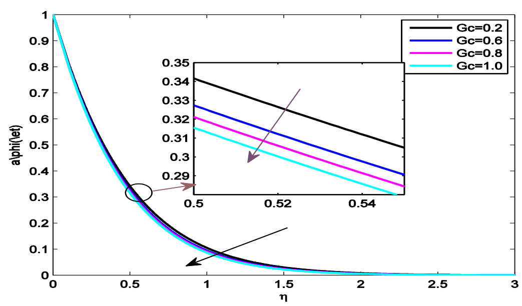

(c)

Figure6. 10: The graph of Velocity, Temperature and Concentration for different values of Concentration Buoyancy parameter (G_c)

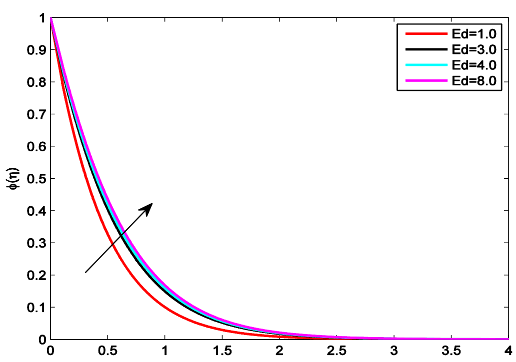

(a)

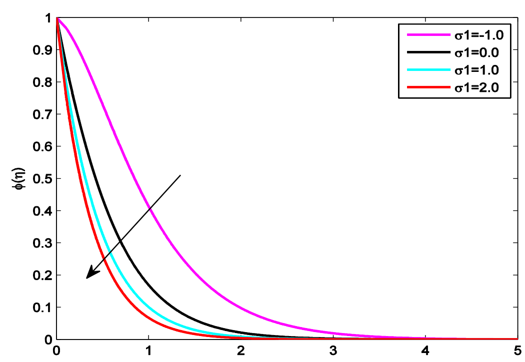

(b)

Figure6. 11: The graph of Concentration for different values of Activation energy ($\mathbf{E_d}$) and reaction rate parameter ($\boldsymbol{\sigma_1}$)

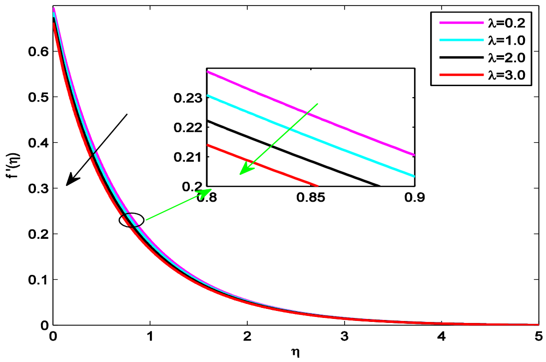

(a)

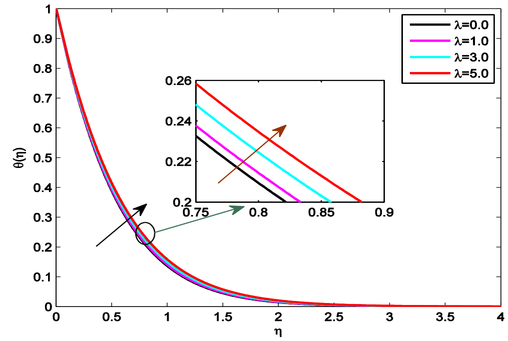

(b)

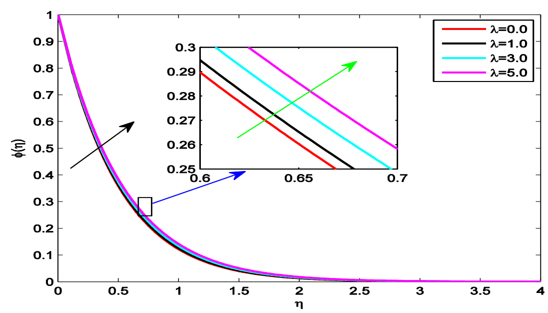

(c)

Figure6. 12: The graph of Velocity, Temperature and Concentration for different values of Williamson Parameter ($\boldsymbol{\lambda}$)

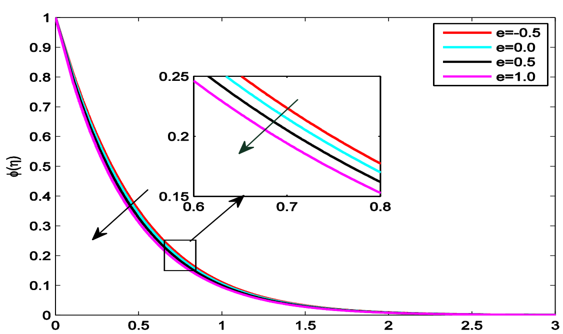

(a)

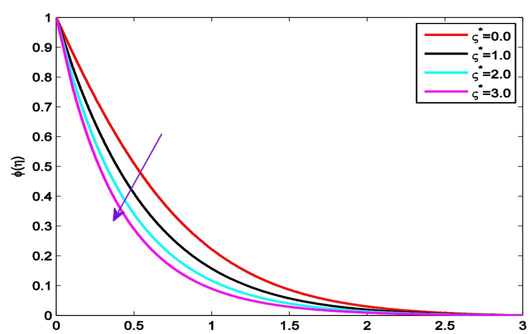

(b)

Figure6. 13: The graph of Concentration for different values of fitted rate constant (e) and Concentration exponent ($\boldsymbol{\varsigma}^*$)

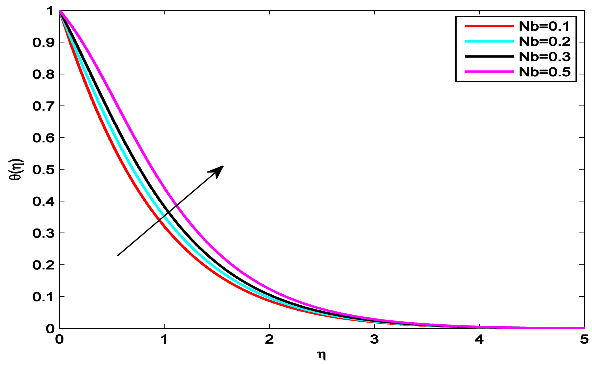

(a)

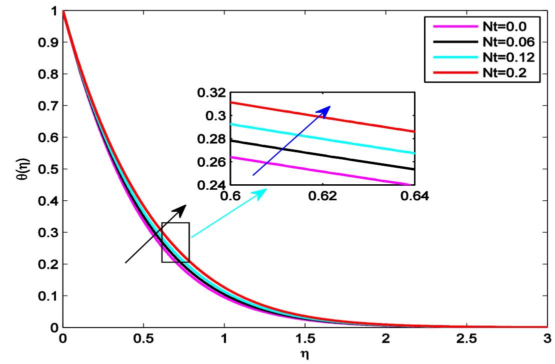

(b)

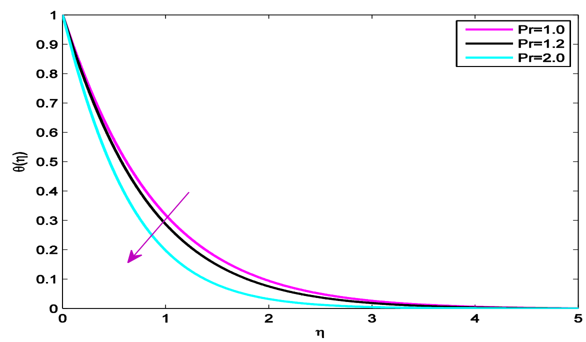

(c)

Figure6. 14: The graph of Temperature for different values of Brownian motion (Nb), Thermophoresis parameter (Nt) and Prandtl number (Pr)

This body force reduced the boundary layer flow and congeals the velocity boundary layers. Furthermore this force creates a resistance force that opposes the fluid motion. Therefore, for the higher magnetic field heat is generated leading to a boost in the temperature and thermal boundary layer thickness. The graph of velocity, temperature and concentration are plotted in figs.6.6 (a)-(c) respectively for different values of porosity parameter. Porous medium causes higher restriction to the fluid flow, which in turn decelerates its motion. Consequently, from fig.6.6 (a) we observed that with an increase of porosity parameter the velocity profiles decreases. But from fig.6.6 (b) and (c) it can be seen that with an increase of permeability parameter both temperature and concentration profiles are increased. The distribution of velocity and temperature for different values of curvature parameter (γ) is plotted in figs.6.7 (a)-(b) respectively. Fig.6.7 (a) displays that the velocity profiles are increased with an increase of

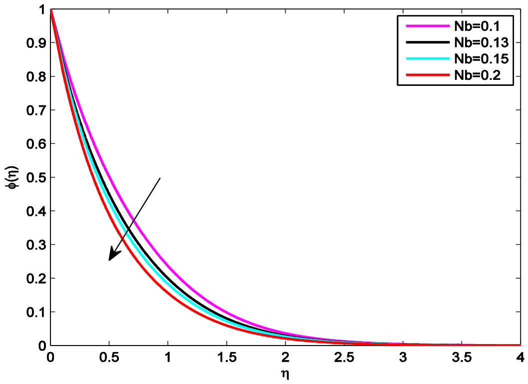

(a)

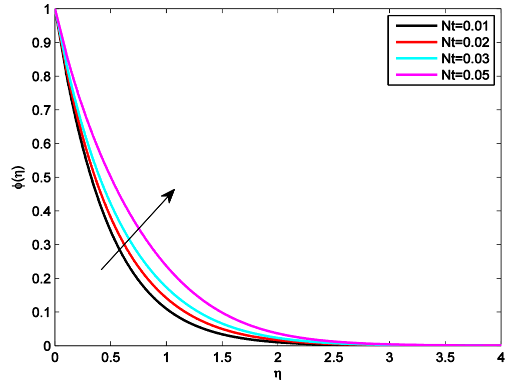

(b)

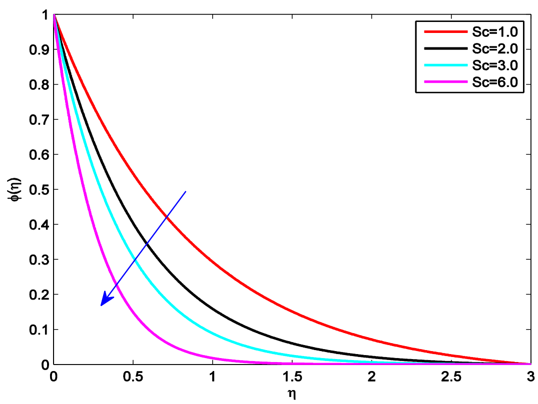

(c)

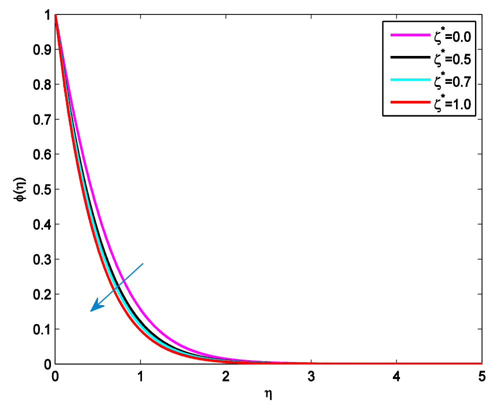

(d)

Figure6. 15: The graph of Concentration for different values of Brownian motion (Nb), Thermophoresis parameter (**Nt**), Schmidt number (**Sc**) and Temperature difference parameter ($\boldsymbol{\zeta}^*$)

curvature parameter, whereas fig.6.7 (b) spectacles that when the values of curvature parameter upsurges the temperature boundary layer thickness declines. This is due to the fact that when curvature parameter increases the radius of the cylinder reduces which deduces that the contact area of the cylinder with the fluid reduces. Hence, less resistance is offered by the surface to the fluid motion and as a result the fluid velocity improved.

For different values of temperature buoyancy parameter (G_t) the graph of velocity, temperature and concentration is presented in figs.6.8 (a)-(c). From these figures we observed that velocity profiles increases with an increase of temperature buoyancy parameter but temperature and concentration field decreases with an increase of temperature buoyancy parameter. Figs.6.9 (a)-(c) shows the graph of temperature for different values of heat source/sink parameter (R) and temperature exponent (α). It is seen that the temperature field increases with an increase of heat source but opposite trend is happen for large values of heat sink and temperature exponent (α). Figs.6.10 (a)-(b) displays the graph of velocity, temperature and concentration respectively, for various values of concentration buoyancy parameter (G_c). The figures illustrates that velocity field increases whereas temperature and concentration fields are declines with an increase of concentration buoyancy parameter.

The effect of activation energy (E_d) and reaction rate parameter (σ_1) on concentration field is plotted in figs.6.11 (a)-(b). From these figures it is seen that when an activation energy upsurges the concentration field raises, but it diminishes with an increase of reaction rate parameter. This is due to the fact that large activation energy and low temperature causes smaller reaction rate constant and thus slow down the chemical reaction. So, the concentration of the solute increases. Figs.6.12 (a)-(c) executes the impact of Williamson parameter on velocity, temperature and concentration fields respectively. Fig.6.12 (a) tells us that with an increase of Williamson parameter the velocity profiles decreases. As we know that Williamson parameter is the ratio of relaxation time to retardation time. Hence, as the values of the retardation time decrease the Williamson parameter increase which displays that there is reduction in velocity field and in addition in boundary layer thickness decrease. On the behalf of figs.6.12 (b) and (c) it is noted that the temperature and concentration fields is upsurges with an enhancement of Williamson parameter.

The variation of concentration profiles for various values of fitted rate constant (e) and concentration exponent (ς^*) is shown in figs.6.13 (a)-(b). It is noticed that the distribution of concentration profiles is decreased with an increase of both fitted rate constant and concentration exponent parameters. This is because when the values of fitted rate constant increased the factor $\sigma(1+\zeta^*\theta)^e exp\left(\frac{-E_d}{1+\zeta^*\theta}\right)$ is augmented. This finally favors the destructive chemical reaction which causes concentration gradient rises. So, the diminution in concentration field is accompanied with a higher concentration gradient at the wall. The impact of Brownian motion (Nb), Thermophoresis parameter (Nt) and Prandtl number (Pr) on temperature is plotted in figs.6.14 (a)-(c). Fig.6.14 (a) indicates that when Brownian motion (Nb) parameter increases, the movement of nanoparticles from the hot surface to cold surface is happened and ambient fluid occurred. Due to this the temperature and thermal boundary layer thickness rises. From fig. 6.14 (b) it is observed that the temperature field grows with an increase of Thermophoresis parameter. A phenomenon in which small particles are pulled away from the hot surface to cold one is called thermophoresis. So, when the surface is heated large number of nanoparticles is moved away which raises the temperature of fluid. Therefore the temperature of fluid increases. Fig.6.14 (c) displays that the effect of Prandtl number (Pr) on temperature. From this it can be seen that when the values of Pr rises the temperature profiles declines. This is because a fluid with higher Pr has relatively low thermal conductivity, which results in heat conduction and there by the thermal boundary layer thickness, and temperature drops. The effect of Brownian motion (Nb), Thermophoresis parameter(Nt), Schmidt number (Sc) and Temperature difference parameter (ζ^*) on concentration profiles are plotted in figs.6.15 (a)-(d). Figs.6.15 (a) indicates that when Brownian motion (Nb) upsurges volume fraction of nanoparticles within the boundary layer reduces. It is interesting to note that Brownian motion of the nanoparticles at the molecular and nanoscale levels is a key mechanism in governing their thermal behavior. In nanofluid system, due to the size of the nanoparticles, Brownian motion affects the heat transfer properties. As the particle size scale approaches to the nano-meter scale, Brownian motion on the surrounding liquids play an important role in heat transfer. Fig.6.15 (b) shows that when with an increase of Thermophoresis parameter concentration profiles rises. From fig.6.15 (c) it is observed that the concentration profiles decrease with an increase of Schmidt number. This is due to the fact that weaker molecular diffusivity appeared for larger Schmidt number and stronger molecular diffusivity corresponds to lower Schmidt number. Fig.6.15 (d) forecasts that with an increase of Temperature difference parameter the concentration profiles declines.

Table6. 1: Comparison of values of skin friction coefficient $\left(\mathbf{f}''(\mathbf{0})\right)$ for various values of λ with earlier scholar results.

λ	Malik et al. (2016) $f''(0)$	Present results $f''(0)$
0.1	-0.9776	-0.9779
0.2	-0.9118	-0.9128
0.3	-0.8413	-0.8417

Table6.1 shows that the comparison of skin friction coefficient with the available published results of (Malik et al., 2016) and found that it is an excellent agreement. Moreover, the comparisons of the values of Nusselt number and Sherwood number with the other published result of (Shafique et al., 2019) have shown in table 6.2. Here from the table it can be seen that there is an excellent agreement.

Table6. 2: Comparison of values of Nusselt number $(-\boldsymbol{\theta}'(\mathbf{0}))$ and Sherwood number $(-\boldsymbol{\phi}'(\mathbf{0}))$ for various values of Pr and E with earlier scholar results.

Pr	E_d	Shafique et al., (2019) $(-\theta'(0))$	Present Result	Shafique et al., (2019) $(-\phi'(0))$	Present Result
1	1	0.51903	0.51913		
2		0.85109	0.85121		
5		1.51553	1.51558		
7		1.84540	1.84547		
10		2.26033	2.26039		
	1			0.95064	0.95069

2		0.75333	0.75338
4		0.58015	0.58020
6		0.53528	0.53530
8		0.52368	0.52371

Straightforwardly, the numerical values of skin friction coefficient, Nusselt number and Sherwood number appears in table 6.3 for different values suction parameter (χ), permeability parameter (d), Curvature parameter (γ) temperature buoyancy parameter (G_t), concentration buoyancy parameter (G_c) and slip parameter (γ^*). It is noticed that the magnitude of skin friction coefficient increase with an increase of suction parameter (χ), permeability parameter (d) and Curvature parameter (γ) whereas with an upsurges of temperature buoyancy parameter (G_t), concentration buoyancy parameter (G_t) and slip parameter (γ^*) the skin friction coefficient magnitude reduced; but it remains constant with an increase of activation energy (E_d) and reaction rate parameter (σ_1). Moreover, from this table it can be seen that when the values of suction parameter (χ), temperature buoyancy parameter (G_t), concentration buoyancy parameter (G_c), activation energy (E_d) and Curvature parameter (γ) increase the magnitude of Nusselt number increases whereas with an increase of permeability parameter (d), reaction rate parameter (σ_1) and slip parameter (γ^*) the magnitude of Nusselt number diminution. Furthermore, from this table it can be seen that Sherwood number declines when the values of permeability parameter (d), activation energy (E_d) and slip parameter (γ^*) raises but opposite trend is happened on Sherwood number as the values of suction parameter (χ) temperature buoyancy parameter (G_t), concentration buoyancy parameter (G_c) and reaction rate parameter (σ_1).

Table6. 3: Numerical results of skin friction coefficient, Nusselt number and Sherwood number for different values of $\boldsymbol{\sigma_1}, \mathbf{d}, \boldsymbol{G_t}, \boldsymbol{G_c}, \boldsymbol{\gamma}, \mathbf{E_d}, \boldsymbol{\chi}, \boldsymbol{\gamma^*}$ **and** $\boldsymbol{\sigma}$ when $\mathbf{Nt = 0.1, Nb = 0.1, M = 0.3}, \boldsymbol{\lambda} = \mathbf{0.1, e = 0.1}, \boldsymbol{\varsigma^*} = \mathbf{1.0}, \boldsymbol{\zeta^*} = \mathbf{0.1, Sc = 3, Pr = 2}, \boldsymbol{\alpha} = \mathbf{1}$, **and** $\mathbf{R = 0.1}$.

χ	d	G_t	G_c	E_d	γ	σ_1	γ^*	$-f''(0)$	$-\theta'(0)$	$-\phi'(0)$
0.0	0.0	0.1	0.1	1.0	0.0	0.1	0.0	1.5944	1.3886	1.8893

0.1						1.7116	1.4823	2.0540
0.2						1.8482	1.5808	2.2277
0.3						2.0143	1.6829	2.4095
	0.0					1.6684	1.6015	2.2530
	0.2					1.8482	1.5805	2.2277
	0.4					2.0500	1.5602	2.2029
	0.6					2.3045	1.5402	2.1784
		0.1				1.7628	1.5895	2.2387
		0.3				1.6121	1.6060	2.2588
		0.5				1.4802	1.6209	2.2771
		1.0				1.2026	1.6534	2.3467
			0.1			1.6992	1.5914	2.2461
			0.3			1.5826	1.6066	2.2600
			0.5			1.4770	1.6171	2.2731
			1.5			1.2469	1.6407	2.3024
				1.0		1.8482	1.5509	1.1909
				2.0		1.8482	1.5534	1.1781
				4.0		1.8482	1.5538	1.1711
				8.0		1.8482	1.5539	1.1699
					0.0	1.5491	1.5273	2.1991

0.15			1.8482	1.5805	2.2277
0.2			1.9930	1.5967	2.2352
0.25			2.2087	1.6117	2.2413
	0.1		1.8482	1.5527	1.1909
	0.3		1.8482	1.5504	1.2315
	0.7		1.8482	1.5463	1.3080
	1.5		1.8482	1.5393	1.4457
		0.0	1.8482	1.5805	2.2277
		0.2	1.1506	1.4413	2.0311
		0.3	0.9958	1.3940	1.9643
		0.4	0.8832	1.3544	1.9083

6.5. Conclusion

This article deals with numerical solution of MHD non-Newtonian nano fluid over stretching cylinder embedded in porous medium with the effect of activation energy and heat generation/ absorption. The impact of various dimensionless physical parameter on velocity, temperature and concentration profiles as well as skin coefficient friction $\left(C_f\right)$, heat transfer rate (Nu_x) and mass transfer rate parameter (Sh_x) are discussed in graphs and tables. The summarized conclusion of numerical study is as follows:

- The suction (χ) parameter interaction reduces the velocity, temperature and concentration profiles of the flow.
- Curvature parameter (γ) improves velocity profiles but it reduces temperature profiles.
- With an increase of porous parameter (d) the profiles of velocity declines whereas temperature and concentration profiles are improved.

- Raise in temperature and concentration buoyancy parameter enhances velocity whereas temperature and concentration are reduced.
- Increase in activation energy (E_d) enhances concentration profiles.
- With an increase of reaction rate parameter (σ_1) the magnitude of skin friction coefficient remain constant but the magnitude of Nusselt number diminution and Sherwood number raises.
- Sherwood number declines when the value of slip parameter (γ^*) rises.

References

Aamir Hamid, Hashim and Masood Khan (2018). Impacts of binary chemical reaction with activation energy on unsteady flow of magneto-Williamson nanofluid. *Journal of Molecular Liquids* 262, 435–442.

Abdullah Al-Mamun, Arifuzzaman S.M., Reza-E-Rabbi Sk., Pronab Biswas, and Shakhaoath Khan Md. (2019). Computational Modeling on MHD Radiative Sisko Nanofluids Flow through a Nonlinearly Stretching Sheet. *International Journal of Heat and Technology*, 37(1), 285-295.

Ambreen N., Rehman A., Sheikh N., Iqbal S., Zulfiqar M. (2019). Boundary-Layer Flow and Heat Transfer over a Rotating Porous Disk in a Non-Newtonian Williamson Nanofluid. *Indian Journal of Science and Technology*, 12(38).

Anuradha Dr.S. and Yegammai M. (2017). MHD Radiative Boundary Layer Flow of Nanofluid Past a Vertical Plate with Effects of Binary Chemical Reaction and Activation Energy. *Global Journal of Pure and Applied Mathematics*, 13(9), 6377-6392.

Anuradha S. and Sasikala K. (2018). MHD Free Convective Flow of a nanofluid over A Permeable Shrinking Sheet with Binary Chemical Reaction and Activation Energy. *International Journal of Engineering Science Invention*, 7(1), 22-30.

Aurang Zaib, Mohammad Mehdi Rashidi, A Chamkha and Krishnendu Bhattacharyya. (2017). Numerical solution of second law analysis for MHD Casson nanofluid past a wedge with activation energy and binary chemical reaction. *International Journal of Numerical Methods for Heat & Fluid Flow*, 27(12), 2816-2834.

Aurangzaib, Kasim A. R. M., Mohammad N. F. and Sharidan Shafie (2013). Unsteady MHD Mixed Convection Flow with Heat and Mass Transfer over a Vertical Plate in a Micropolar Fluid-Saturated Porous Medium. *Journal of Applied Science and Engineering*, 16(2), 141-150.

Bal Reddy G., Shankar Goud B. and Raja Shekar MN. (2019). Numerical Solution of MHD Mixed Convective Boundary Layer Flow of a Nanofluid through a Porous Medium due to an Exponentially Stretching Sheet with Magnetic Field Effect. *International Journal of Applied Engineering Research*, 14(9), 2074-2083.

Bestman AR. (1990). Natural convection boundary layer with suction and mass transfer in a porous medium. *International Journal of Energy Research*, 14, 389–396.

Chuo-Jeng Huang (2019). Arrhenius activation energy effects on free convective about a permeable horizontal cylinder in porous medium. *Transport in porous media*.

Faiz G. Awad, Sandile Motsa, Melusi Khumalo (2014). Heat and Mass Transfer in Unsteady Rotating Fluid Flow with Binary Chemical Reaction and Activation Energy. *PLoS ONE*, 9(9).

Imran Ullah, Sharidan Shafie and Ilyas Khan (2018). Heat generation and absorption in MHD flow of Casson fluid past a stretching wedge with viscous dissipation and Newtonian heating. *Jurnal Teknologi*, 77–85

Jayachandra Babu M. and Sandeep N. (2016). MHD non-Newtonian fluid flow over a slendering stretching sheet in the presence of cross-diffusion effects. *Alexandria Engineering Journal*, 55, 2193–2201.

Kairi R.R. and RamReddy Ch. (2015). The effect of melting on mixed convection heat and mass transfer in non-Newtonian nanofluid saturated in porous medium. *Frontiers in Heat and Mass Transfer (FHMT)*, 6(6).

Khalil Ur Rehman, Malik M.Y, Abid Ali Khan, Iffat Zehra, Mostafa Zahri and M. Tahir, (2017). Numerical solution of chemically reactive non-Newtonian fluid flow. *Eur. Phys. J. Plus* 132: 550.

Krishnamurthy M.R., Prasannakumara B.C., Gireesha B.J. and Rama Subba Reddy Gorla (2016). Effect of chemical reaction on MHD boundary layer flow and melting heat transfer of Williamson nanofluid in porous medium. *Engineering Science and Technology, an International Journal*, 19 53–61.

Malik M. Y., Bibi M., Farzana Khan and Salahuddin T. (2016). Numerical solution of Williamson fluid flow past a stretching cylinder and heat transfer with variable thermal conductivity and heat generation/absorption. *AIP Advances* 6, 035101.

Mlamuli Dhlamini, Peri K. Kameswaran, Precious Sibanda, Sandile Motsa and Hiranmoy Mondal (2018). Activation energy and binary chemical reaction effects in mixed convective nanofluid flow with convective boundary conditions.

Monica M., Sucharitha J. and CH Kishore (2017). Effects of exothermic chemical reaction with Arrhenius activation energy, non-uniform heat source/sink on MHD stagnation point flow of a Casson fluid over a nonlinear stretching sheet with variable fluid properties and slip conditions. *Journal of the Nigerian Mathematical Society*, 36, 163-190.

Muhammad Suleman, Muhammad Ramzan, Shafiq Ahmad and Dianchen Lu (2019). Numerical simulation for homogeneous–heterogeneous reactions and Newtonian heating in the silver-water nanofluid flow past a nonlinear stretched cylinder. *Phys. Scr.* 94, 085702, (9pp).

Mustafa M., Junaid Ahmad Khan, Hayat T., Alsaedi A. (2017). Buoyancy effects on the MHD nanofluid flow past a vertical surface with chemical reaction and activation energy. *International Journal of Heat and Mass Transfer*, 108, 1340–1346.

Nadeem S., Hussain S. T. and Changhoon Lee (2013). Flow of a Williamson fluid over a stretching sheet. *Brazilian Journal of Chemical Engineering*, 30(03), 619 – 625.

Padmavathi K. and Anitha kumari Y. (2017). MHD Mixed Convection Stagnation-Point Flow of a Power - Law Nano fluid towards a Stretching Surface in the presence of viscous dissipation and suction or injection. *Aryabhatta Journal of Mathematics and Informatics*, 09(01), 457-473.

Sameh E. Ahmed, Ramadan A. Mohamed, Abd Elraheem M. Aly, and Mahmoud S. Soliman, (2019). Magnetohydrodynamic Maxwell Nanofluids Flow over a Stretching Surface through a Porous Medium. *International Journal of Mechanical, Industrial and Aerospace Sciences*, 13(6).

Shafique Z., Mustafa M., Mushtaq A. (2016). Boundary layer flow of Maxwell fluid in rotating frame with binary chemical reaction and activation energy. *Results in Physics,* 6, 627–633.

Shakhaoath Khana Md., Mizanur Rahmana Md., Arifuzzaman S.M., Pronab Biswas, Ifsana Karim (2017). Williamson fluid flow behaviour of mhd convective radiative cattaneo–christov heat flux type over a linearly stretched-surface with heat generation and thermal-diffusion. *Frontiers in Heat and Mass Transfer (FHMT),* 9, 15.

Shamshuddin MD., Thirupathi T. and Satya Narayana P.V. (2019). Micropolar Fluid Flow Induced due to a Stretching Sheet with Heat Source/Sink and Surface Heat Flux Boundary Condition Effects. *J. Appl. Comput. Mech*., 5(5), 816-826.

Sravanthi C.S. (2018). Effects of heat source/sink and chemical reaction on MHD Maxwell nanofluid flow over a convectively heated exponentially stretching sheet using homotopy analysis method. *Int. J. of Applied Mechanics and Engineering*, 23(1), 137-159.

Srinivas Maripala, Kishan N. (2015). Unsteady MHD flow and heat transfer of nanofluid over a permeable shrinking sheet with thermal radiation and chemical reaction. *American Journal of Engineering Research (AJER)*, 4(6), 68-79.

Srinivasasai Panuganti and Gnaneswara Reddy Machireddy (2017). Chemical reaction and viscous dissipation effects on radiative MHD boundary layer flow of nanofluids. *Aryabhatta Journal of Mathematics and Informatics*, 09(1), 405-430.

Tasawar Hayat, Ikram Ullah, Muhammad Waqas and Ahmed Alsaedi (2019). Attributes of Activation Energy and Exponential Based Heat Source in Flow of Carreau Fluid with Cross-Diffusion Effects. *J. Non-Equilib. Thermodyn.*; aop.

Vijaya Lakshmi G., Anand Babu L. and Srinivasa Rao K. (2018). MHD mixed convection stagnation point flow of nanofluid through a porous medium over stretching sheet. *International Journal of Pure and Applied Mathematics*, 118 (10), 369-389.

Williamson, R.V., (1929). The theory of pseudoplastic materials. *Ind. Eng. Chem*., 21(11): 1108-1111.

Zeeshan Khan, Haroon Ur Rasheed, Tawfeeq Abdullah Alkanhal, Murad Ullah, Ilyas Khan and Iskander Tlili (2018). Effect of magnetic field and heat source on Upper-convected-Maxwell fluid in a porous channel. *Open Phys.*, 16, 917–928.

Chapter7

The effect of viscous dissipation on mixed convective heat transfer of MHD flow of Williamson nanofluid above a stretching cylinder in the presence of variable thermal conductivity and chemical reaction

7.1. Introduction

The boundary layer flow of mass and heat transfer of non-Newtonian fluids above a stretching cylinder is of numerous interests for researchers, scientists and engineers because of its extensive applications such as thinning of copper wire, extrusion of polymer sheets, annealing, emulsion coated sheets, pipe industry, and so on. Due to dissimilarity of shear stress and additional physical behavior of fluid, the non-Newtonian fluids are classified as Dilatant, Bingham plastic, Pseudoplastic and viscoelastic. Williamson fluid model is one of the models of pseudoplastic fluids. Typical of a non-Newtonian fluid model which can be considered for very small viscosity as well as for very large viscosity effects is Williamson fluid. This fluid model was firstly proposed by (Williamson, 1929). Malik et al., (2016) examined the effect of variable thermal conductivity and heat generation/absorption on Williamson fluid flow past a stretching cylinder. Bilal et al., (2017) used numerical investigation to explore thermally stratified non-Newtonian Williamson fluid flow above a cylindrical surface. MHD flow of Williamson fluid with Viscous Dissipation is discussed by (Manjula et al., 2019). Sumit Gupta et al., (2020) examined the influences of variable thickness and nonlinear thermal radiation on Williamson fluid. Similarly Williamson nanofluid flows examined by (Iqbal et al., 2019), (Liaquat, 2019), (Nagendra et al. 2018), Rashid et al. 2020), (Hashim et al. 2019) and (Ghulam, et al. 2020).

Nanofluid is the homogeneous mixture of base fluids with nanoparticles like Al, Cu, Ag,TiO_2, Al_2O_3, etc. Since the specific heat of metal is very small as compared to base fluids, nano size particles improve the thermal conductivity and heat transfer rate of base fluids. Nanofluids are used in an excess of engineering applications, automotive applications, electronic applications and biomedical applications. Through experiments Choi, (1995) was the first researcher who presented that the thermal behaviors of fluid can be improved through nanoparticles. Afterward, Buongiorno, (2006) was developed a mathematical model which exhibits the characteristic of thermophoresis and Brownian motion of nanoparticles. Until now, many researchers have focused on the development and applications of nanofluids in different directions. Gireesha et al., (2019) analyzed the effect of thermal radiation on three dimensional MHD boundary layer flows of Jaffrey nanofluids past nonlinear stretching sheet. Bilal et al., (2018) examined MHD Maxwell fluid flow in the presence of radiative heat flux. Hayat et al., (2018) scrutinized Entropy generation in bidirectional flow of water-based carbon nanotubes with convective boundary conditions. In mixed convective flow Entropy generation of nanoparticle with effect of Joule heating and thermal radiation was analyzed by (Hayat et al., (2018). Some research related to nanofluid included in (Hayat eta, 2015), (Ramzan and Bilal, 2015), (Hammed et al., 2019), (Kai-Long et al., 2017), (Mohamed et al. 2020), (Anum Shafiq et al. 2020) and (Sohail Aslam, 2020).

When forced convection and natural convection mechanisms performance together to transfer heat, mixed convection happens. Mixed convection also defined as circumstances where both buoyant forces and pressure forces combine. Mixed convection flows happen in several industrial and technological requests in natural surroundings, example, electronic devices cooled by fans, solar receivers unprotected to wind flows, heat exchangers located in a small velocity environment, nuclear reactors cooled throughout emergency shutdown, dry of porous solids, flows in the atmosphere and ocean etc. Accordingly some researchers examined mixed convection flows. Among these Bahlaoui et al., (2016) studied nanofluid flows in a vertical vented rectangular enclosure with mixed convective heat transfer. Entropy generation effectiveness in hydromagnetic mixed convection heat transfer over rotating disk in the existence of partial slip effect was scrutinized by (Ijaz Khan et al., 2018). Moreover, Mamun Billah et al., (2017) inspected mixed convection flow through a rectangular channel. Unsteady three-dimensional mixed convection heat transfer was carried out by (Hayat et al., 2016). Further studies covering mixed convection heat transfer flow concept can be referred through (Manu Chakkingal, 2020), (Hamdi Messaoud, 2017), (Hemalatha, 2015), (Henniche, 2018), (Husein Alzgool, 2019) and (Abbasian Arani, 2017).

In many industrial and engineering sectors the fluid flows above stretching cylinder have extensive application. Due to this it is one of the recent research titles among researchers and scientist. In many of the researches, the impact of variable thermal conductivity on temperature is not considered. But, in Mohamed et al., (2010), Sihem Lahmar et al., (2019) and Mohamed

Kezzar et al., (2020) it can be seen that the effect of variable thermal conductivity powerfully be depending on temperature, especially if there is a great temperature variance. If relatively a slight temperature variance occurred, thermal conductivity can certainly be expected not changed but in the occurrence of nanoparticles, this supposition can lead to a clear mistake (Mohamed Kezzar et al., 2020). Faisal Sultan et al., (2020) presented mixed convective MHD flow of cross fluid above a bidirectional stretching sheet. They deliberated the impact of heat absorption/generation and variable thermal conductivity. Moreover, numerical investigation of nanofluid with mixed convection flow past a stretching sheet in the presence of convective slip boundary conditions and thermal radiation was inspected by (Noreen Sher Akbar and Zafar Hayat Khan, 2016). Hayat et al., (2016) discovered Cattaneo–Christov heat flux model flow of fluid with variable thermal conductivity above a variable thicked surface.

To formulate energy equation a variable thermal conductivity which is depends on temperature is presumed. In the articles Chun-Bao Xiong et al., (2019), Sarojamma et al., (2019), Maatouk Khoukhi et al., (2019), Gbadeyan et al., (2020), Rajneesh Kumar et al., (2019), Nawel Boumaiza et al., (2019), Kai-Long Hsiao, (2016) and Sihem Lahmar et al. (2019) comprise some current literature linked to variable thermal conductivity. Not too much works is obtainable for the effect of temperature dependent variable thermal conductivity and viscous dissipation on mixed convective heat transfer, especially past a stretched cylinder. The main goal of the current article is to examine the impact of thermal radiation and viscous dissipation on mixed convective mass and heat transfer of MHD Williamson nanofluid with variable thermal conductivity and chemical reaction. By using Runge-Kutta method combined with shooting technique, the values of momentum, energy and mass are calculated. Numerical solutions are further supported with software called MATLAB. The graphs of temperature, velocity, and concentration distributions are plotted to observe the dissimilarity for various values of prominent parameters. Also numerical results of local Sherwood number, local Nusselt number and skin-friction coefficient are tabulated.

7.2. Mathematical Formulation

In this research paper, steady, axisymmetric, MHD Williamson nanofluid flow above a linearly stretching cylinder along x-axis is discussed and its geometrical model is revealed through Fig.7. 1. Magnetic field strength B_0 is applied perpendicular to the flow along radial direction with the supposition of minor Reynolds number. Moreover, the mixed convective mass and heat transfer phenomenon are incorporated in the existence of viscous dissipation and heat generation. T_∞ and C_∞ are the ambient fluid temperature and concentration respectively. Further, u and v are velocity component lengthways x and r axes respectively. Except the thermal conductivity the physical behaviors of the fluid are deliberated constant. By using the above supposition the equations of continuity, momentum, energy and mass can be formulated as (Bilal et al., 2018).

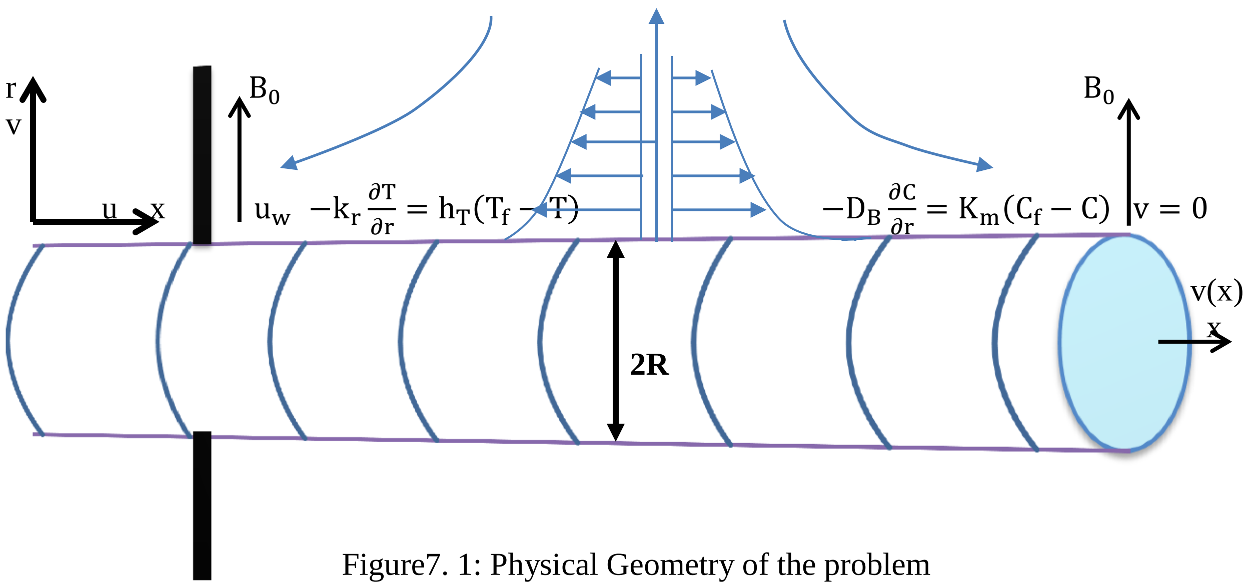

Figure7. 1: Physical Geometry of the problem

$$\frac{\partial}{\partial x}(ru) + \frac{\partial}{\partial y}(rv) = 0 \tag{7.1}$$

$$u\frac{\partial u}{\partial x} + v\frac{\partial u}{\partial r} = \nu\left(\frac{1}{r}\frac{\partial u}{\partial r} + \frac{\partial^2 u}{\partial r^2}\right) + \nu\left(\frac{\Gamma}{\sqrt{2}r}\left(\frac{\partial u}{\partial r}\right)^2 + \sqrt{2}\Gamma\frac{\partial u}{\partial r}\frac{\partial^2 u}{\partial r^2}\right) - \frac{\nu}{k'}u - \frac{\sigma_1 B_0^2}{\rho}u + g\beta_1(T - T_\infty) + g\beta_2(C - C_\infty) = 0, \tag{7.2}$$

$$u\frac{\partial T}{\partial x} + v\frac{\partial T}{\partial r} = \frac{1}{r}\frac{\partial}{\partial r}\left(\alpha_m\frac{\partial T}{\partial r}\right) + \omega\left\{D_B\frac{\partial C}{\partial r}\frac{\partial T}{\partial r} + \frac{D_T}{T_\infty}\left(\frac{\partial T}{\partial r}\right)^2\right\} + \frac{Q}{\rho c_p}(T - T_\infty) - \frac{1}{\rho c_p r}\frac{\partial}{\partial r}(rq_r) + \frac{\mu}{\rho c_p}\left(\frac{\partial u}{\partial r}\right)^2 = 0, \tag{7.3}$$

$$u\frac{\partial C}{\partial x} + v\frac{\partial C}{\partial r} = D_B\frac{1}{r}\left(r\frac{\partial C}{\partial r}\right) + \frac{D_T}{T_\infty}\frac{1}{r}\left(r\frac{\partial T}{\partial r}\right) - k_r(C_w - C_\infty). \tag{7.4}$$

The boundary conditions are (Bilal et al., 2018):

$$u = u_0 \frac{x}{l}, \qquad v = 0, \quad - k_T \frac{\partial T}{\partial r} = h_T\left(T_f - T\right), \qquad -D_B \frac{\partial C}{\partial r} = k_m\left(C_f - C\right) \;\; at \;\; r = R, \qquad (7.5)$$

$$u(\infty) = 0, \;\; T(\infty) = T_\infty, \;\; C(\infty) = C_\infty, \quad as \;\; r \to \infty. \qquad (7.6)$$

Inspiring the following dimensionless resemblance transformations the PDE is converted to non-dimensional system ODE (Bilal et al., 2018).

$$\eta = \frac{r^2-R^2}{2R}\left(\frac{u_0}{l\nu}\right)^{\frac{1}{2}}, \quad \psi = \left(\frac{\nu u_0}{l}\right)^{\frac{1}{2}} xRf(\eta), \;\; u = \frac{u_{0x}}{l} f'(\eta), v = -\left(\frac{\nu u_0}{l}\frac{R}{r}\right)^{\frac{1}{2}} f(\eta), \quad \theta(\eta) = \frac{T-T_\infty}{T_w-T_\infty}, \quad \phi(\eta) = \frac{C-C_\infty}{C_w-C_\infty} \qquad (7.7)$$

In Equation (7.3), α_m is given by (Bilal et al., 2018).

$$\alpha_m = \alpha_\infty\left(1 + \varepsilon\theta(\eta)\right) \qquad (7.8)$$

where α_∞ is the thermal conductivity and ε represents thermal conductivity parameter.

Rosseland approximation for radiation (Bilal et al., 2018).

$$q_r = -\frac{4\sigma^*}{3k^*}\frac{\partial T^4}{\partial y} \qquad (7.9)$$

where k^* and σ^* are the absorption constant and Stefan-Boltzman constant. T^4 can be expressed as the fuunction of temperature by assuming the temperature difference within the flow. The Taylor series of T^4 about T_∞ after neglecting higher orders is $T^4 = 4TT_\infty^3 - 3T_\infty^4$.

Therefore, (Bilal et al., 2018).

$$\frac{\partial q_r}{\partial y} = -\frac{16\sigma^* T_\infty^3}{3k^*}\frac{\partial^2 T}{\partial y^2} \qquad (7.10)$$

Substituting equation (7.7) in to equation (7.1) it is satisfied, while equations (7.2-7.4) are changed in to system of first order ODEs as shown below.

$$\left((1 + 2\eta\gamma\lambda) + (1 + 2\eta\gamma)^{\frac{3}{2}} f''\right) f''' + 2\gamma f'' + ff'' + {}^3\!/_2 \, (1 + 2\eta\gamma)^{\frac{1}{2}}\gamma\lambda f''^2 - f'^2 - (d + M)f' + G_t\theta + G_c\phi = 0, \qquad (7.11)$$

$$(1+2\eta\gamma)(1+\varepsilon\theta+4/3R_d)\theta''+Prf\theta'+2\gamma\theta'+\gamma\varepsilon\theta\theta'+\frac{4}{3}R_d\gamma\theta'+\varepsilon(1+2\eta\gamma)\theta'^2+$$
$$PrR\theta+PrNb(1+2\eta\gamma)\theta'\phi'+PrNt(1+2\eta\gamma)\theta'^2+PrEcf''^2=0, \quad (7.12)$$

$$(1+2\eta\gamma)\phi''+\frac{Nt}{Nb}(1+2\eta\gamma)\theta''+2\gamma\phi'+2\gamma\frac{Nt}{Nb}\theta'+PrLef\phi'-KLe\phi=0. \quad (7.13)$$

The transmuted boundary conditions are

$$f(0)=0,\ \ f'(0)=1, \quad \theta'(0)=-h\big(1-\theta(0)\big), \quad \phi'(0)=-H(1-\phi(0)), \quad (7.14)$$

$$f'(\infty)=0, \quad \theta(\infty)=0, \quad \phi(\infty)=0. \quad (7.15)$$

Where $M=\frac{\sigma_1 B_0^2 l}{\rho u_0}$ is magnetic parameter, $d=\frac{\nu}{k\prime}$ is porosity parameter, $\gamma=\sqrt{\frac{\nu l}{u_0 R^2}}$ is curvature parameter, $\lambda=\Gamma\sqrt{\frac{u_0^3}{2\nu l^3}}x$ is Weissenberg number (Williamson parameter), $G_t=\frac{g\beta_1(T_w-T_\infty)}{Re_x\nu}$ is local temperature buoyancy parameter, $G_c=\frac{g\beta_2(C_w-C_\infty)}{Re_x\nu}$ is concentration buoyancy parameter, $R=\frac{\theta l}{u_0 c_p\rho}$ is heat generation parameter, $R_d=\frac{4\sigma^* T_\infty^3}{k_1 k^*}$ is thermal radiation parameter, $Pr=\frac{\mu c_p}{k}$ is Prandtl number, $Nb=\frac{\omega D_B(C_f-C_\infty)}{\nu}$ is Brownian motion parameter, $Nt=\frac{\omega D_T(T_f-T_\infty)}{\nu T_\infty}$ is thermophoresis parameter, $Ec=\frac{{u_0}^2x^2}{l^2(T_f-T)}$ is Eckert number, $K=\frac{k_0}{u_0 l}$ is chemical reaction parameter, $h=\frac{h_T R}{\sqrt{\frac{\nu l}{u_0 r^2}}}$ is thermal Biot number, $H=\frac{k_m R}{\sqrt{\frac{\nu l}{u_0 r^2}}}$ is concentration Biot number , $Le=\frac{\alpha}{D_B}$ is Lewis number.

The important physical quantities C_f, Nu_x and Sh_x are defined as follows.

$$C_f=\frac{2\tau_w}{\rho u_w^2}, \quad Nu_x=\left(\frac{xq_w}{k(T_f-T_\infty)}+q_r\right)_{r=R}, \quad Sh_x=\frac{xq_m}{D_B(C_f-C_\infty)}, \quad (7.16)$$

$$\text{Where } \tau_w=\mu\left(\frac{\partial u}{\partial r}+\frac{\Gamma}{\sqrt{2}}\left(\frac{\partial u}{\partial r}\right)^2\right)_{r=R}, \quad q_w=-k\left(\frac{\partial T}{\partial r}\right)_{r=R}, \quad q_m=-D_B\left(\frac{\partial C}{\partial r}\right)_{r=R}. \quad (7.17)$$

The non-dimension forms of these physical quantities are:

$$C_f \frac{\sqrt{Re_x}}{2} = f''(0) + \frac{\lambda}{2} f''^2(0), \quad Nu_x Re_x^{-1/2} = -\left(1 + \frac{4}{3}R\right)\theta(0), \quad Sh_x Re_x^{-1/2} = -\phi'(0). \quad (7.18)$$

where $Re_x = \frac{u_0^2 x^2}{\nu l}$ is Reynolds number.

7.3. Method of Solution

The coupled non-linear ODEs (7.11)-(7.13) with the boundary conditions (7.14) - (7.15) are solved using Runge-Kutta method integrated with shooting technique. For the slight variation of initial estimates u_1, u_2 and u_3 Newton Raphson method is practical subject to the patience $\varepsilon_1 = 10^{-7}$. From computational experiments, there is no significant alteration in the outcomes after $\eta = 7$, thus we are allowing for $[0, 7]$ as the domain of the problem in terms of $[0, \infty)$. Equations (8.11)-(8.13) are solved by converting in to system of first order ODEs. System of first order ODEs is defined below.

$$f = y_1, f' = y_2, \; f'' = y_3, f''' = {y'}_3, \; \theta = y_4, \; \theta' = y_5, \; \theta'' = {y'}_5, \phi = y_6, \phi' = y_7, \phi'' = {y'}_7 \quad (7.19)$$

Thus, the systems of first order simultaneous ordinary differential equations are

$${y'}_1 = y_2 \quad (7.20)$$

$${y'}_2 = y_3 \quad 8.21$$

$${y'}_3 = \frac{-2\gamma y_3 - \frac{3}{2}(1+2\eta\gamma)^{\frac{1}{2}}\gamma\lambda y_3^2 - y_1 y_3 + y_2^2 + (d+M)y_2 - G_t y_4 - G_c y_6}{(1+2\eta\gamma) + \lambda(1+2\eta\gamma)^{\frac{3}{2}} y_3} \quad (7.22)$$

$${y'}_4 = y_5 \quad (7.23)$$

$${y'}_5 = \frac{-PrNb(1+2\eta\gamma)y_5 y_7 - 2\gamma y_5 - Pr y_1 y_5 - \gamma\varepsilon y_4 y_5 - \frac{4}{3}R_d y_5 - \varepsilon(1+2\eta\gamma)y_5^2 - PrNt(1+2\eta\gamma)y_5^2 + PrR y_4 + PrEc y_3^2}{(1+2\eta\gamma)\left(1 + \varepsilon y_4 + \frac{4}{3}R_d\right)}$$

(7.24)

$${y'}_6 = y_7 \quad (7.25)$$

$${y'}_7 = -\frac{Nt}{Nb}(1 + 2\eta\gamma){y'}_5 - 2\gamma y_7 - 2\gamma \frac{Nt}{Nb} y_5 - PrLe y_1 y_7 + KLe y_6$$ or

$$y'_7 = \frac{\begin{array}{c} NtPr(1+2\eta\gamma)y_5y_7+\frac{Nt}{Nb}\gamma\varepsilon y_4y_5+\frac{4Nt}{3Nb}R_d\gamma y_5+2\frac{Nt}{Nb}\gamma y_5+\frac{Nt}{Nb}Pry_1y_5+\varepsilon\frac{Nt}{Nb}(1+2\eta\gamma)y_5^2+\frac{Nt^2}{Nb}(1+2\eta\gamma)y_5^2 \\ +Pr\frac{Nt}{Nb}Ry_4+\frac{Nt}{Nb}PrEcy_3^2-2\left(1+\varepsilon y_4+\frac{4}{3}R_d\right)\gamma y_7-\frac{Nt}{Nb}\left(1+\varepsilon y_4+\frac{4}{3}R_d\right)\gamma y_5-PrLe\left(1+\varepsilon y_4+\frac{4}{3}R\right)y_1y_7+KLe\left(1+\varepsilon y_4+\frac{4}{3}R_d\right)y_6 \end{array}}{(1+2\eta\gamma)\left(1+\varepsilon y_4+\frac{4}{3}R_d\right)} \tag{7.26}$$

$$y_1(0) = 0, y_2(0) = 1, y_3(0) = u_1, y_4(0) = u_2, y_5(0) = -h(1-u_2), y_6 = u_3, y_7 = -H(1-u_3) \tag{7.27}$$

7.4. Result and Discussion

The effect of various protuberant parameters on concentration, temperature, and velocity is deliberated. The calculation has been carried out by taking $0.0 \le \mathrm{M} \le 0.6$, $0.1 \le \mathrm{Nt} \le 0.9$, $0.2 \le \mathrm{Nb} \le 0.8$, $0.2 \le \gamma \le 0.8$, $1.0 \le \mathrm{Le} \le 2.5$, $0.2 \le \mathrm{d} \le 0.8$, $0.0 \le \lambda \le 0.6$, $0.1 \le \mathrm{K} \le 0.4$, $0.01 \le \mathrm{Ec} \le 0.07$, $0.01 \le \mathrm{R} \le 0.1$, $0.1 \le \varepsilon \le 0.9$, $0.01 \le \mathrm{h} \le 0.2$, $0.0 \le \mathrm{G_t} \le 5.0$, $0.0 \le \mathrm{G_c} \le 3.0$, $0.0 \le \mathrm{H} \le 3.0$, $0.2 \le \mathrm{R}_d \le 0.5$ and $1.0 \le \mathrm{Pr} \le 3.0$. The accuracy and validity of the present work are ensured by comparing with the pupblished paper of (Bilal et al., 2018) and as it is shown in Table 7.1 it has very good agreement. This ensures the validity and accuracy of the present work. The properties of Local skin friction coefficeint, Local Sheerwood and Nusselt number are considered in Table7.2 for various values of ε, d, Gt, Gc, h, H, and R. From this table it can detect with an increase of ε $-f''(0)$ and $-\phi'(0)$ are raised whereas $-\theta'(0)$ is decreased. Moreover, $-\theta'(0)$ and $-\phi'(0)$ are decreased with an upsurge of d but reverse trend occurred for $-f''(0)$. As the values of $\mathrm{G_t}$ and $\mathrm{G_c}$ upsurges $-f''(0)$ rises whereas $-\theta'(0)$ and $-\phi'(0)$ have opposite trend for these parameters. Furthermore, from this table it can be observing that $-f''(0)$ and $-\phi'(0)$ declines with an increase of h. But $-\theta'(0)$ raises with an increases of h. Still furthermore, as the values of H and S rises $-f''(0)$ and $-\theta'(0)$ diminished whereas $-\phi'(0)$ upsurges.

In Figs. 7.2–7.36 it can be seen that the insight behavior of various parameters on temperature, velocity, and concentration. Figs.7. 2-7.4 are plotted to show the influence of Magnetic parameter on temperature, velocity, and concentration. The figures shows that velocity profiles declines with a growth of Magnetic field M whereas the temperature and concentration profiles have opposite trend with this paremeter. This is because a resistive force which is a Lorentz force is created when the influence of the magnetic field is boosted. This resistive force is liable for the reducement of velocity. The behavior of temperature and concentration for different values of Thermophoresis parameter (Nt) are shown in Figs.7.5-7.6. From the graphs it is observed that both concentration and temperature profiles are upsurges with a growth of this parameter.

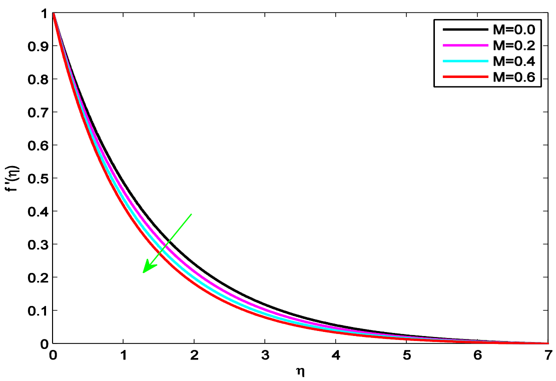

Figure7. 2: The graph of velocity for different values M

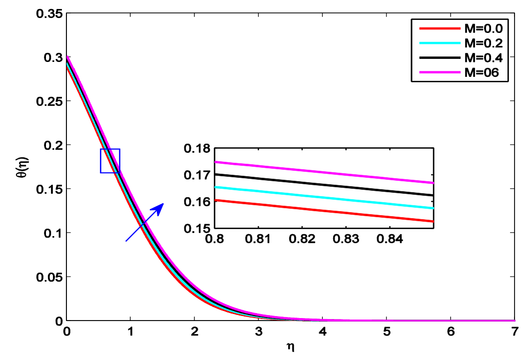

Figure7.3: The graph of temperature for different values of M

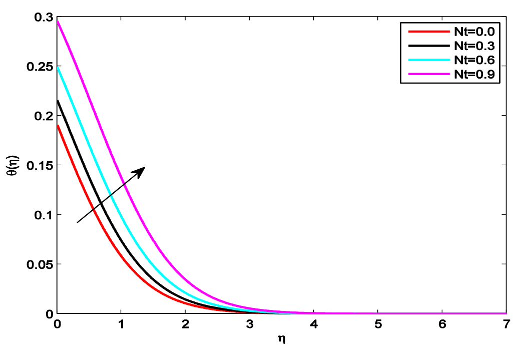

Figure7. 4: The graph of Concentration for different values of M

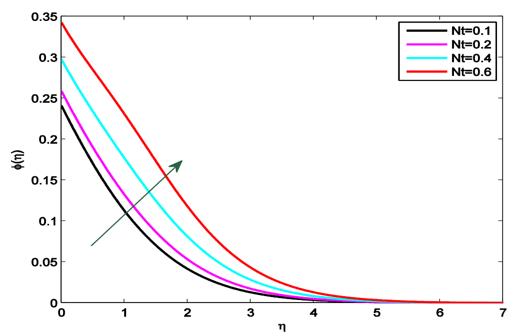

Figure7. 5 Concentration graph for various values of Nt

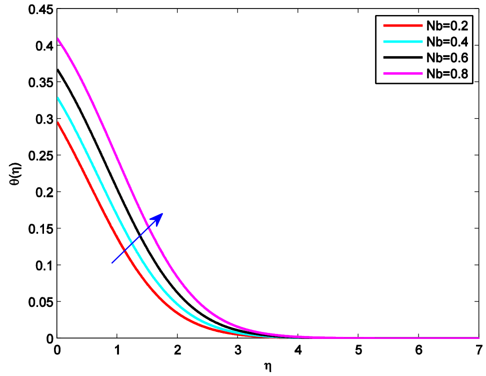

Figure7. 6: Temperature graph of for various values of Nt

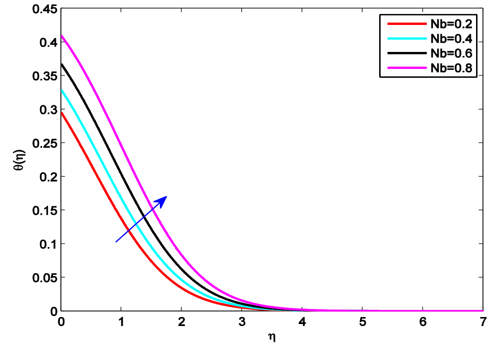

Figure7. 7: Temperature graph for various values of Nb

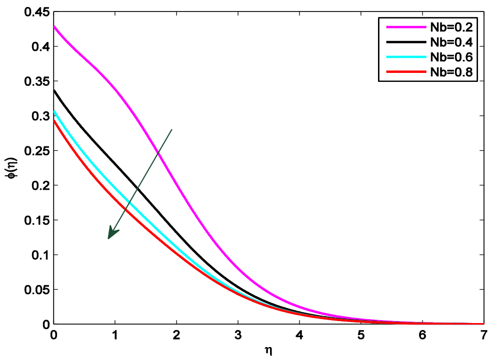

Figure7. 8: Concentration graph for various values of Nb

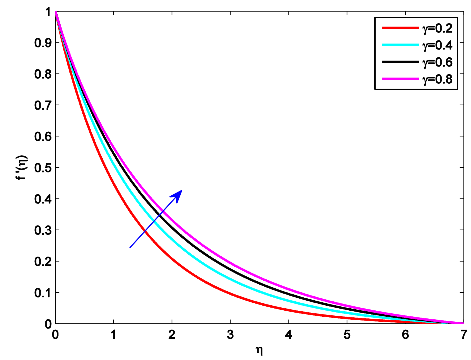

Figure7. 9: The graph of Velocity for different values of **γ**

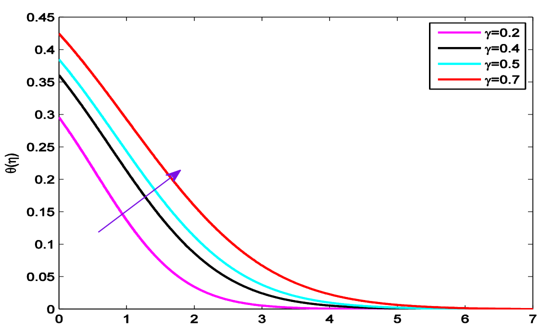

Figure7. 10: The graph of Concentration for different values of **γ**

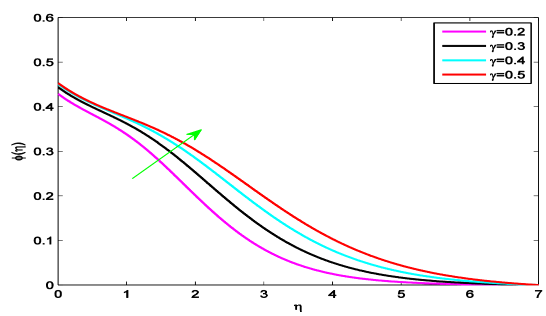

Figure7. 11: The graph of temperature for different values of **γ**

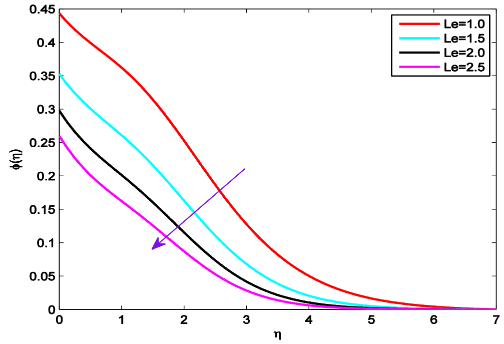

Figure7. 12: Concentration graph for various values of Le

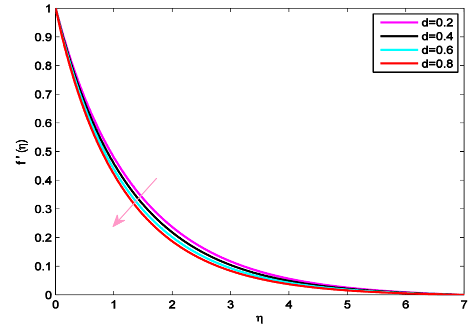

Figure7. 13: Velocity graph for various values of d

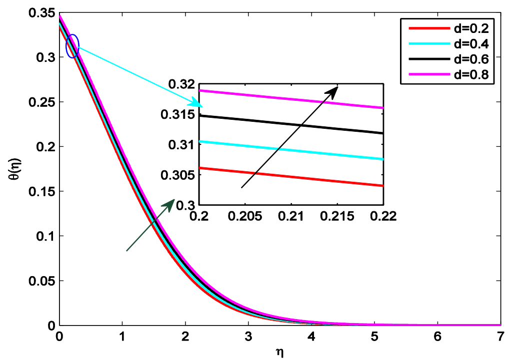

Figure7.14: Temperature graph for various values of d

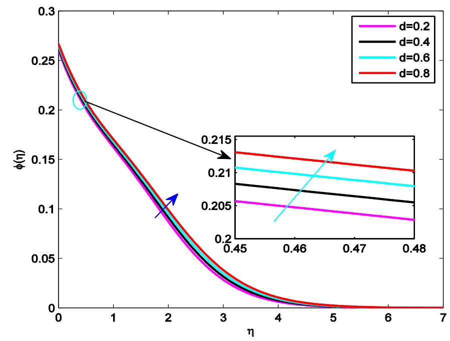

Figure7.15: Concentration graph for various values of d

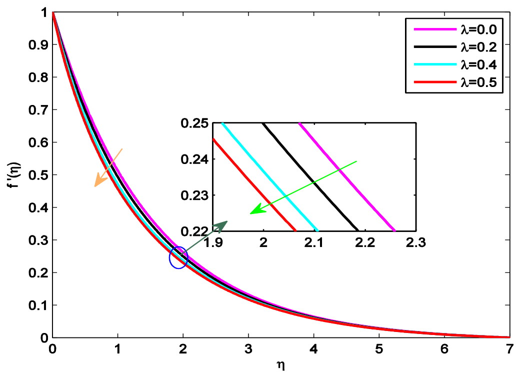

Figure7. 16: Velocity graph for various values of **λ**

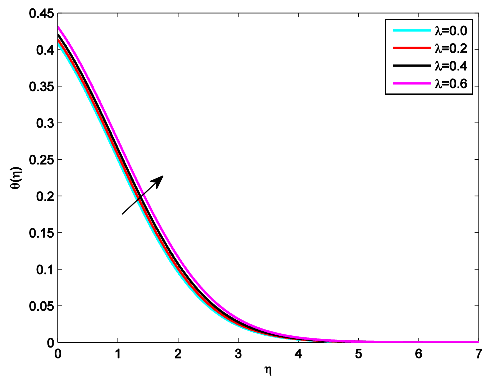

Figure7. 17: Temperature graph for various values of **λ**

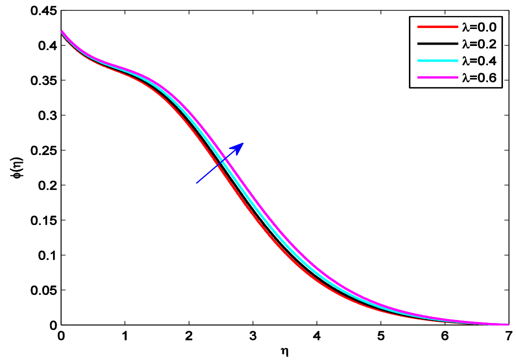

Figure7. 18: Concentration graph for various values of **λ**

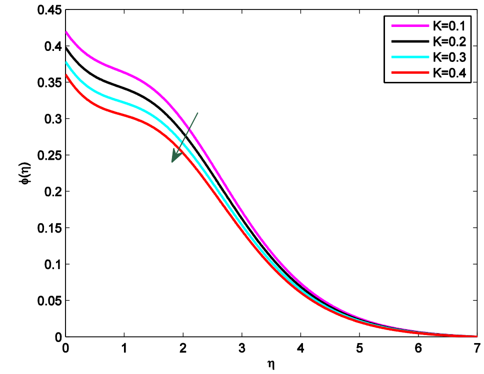

Figure7. 19: Concentration graph for various values of K

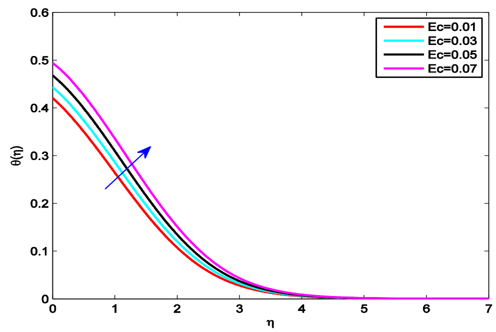

Figure7. 20: Temperature graph for various values of Ec

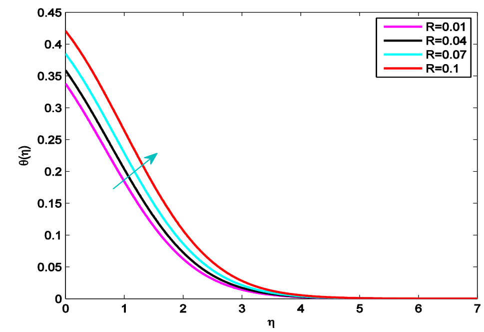

Figure7. 21: Temperature graph for various values of R

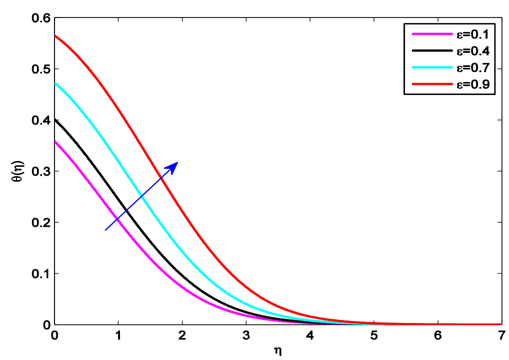

Figure7. 22: Temperature graph for various values of **ε**

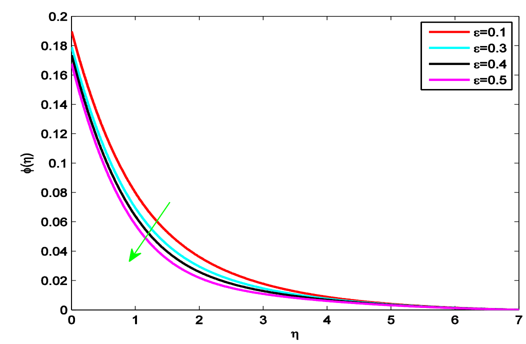

Figure7.23: Concentration graph for various values of **ε**

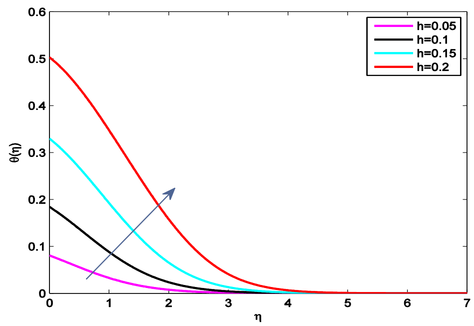

Figure7. 24: Temperature graph for various values of h

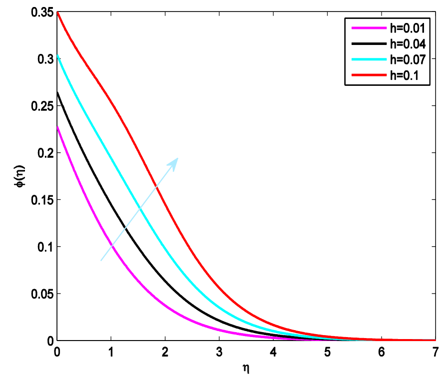

Figure7.25: Concentration graph for various values of h

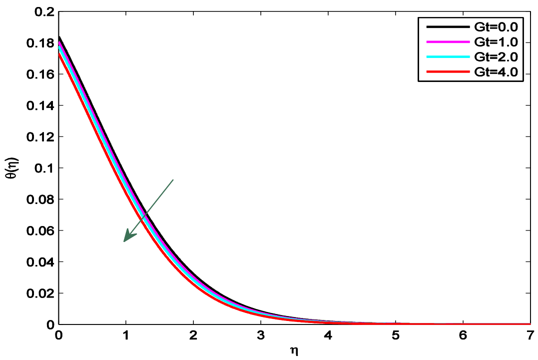

Figure7.26: Temperature graph for various values of Gt

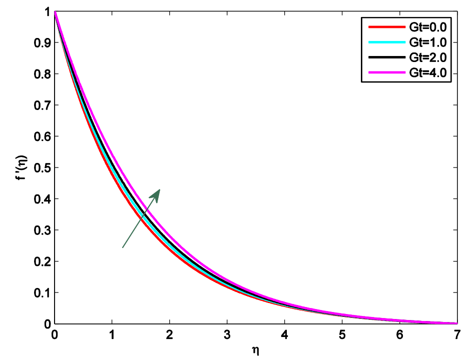

Figure7.27: Velocity graph for various values of Gt

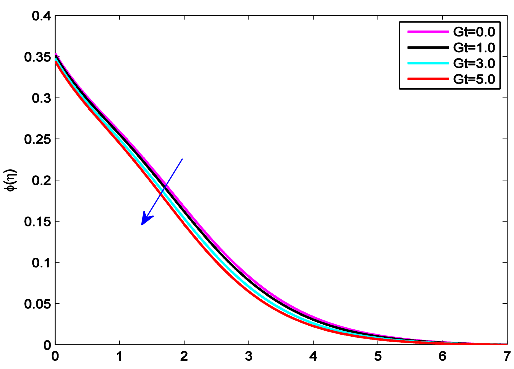

Figure7. 28: Concentration graph for various values of Gt

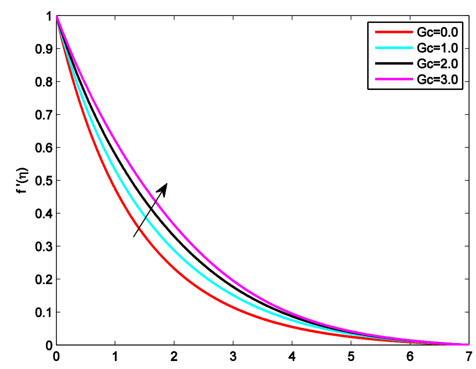

Figure7.29: Velocity graph for various values of Gc

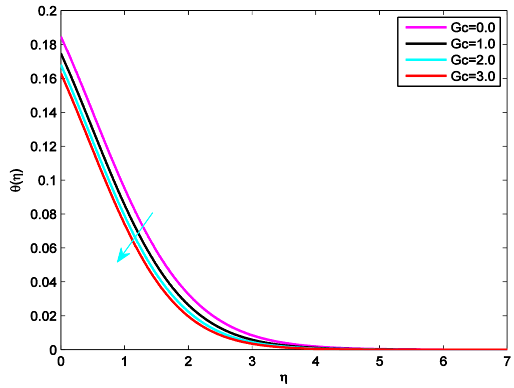

Figure7. 30: Temperature graph for various values of Gc

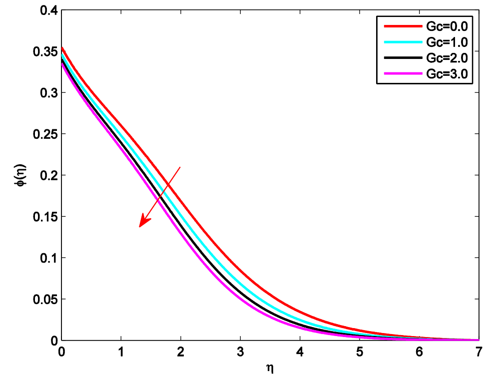

Figure7. 31: Concentration graph for various values of Gc

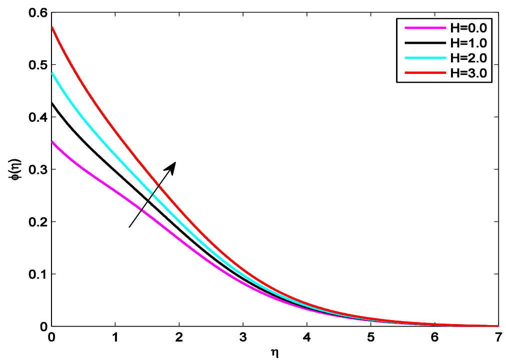

Figure7.32 Concentration graph for various values of H

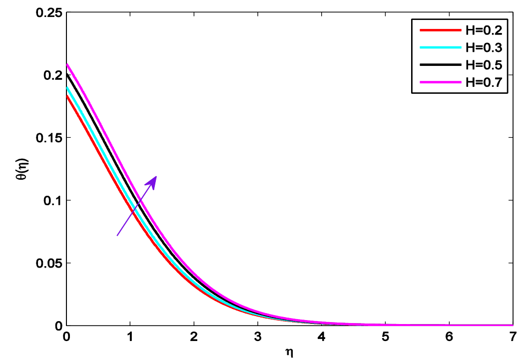

Figure7. 33: Temperature graph for various values of H

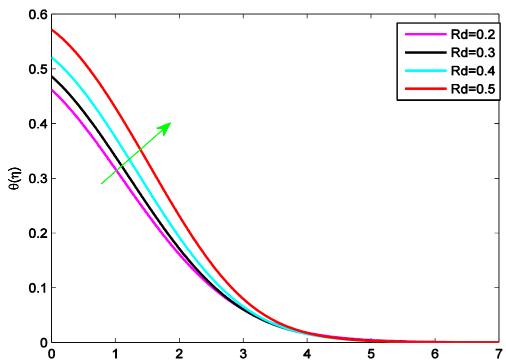

Figure7.34: Concentration graph for various values of R_d

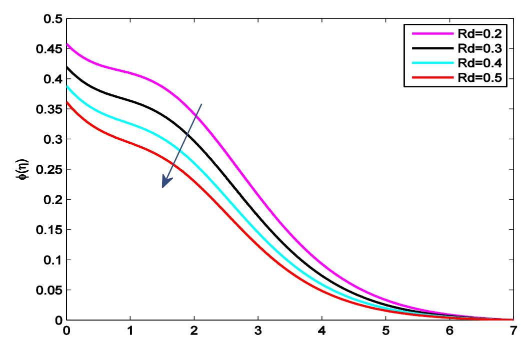

Figure7.35: Temperature graph for various values of R_d

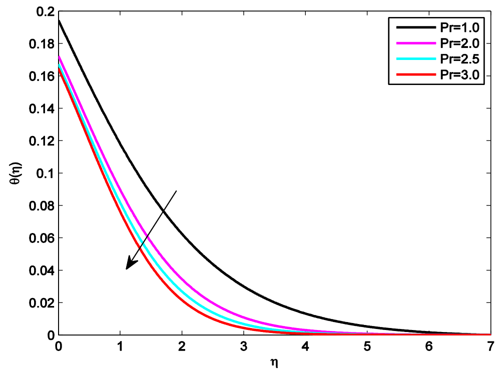

Figure7. 36: Temperature graph for various values of Pr

Figs.7.7-7.8 are displayed to examine the influence of Brownian motion on concentration and temperature profiles. From these figures we noticed that the temperature profile is upsurges whereas concentration profile has opposite trend for this parameter. The effect of curvature parameter γ on temperature, velocity, and concentration are sketched in Figs. 7.9-7.11.These figures reveals that an increment of curvature parameter γ results an increment of the temperature, velocity, and concentration profiles. From Fig. 7.12 it can be noticed that as the values of Lewis number Le raises the concentration field boosted. This is because greater Lewis number produce the slighter Brownian diffusion coefficient. From Figs. 7.13-7.15 it is noticed that when porosity parameter d increases the velocity profile reduced whereas the concentration and temperature distributions are upsurges. The graph of temperature, velocity and concentration are plotted in Figs. 7.16-7.18 for various values of Williamson parameter. These figures displayed that an increment of Williamson parameter causes a decrement of velocity profile and an increment of temperature and concentration profiles. Fig.7.19 is exhibited to show the nature of concentration profiles for dissimilar values of chemical reaction K. The figure revealed that as chemical reaction K upsurges the concentration distribution decreased. This is because chemical reaction in this system results in intake of the chemical and hence results the decrement of concentration. Figs.7.20-7.21 is plotted to examine the effect heat generation R and Eckert number Ec on temperature profiles. From the figures it can be seen that the temperature is boosted with an upsurge of both Eckert number Ec and heat generation R. The impacts of thermal conductivity ε on temperature and nanoparticle concentration are portrayed in Figs. 7.22-7.23. The temperature field is boosted with a growth of thermal conductivity ε whereas opposite trends happens for concentration profiles. This is due to the fact that when thermal conductivity of the fluid boosted the fluid gets heated more which causes an increment of temperature. The behavior of thermal Biot number h on concentration and temperature fields are discussed through Figs. 7.24-7.25. These figures displayed that when thermal Biot number h upsurges both temperature and concentration fields are boosted. Figs. 7.26-7.31 are displayed to spectacle the impact of temperature buoyancy parameter G_t and concentration buoyancy parameter G_c on velocity, temperature and concentration profiles. Physically, buoyancy force acts as a favorable pressure gradient which accelerates the fluid within the boundary layer. Also, it is observed that the enhanced thermal buoyancy leads to the formation of thicker boundary layers. It can be noticed that when temperature and concentration buoyancy parameter G_t and G_c respectively boosted velocity profile is raised whereas concentration and temperature profiles are declines. Figs. 7.32-7.33 show the sketch of temperature and concentration profiles for various values of solutal Biot number H.

Table7.1: Comparison of skin friction coefficient, Nusselt and Sherwood number for different values of γ, λ and M with previous researcher results.

γ	λ	M	Bilal et al. (2018) $\frac{C_f\sqrt{Re}}{2}$	Present Result	Bilal et al. (2018) $\frac{Nu}{\sqrt{Re}}$	Present result	Bilal et al. (2018) $\frac{Sh}{\sqrt{Re}}$	Present Result
0.3			2.006048	2.006048	0.137640	0.137639	0.110563	0.110563
0.4			2.110885	2.110891	0.135243	0.135243	0.114124	0.114125
0.5			2.225691	2.225691	0.133668	0.133668	0.118619	0.118620
0.6			2.355524	2.355524	0.132713	0.132713	0.123362	0.123364
	0.1		1.383508	1.383508	0.141313	0.141313	0.110321	0.110321
	0.2		1.529184	1.529184	0.140342	0.140342	0.110272	0.110272
	0.3		1.716811	1.716812	0.139165	0.139165	0.110324	0.110318
	0.4		2.006048	2.006048	0.137640	0.137640	0.110563	0.110563
		0.3	2.006048	2.006048	0.137640	0.137640	0.110563	0.110563
		0.4	2.131195	2.131195	0.135695	0.135698	0.110978	0.110980
		0.5	2.267197	2.267193	0.133703	0.133700	0.111715	0.111715
		0.6	2.422030	2.422030	0.131660	0.131660	0.112784	0.112784

It is observed that both concentration and temperature profiles are upsurges with a growth of solutal Biot number H. The graph of temperature and concentration for various thermal radiation parameters R_d is displayed through Figs. 7.34-7.35. The figures displayed that the temperature distributions increased when this parameter increased whereas concentration has opposite trends. Fig. 7.36 is sketched to show the behavior of the temperature profiles. The revealed figure with an increase of Prandtl number Pr the temperature profiles rises. This is due the fact that Prandtl number is a ratio of momentum diffusivity to thermal diffusivity. When Prandtl number is high fluid has low thermal conductivity, which decreases the thermal boundary layer thickness and conduction.

Table7. 2: Numerical values of $-f''(0)$, $-\theta'(0)$ and $-\phi'(0)$ for various values of $\beta, \mathrm{d}, \mathrm{Gt}, \mathrm{Gc}, \mathrm{h}, \mathrm{H}, \text{and R}$ when $\mathrm{Nb} = 0.2$, $\mathrm{Le} = 1, \mathrm{M} = 0.3$, $\mathrm{K} = 1.0, \mathrm{Ec} = 0.1, \lambda = 0.3, R_d = 0.4, \mathrm{Nt} = 0.9, \mathrm{Pr} = 3$ and $\gamma = 0.3$.

β	D	Gt	Gc	H	H	R_d	$-f''(0)$	$-\theta'(0)$	$-\phi'(0)$
0.3							0.649363	0.075162	0.128253
0.4							0.649388	0.074699	0.129217
0.5							0.649405	0.074198	0.130207
0.6							0.649414	0.074512	0.131230
	0.2						0.649552	0.073965	0.123826
	0.3						0.671949	0.073407	0.123552
	0.4						0.694065	0.072838	0.123292
	0.5						0.715840	0.074405	0.123046
		0.1					0.649284	0.074136	0.123280
		0.2					0.643310	0.074275	0.123347
		0.3					0.637447	0.074409	0.123413
		0.4					0.631691	0.074538	0.123477
			0.1				0.649284	0.074136	0.123280
			0.2				0.637262	0.074486	0.123495
			0.3				0.625566	0.074812	0.123697
			0.4				0.614167	0.075115	0.123889
				0.01			0.660212	0.009445	0.147381
				0.05			0.655984	0.043125	0.137269
				0.1			0.649069	0.073192	0.124290
				0.15			0.640188	0.086498	0.110799
					0.2		0.649363	0.075162	0.128253

0.3		0.646389	0.074860	0.162602
0.4		0.644220	0.074636	0.187772
0.5		0.642568	0.074463	0.207016
	0.01	0.650915	0.078015	0.122031
	0.05	0.650269	0.076259	0.122978
	0.1	0.649069	0.073192	0.124290
	0.15	0.646770	0.067857	0.125598

7.5. Conclusion

This article was deals with to explore the influences of variable thermal conductivity and viscous dissipation on MHD flow of Williamson fluid above a stretching cylinder. By employing similarity transformations from the governing equations system of first order ODEs are achieved. Then, system of first order ODEs are solved numerically by applying Runge-Kutta method integrated with shooting technique using MATLAB software. The temperature, velocity, concentration, skin-friction coefficient, local Nusselt and Sherwood number for various values of dimensionless parameters are revealed and pondered using tables and graphs.

From the numerical results attained, some of the summarized conclusions are:

1. Enhancement of temperature and concentration buoyancy parameter results an increment of fluid motion whereas results a decrement of temperature and concentration.
2. With an increase of porous parameter d the profiles of velocity declines whereas temperature and concentration profiles are improved.
3. Velocity, temperature and concentration distributions are augmented with an increment of curvature parameter.
4. Williamson parameter has an increasing effect on temperature and concentration distribution whereas this parameter has a decreasing result on velocity distribution.
5. Higher Eckert number Ec and heat generation R implies higher temperature and concentration distribution
6. Temperature distributions increases and concentration distributions decreases for the growing of thermal conductivity parameter.
7. $-f''(0)$ decreases whereas $-\theta'(0)$ and $-\phi'(0)$ are increases when thermal and solutal buoyancy parameters are increased.

References

Abbasian Arani A., Abbaszadeh M., and Ardeshiri A. (2017). Mixed convection fluid flow and heat transfer and optimal distribution of discrete heat sources location in a cavity filled with nanofluid. *Trans. Phenom. Nano Micro Scales*, 5(1), 30-43. DOI:10.7508/tpnms.2017.01.004.

Anum Shafiq, Ghulam Rasool, Chaudry Masood Khalique, and Sohail Aslam (2020.) Second Grade Bioconvective Nanofluid Flow with Buoyancy Effect and Chemical Reaction. *Symmetry*, 12, 621; doi:10.3390/sym12040621.

Anum Shafiq, Ilyas Khan, Ghulam Rasool, El-Sayed M. Sherif, and Asiful H. Sheikh (2020). Influence of Single- and Multi-Wall Carbon Nanotubes on Magnetohydrodynamic Stagnation Point Nanofluid Flow over Variable Thicker Surface with Concave and Convex Effects. *Mathematics*. 8, 104. doi:10.3390/math8010104.

Bahlaoui A., Raji A., Hasnaoui M., and Naïmi M. (2016). Mixed Convection Heat Transfer Enhancement in a Vented Cavity Filled with a Nanofluid. *Journal of Applied Fluid Mechanics*, 9 (2), 593-604, http://www.jafmonline.net.

Bilal M., Sagheer M., and Hussain S. (2018). Numerical study of magnetohydrodynamics and thermal radiation on Williamson nanofluid flow over a stretching cylinder with variable thermal conductivity. *Alexandria Engineering Journal*, 57, 3281–3289. https://doi.org/10.1016/j.aej.2017.12.006.

Bilal M., Sagheer M., and Hussain S. (2018). Three dimensional MHD upper-convected Maxwell nanofluid flow with nonlinear radiative heat flux. *Alexandria Engineering Journal*. 57, 1917–1925, http://dx.doi.org/10.1016/j.aej.2017.03.039.

Bilal S., Khalil Ur Rehman, and Malik M.Y. (2017). Numerical investigation of thermally stratified Williamson fluid flow over a cylindrical surface. http://dx.doi.org/10.1016/j.rinp.2017.01.032.

Buongiorno J. (2006). Convective transport in nanofluids, *ASME J. Heat Tran*, 128 240–250.

Choi S.U.S. (1995). Enhancing Thermal Conductivity of Fluids with Nanoparticles, *ASME, USA.*

Chun-Bao Xiong, Li-Na Yu , and Yan-Bo Niu. Effect of Variable Thermal Conductivity on the Generalized Thermo elasticity Problems in a Fiber-Reinforced Anisotropic Half-Space. *Advances in Materials Science and Engineering*. 2019. https://doi.org/10.1155/2019/8625371.

Faisal Sultan, Waqar Azeem Khan,·Muhammad Shahzad, ·Mehboob Ali, and Zakir Hussain (2019). Physical assessments on variable thermal conductivity and heat generation/absorption in cross magneto-flow model. *Journal of Thermal Analysis and Calorimetry*. https://doi.org/10.1007/s10973-019-08957-4.

Gbadeyan J.A., Titiloye E.O., and Adeosun A.T. (2020). Effect of variable thermal conductivity and viscosity on Casson nanofluid flow with convective heating and velocity slip. *Heliyon*, 6. https://doi.org/10.1016/j.heliyon.2019.e03076.

Ghulam Rasool, Ting Zhang, Ali J. Chamkha, Anum Shafiq, Iskander Tlili, and Gullnaz Shahzadi (2020). Entropy Generation and Consequences of Binary Chemical Reaction on MHD Darcy–Forchheimer Williamson Nanofluid Flow over Non-Linearly Stretching Surface. *Entropy* 22, 18. doi:10.3390/e22010018.

Gireesha B.J., Umeshaiah M., Prasannakumara B.C., Shashikumar N.S., and Archana M. (2019). Impacts of nonlinear thermal radiation on magnetohydrodynamic three dimensional boundary layer flow of Jeffrey nanofluid over a nonlinearly permeable stretching sheet. *Physica A*. doi: https://doi.org/10.1016/j.physa.2019.124051.

Hamdi Messaoud1, Meziani Bachir, and Sadaoui Djamel. (2017). Numerical study of mixed convection and flow pattern in various across-shape concave enclosures. *International journal of heat and technology*, 35(3), 567-575, DOI: 10.18280/ijht.350313.

Hammed Abiodun Ogunseye, and Precious Sibanda (2019). A mathematical model for entropy generation in a Powell-Eyring nanofluid flow in a porous channel. *Heliyon*, 5 https://doi.org/10.1016/j.heliyon.2019.e01662.

Hashim,Aamir Hamid, and Masood Khan (2019). Transient flow and heat transfer mechanism for Williamson nano materials caused by a stretching cylinder with variable thermal conductivity. *Microsystem Technologies*, https://doi.org/10.1007/s00542-019-04364-9.

Hayat T., Ijaz Khan M., Farooq M., Alsaedi A., Waqas M., and Tabassam Yasmeen (2016). Impact of Cattaneo–Christov heat flux model in flow of variable thermal conductivity fluid over a variable thicked surface. *International Journal of Heat and Mass Transfer*, 99 702–710. http://dx.doi.org/10.1016/j.ijheatmasstransfer.2016.04.016.

Hayat T., Ijaz Khan M., Farooq M., Numra Gull, and Alsaedi A. (2016). Unsteady three-dimensional mixed convection flow with variable viscosity and thermal conductivity. *Journal of Molecular Liquids*, http://dx.doi.org/10.1016/j.molliq.2016.09.069.

Hemalath, Peri K Kameswaran, and Madhavi M V D N S. (2015). Mixed convective heat transfer from a vertical plate embedded in a saturated non-Darcy porous medium with concentration and melting effect. *Indian Academy of Sciences*, 40(2), 455–465.

Henniche R., Korichi A., and Ziane F. (2018). Mixed Convection Heat Transfer in a Channel in Presence of Baffles. *CFD and Tech*.

Husein Alzgool A., Hamzeh Alkasasbeh T., Sana Abu-ghurra, Zain Al-houri, Mohammed Swalmeh Z. (2019). Numerical Solution of Heat Transfer in MHD Mixed Convection Flow Micropolar Casson Fluid about Solid Sphere with Radiation Effect. *International Journal of Engineering Research and Technology*, 12(4), 519-529. http://www.irphouse.com.

Ijaz Khan M., Hayat T., Imran Khan M., Waqas M., and Alsaedi A. (2018), Numerical simulation of hydromagnetic mixed convective radiative slip flow with variable fluid properties. A mathematical model for entropy generation. *Journal of Physics and Chemistry of Solids*. https://doi.org/10.1016/j.jpcs.2018.10.015.

Iqbal W., Naeem M. N., and Jalil M. (2019). Numerical analysis of Williamson fluid flow along an exponentially stretching cylinder. *AIP Advances*, 9, 055118, doi: 10.1063/1.5092737.

Kai-Long Hsiao (2016). Stagnation Electrical MHD Nanofluid Mixed Convection with Slip Boundary on a Stretching Sheet, *Applied Thermal Engineering*, 98, 850–86. http://dx.doi.org/10.1016/j.applthermaleng.2015.12.138.

Kai-Long Hsiao (2017). Micropolar nanofluid flow with MHD and viscous dissipation effects towards a stretching sheet with multimedia feature. *International Journal of Heat and Mass Transfer*, 112: 983–990. http://dx.doi.org/10.1016/j.ijheatmasstransfer.2017.05.042.

Liaquat Ali Lund, Zurni Omar, and Ilyas Khan. (2019). Analysis of dual solution for MHD flow of Williamson fluid with slippage. *Heliyon*, 5 e01345.doi: 10.1016/j.heliyon.2019.e01345.

Maatouk Khoukhi, Ahmed Hassan, and Shaimaa Abdelbaqi, (2019). The Impact of Variable Thermal Conductivity of Insulation Materials on the Building Energy Performance in Hot Climate. *E3S Web of Conferences*, https://doi.org/10.1051/e3sconf/201910302001.

Malik M. Y., Bibi M., Farzana Khan, and Salahuddin T. (2016). The effect of variable thermal conductivity on Williamson fluid flow over a stretching cylinder and heat transfer with heat generation/absorption. 6, 035101; doi: 10.1063/1.4943398

Mamun Billah Md., Imran Khan Md, Mohammed Mizanur Rahman, Muntasir Alam, Sumon Saha, and Mohammad Nasim Hasan (2017). Numerical Study of Mixed Convection Heat Transfer Enhancement in a Channel with Active Flow Modulation. *AIP Conference Proceedings*, http://dx.doi.org/10.1063/1.4984733.

Manjula N., Govardhan K., Rajashekar M. N. (2019). A numerical investigation of the steady state flow of MHD Williamson nanofluid with viscous dissipation in porous medium. *International Journal of Recent Technology and Engineering*. 8(3), DOI:10.35940/ijrte.C4861.098319.

Manu Chakkingal, Julia de Geus, Sasa Kenjeres, Iman Ataei-Dadavi, M.J. Tummers, and Chris R. Kleijn (2020). Assisting and opposing mixed convection with conjugate heat transfer in a differentially heated cavity filled with coarse-grained porous media. *International Communications in Heat and Mass Transfer*, 111. https://doi.org/10.1016/j.icheatmasstransfer.2019.104457.

Mohamed Kezzar, Ismail Tabet, Mohamed R. Eid. (2020). A new analytical solution of longitudinal fin with variable heat generation and thermal conductivity using DRA. *Eur. Phys. J. Plus*. 135:120. https://doi.org/10.1140/epjp/s13360-020-00206-0.

Mohamed R. Eid & Mohamed A. Nafe (2020). Thermal conductivity variation and heat generation effects on magneto-hybrid nanofluid flow in a porous medium with slip condition*: Waves in Random and Complex Media*. https://doi.org/10.1080/17455030.2020.1810365.

Mohamed R. Eid1, Ahmed F. Al-Hossainy (2020). Synthesis, DFT calculations, and heat transfer performance large-surface TiO2: ethylene glycol nanofluid and coolant applications. *Eur. Phys. J. Plus*. 135:596. https://doi.org/10.1140/epjp/s13360-020-00599-y

Muhammad Ramzan and, Muhammad Bilal (2015). Time Dependent MHD Nano-Second Grade Fluid Flow Induced by Permeable Vertical Sheet with Mixed Convection and Thermal Radiation. *PLOS ONE*. DOI:10.1371/journal.pone.0124929.

Nagendra N., Amanulla CH., Sudhakar Reddy M., and Ramachandra Prasad V. (2018). Hydromagnetic Flow of Heat and Mass Transfer in a Nano Williamson Fluid Past a Vertical Plate With Thermal and Momentum Slip Effects. *Nonlinear Engineering*. aop. https://doi.org/10.1515/nleng-2017-0057.

Nawel Boumaiza, Mohamed Kezzar, Mohamed R. Eid & Ismail Tabet (2019). On numerical and analytical solutions for mixed convection Falkner-Skan flow of nanofluids with variable thermal conductivity, *Waves in Random and Complex Media*. DOI: 10.1080/17455030.2019.1686550

Noreen Sher Akbar, and Zafar Hayat Khan (2016). Effect of variable thermal conductivity and thermal radiation with CNTS suspended nanofluid over a stretching sheet with convective slip boundary conditions: Numerical study. *Journal of Molecular Liquids*. 222 279–286. http://dx.doi.org/10.1016/j.molliq.2016.06.102.

Rajneesh Kumar, Anil K. Vashishth, and Suniti Ghangas (2019). Variable thermal conductivity approach for bio heat transfer during thermal ablation. *Arab Journal of Basic and Applied Sciences*, 26(1), 78-88. DOI: 10.1080/25765299.2019.1566982.

Rashid M., Ansara K., and Nadeem S. (2020). Effects of Induced Magnetic Field for Peristaltic flow of Williamson Fluid in A Curved Channel. *Physica Adoi*, https://doi.org/10.1016/j.physa.2019.123979.

Sarojamma G., Vijaya R. Lakshmi, Satya Narayana P. V., and Vajravelu K. 2019. Variable Thermal Conductivity and Thermal Radiation Effect on the Motion of a Micro Polar Fluid over an Upper Surface. *J. Appl. Comput. Mech*. 5(2) 441-453. DOI: 10.22055/JACM.2018.27138.1380.

Sihem Lahmar, Mohamed Kezzar, Mohamed R. Eid, Mohamed Rafik Sari (2019). Heat transfer of squeezing unsteady nanofluid flow under the effects of an inclined magnetic field and variable thermal conductivity, *Physica A*. doi: https://doi.org/10.1016/j.physa.2019.123138.

Sihem Lahmar, Mohamed Kezzar, Mohamed R. Eid, Mohamed Rafik Sari (2019). Heat transfer of squeezing unsteady nanofluid flow under the effects of an inclined magnetic field and variable thermal conductivity. *Physica A.*, https://doi.org/10.1016/j.physa.2019.123138

Sumit Gupta, Devendra Kumar, and Jagdev Singh (2020). Analytical investigation of the effects of variable thickness on MHD flow of Williamson nanofluid with the nonlinear thermal radiation. *SN Applied Sciences*, 2438. https://doi.org/10.1007/s42452-020-1995-x.

Tasawar Hayat, Bilal Ashraf, Sabir Ali Shehzad, Alsaedi A., and Bayomi N. (2015). Three-dimensional mixed convection flow of viscoelastic nanofluid over an exponentially stretching surface. *International Journal of Numerical Methods for Heat & Fluid Flow*. 25(2), 333 – 357, http://dx.doi.org/10.1108/HFF-01-2014-0024.

Tasawar Hayat, Ijaz Khan M., Tufail Ahmad Khan, Khan M.I., Salman Ahmad, Ahmed Alsaedi (2018). Entropy generation in Darcy-Forchheimer bidirectional flow of water-based carbon nanotubes with convective boundary conditions. *Molliq*. doi:10.1016/j.molliq.2018.06.017.

Tasawar Hayata, Muhammad Ijaz Khan, Sumaira Qayyum, and Ahmed Alsaedi (2018). Entropy generation in flow with silver and copper nanoparticles. *Colloids and Surfaces A*. 539 335–346, https://doi.org/10.1016/j.colsurfa.2017.12.021.

Williamson R.V. (1929). The flow of pseudo plastic materials. *Ind Eng Chem Res.*; 21(11):1108-1111.

Chapter 8

General Conclusion and Recommendation

8.1. General Conclusion

The present investigation entitled **"**Boundary Layer Analysis of non-Newtonian Nanofluid Past Stretching/Shrinking Surface**"** has been made to study the effects of different phenomena on boundary layer non-Newtonian nanofluid flow processes through different shaped bodies. The governing non-linear ordinary differential equations are solved by means of very efficient numerical techniques such as Keller box method and 5^{th} order Runge-Kutta method with shooting technique. The effects of various parameter such as Deborah number, Brownian motion parameter, Thermophoresis parameter, Weissenberg number, suction/injection, melting parameter, wedge angle, unsteady parameter, activation energy parameter, magnetic field, temperature buoyancy parameter, concentration buoyancy parameter, heat source parameter, radiation effect, porosity, chemical reaction and boundary layer slip past stretching/shrinking surface are discussed. Variation of velocity, temperature and concentration with various physical parameters has been studied. Numerical values of Skin-friction coefficient, Nusselt number and Sherwood number have also been computed and analyzed with the variation of some physical parameters involved in the study.

Chapter 1 is purely introductory and is designed in such a way that it introduces core concepts and foundation required for the study. It includes the classification of fluids. The governing equations of continuity, momentum, energy and diffusion have also been presented. Phenomena of physical quantity and non-dimensional number were also explained. Moreover, the objective of the study, statement of the problem, significance of the study and the methods those are used in this study are discussed in this chapter.

The review of literature to accommodate majority of available past research works is given in chapter 2. It contains a summary of the subject interest and includes an overview of the entire topic and segments of related works and materials that will reflect the total relevance with the present study. The literature related to applications of nanofluid and non-Newtonian is also reviewed in this chapter. Some model of nanofliud and application of some shaped bodies are discussed in this chapter.

In chapter 3, MHD Slip Flow of Upper-Convected Maxwell Nano Fluid over a Stretching Sheet with Chemical Reaction is studied. The governing partial differential equations are converted into dimensionless form of non-linear ordinary differential equation by using suitable transformations. For the numerical solution of the reduced dimensionless ordinary differential equations, the Keller Box method is applied. To show the accuracy and authenticity of our results, a comparison is made with literature for some special cases. The impacts of non-dimensional governing parameters such as Brownian motion parameter, velocity ratio, velocity slip parameter, suction/injection parameter, Lewis numbers, upper-convected Maxwell parameter, magnetic field, thermophoresis parameter, chemical reactions parameter, thermal slip parameter, solutal slip parameter, and heat source parameter on the velocity field, heat and mass transfer characteristics are discussed and presented through graphs. The results indicate that when the magnetic field is intensified, it reduces velocity profiles, whereas it rises temperature and concentration profiles.

Chapter 4 is focused to analyze melting and viscous dissipation effect on upper-convected Maxwell and Williamson Nanofluid over a stretching sheet embedded in porous media. System of partial differential equation which is obtained by conservation principles is transformed by means of appropriate similarity transformation into system of ordinary differential equations. Employing the Keller box method numerical results are obtained. Impacts of different appropriate parameters on velocity profiles, thermal and concentration fields, Nusselt number, skin friction coefficient and Sherwood number are deliberated with graphical and tabular representations. The study revealed that dimensionless melting parameter increases the flow and velocity boundary layer whereas the thermal and concentration profiles decrease. Melting parameter affects harmfully the velocity boundary layer thickness of Williamson nanofluid when compared to upper-convected Maxwell nanofliud. Moreover, radiation parameter has opposite effect on temperature and concentration graph. As the values of radiation parameter upsurges the temperature decreases whereas concentration rises.

In chapter 5, the effect of viscous dissipation on unsteady Williamson nanofluid over stretching/ shrinking wedge with thermal radiation and chemical reaction is discussed. The governing partial differential equations are converted to ordinary differential equations by means of a similarity transformation before being solved numerically by finite difference scheme called Keller-Box method. The flow, heat transfer and mass transfer characteristics are analyzed through governing parameters such as wedge angle, unsteadiness, Williamson, slip, Brownian motion, thermophoresis, chemical reaction parameters, Prandtl number, Biot-number, Eckert number and Lewis number. The result of the study described that the velocity profiles increased with an upsurge of wedge angle, unsteady parameter and suction parameter while it is diminished with an increase of Williamson and injection parameter. Moreover, the temperature profiles upsurges with the distended Williamson parameter, Biot number and injection parameter, while it is declined for large values of wedge angle, unsteady and suction parameter. With an increase of Williamson, unsteady and suction parameter the concentration profiles upsurges, while it is decreased with an increase of wedge angle and injection parameter.

Chapter 6 presents the analysis of effect of activation energy on mixed convective heat and mass transfer of Williamson nano fluid with heat generation or absorption over stretching cylinder. Mathematical model for Williamson fluid in cylindrical coordinate system is developed in terms of nonlinear partial differential equations and transformed in to system ordinary differential equations. The numerical solution is obtained by using Runge-Kutta method in conjugation with shooting technique. Numerical results of Nusselt number, skin friction coefficient and Sherwood number for different values of physical parameter are computed in tables. The effects of different physical parameter on dimensionless velocity, temperature and concentration are presented in graphs. The result of the study shows that the velocity profiles are increased with an increase of curvature parameter whereas when the values of curvature parameter upsurges the temperature boundary layer thickness declines. Moreover, from the study it can be seen that when an activation energy upsurges the concentration field raises, but it diminishes with an increase of reaction rate parameter. With an increase of reaction rate parameter the magnitude of skin friction coefficient remain constant but the magnitude of Nusselt number diminution and Sherwood number raises.

In chapter 7, we presented the combined effects of the effect of viscous dissipation on mixed convective heat transfer of magnetohydrodynamics flow of Williamson nanofluid above a stretching cylinder in the presence of variable thermal conductivity and chemical reaction. By proposing applicable similarity transformations nonlinear ordinary differential equations are attained from partial differential equations. These non-dimensional ordinary differential equations are computed through Runge-Kutta method integrated with shooting method. The graphs of temperature, velocity, and concentration distributions are plotted to observe the dissimilarity for various values of prominent parameters. Also numerical results of local Sherwood number, local Nusselt number and skin-friction coefficient are tabulated. From the result it can be noticed that when temperature and concentration buoyancy parameter respectively boosted velocity profile is raised whereas concentration and temperature profiles are declines. Also, from the computation it is concluded that the temperature field is boosted with a growth of thermal conductivity whereas opposite trends happens for concentration profiles.

8.2. Recommendation for the future work

The present study discusses boundary layer analysis of non-Newtonian nanofluid past stretching/ shrinking surface. In this dissertation 2-D model and non-Newtonian nanofluid have considered. Therefore, the researcher suggests the following future areas of research:

- The problem can be extended to non-Newtonian dusty nanofluids.
- It is also possible to consider inclined stretching/shrinking surfaces.
- The problem can be extended for 3-D model non-Newtonian nanofluids.
- One also consider compressible and turbulence flow with entropy generation.

List of published papers

MHD slips flow of upper-convected Maxwell nanofluid over a stretching sheet with chemical reaction. Journal of the Egyptian Mathematical Society (2020) 28:7 https://doi.org/10.1186/s42787-019-0057-2

Melting and viscous dissipation effect on upper-convected Maxwell and Williamson nanofluid. Engineering Reports. 2020; 2:e12159. wileyonlinelibrary.com/journal/eng2 1 of 25, https://doi.org/10.1002/eng2.12159.

Viscous dissipation effect on Williamson nanofluid over stretching/ shrinking wedge with thermal radiation and chemical reaction J. Phys. Commun. 4 (2020) 045015. https://doi.org/10.1088/2399-6528/ab8a68.

The Investigation of MHD Williamson Nanofluid over Stretching Cylinder with the Effect of Activation Energy. Advances in Mathematical Physics Volume 2020, Article ID 9523630, 16 pages. https://doi.org/10.1155/2020/9523630.

Viscous dissipation effect on mixed convective heat transfer of MHD flow of Williamson nanofluid over a stretching cylinder in the presence of variable thermal conductivity and chemical reaction. DOI: 10.1002/htj.21985.